Control of Sound Transmission with Active-Passive Tiles

Andre L. Goldstein

Dissertation submitted to the faculty of the Virginia Polytechnic Institute and State University in partial fulfillment of the requirements for the degree of

Doctor of Philosophy
In
Mechanical Engineering

Dr. Chris R. Fuller, Chair
Dr. Daniel J. Inman
Dr. Ricardo A. Burdisso
Dr. Marty E. Johnson
Dr. James P. Carneal
Dr. Douglas K. Lindner

May, 2006
Blacksburg, VA

Keywords: noise control, payload fairing, double panel, Thunder actuator, vibration isolation

Control of Sound Transmission with Active-Passive Tiles

Andre L. Goldstein

(ABSTRACT)

Nowadays, numerous applications of active sound transmission control require lightweight partitions with high transmission loss over a broad frequency range and simple control strategies. In this work an active-passive sound transmission control approach is investigated that potentially addresses these requirements. The approach involves the use of lightweight stiff panels, or tiles, attached to a radiating base structure through active-passive soft mounts and covering the structure surface. The resulting double-partition configuration was shown to have good high frequency passive isolation, but poor low frequency transmission loss due to the coupling of the tiles to the base vibration through the air gap. The low frequency transmission loss performance of the partition was increased by using the active mounts to cancel the local volume velocity of the tiles. The use of a decentralized control approach with independent single channel controllers for each tile facilitates the implementation of a multiple tile system in a large scale application.

A coupled structural-acoustic model based on an impedance mobility matrix approach was formulated to investigate the potential performance of active-passive tile approach in controlling sound transmission through plates. The model was initially applied to investigate the sound transmission characteristics of a double-panel partition consisting of a single tile-plate configuration and then extended to model a partition consisting of multiple-tiles mounted on a plate. The system was shown to have significant passive performance above the mass-spring-mass resonance of the double-panel system. Both feedback and feedforward control approaches were simulated and shown to significantly increase the transmission loss of the partition by applying control forces in parallel with

the mounts to reduce the tile normal velocity. A correspondent reduction in sound radiated power was obtained over a broad frequency range limited by the tile stiffness.

The experimental implementation of the active-passive tile approach for the control of sound transmission through plates was also performed. Two main experimental setups were utilized in the investigations, the first consisting of a single tile mounted on a clamped plate and the other consisting of four active tiles mounted of a simply supported plate. Tile prototypes were implemented with lightweight stiff panels and integrated active-passive mounts were implemented with piezoelectric Thunder actuators. Both analog feedback and digital feedforward control schemes where designed and implemented with the objective of reducing the normal velocity of the tiles. Experimental results have demonstrated significant broad frequency range reductions in the sound transmission through the partition by active attenuation of the tile velocity. In addition, the experiments have shown that decentralized control can be successfully implemented for multiple tiles systems. The active-passive sound transmission control characteristics of the systems experimentally studied were observed to be in accordance with the analytical results.

Acknowledgements

I would like to thank my research advisor, Dr. Chris Fuller for the opportunity to work under his guidance on a challenging project and for providing an excellent research environment, which made it possible to carry out my Ph.D. studies. I would also like to thank Dr. Daniel Inman, Dr. Ricardo A. Burdisso, Dr. Marty E. Johnson, Dr. James P. Carneal and Dr. Douglas K. Lindner for serving as members of my dissertation committee. Special thanks to Dr. Leonardo Goldstein Jr. for his invaluable input on the organization of this dissertation. Thanks are also due to the staff of the Mechanical Engineering Department and the Vibration and Acoustics Laboratory for their support and to research fellows Kenji Homma, Yu Du and Pierre Marcotte for their support and friendship.

I also wish to acknowledge the Brazilian sponsoring agency CAPES and the U.S. Air Force Office of Scientific Research for their sponsorship during the project.

Last, but not least, I wish to express my gratitude to my parents in Brazil for their support and encouragement throughout my graduate studies. Above all, I would like to thank my wife, Gisele, for her wholehearted support that was invaluable for the completion of my degree.

Contents

List of Figures

List of Tables

Chapter 1

1 Introduction

The control of sound transmission constitutes an important noise control problem in modern structures such as aircrafts, helicopters, automobiles, and rocket payload fairings. Acoustic noise can affect human health, with effects ranging from discomfort to serious hearing loss. Excessive acoustic noise can also present a serious threat to mechanical and electrical systems by producing excessive vibration, stress, fatigue damage, and malfunction [1].

In the case of the rocket payload fairing the severe vibration/acoustic environment that exists during launch was blamed for 30% to 60% of satellite first-day failures [2]. The main cause of the high intensity noise is the burn of the rockets; aerodynamic noise during the transonic stage and explosions that occur during the separation can also contribute. The burn of the rockets during launch generates an acoustic load that excites the fairing walls. The vibration of the fairing walls couples with the acoustic field of the fairing interior and can generate very high sound pressure levels (SPL). The high levels inside the fairing can excite and damage lightweight structures of the spacecraft, such as solar panels.

The large acoustic transmission problem is augmented by the development of more powerful engines and by use of larger fairings built with lightweight composite materials, aiming at reducing fairing weight, maximizing payload capability and reducing costs. Typical maximum SPL expected for the fairing of a Boeing Delta launch vehicle are shown in Figure 1.1. Levels between 125 dB and 130 dB can be expected in the 50 Hz to 400 Hz, and the overall SPL reaches 140 dB.

Because of the high costs involved in a rocket launch, the mass and free volume of the fairing are very important parameters that limit the amount of treatment that can be applied to the fairing interior to control the sound levels. The currently employed

passive control method of increasing the transmission loss consists of covering the fairing interior walls with 2 to 4 inches thick acoustic foam blankets. Although this method works for high frequency noise, it has proven ineffective at low frequencies [4]. The inefficiency of current noise control treatments helps motivating the recent great research interest in novel solutions for controlling the low frequency sound transmission in the payload fairing application.

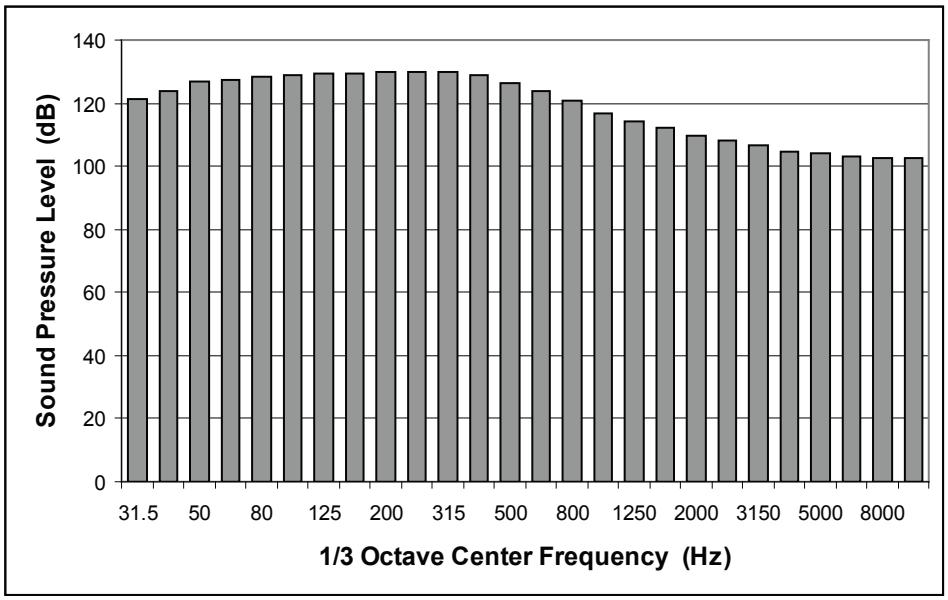

Figure 1.1: Typical sound pressure levels experienced by spacecraft during launch [3].

1.1 Active Control of Sound Transmission

The initial applications of active sound transmission control were based on the use of acoustic sources located in the acoustic medium next to the structure. The basis of this technique is reducing the acoustic radiation impedance seen by the structure [5,7]. Another approach that has received great research interest is active structural acoustic control [6] in which active forces are applied directly on the structure and used for modifying its radiating characteristics.

Fuller first demonstrated the active structural acoustic control (ASAC) approach in an analytical investigation of the control of the sound radiated by a panel over a large frequency band using several point force actuators [19]. This work revealed that for control of the structural sound radiation it is necessary to control only the structural modes that are well coupled to the sound field. Further work [20,21] demonstrated that piezoelectric actuators could be used for reduction of the far-field acoustic radiated power with proper selection of the number, location and size of the actuators, with higher reductions observed with increased number of actuators.

The reduction in sound radiation using ASAC results from the modification of the surface velocity of the structure by two distinct physical mechanisms: modal suppression and modal rearrangement [8,22]. Modal suppression involves a decrease in the amplitude of the dominating structural modes, while modal rearrangement involves an adjustment of the amplitude and phases of the structural modes resulting in a decrease of the radiation efficiency of the structure.

1.1.1 Active Control for the Fairing Noise Problem

Active control techniques have been considered as a potential solution for the low frequency noise problem in payload fairings. However, there are several requirements for a successful implementation of an active control system to control the internal acoustic noise levels in a rocket fairing. The overall control system should have the following characteristics [14]:

The entire control system should be lightweight and compact, contained within a few inches of the fairing wall;

- The control system should be rugged enough to withstand the severity of the launch environment;
- The controller should be able to control broadband disturbances and both

structural and acoustic dominated system responses;

- The control system should impose reduced or no additional interface requirements on the launch vehicle;

- The actuators should have adequate control authority to control the very high SPL that occur during launch; and

- The control system should draw reasonable amounts of electric power or current from the launch vehicle.

Recently, several authors have investigated the application of active control techniques to the rocket fairing sound transmission problem. In [17] MIMO feedback and feedforward control approaches were investigated. Loudspeakers inside the fairing and piezoelectric actuators attached to the fairing were used as actuators. The error and residual sensors consisted of microphones inside the fairing and accelerometers at the fairing walls. The trade-offs involved in implementing a practical active noise control system for the fairing are discussed, including: the feedback versus feedforward control, acoustic versus structural actuators and acoustic versus structural error sensors. The results showed that reaching the desired noise reduction levels using the MIMO controller depended on the use of a large number of microphones as error sensors inside the fairing. In addition, the use of both loudspeakers inside the fairing or piezoelectric actuators were recommended, as well as large number of actuators because of the required control authority.

The application of a MIMO optimal feedback controller for reducing the interior sound field of an enclosure using only structural sensors and actuators was proposed in [16]. Controlling the radiation modes of the system eliminates the need for interior microphones. However, practical implementation was pointed as being constrained by the large complexity of the control system as well as difficulty in modeling the large number of structural modes and including robustness in the presence of model uncertainty.

Other studies have been performed investigating the control of the interior acoustic noise by actively adding damping to the structural and acoustic modes of the fairing. Piezoelectric sensors and actuators were used with local feedback control for applying broadband damping to the structure aiming at reducing the SPL inside the payload fairing [31,32] but performance in large fairings is limited by necessary actuator authority. Control authority issues also limit the use of active proof-mass actuators with local feedback controllers, as shown in [34]. Damping can be added to the acoustic modes of the fairing using acoustic sensor and actuators and local feedback loops. The use of an array of spatially weighted loudspeakers driven by feedback control was demonstrated for controlling low frequency acoustic modes of a small-scale fairing [35]. Still, the limited authority of current actuator technology constrained the practical application of the approach in large fairings and realistic SPL.

The use of active-passive distributed vibration absorbers for reducing the interior noise of a composite cylinder excited by a high-level reverberant acoustic field was investigated by Johnson et al. [36,37]. The passive devices were tuned to the resonance frequencies of the structure and the actuators were driven using a MIMO feedback controller. The results demonstrated that it is possible to reduce the sound transmission resulting from structural modes by damping to the structure. However, in order to control the interior sound field caused by acoustic resonances requires additional acoustic tuned resonators. Both the feedback and optimally tuned absorbers were based on a detailed model of the system response for a specific payload fill condition.

Esteve and Johnson [61] demonstrated the simultaneous use of distributed vibration absorbers (DVA) and Helmholtz resonators (HR) for controlling the interior sound levels of a cylinder. Using a fully coupled model of the system it was demonstrated that significant interior noise reduction could be achieved by optimally tuning the resonant devices to add damping to both acoustic and structural modes in the bandwidth of interest. Good performance is however, restricted to lightly damped structure and acoustic cavity.

Although a great amount of research has been dedicated to the rocket fairing noise

problem, limited success has been obtained. This limited success can be attributed to requirements listed at the beginning of this section, requisite for practical implementation active control method to reduce sound transmission into a rocket payload fairing. The high stiffness of the payload structure limits the implementation of a system based on the ASAC approach because of lack of readily available commercial off-the-shelf high authority actuators that are required [15]. The implementation of an ANC system requires microphones error sensors positioned in the interior of the fairing, which would complicate the payload integration aspects of launch vehicle operations [16]. In addition, the necessity of controlling high SPL at low frequencies imply in the bulky and heavy loudspeakers, which consume large amounts of electrical power.

Furthermore, as the payload fairing system is a coupled structural-acoustic system it is necessary to control both acoustic-dominated and structural-dominated modes. In general, the control of a structural-acoustic coupled system requires a multiple-input, multiple-output (MIMO) controller, and possibly a hybrid ANC/ASAC system [17, 18]. The use of a MIMO control system with a large number of channels results in very complex control system implementation at the expense of great computational power and complex integration of the actuators and sensors in the fairing. In addition as the controller design depends on a system model, practical implementation is constrained by the high order model [16], and controller performance and stability can suffer if the system changes or if a transducer fails.

The use of feedforward control is limited by the difficulty in obtaining an adequate reference signal that gives time-advanced information about the disturbance, given its random and broadband nature. Another difficulty is the necessity of reducing the control system interface requirements, which eliminates the possibility of using an external array of microphones as reference sensors.

1.1.2 Other Approaches in Active Control of Sound Transmission

The great amount of research in the area of active systems for controlling sound transmission through a partition has resulted in alternative concepts, such as

active-passive hybrid systems [38,39] and active (or smart) skins [40] which are reviewed next.

Partition Segmentation

An important aspect of several of the alternative active control approaches for controlling sound transmission has been the division of the partition to be controlled in segments. These segments are individually actuated in such a way as to minimize sound radiation. In general, this approach involves the use of actuators for reducing either the vibration of the sub panel or its radiation efficiency. A potential benefit of such approach includes the simplification of the control requirements with the use of decentralized single-input single-output (SISO) control loops for controlling each segment, based on local structural or acoustic information.

Several approaches have been proposed for the implementation of the active control of sound transmission using segmented partitions. A theoretical investigation of partition segmentation by modeling the segment/actuator configurations using electro-mechanical-acoustical circuits is given in [41]. Hirsch et al. [42,43] presented an analytical and experimental investigation of the use of segmented trim panels as acoustic control sources for controlling interior noise levels of a cylinder. The numerical results presented, suggested that an increase in the number of segments increases the frequency range in which the acoustic pressure can be controlled. In an experimental investigation, flat aircraft trim panels restricted to move in the piston mode and driven by a small shaker, were used as acoustic sources for controlling both structural and acoustic sound transmission through a cylinder.

Ross and Burdisso [44] proposed the concept of a weak sound-radiating cell, which consists of two mechanically coupled surfaces whose response is out-of-phase and of nearly equal magnitude and that radiate as an acoustic dipole. When placed on a vibrating structure, it converts the motion of the base vibrating structure into an inefficient radiator, in this case a dipole radiator. Attenuation of sound radiation by a structure was obtained by covering the surface of the structure with arrays of weak

radiating cells. A requirement of this method is that the resonance frequency of the cell should be lower than frequency bandwidth where reduction is desired. This reduction in the resonance frequency is obtained either by increasing the mass of the cell's vibrating surface or reducing the stiffness of the system. Experimental implementation validated the potential of the proposed approach in the frequency range from 400 to 1600 Hz.

Double Panel Partitions

Double panel partitions are often used for controlling the transmission of sound when high transmission loss is required with a relatively lightweight structure, such as aircraft fuselage walls. However, the transmission loss performance of the double panel degrades at low frequencies because of the coupling between the partition panels and can even be lower than that of a single panel [23]. The poor low frequency transmission loss of double panel partitions has motivated the use of active control methods aiming at improving the low frequency transmission loss performance.

Active control of double wall partition can be implemented with control of the interior SPL inside the air gap [25,27] or control of the structural vibration [24,46]. Carneal and Fuller [24] demonstrated the use of ASAC to control of sound transmission through double-panels applied to noise reduction in aircraft interiors. Piezoelectric actuators were used to apply control forces to the structure and a feedforward controller minimized the radiated power sensed by microphones located in the acoustic far field. It was shown that the application of the control inputs to the radiating panel resulted in better performance than when the control forces were applied to the base panel. In addition, increased performance, by passive and active effects, was demonstrated with the use of a stiffer radiating panel with lower modal density.

It is well known that at low frequencies the volume velocity of the radiating panel controls the sound radiation. For the case of a flexible panel, a single shaped error sensor can be employed to achieve large reductions in the radiated power [26,33]. In the case of the sound transmission through a stiff panel, the rigid body modes were shown to dominate the sound transmission at low frequencies [22]. In this case, large attenuations

of the sound transmission can be obtained using three actuators, one for each vibration mode (one piston and two rocking modes). In addition high levels of attenuation of sound transmission can be achieved with a single actuator if the panel is restricted to move in the piston mode. Several works explored this concept as discussed below.

Thomas et al. [46] presented an experimental investigation on the control of single frequency sound transmission through a double-panel partition consisting of a clamped steel plate and a freely mounted aluminum honeycomb plate. A feedforward controller was used to generate control signals sent to electrodynamic shakers between the plate and honeycomb panel for minimization of the sound pressure at error microphones positioned in the acoustic far field. Flanking paths in the experimental setup ensured appreciable sound transmission, even if the radiating panel remained motionless and in order to attain further reductions in radiated pressure, the panel had to act as a secondary acoustic source. Significant improvement in performance was obtained when using four smaller panels. A better control of the rotational modes of the composite panels and better control of the sound radiated by the flanking path were given as possible reasons for this improvement, resultant from the increased number of secondary acoustic sources. The need for microphones in the far field as error sensors and bulky electrodynamic actuators as control actuators limit the practical implementation of this approach in real world applications.

In a related work [50], the same authors used a modified loudspeaker as an actuator for applying a control force between two aluminum honeycomb panels. The panels were mounted on flexible gaskets and positioned in a window between two acoustic chambers. The first panel, which served as the base structure, was excited with broadband noise by an electrodynamic shaker. Attenuation of the radiating panel sound was achieved through the use of optimal digital feedback control with the objective of minimizing the signal from an accelerometer mounted at the center of the radiating panel surface. The excitation of the radiating panel rocking modes of vibration was shown to limit the frequency band where sound attenuation could be achieved. The results obtained in this work were encouraging for demonstrating the possibility of reducing sound radiation by

minimizing the velocity of the radiating panel with a single acceleration sensor. However, the implementation made use bulky electrodynamic actuators and no analytical model to predict the behavior of the system was presented.

In [27] the active control of sound transmission through double panels was investigated analytically considering the simultaneous use of acoustic actuators in the air gap and active vibration isolators connecting the panels. Loudspeakers were shown to be effective control sources at low frequencies, when the sound transmitted is resultant of the coupling of the panels through the air in the cavity (that has a spring like behavior at low frequencies). At higher frequencies, above the first resonance of the cavity, coupling of the panel structural modes and cavity acoustic modes controlled the sound transmission. The active mount configuration studied was effective in reducing sound transmission only when used in combination with loudspeakers. This failure in reducing sound transmission through the use of active mounts was attributed to the positioning of the mounts at the corners of the panels, where they were unable to control structural modes that radiated efficiently or the mass-spring-mass coupling mechanism of the double panel system.

1.2 Active-Passive Tile Concept

This work investigates a novel active-passive sound transmission control approach that consists of arrays of lightweight stiff panels (or tiles) attached to a radiating surface through active-passive mounts and covering the entire (or most of the) structure surface. At low frequencies, the sound radiated by the tiles mostly due to the tile piston mode of vibration (or volume velocity mode) is proportional to the normal velocity of the tiles. Thus reductions in the total sound radiated power can be achieved by reducing the vibrations levels of the surface.

Each active-passive tile element consists of a lightweight, stiff panel connected to the base structure through integrated active-passive soft mounts, which ideally behave as a spring-damper systems with an active force applied in parallel. The use of soft mounts

provides good passive isolation characteristics at high frequencies. The active element is used apply control forces to improve the isolation performance at low frequencies without weight or size penalties. Each tile has its normal velocity, measured by a single point sensor, minimized by independent single-input, single-output (SISO) control loops. As long as the tiles behave rigidly and the volume velocity mode is the main contributor to sound radiation, the acoustic radiated power is proportional to the normal velocity of the tiles. Figure 1.2 shows an illustration of a structured covered with arrays of tiles connected to the structure via active-passive mounts. Figure 1.3 shows a schematic of the proposed decentralized control approach.

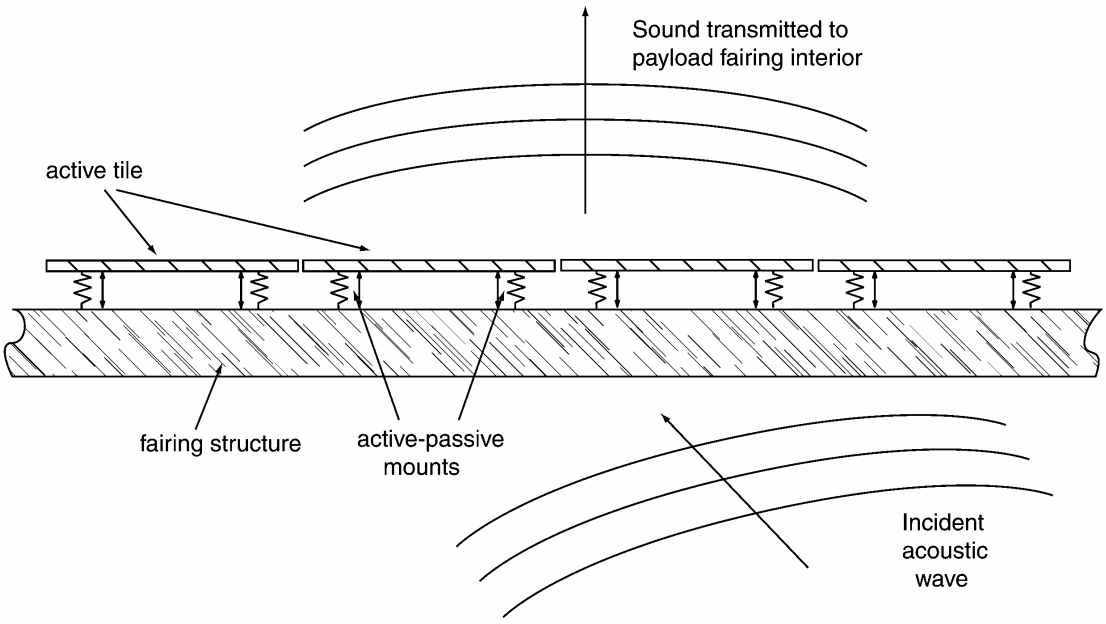

Figure 1.2: Schematic of surface treatment using active tiles.

The active-passive tile approach for active control of sound transmission is an alternative to ASAC systems specially when the partition is large and has low mechanical mobility, which would require an overly complex MIMO control system and high authority control actuators. The surface treatment approach of the active tile method also provides an alternative to ANC systems for controlling high-level low-frequency sound, which

requires large acoustic actuators (loudspeakers).

The active tile approach also potentially reduces the control system implementation costs and simplifies the controller design through the use of a decentralized control scheme. As mentioned earlier, the use of a centralized MIMO control system for a large system has several disadvantages. The complexity of a centralized controller increases rapidly with number of sensors and actuators requiring a great amount of wiring for connecting all transducers to a single controller and large amounts of processing power. In addition, since the MIMO controller is based on a complex model of the system, the control performance and stability are threatened by transducer failure or changes in the system not taken into account by the model. The use of a decentralized control system with multiple independent loops has the advantages of reduced complexity and wiring. In addition, the system can be made modular and systems of increased complexity can readily be implemented with a larger number of similar control units.

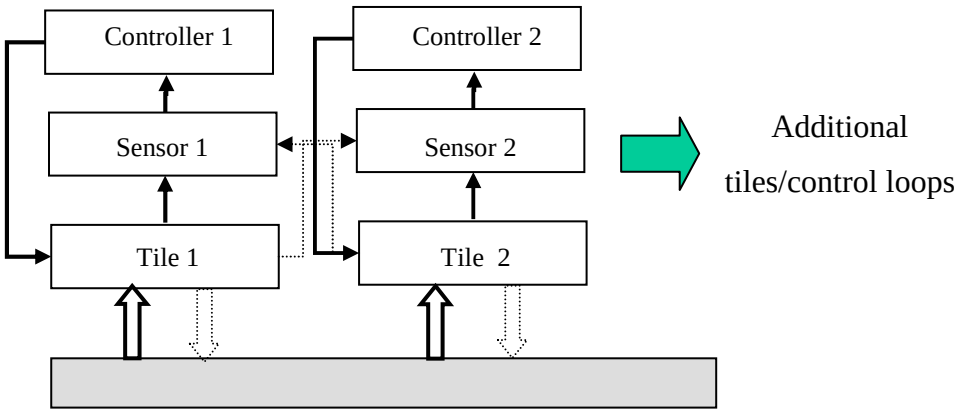

Figure 1.3: Schematic of active tiles with decentralized control

1.3 Dissertation Goals and Contributions

The main goal of the present work is to investigate the sound transmission control characteristics of the proposed active-passive tile approach. This approach can be applied to numerous applications of active sound transmission control that require lightweight partitions with high transmission loss over a broad frequency range and simple control strategies. In particular the proposed method addresses several of the practical requirements of an active control system to be used in the fairing noise problem:

- The control system can be made lightweight and compact, and contained within a few inches of the fairing wall;
- A simple decentralized control system can be implemented;
- Simple integration with the launch vehicle and be possible integration with passive blankets;
- The control system is modular and the tile can be manufactured as a stand-alone device with integrated battery, controller, actuator and sensor.
- The control system and hardware can be readily expanded to multiple tiles.
- The actuators are demonstrated to have adequate control authority suitable for application in the very high SPL environments.

The investigation is divided into an analytical and an experimental effort. The motivation for the analytical component of the work is to determine the potential sound transmission control performance of the system. A coupled structural-acoustic model based on an impedance-mobility matrix approach is formulated to represent double-panel systems consisting of a rectangular base plate connected to a single or multiple tiles through active-passive isolators and an acoustic cavity. The base plate is acoustically excited and the sound radiated power is computed using the tiles surface

velocity in the active and passive cases. The theoretical model is also used to efficiently study the effect of parameter variation on the system performance and trade-offs involved in the tile design, including the model the effect of tile flexibility on the sound transmission performance.

An extensive experimental effort was performed to evaluate the practical application of the active tiles approach in controlling sound transmitted through plates. Active tile prototypes were designed using lightweight composite panels and Thunder piezoelectric elements as integrated passive-active mounts. Two main experimental setups were used for the investigations. The first consisting of a single tile-plate double partition mounted in a window between acoustic chambers and the second consisting of a simply-supported plate and four active tiles, creating a double panel partition separated by a sealed acoustic cavity. Both feedforward and feedback controllers were designed and evaluated. Single-input single-output (SISO) feedback controllers were designed and implemented with analog electronic circuits, minimizing the cost and complexity of the overall control system. In addition, active tiles were tested using filtered-x LMS feedforward digital controller and tests were done for feedforward controllers using ideal reference and realistic (acceleration and pressure measurements) reference signals. Although the use of feedforward control would potentially increase cost and complexity, it serves as a benchmark to judge the performance of the feedback controller. The experimental system with multiple tiles was used for investigating inter-tile coupling and performance of decentralized control schemes.

Contributions of this work to the current state of the art can be summarized as follows:

- The development of a new active-passive tile approach for active control of sound transmission through partitions. The proposed approach meets the requirements of being compact, lightweight, with simple control strategy and can be applied to large structures.

- The novel implementation of active-passive tiles prototypes taking advantage of both active and passive effects provided by Thunder actuators

- The formulation of a fully coupled structural-acoustic model of plate-tile systems based on a mobility-impedance matrix approach and applied to single and multiple tile systems.

- Analytical investigation of the passive and active performance of single and multiple tile systems including different control strategies and physical parameter variations.

- Analytical and experimental investigation of inter-tile coupling mechanisms and its effect on the decentralized control system performance.

- Experimental implementation of the active-tile approach in a multiple tiles system utilizing feedback and feedforward decentralized control schemes. In addition, the implementation of feedforward control with a realistic reference signal was demonstrated.

1.4 Dissertation Outline

Following the introduction and literature review in Chapter 1, Chapter 2 presents the theoretical modeling and simulation approach used to study the sound transmission characteristics of tile-plate double panel partitions. The impedance mobility approach is introduced and initially applied to the modeling of a single tile-plate system excited by a plane acoustic wave. The passive and active sound radiation response of the system is simulated for velocity feedback and harmonic feedforward control. The analytical model is then extended to include multiple tiles and to investigate inter-tile coupling mechanisms. In addition, the analytical model is used to investigate the effect of parameter variations, such as tile stiffness, mount stiffness and damping and air gap volume, on the active and passive isolation performance of the tile. Chapter 3 presents the design and experimental tests of active tile prototypes. It includes the selection of the tile material and actuator and the construction of active tile prototypes. An investigation of the vibration isolation characteristics of a single mount tile is presented for the passive and active control cases, using both feedforward and feedback control. Then an

experimental setup consisting of a single tile/base plate system is described and results of the control of sound transmission using a feedforward controller are presented. Chapter 4 investigates a single tile base plate system with a larger base plate that was also used in a multiple tiles setup. A SISO feedback controller is designed and implemented with analog electronic circuits. Experimental results of the reduction of tile velocity and estimated sound radiated power obtained using feedforward and feedback are presented and compared. Both ideal and practical reference signals are used in the feedforward control tests. Chapter 5 covers the experimental testing of a system with multiple tiles. An experimental setup is described that is used to test the performance of four active tiles covering a simply supported plate. The performance of the multi-tile system is tested using decentralized control schemes. First, multiple independent SISO feedback controllers are designed and implemented with analog electronic circuits. The design of the analog feedback controller is detailed, including the plant estimation, controller design via loop shaping and controller implementation using operational amplifier circuits. Additional tests are performed using digital feedforward controller with both ideal and realistic reference signal implementations. Chapter 6 presents conclusions, summarizes the main contribution of this dissertation and presents suggestions for future research.

Chapter 2

2 Analytical Modeling

This work investigates the control of sound transmission through a double panel partition consisting of plate and lightweight stiff panels (tiles). Each tile is attached to the base structure through an active-passive mount used to apply a reactive force between the tile and the base structure to reduce the tile velocity. The effectiveness of the approach is based on minimization of the tile surface velocity so that the vibration of the base structure is decoupled from the associated sound field. This approach for control of sound radiation should be particularly useful in the control of sound radiation by large and low mobility structures.

Assuming that each tile behaves as a rigid body and is constrained to move perpendicularly to the base structure, there are only three possible modes of vibration, a piston mode and two rocking modes. At low frequencies the piston mode is responsible for most of the sound radiation. For the rocking modes of vibration, the tile radiation resembles that of an acoustic dipole, which is like two monopoles of same strength vibrating 180 degrees out of phase. It is known that a dipole is a very inefficient radiator at frequencies where the acoustic wavelength is much larger than the dimensions of the source. Thus, depending on the frequency range and the tile size, the contribution of the rocking modes to the sound radiation should be small and the control of the rocking modes can be neglected [48].

A reactive control force is applied between the tile and the base by active mounts for minimizing the tile normal velocity as measured by point error sensors positioned on the tile surface. The flexible behavior of the tile at high frequencies limits the effectiveness of controlling the surface velocity at a single point for reducing the tile radiation. Thus, it is important to investigate how the flexibility of the tiles limits the effectiveness of the active tile approach, which can be performed using the structural acoustic model

developed in this Chapter.

The problem of suppressing the normal velocity of the tile to attenuate the piston mode of vibration is similar to a vibration isolation problem when it is desired to isolate the tile (equipment or receiver) from the vibration of the base structure (source of vibration). An important difference is that in the active tile problem there is the additional air borne path of vibration transmission. As mentioned previously, there is great practical interest in keeping the control system as simple as possible for simplifying the practical implementation of the approach in a large structure. Independent SISO control loops implemented with simple analog electronic circuits are utilized for reducing overall complexity and cost.

Two control approaches are investigated in this Chapter: velocity feedback (skyhook damping) control and harmonic feedforward control. Direct velocity feedback using a reactive actuator between the source and receiver, also know as “skyhook damping,” is a well-known technique to implement active vibration isolation [6]. This approach is studied given its simplicity and potential to provide both good performance and stability when used to actively increase damping. Feedforward control is a possible alternative for active vibration isolation in the cases where it is possible to obtained advanced information about the disturbance that can be used as a reference signal. Harmonic feedforward control is considered in this chapter providing results that illustrate the best possible achievable performance for a feedforward control system.

In this Chapter, the velocity feedback control and harmonic feedforward control schemes are briefly reviewed, followed by a review of the sound transmission characteristics of double-leaf partitions. Then a coupled structural-acoustic model of a flexible tile on a flexible plate is formulated based on an impedance mobility matrix approach. The model is used to investigate the passive and active performance of the tile using the feedback and feedforward control approaches. Finally the model is extended to include multiple tiles. A comparison of the impedance-mobility approach to a model based on modal coupling theory is presented in Appendix D.

2.1 Control Strategies

Next, the application of feedback and feedforward control to the vibration isolation of a single degree of freedom (SDOF) mass spring system on a rigid base is reviewed.

2.1.1 Feedback Control

Feedback control is the control strategy of choice for the implementation of active vibration isolation system in the case of random disturbances, when a reference signal required for a feedforward controller is not available. One common approach for implementing feedback control for vibration isolation is placing a reactive actuator in parallel with the passive isolator producing a force proportional to the velocity of the system being isolated. The components of a vibration isolation system with velocity feedback control (skyhook damping [6]) are shown in Figure 2.1. Note that for an active tile system in the low frequency range, when the acoustic wavelength is larger than the dimensions of the physical system, the air trapped in the gap between the tile and the base structure has the effect of an additional mechanical spring in parallel with the isolator stiffness.

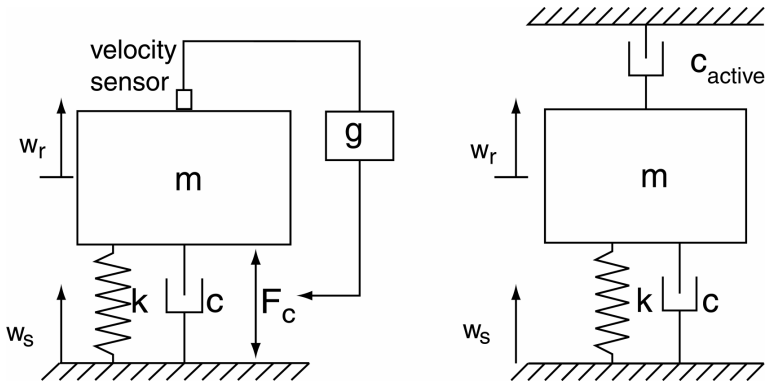

Figure 2.1: Vibration isolation of a SDOF base excited system using velocity feedback

For the system in Figure 2.1, the equation of motion of the mass to be isolated can be written as:

$$-\omega^2 m w_r(\omega) + j\omega c(w_r(\omega) - w_b(\omega)) + k(w_r(\omega) - w_b(\omega)) = F_c \qquad (2.1)$$

where wb is the base displacement and wr is the receiver (or equipment) displacement. Assuming that Fc is proportional to the velocity of the receiver mass multiplied by a gain g it is possible to write:

$$-\omega^2 m w_r(\omega) + j\omega c(w_r(\omega) - w_b(\omega)) + k(w_r(\omega) - w_b(\omega)) = g(j\omega w_r) \qquad (2.2)$$

and the displacement transmissibility becomes:

$$\frac{w_r(\omega)}{w_b(\omega)} = \frac{j\omega c + k}{\omega^2 m + j\omega(c+g) + k} \qquad (2.3)$$

This expression can be rewritten as:

$$\frac{w_r(\omega)}{w_b(\omega)} = \frac{1 + 2i\xi_p \Omega}{1 - \Omega^2 + 2i(\xi_p + \xi_a)\Omega} \qquad (2.4)$$

where, ωn is the mounted mass resonance frequency, Ω = ω/ωn is the normalized frequency, ξp is the passive damping ration, ξa is the active damping ratio and g is the feedback gain. The displacement ratio given by equation 4 is plotted in Figure 2.2 for a low-damping passive isolator (ξp = 2.5), a high-damping passive isolator (ξp = 40) and a low-damping active isolator (ξp = 2.5 and ξa = 40). This graph illustrates the disadvantage of using a purely passive isolation system: for low values of ξp there is the possibility of resonant amplification of the disturbance, whereas for higher values of ξp the transmissibility increases. In the case of active vibration isolation, higher values of ξa decreases the transmissibility at resonance without deterioration of the system isolation performance at high frequencies, as occurs in the passive isolator case.

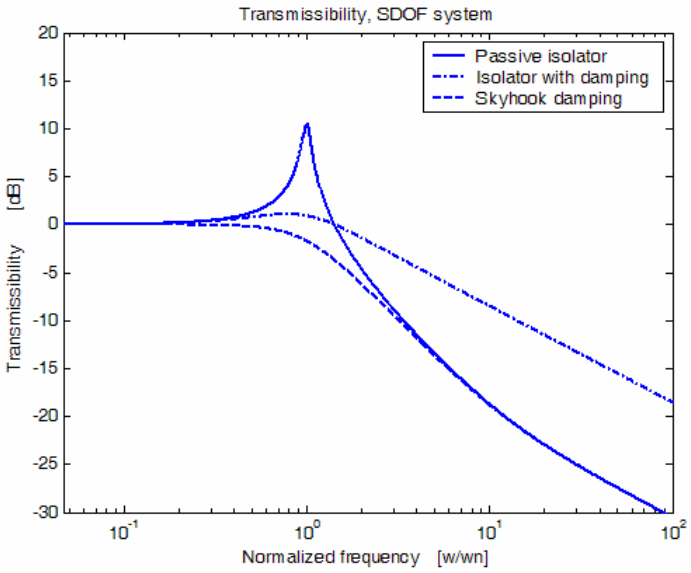

Figure 2.2: Transmissibility of base excited SDOF with passive isolator and velocity feedback.

It should also be noted that when linear quadratic Gaussian (LQG) modern control theory is applied to the vibration isolation of a base excited SDOF mass-spring system shown in Figure 2.1, with cost function given by:

$$J = E[q\dot{w}_r^2(t) + rf_s^2(t)] \tag{2.5}$$

where q is a weighting on the mean square velocity and r is a weighting on the mean square control effort, the feedback control law that minimizes J can be shown to be $f_s = -\sqrt{q/r}\,\dot{w}_r^2(t)$, which is exactly the "skyhook damping" feedback law with $g = \sqrt{q/r}$. The complete analysis, which can be found in [6], demonstrates that "skyhook damping" can be considered an optimal control strategy, since it minimizes the mean square velocity of the mass to be isolated.

2.1.2 Feedforward Control

In the feedback control approach discussed in the last section, no advanced knowledge of the primary source of random excitation of the base structure was assumed. However, in some applications it is possible to obtain such information, which allows the use of a feedforward control approach. Advanced knowledge of the primary source excitation can be obtained, for example, when the disturbance is deterministic or when the disturbance propagates through an acoustic or structural system. In this case a reference sensor is able to measure the incident disturbance, which can be used by the feedforward controller.

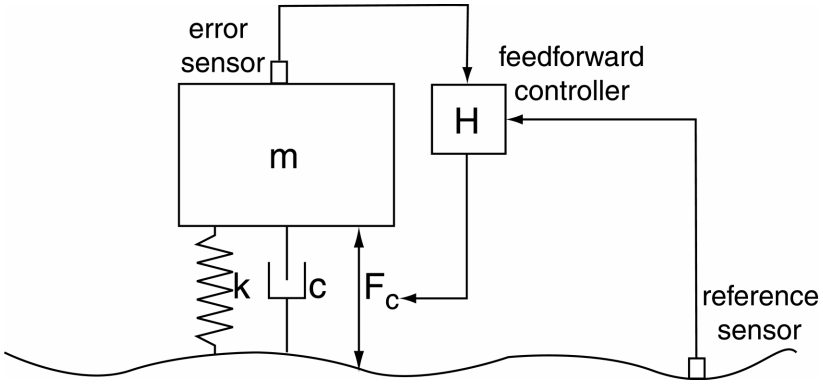

Figure 2.3: Illustration of the concept of applying feedforward control to a SDOF to provide vibration isolation.

The schematic of a feedforward control system for isolating the receiver from the base vibration is shown in Figure 2.3. A reference sensor measures in advance the disturbance input to the system, which should be well correlated with the vibration of the controlled system for successful operation of the feedforward controller. This signal is detected and processed by a digital control filter prior its use in driving the control actuators. The digital filter is computed so that the control forces minimize the mean square measure of the system response, for example the displacement, velocity or acceleration. In the case of an acoustically excited structure, an alternative arrangement would be to use a microphone to detect in advance the disturbance signal.

In the case of a harmonic disturbance and a linear system the feedforward control

problem can be solved frequency by frequency. The analysis of a feedforward control system for random disturbances is more complex, since the controller response has to be prescribed at all frequencies of interest and the constraint of causality that has to be satisfied so that the controller is realizable [6]. The study of the active tile system with feedforward control and random disturbances is investigated in the next chapter with a real-time experimental implementation of feedforward control using an adaptive filtered-x LMS algorithm.

The equivalent block diagram that describes the feedforward control system is shown in Figure 2.4 with the signals represented by the Fourier transforms of the time signals and the physical components by their frequency response [5,6]. The contribution of the primary excitation (external disturbance) to the error signal E(ω) is denoted as D(ω), the output of the controller (secondary source) is denoted as U(ω) and the estimate of the primary excitation (reference signal) used to drive the feedforward controller is denoted as X(ω).

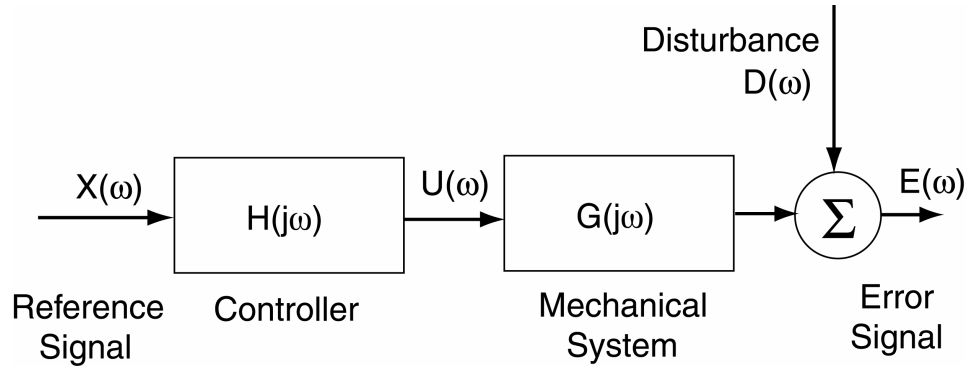

Figure 2.4 : Equivalent block diagram of a feedforward control system [5,6]

Assuming linearity, the output of the error sensor is the superposition of the contribution of the primary disturbance source D(ω), and of the secondary source U(ω), modified by the primary path (mechanical system) G(jω), so that the error signal can be written as:

$$E(\omega) = D(\omega) + G(\omega)U(\omega) \tag{2.6}$$

Assuming that the controller has frequency response H(ω), the control signal

$$U(\omega) = H(\omega)X(\omega)$$

and the total error signal can be rewritten as follows:

$$E(\omega) = D(\omega) + G(\omega)H(\omega)X(\omega) \tag{2.7}$$

The optimal control signal $U(\omega)$ is that which minimize the mean square value of the error signal defined by:

$$J(\omega) = e^2(\omega) = E^*(\omega)E(\omega) \tag{2.8}$$

This expression can be expanded as a Hermitian quadratic form [5]:

$$J(\omega) = U^H(\omega)A(\omega)U(\omega) + U^H(\omega)b(\omega) + b^H(\omega)U(\omega) + c(\omega) \tag{2.9}$$

where

$$A(\omega) = G^H(\omega)G(\omega) \tag{2.10}$$

$$b(\omega) = G^H(\omega)D(\omega) \tag{2.11}$$

$$c(\omega) = D^H(\omega)D(\omega) \tag{2.12}$$

A quadratic function like J(ω) can be shown to have a unique global minimum associated with the optimal values of control input given by:

$$U_{opt} = -A(\omega)^{-1}b(\omega) \tag{2.13}$$

This approach for computing the optimal control signals is applied to the coupled structural acoustic system discussed in the next sections.

2.2 Transmission of Sound through a Double-Panel Partition

In this section an idealized model is studied to understand the general sound transmission characteristics of a finite double-panel partition. A similar derivation for unbounded double-leaf partitions is found in [11]. As a first approximation to the problem, the model assumes non-flexible panels and a cavity width much smaller that the acoustic wavelength. The model is used to investigate how the transmission characteristics depend on the physical parameters of the system.

The double-panel model is illustrated in Figure 2.5, two panels with masses m_1 and m_2 are separated by a distance d and are assumed mounted on ideal spring-dampers, which have respectively damping and stiffness coefficients c_1, c_2, k_1, k_2. In addition, the panels are connected by a spring with mechanical stiffness k_m. The panels 1 and 2 have areas S and displacements ξ_1 and ξ_2. It is also assumed no energy dissipation and adiabatic pressure-density relationship. The primary disturbance is assumed to be a harmonic plane wave normally incident on panel 1.

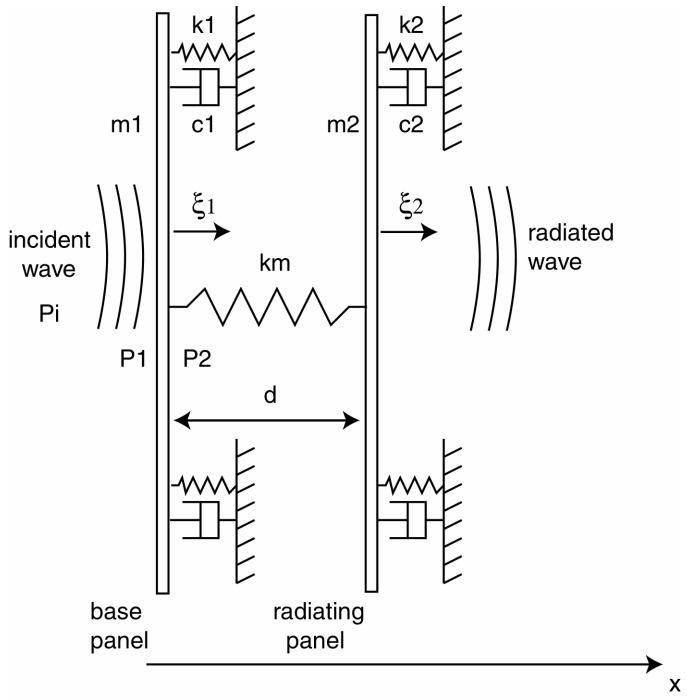

Figure 2.5: Schematic of normal incident sound transmission through a double-panel partition

The equations of motion of the panels 1 and 2 are respectively:

$$(-\omega^2 m_1 + j\omega c_1 + k_1)\xi_1 + k_m(\xi_2 - \xi_1) + P_2 S = P_1 S \tag{2.14}$$

$$(-\omega^2 m_2 + j\omega c_2 + k_2)\xi_2 + k_m(\xi_2 - \xi_1) + P_2 S = 0 \tag{2.15}$$

Assuming that the cavity width is very small compared with an acoustic wavelength, which is to assume that the cavity pressure is uniform, the pressure P2 can be shown to be given by [11]:

$$P_2 = \rho c^2 \frac{\Delta V}{V} = \rho c^2 \frac{S(\xi_2 - \xi_1)}{V} \tag{2.16}$$

The expression above indicates that the air trapped between the panels is equivalent to a spring with stiffness given by:

$$k_a = \rho c^2 \frac{S^2}{V} \tag{2.17}$$

Substituting expression (16) in expressions (14) and (15) gives:

$$(-\omega^2 m_1 + j\omega c_1 + k_1 + k_m + \rho c^2 \frac{S^2}{V})\xi_1 - (k_m + \rho c^2 \frac{S^2}{V})\xi_2 = P_1 S \tag{2.18}$$

$$(-\omega^2 m_2 + j\omega c_2 + k_2 + k_m + \rho c^2 \frac{S^2}{V})\xi_2 - (k_m + \rho c^2 \frac{S^2}{V})\xi_1 = 0 \tag{2.19}$$

If the mechanical damping and stiffness of the panels and mounts are ignored, it can be shown that the maximum transmission of sound occurs at a frequency given by:

$$f_0 = \frac{1}{2\pi}\sqrt{k_a \frac{(m_1 + m_2)}{m_1 m_2}} \tag{2.20}$$

This frequency is called mass-air-mass resonance [11] and it is inversely proportional to the panel separation d.

Below the *mass-air-mass resonance* frequency, the partition behaves as a single panel partition with mass equal to the sum of the masses of the two panels. For frequencies above the mass-air-mass resonance frequency the system behaves with panel 2 being driven through the air spring by the motion of panel 1 and the sound transmission decreases at 18dB/octave.

In the case where the double panels are mechanically coupled, it is beneficial to have a very flexible connection or soft spring. In this case the response of panel 2 in response to panel 1 movement can be modeled approximately as a base-excited mass-spring system [59]. For such a system it is well known [11] that the velocity ratio of the base (panel 1) and the receiver (panel 2) decrease proportionally to the square of the frequency above the fundamental resonance which result in a decrease of the sound power transmitted.

2.2.1 Simulation Results

The equations developed in the last section are used to compute the displacement frequency response of the base and the radiating panels for an acoustic pressure disturbance incident on the base panel. The physical parameters of the panels and air cavity used in the simulations are listed respectively in Table 1 and Table 2.

The in vacuum natural frequencies of the panels are defined as

$$\omega_1 = \sqrt{\frac{k_1}{m_1}} \quad \text{and} \quad \omega_2 = \sqrt{\frac{k_2}{m_2}} \tag{2.21}$$

Note also that the damping ratio ζ is related to the damping constant c as:

$$c = 2\zeta m \omega_n kg / s \tag{2.22}$$

Table 2.1: Dimensions and physical constants for the base panel and tile

Parameter	Base panel	Receiver panel
Dimensions	0.38 x 0.30 m	0.38 x 0.30 m
Mass	0.615 kg	0.135 kg
Natural frequency	722 rad/s	60 rad/s
Damping ratio	0.10 kg/s	0.10 kg/s

Table 2.2: Dimensions and physical constants for air filled cavity

Parameter	Value
Dimensions	0.38 x 0.30 m
Depth	0.05 m
Air density	1.21 kg/m^3
Speed of sound	344 m/s

The plot of the magnitude and phase of the displacements of the base and radiating panels is presented in Figure 2.6. Two-peaks are observed in the magnitude response corresponding to the in-phase and out-of-phase modes of vibration of the two-panel systems.

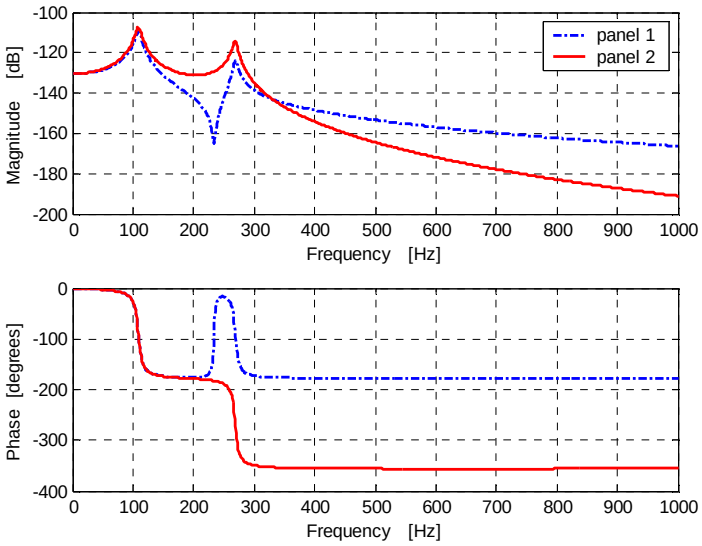

Figure 2.6: Displacement of base and radiating panels

The sound pressure radiated by the radiating panel is plotted in Figure 2.7 together with the sound pressure radiated by a single panel system with the physical characteristics of the base panel. Note that in the double panel system the resonance peak of the single panel case is shifted from around 180 Hz to 115 Hz and that second peak is created around 285 Hz, with sound radiation higher that in the single panel case. The double-panel system presents higher transmission loss than the single panel system above around 335 Hz with an 18dB/octave roll-off versus 6dB/octave roll-off for the case of the single panel system case. Figure 2.8 shows the ratio of the sound pressure transmitted by the double panel system versus the single panel system.

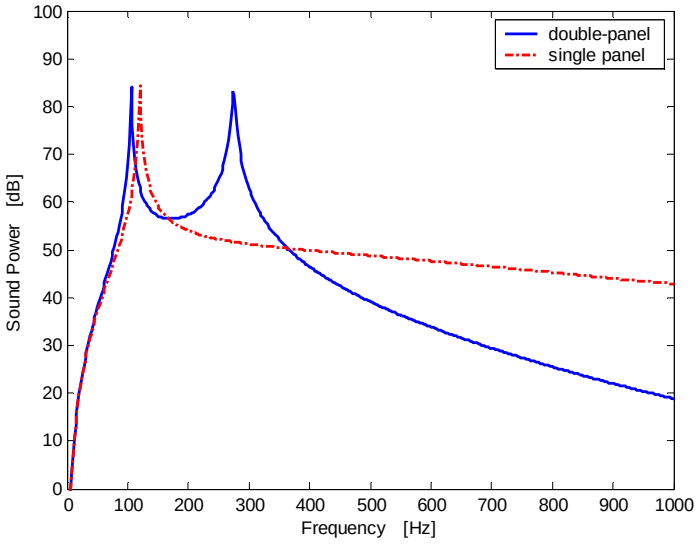

Figure 2.7: Sound power radiated by the double-panel system and for the base panel system

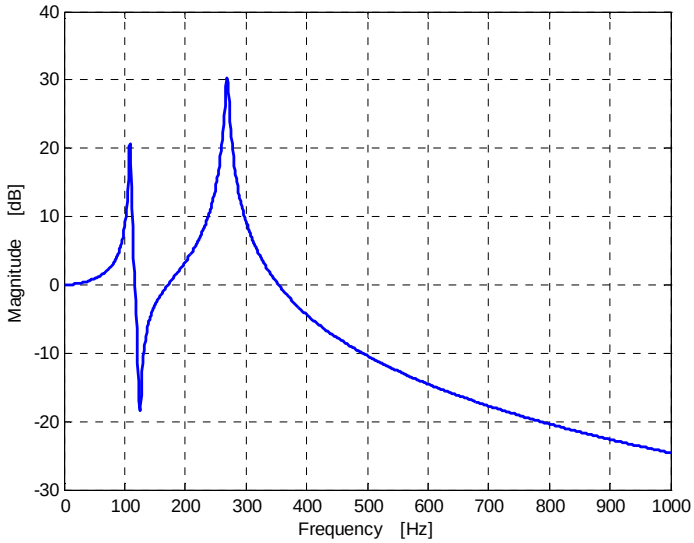

Figure 2.8: Ratio of the sound pressure radiated by the double-panel system over the single base panel system

2.2.2 Influence of Parameter Variations

The model developed last section can be used for analyzing how the sound transmission is affected by variation of system parameters. Initially, in order to investigate how the inter panel distance affects the sound transmission, the inter-panel distance is varied from 5 cm to 10 cm and 20 cm, and the ratio of sound radiated pressure of the double-panel system to the single panel system is presented in Figure 2.9. The results show that the increase in panel distance (increase in the air gap) decouples the vibration of the radiating panel from the vibration of the base panel through the air gap, which causes a shift of the 2nd resonant peak to a lower frequency and improved transmission loss.

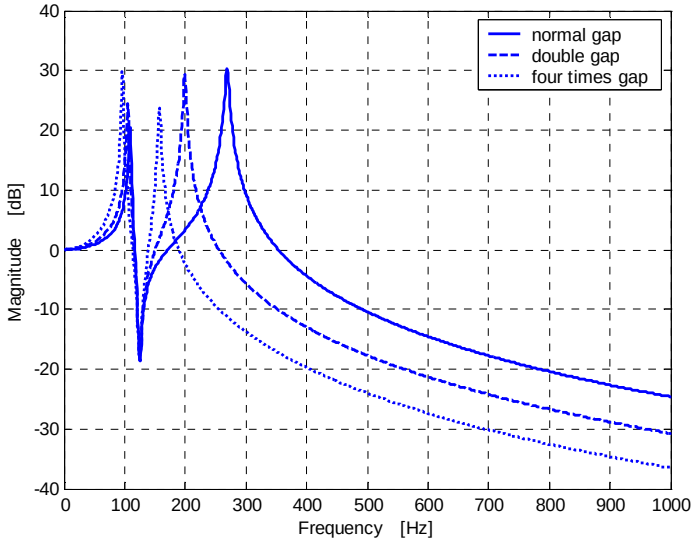

Figure 2.9: Ratio of the sound pressure radiated by the double-panel system over the single base panel system for different gap distances

The effect of adding the isolators connecting the panels on the transmission loss of two-panel system can also be investigated using the model. Figure 2.10 shows the displacement of the radiating panel for increasing values of isolator stiffness. Note that as long as the isolator stiffness is low, the coupling is controlled by the air gap stiffness. If the isolator stiffness is relatively, the second resonant peak is shifted to a higher

frequency, affecting the high frequency passive isolation.

The effect of the isolator damping on the coupling between the plates can be observed by plotting the transmissibility curve, which is the ratio of the displacement of the radiating plate over the base plate, for different isolator damping values. Note that increasing the isolator damping decreases the magnitude of the peak of the displacement transmissibility curve, but degrades the passive isolation at higher frequencies. Note also that similar effects are obtained by increasing the air gap damping.

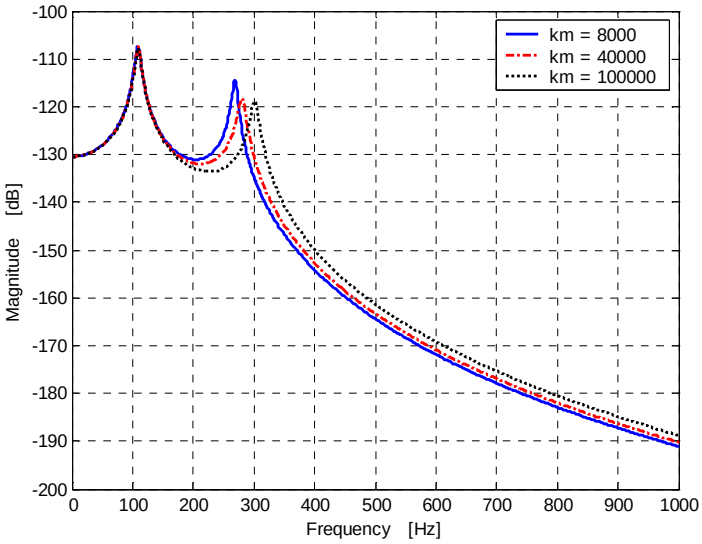

Figure 2.10: Displacement of the radiating panel for different isolator stiffness

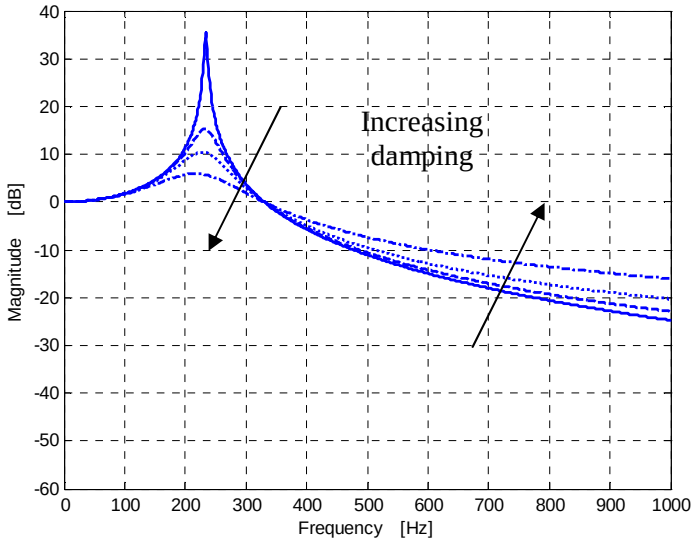

Figure 2.11: Base panel and radiating panel displacement ratio for increasing values of isolator damping

2.2.3 Velocity Feedback Control

The use of feedback control to increase the transmission loss of the double panel system is considered in this section. Actuators placed between the panels in parallel with the passive isolators apply a control force to the panels that is proportional to the negative velocity of the radiating panel. The effect of the applying negative velocity feedback is shown in Figure 2.12, which plots the displacement transmissibility for increasing values of feedback gain. Increasing the feedback control gain results in an accentuated attenuation of the transmissibility around the peak region of the transmissibility response, without degradation of the high frequency isolation characteristics, as is the case for increased values of passive damping.

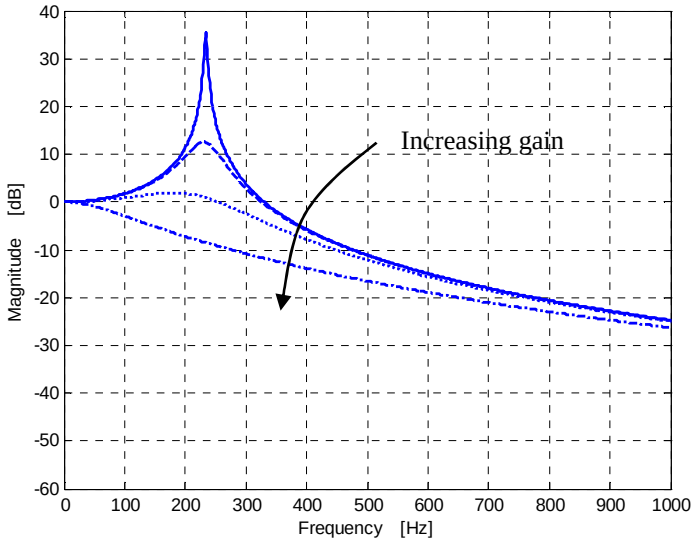

Figure 2.12: Base panel and radiating panel displacement ratio for increasing values of feedback control gain

Figure 2.13 shows the results of applying feedback control on the sound pressure radiated by the radiating panel. Note that increasing values of feedback gain result in greater attenuation of the sound radiated in the frequency range around the second peak of the magnitude response, which extends the active attenuation close to the resonance of the first peak. Figure 2.14 shows the ratio of the sound pressure transmitted by the double panel system over that of the single panel system formed by the base plate only. For high enough values of gain, the double panel system presents less sound radiation than the single panel over the entire frequency range.

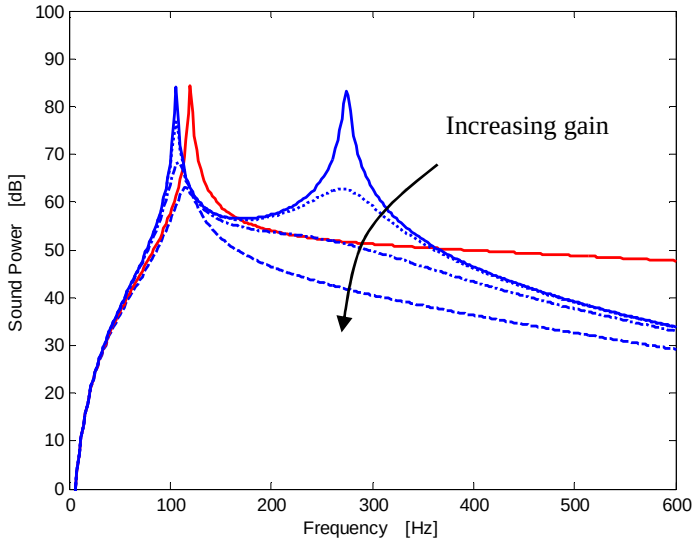

Figure 2.13 Sound pressure radiated by the double-panel system and for the base panel system for increasing values of feedback control

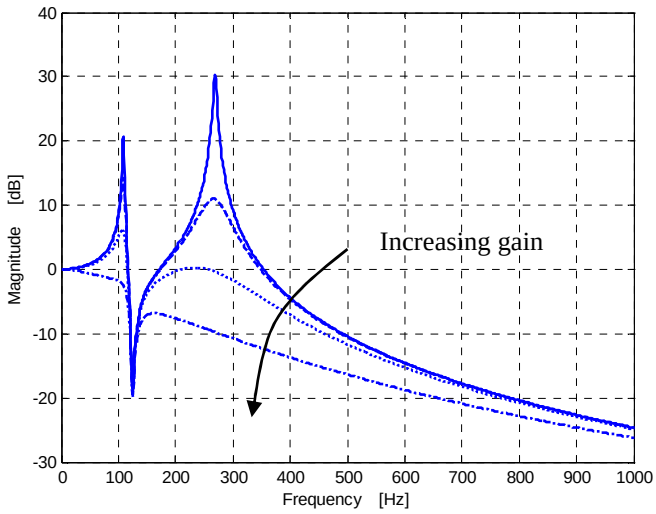

Figure 2.14 Ratio of the sound pressure radiated by the double-panel system over the single base panel system for increasing feedback control gain

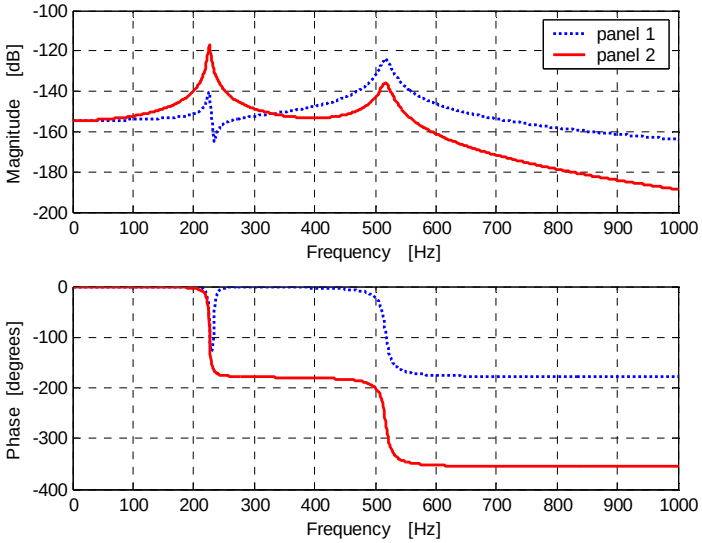

Figure 2.15 Displacement of base and radiating panels

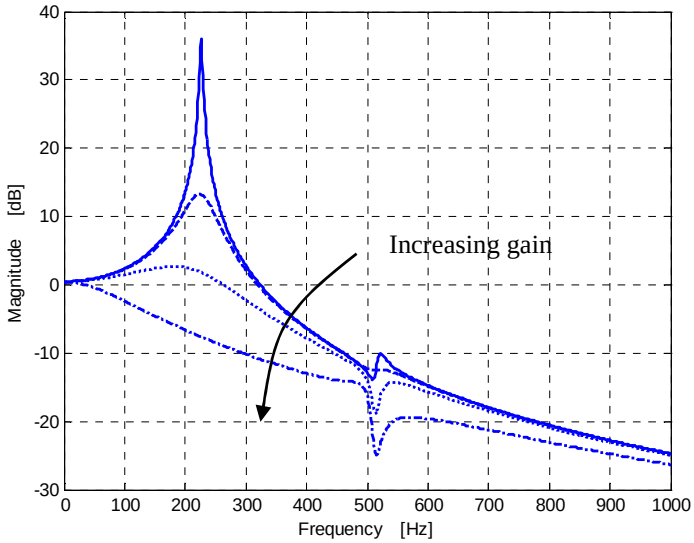

Figure 2.16 Ratio of the sound pressure radiated by the double-panel system over the single base panel system for increasing feedback control gain

2.3 Single Tile Coupled Structural Acoustic Model

This section presents an analytical model developed for investigating the attenuation performance of a double panel system with a single active tile using an impedance mobility approach. A comparison of the impedance-mobility approach to a model based on modal coupling theory is presented in Appendix D. A plate with clamped boundary conditions is assumed as the base panel and the radiating panel is a stiff tile, which is modeled as an isotropic plate with free boundary conditions, and is connected to the base plate via two spring-dampers mounts. Active forces are assumed to act in parallel with the spring-damper mounts. The model assumes a fully coupled structural acoustic system.

The system studied is shown schematically in Figure 2.17. The clamped plate is acoustically excited by an incident plane wave and the tile is assumed mounted on an infinite baffle radiating into free space. Simulation results are presented for the velocity of the tile and sound power radiated by the partition, with and without active control. In addition, simulation results using velocity feedback and optimal feedforward control, are presented.

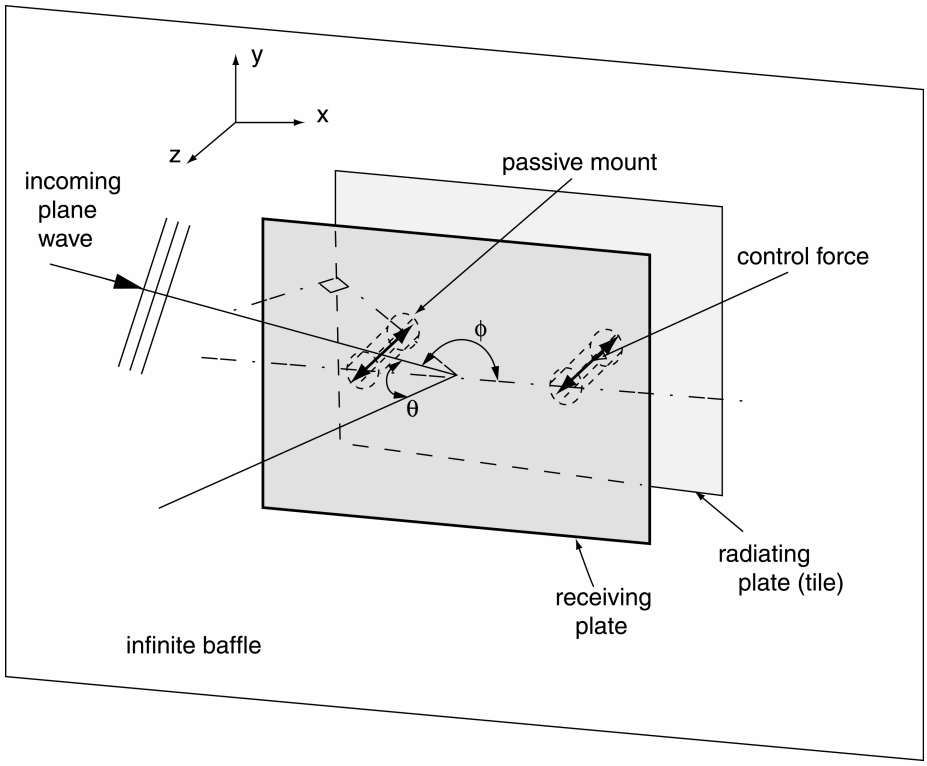

Figure 2.17: Double panel and incident acoustic wave coordinate system for the analytical model.

2.3.1 Impedance Mobility Model

In this section the development of the impedance mobility model [27] for the system shown in Figure 2.17 is presented. The impedance mobility formulation assumes that the system is divided into individual components, which are the source panel (base clamped rectangular plate), the transmitting system (airborne and structural borne transmitting paths), and the receiving panel (stiff tile). The transmitting system consists of an airborne path, which is the air confined between the base plate and the tile, and a structural borne path, which is consists of the spring-damper mounts connecting the base plate and the tile. The dynamics of each of these components is modeled using point and transfer mobilities or impedances. The general schematic of the system showing the three individual components is illustrated in the Figure 2.18.

The structural transmitting path consists of n mounts connecting the base plate and the receiving tile at a finite number of junctions. The forces and velocities transmitted at each junction are restricted in this model to the components of force and motion that are perpendicular to the surface of the system. Thus, at each element, for each frequency of excitation, the motion and forces transmitted are given by a single complex parameter that can be written as:

$$v_{mi} = \dot{u}_i \tag{2.23}$$

$$f_{mi} = F_{zi} \tag{2.24}$$

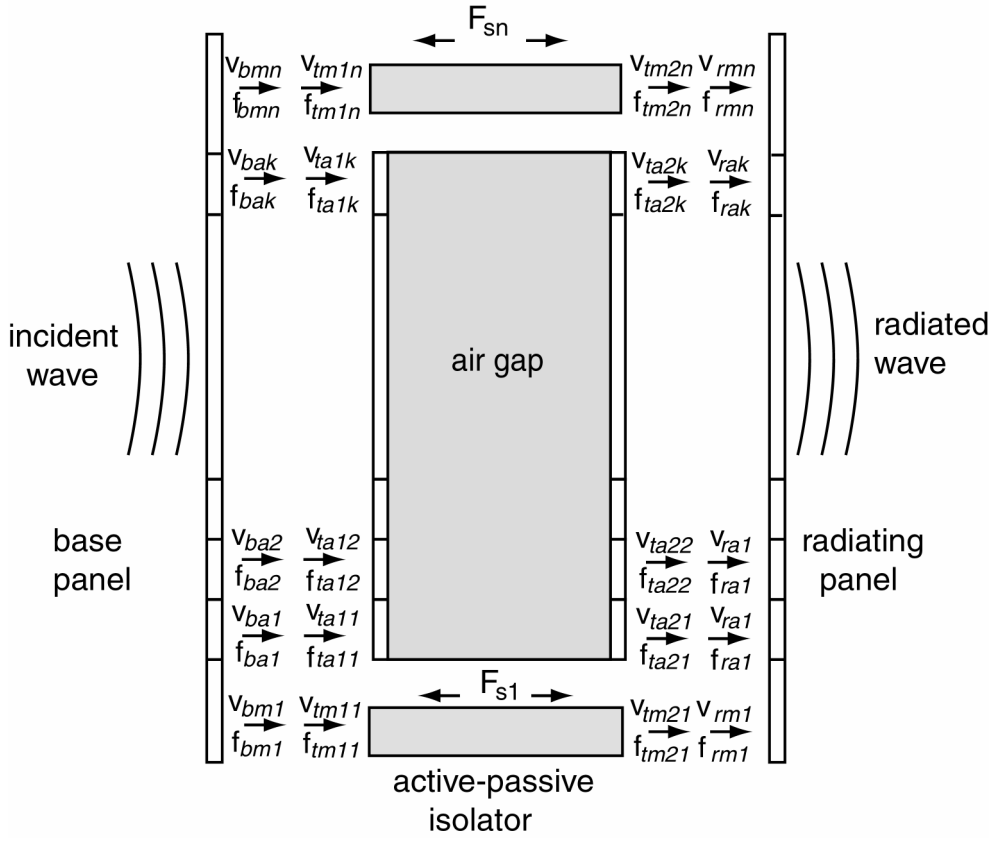

Figure 2.18: Schematic of structural-acoustic model using the impedance-mobility method

The airborne transmitting path, which is the acoustic transmission through the air confined between the base plate and the receiving tile, is taken into account by dividing the boundary surface of the cavity with the base plate and tile in k small elements much smaller than the acoustic wavelength. Each of these elements in the boundary surface is connected to either the base plate or to the receiving tile at the geometrical center of the element. In addition, each element is assumed to vibrate only in the direction perpendicular to the surface. Thus, at each element, the motion and forces transmitted are given, for each frequency, by a single complex parameter written as:

$$v_{ai} = \dot{w}_i \tag{2.25}$$

$$f_{ai} = F_{zi} \tag{2.26}$$

The velocity and force components at the isolator mounts and at the acoustic boundary elements junctions are grouped together to form three pair of vectors: the base velocity vector and the base force vector, the transmitting system velocity vector and force vector, and the receiver velocity vector and force vector. The base velocity vector and force vector are given as:

$$v_b \equiv \begin{Bmatrix} v_{bm} \\ v_{ba} \end{Bmatrix} \equiv \begin{Bmatrix} v_{bm1} \\ \vdots \\ v_{bmn} \\ v_{ba1} \\ \vdots \\ v_{bak} \end{Bmatrix} \tag{2.27}$$

$$f_b \equiv \begin{Bmatrix} f_{bm} \\ f_{ba} \end{Bmatrix} \equiv \begin{Bmatrix} f_{bm1} \\ \vdots \\ f_{bmn} \\ f_{ba1} \\ \vdots \\ f_{bak} \end{Bmatrix} \tag{2.28}$$

where v_{bmi}, f_{bmi} are the velocities and forces at the junctions between the base plate and

the j^{th} mount, and f_{bai}, v_{bai} are the velocities and forces at the junctions between the base plate and the j^{th} acoustic element.

The receiver velocity vector and force vector are given as:

$$v_r \equiv \begin{Bmatrix} v_{rm} \\ v_{ra} \end{Bmatrix} \equiv \begin{Bmatrix} v_{rm1} \\ \vdots \\ v_{rmn} \\ v_{ra1} \\ \vdots \\ v_{rak} \end{Bmatrix} \tag{2.29}$$

$$f_r \equiv \begin{Bmatrix} f_{rm} \\ f_{ra} \end{Bmatrix} \equiv \begin{Bmatrix} f_{rm1} \\ \vdots \\ f_{rmn} \\ f_{ra1} \\ \vdots \\ f_{rak} \end{Bmatrix} \tag{2.30}$$

where v_{rmi} and f_{rmi} are the velocities and forces at the junctions between the receiver plate and the j^{th} mount, and v_{rai} and f_{rai} are the velocities and forces at the junctions between the receiver plate and the j^{th} acoustic element.

Finally, the transmitting system velocity and force vectors are given as:

$$v_t \equiv \begin{Bmatrix} v_{tm1} \\ v_{ta1} \\ v_{tm2} \\ v_{ta2} \end{Bmatrix} = \begin{Bmatrix} v_{tm11} \\ \vdots \\ v_{tm1n} \\ v_{ta11} \\ \vdots \\ v_{ta1k} \\ v_{tm21} \\ \vdots \\ v_{tm2n} \\ v_{ta21} \\ \vdots \\ v_{ta1k} \end{Bmatrix} \tag{2.31}$$

where v_{tm1i} , f_{tm1i} are the velocities and forces at the junctions between the base plate and the j^{th} mount, and v_{ta1i} , f_{ta1i} are the velocities and forces at the junctions between the base plate and the j^{th} acoustic element, v_{tm2i} , f_{tm2i} are the velocities and forces at the junctions between the receiver plate and the j^{th} mount, and v_{ta2i} , f_{ta2i} are the velocities and forces at the junctions between the receiver plate and the j^{th} acoustic element.

Using a mobility matrix approach to model the dynamics of the source and receiver panels allow the velocity and force vectors to be written as:

$$v_b = M_{b1} f_b + M_{b2} q_p \tag{2.32}$$

$$v_r = M_{r1} f_r + M_{r2} q_f \tag{2.33}$$

where Mb1 and Mb2 are mobility matrices of the base panel, Mr1 is a mobility matrix of the receiver panel, qp is the primary excitation vector, and qf is a flanking excitation vector.

The transmitting system dynamics are expressed using an impedance matrix approach.

The receiver force vector can be written as:

$$f_r = Z_{t1} v_t + Z_{t2} q_s \tag{2.34}$$

where Z_{t1} and Z_{t2} are impedance matrices of the transmitting systems and q_s is the force control vector acting at the mounts.

Grouping the source equation (32) and receiver equation (33) together in one equation we get:

$$v_{br} = M_{br1} f_{br} + M_{br2} q_{pf} \tag{2.35}$$

where:

$$M_{br1} = \begin{bmatrix} M_{b1} & 0 \\ 0 & M_{r1} \end{bmatrix} \tag{2.36}$$

$$M_{br2} = \begin{bmatrix} M_{b2} & 0 \\ 0 & M_{r2} \end{bmatrix} \tag{2.37}$$

$$q_{pf} = \begin{Bmatrix} q_p \\ q_f \end{Bmatrix} \tag{2.38}$$

The junction velocity and force vectors, shown below, are called respectively source-receiver velocity vector and source-receiver force vector:

$$v_{br} = \begin{Bmatrix} v_b \\ v_r \end{Bmatrix} \tag{2.39}$$

$$f_{br} = \begin{Bmatrix} f_b \\ f_r \end{Bmatrix} \tag{2.40}$$

The source-receiver velocity vector equation (39) and the transmitting system vector must

satisfy the continuity principle at each junction:

$$v_t = v_{br} \tag{2.41}$$

while the source-receiver force vector and the transmitting system force vector must satisfy the equilibrium principle at each junction:

$$f_t = -f_{br} \tag{2.42}$$

Using the expressions for continuity of velocity and equilibrium of forces presented above, (29) and (30) can be related in such a way as to find the velocities of the source and receiver panel elements as function of the primary, flanking and control sources [27]:

$$v_{br} = Q_{pv} q_{pf} + Q_{sv} q_s \tag{2.43}$$

where

$$Q_{pv} = (I + M_{br1} Z_t)^{-1} M_{br2} \tag{2.44}$$

$$Q_{sv} = -(I + M_{br1} Z_t)^{-1} M_{br1} Z_{t2} \tag{2.45}$$

In a similar fashion, the source-receiver force vector can be written as a function of the primary and control sources as:

$$f_{br} = Q_{pf} q_{pf} + Q_{sf} q_s \tag{2.46}$$

where

$$Q_{pf} = -Z_{t1} (I + M_{br1} Z_{t1})^{-1} M_{br2} \tag{2.47}$$

To solve for the displacement of the source and receiver plates for a given configuration of force disturbances, it is necessary to have the mobility matrices describing the dynamics of the source and receiver plates, and the impedance matrices of the mounts and

acoustic cavity.

The dynamics of the source and receiver plates are described by their mobility function. The mobilities of the base and receiver plates are given by:

$$M_b(\omega) = \frac{\dot{w}}{F} i\omega \sum_{m=1}^{M}\sum_{n=1}^{N} \frac{\Phi_{m,n}(x_2, y_2)\Phi_{m,n}(x_1, y_1)}{\Lambda_m(\omega_i^2(1+i\eta) - \omega^2)} \tag{2.48}$$

$$M_r(\omega) = \frac{\dot{w}}{F} i\omega \sum_{m=1}^{M}\sum_{n=1}^{N} \frac{\Psi_{m,n}(x_2, y_2)\Psi_{m,n}(x_1, y_1)}{\Lambda_m(\omega_i^2(1+i\eta) - \omega^2)} \tag{2.49}$$

where Φ are the mode shapes of the base plate, Ψ are the mode shapes of the receiver (tile), Λ are the respective modal masses, and η are the loss factors. The mode shapes, natural frequencies and modal masses for the plate and tile are obtained using a finite element analysis software (ANSYS), because of the lack of analytical closed-form solutions for computing the modal information of plates with clamped and free boundary conditions.

The isolator mounts are assumed to be simple spring-dampers and the mount mechanical impedance can be written as:

$$Z_m = c_m + \frac{k_m}{i\omega} \tag{2.50}$$

The dynamics of the acoustic cavity is described in an impedance matrix formed by point and transfer impedances between each of the finite number of boundary interface elements at the base and receiver plates. The impedance relates the pressure at one cavity element with the normal velocity imposed at the same element (in the case of a point impedance) or at another element (in the case of a transfer impedance). These impedance functions can be derived using a modal formulation as presented in Chapter 10 of reference [5]. An expression for the pressure at any position in the cavity can be expressed as:

$$p(x,y,z) = \sum_{k=0}^{K} \frac{\omega\rho c^2 \Theta_k(x,y,z)}{V[\omega c_0 D_k + i(\omega^2 - \omega_k^2)} \int_S \Theta_k(z) u(z).\mathbf{n} dS \tag{2.51}$$

where Θ, are the acoustic mode shapes, V is the cavity volume, and D_k is a modal damping term. The damping term is defined for the compliant mode, that is, when all the modal integers are zero by:

$$\omega c_0 D_{000} = \frac{\omega\rho c_0^2}{R_a V} \tag{2.52}$$

It should be noted that at low frequencies, when the wavelength is much larger than the physical dimensions of the system and when only the compliant mode is excited, expression (41) reduces to:

$$\frac{p}{q} = \frac{\omega\rho c_0^2 / V}{\omega\rho c_0^2 / R_a V + i\omega} = \frac{R_a}{1 + i\omega C_a R_a} \tag{2.53}$$

where $C_a = V / \rho c_0^2$ is the acoustic compliance of the cavity volume and R_a is the acoustic resistance that accounts for losses and leaks in the cavity. Thus, the impedance of the cavity in its first mode can be interpreted as a parallel combination of an acoustic compliance and an acoustic resistance.

As the boundary surface is divided in elements, the normal velocity surface integral in equation (51) can be replaced by a summation. The expression for the force is obtained by dividing the expression of the pressure by *S*. Thus it is possible to arrive at the following expression for the acoustic impedance function:

$$\frac{F_k}{u_k} = \sum_{k=0}^{K} \frac{\omega\rho c^2 \Theta_k(x_1, y_1)\Theta_k(x_2, y_2)}{\Lambda_a[\omega c_0 D_k + i(\omega - \omega_k^2)]} ds^2 \tag{2.54}$$

For the case of a rectangular cavity, the mode shapes and natural frequencies can be respectively written as:

$$\Theta_k = \sqrt{e_1 e_2 e_3}(\cos k_x x \cos k_y y \cos k_z z) \tag{2.55}$$

$$\omega_k = c\sqrt{k_x^2 + k_y^2 + k_z^2} \tag{2.56}$$

where k_x , k_y and k_z are the acoustic wavenumbers and $e_i = 1$ if $k_i = 0$ and $e_i = 2$ if $k_i \neq 0$, where the subscript i, can be 1, 2, and 3.

2.3.2 Using the FEM Modal Parameters

This section explains how the "in vacuo" modes of the plates, which are exported into Matlab for performing the structural-acoustic coupled analysis, are obtained using the commercial FEM package ANSYS. After creating the system geometry, a thin shell elastic element (Shell-63) with four nodes was used to mesh the plate. After applying the appropriate boundary conditions, a modal analysis was performed using the Subspace algorithm [58].

ANSYS allows the mode shape vectors of the structure to be normalized to either unity or the mass matrix. The *reduced mass matrix* option that deletes the rotational inertia terms from the mass matrix of the Shell-63 element was chosen to extract the modal mass data. Note that it is assumed that the mode shape is given by the out of plane displacements.

In order to extract the modal mass information from the mode shape results, an expression for the relation between the mass normalized mode shape $\hat{\Phi}_k$ and the unity normalized mode shape Φ_k was used [57]:

$$\Phi_k = \frac{\hat{\Phi}}{\sqrt{\Lambda_k}} \tag{2.57}$$

Because the maximum value of $\hat{\Phi}_k$ is unity, the value of Λ_k is given by the inverse of the maximum value of Φ_k, squared, that is:

$$\Lambda_k = \frac{1}{\max(\Phi_k)} \tag{2.58}$$

The modal data was then formatted in a way proper to be imported by MATLAB, and then used to solve the coupled equations of the structural-acoustic system.

2.3.3 Plane Wave Acoustic Excitation

Assuming a plane wave incident on the base plate with angles of incidence ψ and θ (refer to Figure 2.17), the resultant force applied to the plate can be obtained by solving the following integral:

$$P_{inc} = 4\int_S \Phi_m \, p_{inc}^{-i(k_x x + k_y y)} dS \tag{2.59}$$

where k_x is the acoustic wavenumber component in the x direction and k_y is the acoustic wavenumber component in the y direction.

This integral was solved for a simply supported plate by [21]. Equation (49) can be approximated by a summation to compute the pressure excitation in the case where the modes shapes were obtained by using the finite element method (FEM).

2.3.4 Acoustic Radiated Power

The acoustic radiated power is obtained by assuming a baffled radiating plate and by discretization of the surface of the structure in small elements, each of area ΔS. Then the surface elemental velocity V can be obtained as:

$$V = \frac{\Delta S}{2} \boldsymbol{v}^H \boldsymbol{v} \tag{2.60}$$

where the superscript H denotes the Hermitian (conjugate transposed) of the vector of elemental velocities $\boldsymbol{v}$.

The sound radiated power Π can be approximated as [45]:

$$\Pi = \frac{\Delta S}{2} \sum_{j=1}^{J} \mathrm{Re}(v_j^* p_j) \tag{2.61}$$

where M is the total number of discrete elements p_j and v_j are the pressure and velocity of the element j. In vector form this becomes:

$$\Pi = \frac{\Delta S}{2} \sum_{j=1}^{J} \mathrm{Re}(\boldsymbol{v}^H \boldsymbol{p}) \tag{2.62}$$

The pressure at the surface of the structure is related to the velocities by an M by M matrix of radiation impedances $\boldsymbol{Z}$. The total radiated acoustic power can then be expressed as:

$$\Pi = \frac{\Delta S}{2} \sum_{j=1}^{J} \mathrm{Re}(\boldsymbol{v}^H \boldsymbol{Z} \boldsymbol{v}) = \frac{\Delta S}{2} \sum_{j=1}^{J} \mathrm{Re}(\boldsymbol{v}^H \boldsymbol{R} \boldsymbol{v}) \tag{2.63}$$

where $\boldsymbol{R}$ is the real part of the radiation impedance matrix. For the case of a plane baffled structure radiating into the free field, the elements of $\boldsymbol{R}$ can be calculated analytically using

$$R_{ij} = \frac{\omega^2 \rho \Delta S}{4\pi c} \left[\frac{\sin(k_a r_{ij})}{k_a r_{ij}} \right] \tag{2.64}$$

given in [45], where $k_a = \omega/c$ is the acoustic wavenumber, ω is the frequency and r_{ij} is the distance between the elements i and j.

2.3.5 Feedforward Control

The feedforward control approach is based on minimizing the quadratic that can be written as:

$$J = \mathbf{q_s^H A q_s} + \mathbf{q_s^H b} + \mathbf{b^H q_s} + \mathbf{c} \tag{2.65}$$

The quadratic function J(ω) given in equation (55) can be shown to have a unique global minimum associated with the optimal values of control input given by the equation below [5]:

$$q_{sopt} = -A^{-1}b \tag{2.66}$$

Two control strategies are investigated: 1) minimization of the normal velocity of the tile at the mount locations applying optimal control forces in parallel with the mounts; 2) minimization of the total sound power radiation of the tile applying optimal control forces in parallel with the mounts.

In the case of velocity cancellation the quadratic cost function is $J_{vel} = v_{rm}^H v_{rm}$ where v_{rm} contains only the normal velocity of the tile at the mount-tile junctions, $v_{rm} = S_{vm} v_{br}$. Matrices *A* and *b* in equation (2.66) are given in [27]:

$$A_{vel} = Q_{sv}^H S_{vm}^T S_{vm} Q_{sv} \tag{2.67}$$

$$b_{vel} = Q_{sv}^H S_{vm}^T S_{vm} Q_{pv} q_{pf} \tag{2.68}$$

In the case of total sound power radiation cancellation the quadratic cost function is $J_{sp} = v_{ra}^H v_{ra}$ where v_{ra} contains the normal velocity of all tile elements $v_{ra} = S_{ra} v_{br}$. Matrices *A* and *b* in equation (55) are given by [27]:

$$A_{sp} = Q_{sv}^H S_{ra}^T R S_{ra} Q_{sv} \tag{2.69}$$

$$b_{sp} = Q_{sv}^H S_{ra}^T R S_{ra} Q_{pv} q_{pf} \tag{2.70}$$

2.3.6 Feedback Control

In the case of negative velocity feedback control, the control force is:

$$q_s = -gv_{rm} = -gS_{vm}v_{br}$$

where g is the control gain.

Equation (2.43) can be rewritten as:

$$v_{br} = Q_{pv}q_{pf} + Q_{sv}(-gS_{vm}v_{br}) = (I + gS_{vm}Q_{sv})^{-1}Q_{pv}q_{pf}$$

2.4 Single Tile System Simulations

In this section a single tile-plate system is investigated using the impedance mobility matrices developed above.

2.4.1 System Parameters

This section presents the active attenuation performance results computed for a single active-tile mounted to a rectangular clamped plate (see Figure 2.17) using the equations presented above. Initially, the analytical model is used to investigate the contribution of the structure-borne and air-borne transmission paths to the total sound power radiated by the tile. Next, the sound transmission attenuation performance of the tile using feedback and feedforward control approaches was investigated.

The length and width of the tile and the base plate are respectively $Lx = 0.30m$ and $Ly = 0.38m$. The tile and plate are separated by an air gap with height $Lz = 0.05m$. The spring-damper passive isolator is assumed to have a mechanical stiffness $k = 4000N/m$ and loss factor $c = 2.5Ns/m$. The mounts are attached to the plate and tile at the coordinates

{*Lx/4,Ly/2*} and {*3/4Lx, Ly/2*}. Note that the physical parameters utilized in the model are chosen to correspond with the physical values of the experimental system investigated in Chapter 3. The geometry and physical constants for the cavity and panels are presented respectively in Table 2.3 while Table 2.4 summarizes the natural frequencies of the base plate and tile. The first four flexible vibration modes of the tile with free boundary conditions as computed using FEA are shown in Figure 2.19. The geometry and physical constants of the air cavity are summarized in Table 2.5 while the first four natural frequencies are listed in Table 2.6.

Table 2.3: Dimensions and Physical constants for the base panel and tile

Parameter	Base plate	Tile
Dimensions	0.38 x 0.30 m	0.38 x 0.30 m
Thickness	0.0015 m	0.006m
Young's Modulus	64e9 N/m2	N/m2
Density	2700 kg/m3	20 kg/m3
Poison's ratio	0.33	0.33
Loss factor	0.01	0.01

Table 2.4: Resonance frequencies of the base panel and tile

Base Plate			Receiver Plate (Tile)	
m	n	f_r Hz	m	f_r Hz
1	1	113	1	130
2	1	198	2	330
1	2	258	3	426
2	2	334	4	487
3	1	336	5	570
3	2	461	6	758
1	3	478		
4	1	522		
2	3	547		
4	2	637		

Table 2.5: Dimensions and physical constants for air filled cavity

Parameter	Value
Dimensions	0.38 x 0.30 m
Depth	0.05 m
Air density	1.21 kg/m^3
Speed of sound	344 m/s

Table 2.6: Resonance frequencies of the air gap between the two panels

m	n	p	f_r Hz
0	0	0	0
1	0	0	452
0	1	0	573
1	1	0	730

The performance of the system was measured by comparing the total sound power radiated without control and with control. Three control strategies were considered: (1) negative velocity feedback control, (2) minimization of the tile velocity at the mounts positions using harmonic feedforward control, and (3) minimization of the total radiated power using harmonic feedforward control. The last subsection shows results illustrating the influence of the tile stiffness on the active performance of the system.

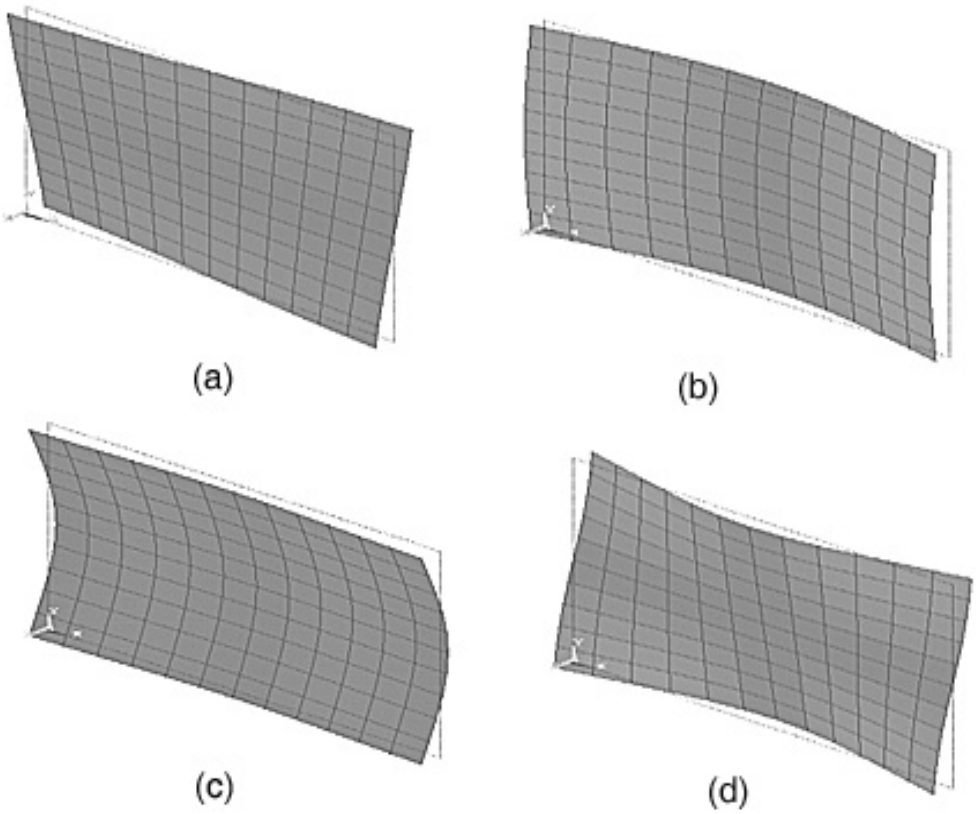

Figure 2.19: First four flexible vibration modes of tile

2.4.2 Model Validation of Sound Radiated Power

In Figure 2.20 the sound power radiated by the radiating panel using the double-panel system equations just discussed in Section 2.2 is compared to the sound power calculated using the impedance-mobility model discussed in Section 2.3, where it is observed the good agreement between the results for the low frequency range. The influence of the flexible modes of the panels and cavity predicted with the impedance mobility model, are observed above 300 Hz.

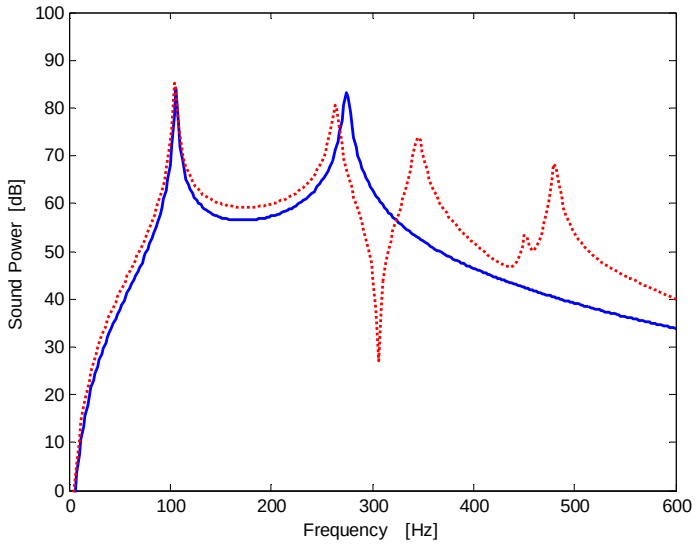

Figure 2.20 Sound power radiated by the radiating panel using the double-panel system equations (solid trace) compared to the sound power calculated using the impedance-mobility model (dashed trace)

Using the equations presented in the previous section programmed in MATLAB, the total sound power radiated by the clamped plate excited by a 45 degrees incident plane wave was computed. The sound radiated power computed using the model is compared to the experimental results measured for single tile-plate system (see Section 3.4, Figure 3.25), as presented in Figure 2.21. Comparing the two plots it is possible to observe the good general agreement between the model and the measured results for the sound radiated

power. Note that the peaked response of the measured sound radiated curves is due to the reverberant nature of the measurement room where the measurements were taken.

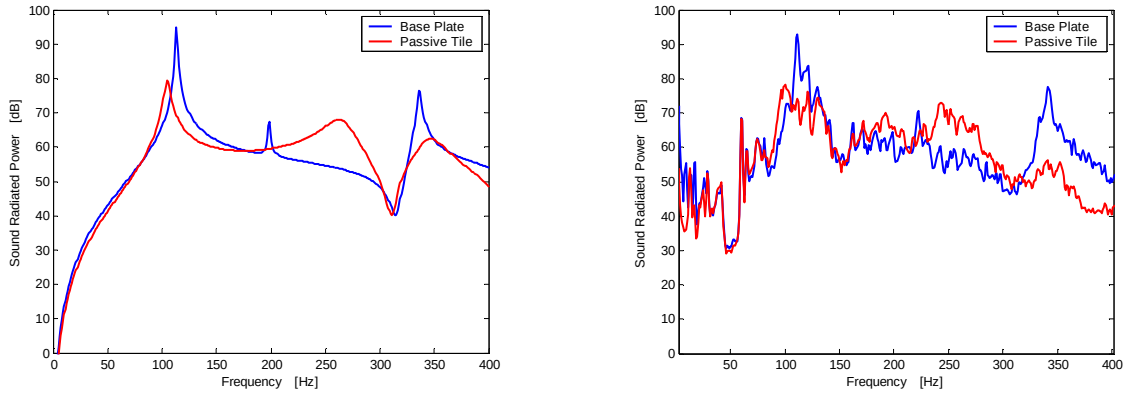

Figure 2.21: Simulated (left plot) and measured (right plot) sound radiated power for base plate and plate with passive tile

2.4.3 Tile-Plate Partition Passive Attenuation Performance

The effect of mounting the tile on the clamped plate on the passive transmission loss of the partition is investigated next. The sound power radiated by the passive tile is compared to the sound power radiated by the clamped base plate only, before adding the tile, which gives the passive attenuation performance of the tile-plate partition.

Figure 2.22 presents the sound radiated power computed using the model for the single plate partition and for the plate-passive tile partition. In the low frequencies, the double panel system with the passive tile has poor attenuation performance due to the strong coupling to the base vibration through the air cavity. Note the increase in the transmitted power between 250 and 300 Hz caused by the second rigid body resonance of the tile-plate system. At frequencies above about 250 Hz, passive isolation effects occur and the sound radiated by the tile is less than the sound radiated by the plate. This behavior agrees with the low-frequency model of the double panel partition, shown in Figure 2.7.

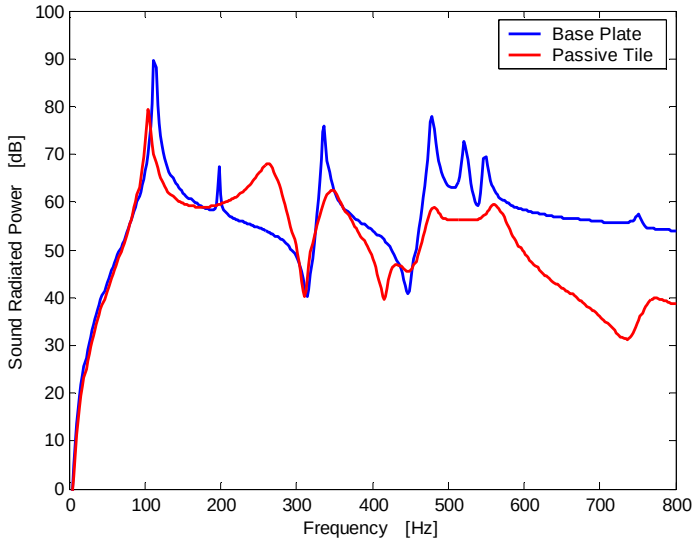

Figure 2.22: Total sound power radiated by a clamped plate (blue line) and by clamped plate covered with a single passive tile (red line), when base plate is excited by a plane acoustic wave.

2.4.4 Structure-borne and Air-borne Transmission Paths

The impedance-mobility model of the system is used for investigating the individual contributions of the structural-borne and air-borne paths to the total sound radiated power by the tile. By structural-borne path it is meant only the vibration transmitted from the base plate to the tile through the passive mounts. By air-borne path, it is meant the vibration transmission from the base plate to the tile due to the coupling caused by air confined between the plate and the tile. As mentioned earlier, the air confined in the cavity between the base plate and the tile acts at low frequencies as a stiffness in parallel with a resistance. The value of the acoustic compliance depends on the volume of the air cavity, while the damping depends on air leaks and the total absorption due to damping of the walls of the cavity. Figure 2.23 shows the total sound radiated power for structural borne path, acoustic borne paths and both structural and acoustic borne paths. For the case of acoustic borne path, two different air cavity sizes are considered, with the tile and plate separated by *0.05m* and *0.10m*, giving cavity volumes of *57e-4* m^3 and *114e-4* m^3

respectively. Note that when the volume of the air gap is increased by a factor of two, the second resonance of the double plate system shifts down to about 190 Hz and passive vibration isolation is obtained above this frequency.

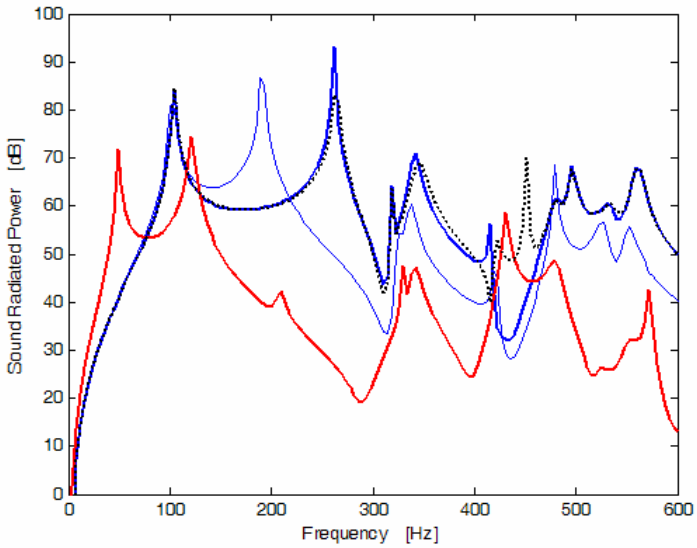

Figure 2.23: Total sound power radiated by the tile when the base plate is excited with an acoustic plane wave. (a) black dashed trace: double panel coupled by air-borne and structure-borne paths. (b) blue thick trace: double panel coupled only by air-borne path. (c) blue thin trace: double panel coupled only by air-borne path and double size gap (d) red trace: double panel coupled only by structure-borne path.

Note that for the system studied the air-borne path is responsible for most of the vibration transmission from the base plate to the tile, as the sound radiated by the tile with air-borne path only is very similar to the sound radiated power with both structural and air-borne paths. When the vibration is transmitted only through the mounts, which is the structural-borne path only, we observe high passive isolation at the high frequencies with low sound transmission. As expected, increasing the air gap volume helps improving the high frequency passive isolation by decreasing the stiffness of the air gap.

2.4.5 Feedback Control Plant Model Validation

The control plant frequency response is given by the absolute velocity at the error sensor v_e location divided by the force acting to the tile f_a, which can be written in the frequency domain as:

$$G_{vel}(j\omega) = \frac{v_e(j\omega)}{f_a(j\omega)}$$

This transfer function is obtained by solving equation (34) repeated below with q_{pf} equal to zero:

$$v_{br} = Q_{sv} q_s$$

The control sources q_s vector set to $q_s = \begin{bmatrix} 1 \\ 0 \end{bmatrix}$ for the left actuator and $q_s = \begin{bmatrix} 0 \\ 1 \end{bmatrix}$ for the plant response of the second actuator.

The transfer functions between the output at the collocated and non-collocated sensors for an input at the actuator located at {Lx/4,Ly/2} are shown in the left plot of Figure 2.24. The right plot in Figure 2.24 shows corresponding measured plant response. The mode near 30 Hz corresponds to the pitch mode of vibration of the tile. Note that good agreement is observed between the simulated and measured plant responses except for frequencies below about 50 Hz where the measured plant response presents additional dynamics possibly caused asymmetries in the experimental setup (for example difference in actuator stiffness), which does not occur in the model.

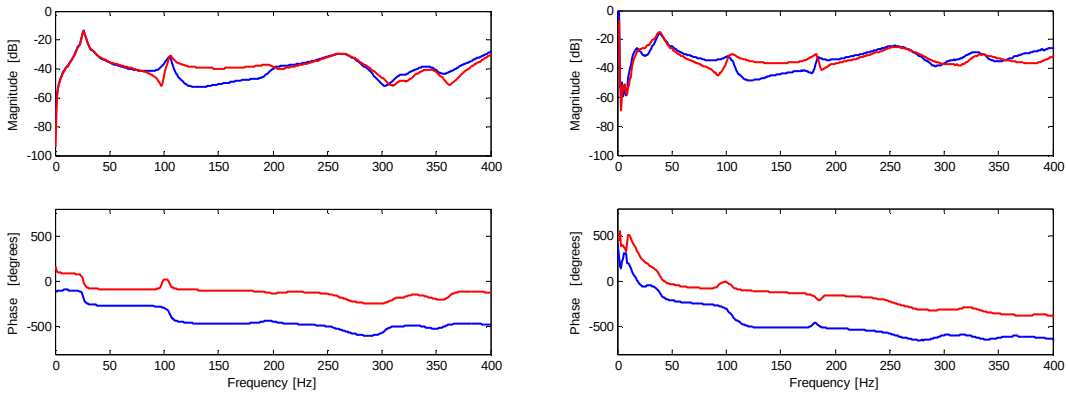

Figure 2.24: Simulated (left plot) and measured (right plot) plant response for input on left mount. Blue trace is plant collocated response and red trace is response for non-collocated sensor.

2.4.6 Velocity Feedback Control Results

In this section the computed results for velocity feedback control applied to the single tile system are presented. Velocity feedback has been successfully applied to vibration isolation of equipment from broadband random base excitation [76]. Ideally, the control force, which is proportional to the absolute receiver velocity, reacts of an inertial ground. In this case, the actuator control force and the measured velocity are collocated and the system is unconditionally stable.

In practice, as an inertial ground is not available, the control force reacts off the base structure, with the control force appearing in parallel with the passive mount. In the case of a flexible base structure, although one end of the actuator is collocated with the sensor, the system is not collocated due to the additional non-collocated reactive force acting on the base structure and which could have dynamics strongly coupled with the mounted receiver. In other words, the reactive force changes the velocity of the base structure, which is also part of the plant being controlled, and that in turn affects the velocity of the receiver. Even in the case of a flexible base, the system was shown to be unconditionally stable for the case of a rigid receiver and mass-less mount [66].

In [74] the vibration isolation between a flexible receiver structure and a either rigid or flexible base structure is investigated. The system employed four reactive actuators and decentralized velocity feedback control and was found to be robustly stable and presenting good performance.

The Nyquist plot of the active tile control plant shown in Figure 2.25 shows a loop on the left hand side of the imaginary axis indicating that the feedback control system is conditionally stable, which means that the system can be unstable for certain values of feedback gain.

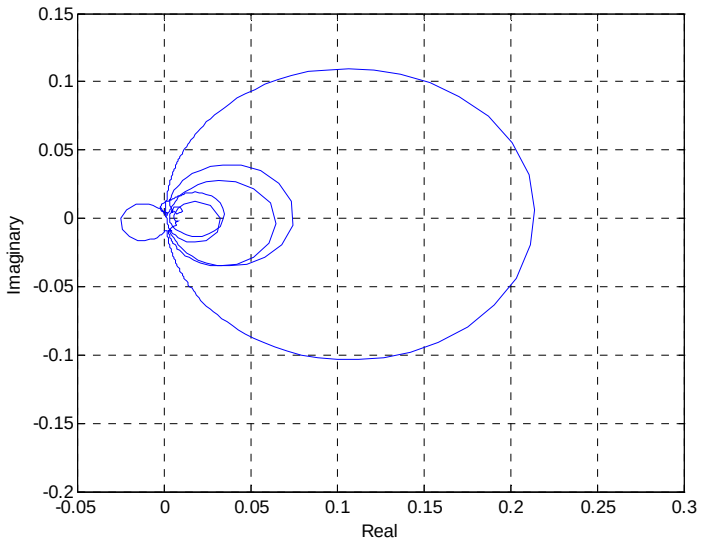

Figure 2.25: Simulated Nyquist plot for the plant response of the single tile-plate system

The tile velocity in the passive and active cases for different feedback gains is shown in Figure 2.26. Good attenuation of the tile mass-spring resonance close to 250 Hz is obtained with some attenuation at the resonance around 120 Hz. In addition some enhancement (spillover) of the tile velocity occurs at higher frequencies, which is followed by the increase in gain values indicating that the feedback system approaches an instability condition.

The sound power radiated by the tile for the passive case and active case with different

feedback gains is presented in Figure 2.27. Observe the good correspondence between the attenuation of the tile velocity and the attenuation of the sound radiated power for the frequency range below about 300 Hz, corresponding to the frequency range below the second flexible vibration mode of the tile. At frequencies when the tile behaves as a flexible structure, attenuation of the tile velocity at the error location does not necessarily correspond to attenuations of sound radiation, as can be observed above 350Hz.

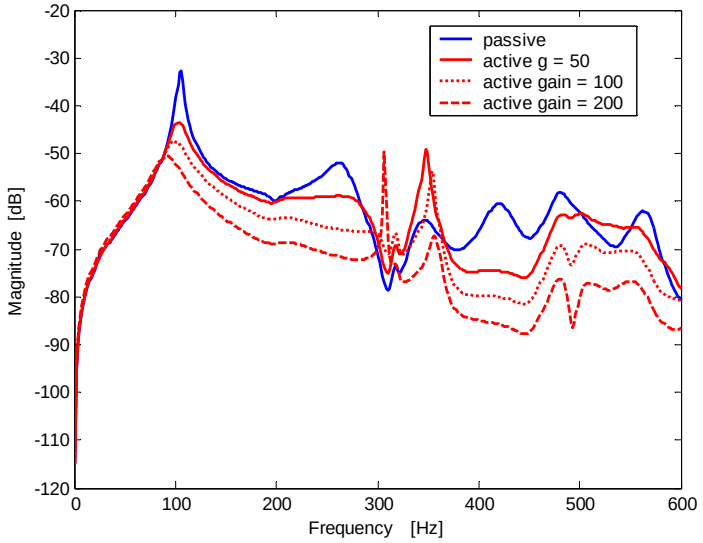

Figure 2.26: Magnitude of the tile velocity at the error sensor for the passive case (blue trace) and active case with different feedback gains (red traces)

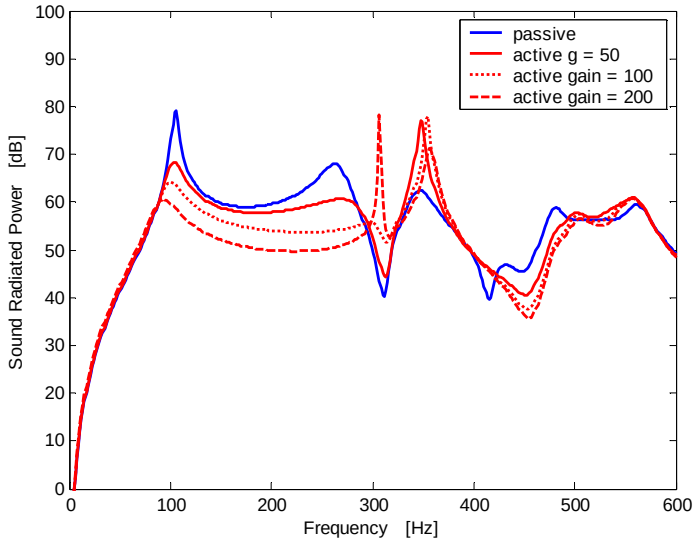

Figure 2.27: Sound power radiated by the tile for the passive case (blue trace) and active case with different feedback gains (red traces)

2.4.7 Feedforward Control

This section presents the active attenuation results computed for the velocity of the tile and sound radiated power using feedforward control. Two control strategies are investigated, as described earlier: 1) minimization of the normal velocity of the tile at the mount locations applying optimal control forces in parallel with the mounts; 2) minimization of the total sound power radiation of the tile applying optimal control forces in parallel with the mounts.

The results obtained for the velocity of the tile at one of the error sensors without control and with different control strategies applied are presented Figure 2.28. The plot shows resultant tile velocity for the cases: a) feedforward control for minimizing the tile velocity at the error sensor, b) velocity feedback control and c) feedforward control with minimization of sound radiated power. Note that in case a) the velocity results with harmonic feedforward control are not visible in the plot because of the limited range of the plot magnitude axis.

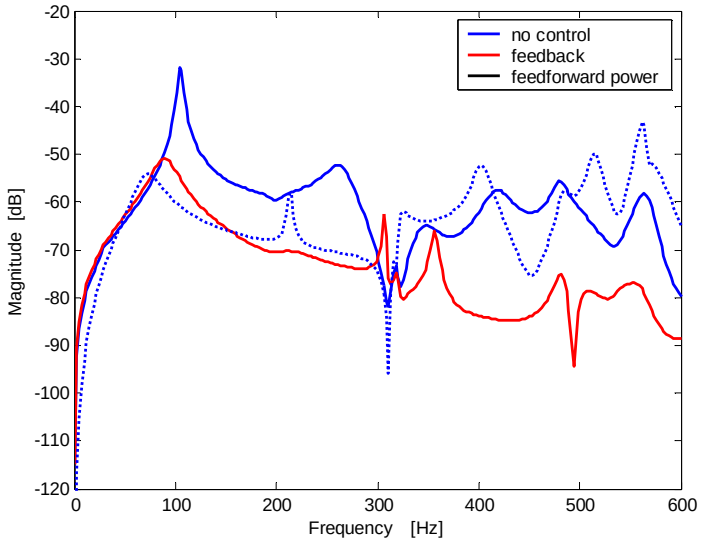

Figure 2.28: Velocity of the tile at one of the mount positions. (a) blue solid trace: no control (b) red solid trace: velocity feedback control. (c) blue dashed trace: feedforward control and minimization of the radiated acoustic power.

The application of active control for minimization of the sound power radiated by the tile assumes the presence of sensors capable of measuring the radiated power as for example, microphones in the far-field or distributed vibration sensors that measure the radiation modes of the structure. The use of error sensors capable of measuring the sound power it is possible to extend the bandwidth of control to higher frequencies than the range obtained by controlling the tile velocity. The resulting sound radiated power obtained when applying the various control strategies is shown in Figure 2.29.

Note that although the application of feedforward control results in large cancellation of the tile velocity at the error sensor location as shown in Figure 2.28, this does not result in a corresponding level of attenuation of the sound radiated power as shown in Figure 2.29. This result indicates that while the velocity of the tile is effectively reduced at the error sensor location there is still a ‘residual’ tile vibration away from the sensor location. The attenuation of the radiated power should be more effective if a stiffer tile is used as shown below. Note also in Figure 2.29 that the application of feedforward control for direct minimization of the sound radiated power results in a bandwidth of effective

control extended to above 500 Hz.

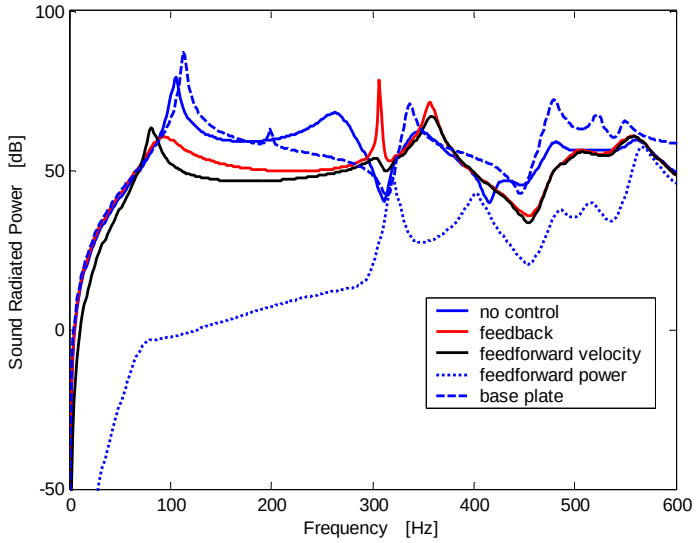

Figure 2.29: Total sound power radiated by tile when the base plate is excited by an acoustic plane wave for the baseline plate and for the tile, passive and active with different control strategies.

In addition, note that the application of feedforward control for minimization of the total sound radiated power in an enhancement of the velocity of the tile compared to the case without control for frequencies above 300 Hz. This amplification of the tile velocity at higher frequencies can be explained by the flexible behavior of the tile with vibration modes that are efficient radiators. The feedforward controller generates a secondary force that results in a reduction in the total radiated power by the modal rearrangement mechanism (Figure 2.29), extending the bandwidth of control above that obtained using velocity cancellation approach.

2.4.8 Active Control Results Using a Stiffer Tile

In this section the model of the tile-plate system is used to investigate the effect of an increase in the tile stiffness on the control bandwidth and performance of the active-tile system. Simulations are performed for a tile with increased stiffness and resonance

frequencies twice the value of those presented in Table 2.4. This increase in stiffness can be realized in practice with little weight increase by using a honeycomb type composite panel with thicker core material layer.

Shown respectively in Figure 2.30 and Figure 2.31 are the plots for the tile velocity and the total sound radiated power for a stiffer tile, in the passive and active configurations using feedforward control. Comparing to the plots shown in Figure 2.28 and Figure 2.29 for the less stiff tile, it can be noted that the system performance is improved. In addition the control frequency bandwidth where attenuation of the total radiated power occurs extends up to 500 Hz. It also can be noted that in the case of the stiffer tile, the use of feedforward control to minimize the total radiated power results in a reduction of the tile velocity throughout the frequency band up to 700 Hz. The direct correspondence between reduction of the tile velocity and the reduction in total sound radiated power demonstrates the importance of the tile stiffness in defining the frequency band where the active-tile has good control performance.

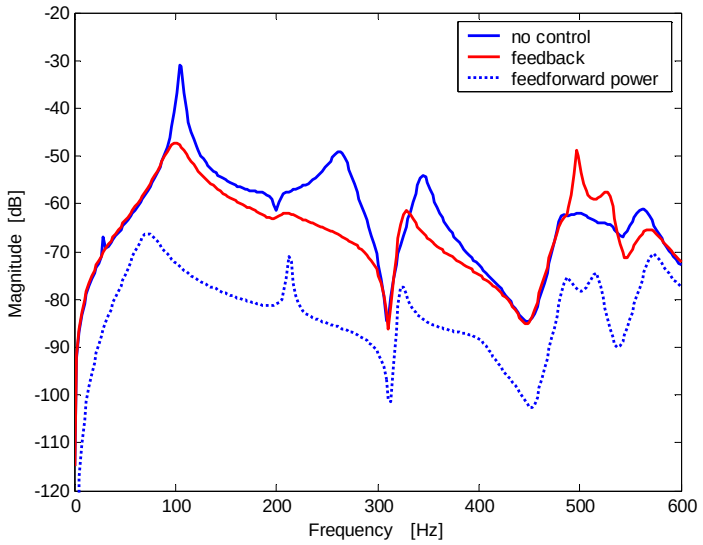

Figure 2.30: Velocity of a stiffer tile at error sensor (mount position). (a) blue solid trace: no control (b) red solid trace: velocity feedback control. (c) blue dashed trace: feedforward control and minimization of the radiated acoustic power.

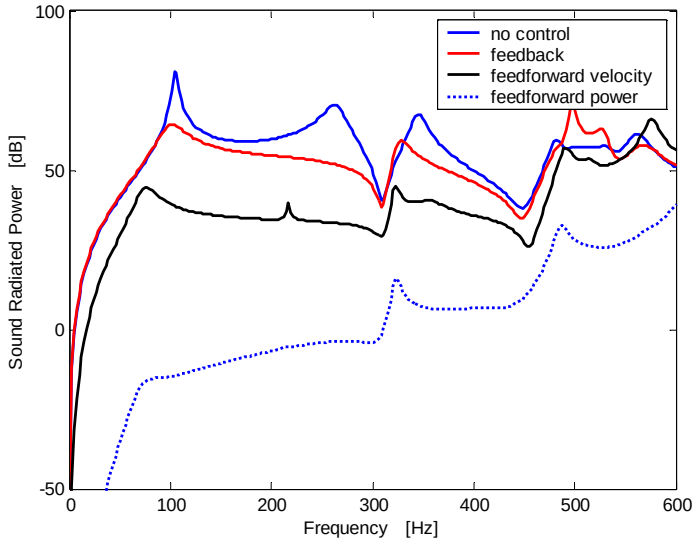

Figure 2.31: Total sound power radiated by a stiffer tile when the base plate is excited by a acoustic plane wave. (a) blue solid trace: no control (b) red solid trace: velocity feedback control. (c) black solid trace: feedforward control and minimization of the tile velocity. (d) blue dotted trace: feedforward control and minimization of the radiated acoustic power.

2.5 Multiple Tiles System

In this section, the impedance mobility model discussed above and applied to a single tile-plate system is extended to a system comprising four tiles on a simply supported plate. Initially, the model details are outlined followed by a description of the system physical parameters. Then both velocity feedback and harmonic control are applied to the system to reduce the sound radiated by the tiles.

2.5.1 System model

The multi-tile system is modeled using the same mobility matrix approach detailed earlier. The receiver velocity vector and force vector are written as equations (20) and

(21) repeated below:

$$v_r \equiv \begin{Bmatrix} v_{rm} \\ v_{ra} \end{Bmatrix} \equiv \begin{Bmatrix} v_{rm1} \\ \vdots \\ v_{rmn} \\ v_{ra1} \\ \vdots \\ v_{rak} \end{Bmatrix} \tag{2.71}$$

$$f_r \equiv \begin{Bmatrix} f_{rm} \\ f_{ra} \end{Bmatrix} \equiv \begin{Bmatrix} f_{rm1} \\ \vdots \\ f_{rmn} \\ f_{ra1} \\ \vdots \\ f_{rak} \end{Bmatrix} \tag{2.72}$$

where v_{rmi} and f_{rmi} are the velocities and forces at the junctions between the receiver plate and the j^{th} mount, and v_{rai} and f_{rai} are the velocities and forces at the junctions between the receiver plate and the j^{th} acoustic element.

The dynamics of the source and receiver panels allow the velocity and force vectors to be written as given in equations (23) and (24) repeated below:

$$v_b = M_{b1} f_b + M_{b2} q_p \tag{2.73}$$

$$v_r = M_{r1} f_r + M_{r2} q_f \tag{2.74}$$

where M_{b1} and M_{b2} are mobility matrices of the base panel, M_{r1} is a mobility matrix of the receiver panel, q_p is the primary excitation vector, and q_f is a flanking excitation vector.

For the single tile system, with the tile divided in N elements, the vectors the vectors v_r and f_r containing respectively the receiver panel velocities and forces have size (N x 1). The matrix M_{r1} containing the tile mobilities has size (N x N) and is fully populated.

In the case of the multiple tile system with *M* tiles, the vectors v_r and f_r have size *(1 x (M*N))*, where * denotes multiplication, and contain elements belonging to different tiles. The matrix M_{r1} for the multiple tile system has size *((M*N) x (M*N))* and is a block matrix constructed using smaller block matrices of the original single mobility matrix.

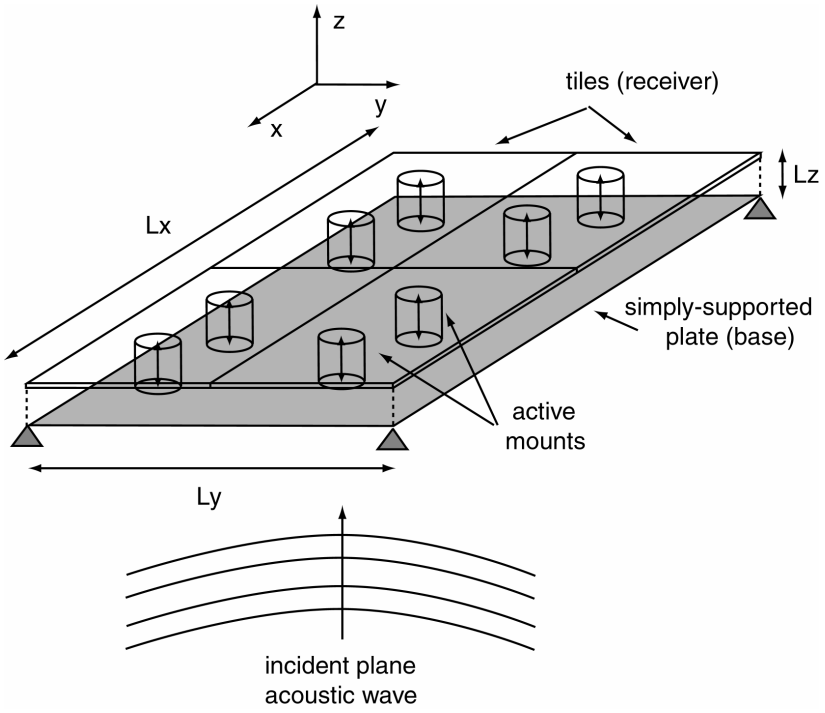

Figure 2.32: Schematic of multi-tile system modeled using the impedance-mobility method

2.5.2 System Parameters

In this section a multiple active-tile system consisting of four tiles mounted on a rectangular aluminum simply supported plate, as depicted in Figure 2.32 , is investigated. The length and width of each tile are respectively Lx_tile = 0.30 m and Ly_tile = 0.38 m and length and width of the base plate are respectively Lx = 0.60 m and Ly = 0.76 m. The tiles and base plate are separated by an air gap with height Lz = 0.05m. The spring-damper passive isolator is assumed to have a mechanical stiffness k = 4000N/m and loss factor c = 2.5 Ns/m. The mounts are attached to the plate and tile at the coordinates

{Lx/4,Ly/2} and {3/4Lx, Ly/2}. The geometry and physical constants for the cavity and panels are listed in Table 2.7, while Table 2.8 summarizes the natural frequencies of the base plate and tile. The geometry and physical constants for the cavity is summarized in Table .2.9 and the first its four natural frequencies are listed in Table 2.10.

Table 2.7: Dimensions and Physical constants for the base panel and tile

Parameter	Base plate	Tile
Dimensions	0.76 x 0.60 m	0.38 x 0.30 m
Thickness	0.00635 m	0.01 m
Young's Modulus	64e9 N/m2	35e10N/m2
Density	2700 kg/m3	1700 kg/m3
Poison's ratio	0.33	0.33
Loss factor	0.01	0.01

Table 2.8: Resonance frequencies of the base panel and tile

Base panel			Tile panel	
m	n	f_r Hz	m	f_r Hz
1	1	66	1	261
2	1	144	2	660
1	2	190	3	852
2	2	272	4	974
3	1	267	5	1141
3	2	396	6	1516
1	3	397		
4	1	452		
2	3	576		
4	2	602		

Table 2.9: Dimensions and physical constants for air filled cavity

Parameter	Value
Dimensions	0.76 x 0.60 m
Depth	0.05 m
Air density	1.21 kg/m^3
Speed of sound	344 m/s

Table 2.10: Resonance frequencies of the air gap between the two panels

m	n	p	f_r Hz
0	0	0	0
1	0	0	226
0	1	0	286
1	1	0	365
2	0	0	452
2	1	0	535
0	2	0	573
1	2	0	616

2.5.3 Passive Vibration Isolation Results

As discussed earlier, the tile vibration is coupled to the base vibration through the air cavity and the passive tile system presents poor low-frequency vibration isolation characteristics. Plotting together the velocity of the base plate and the velocity of the tile one can evaluate the passive vibration isolation of the tiles in the multiple tile system. The velocity of the base plate and the velocity of the tile at the mount location for different air gap volumes are presented in Figure 2.33. Note that in the case of the original air cavity volume *V* passive isolation from the base vibration starts occurring above around 500 Hz. As the air cavity volume is increased, better low frequency vibration isolation is observed, as expected.

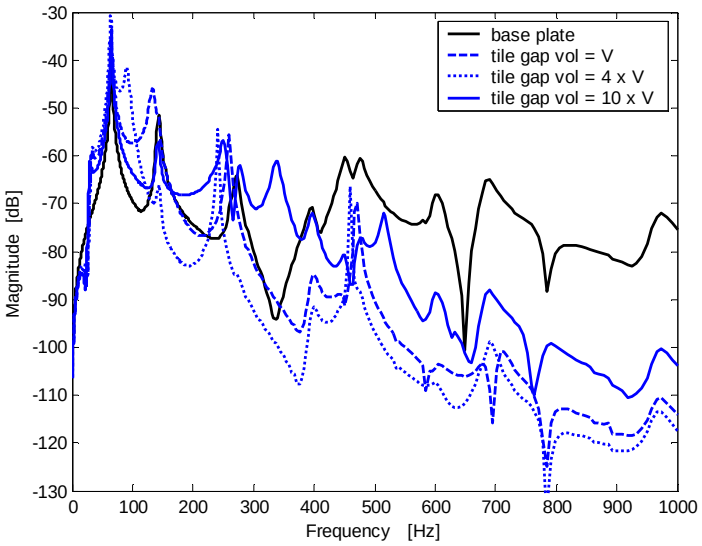

Figure 2.33: Velocity magnitude at the mount location for base plate and passive tile for different air cavity volumes

The surface displacement of the tiles and base plate at the frequencies of 35 Hz, 65 Hz, 151 Hz and 280 Hz corresponding to the first four peaks of the tile response curve shown in Figure 2.33 are shown in Figure 2.34 to Figure 2.37. Figure 2.34 shows the tiles in a rocking type vibration. In Figure 2.35 and Figure 2.36 the all the tiles have the same phase but while in Figure 2.35 the tiles and base plate vibration are in phase, in

Figure 2.36 the tiles and base vibration are 180 degrees out of phase.

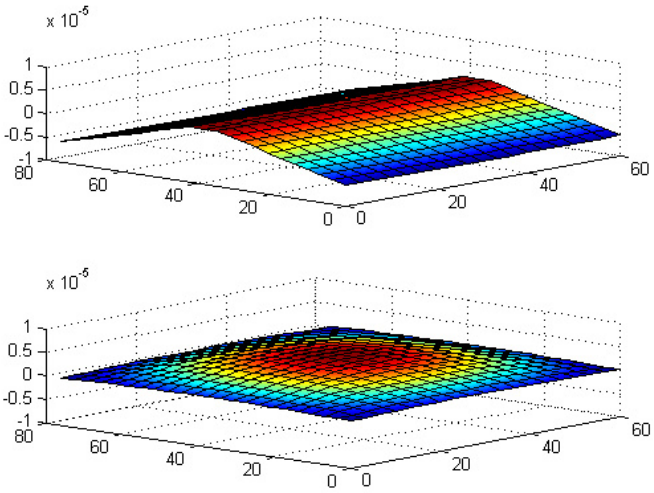

Figure 2.34: Displacement of the tiles (top) and base plate (bottom) at 35 Hz

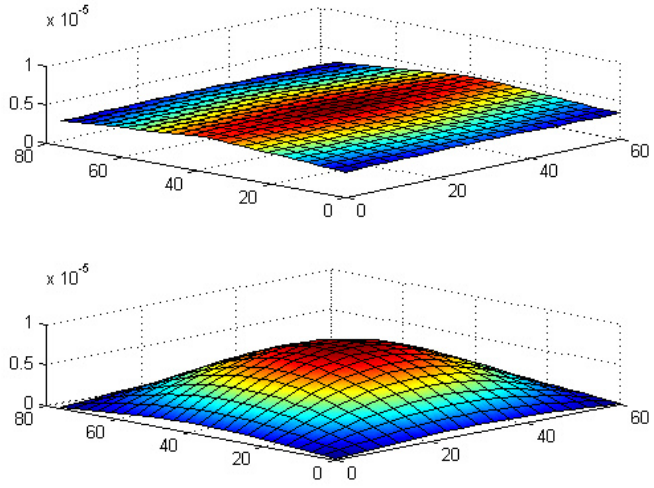

Figure 2.35: Displacement of the tiles (top) and base plate (bottom) at 65 Hz

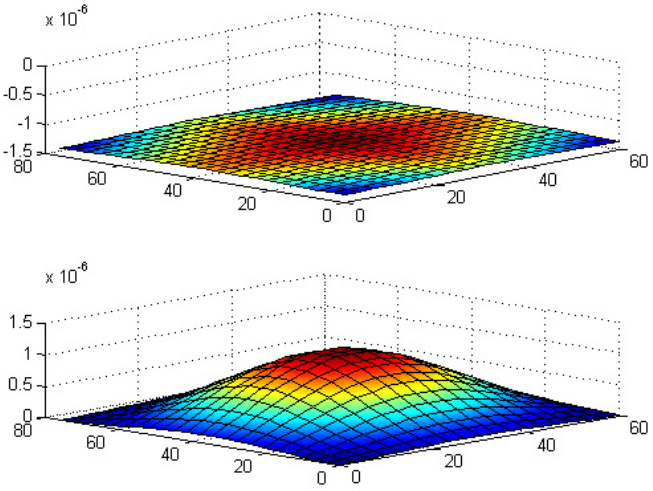

Figure 2.36: Displacement of the tiles (top) and base plate (bottom) at 151 Hz

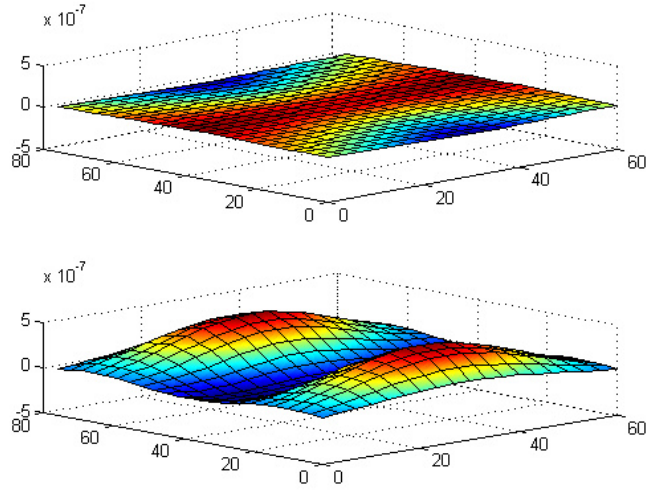

Figure 2.37: Displacement of the tiles (top) and base plate (bottom) at 280 Hz

2.5.4 Velocity Feedback

In this section the simulation results of velocity feedback control applied to the multiple tile system are presented.

The plant response is given by the absolute velocity at the error sensor location v_e, to the force acting to the tile f_a, which can be written in the frequency domain as:

$$G_{vel}(j\omega) = \frac{v_e(j\omega)}{f_a(j\omega)}$$

The plant response for a single collocated actuator sensor pair is shown in Figure 2.38.

The Nyquist plot shown in Figure 2.39 is restricted to the right side of the imaginary axis, indicating that the feedback control system is unconditionally stable.

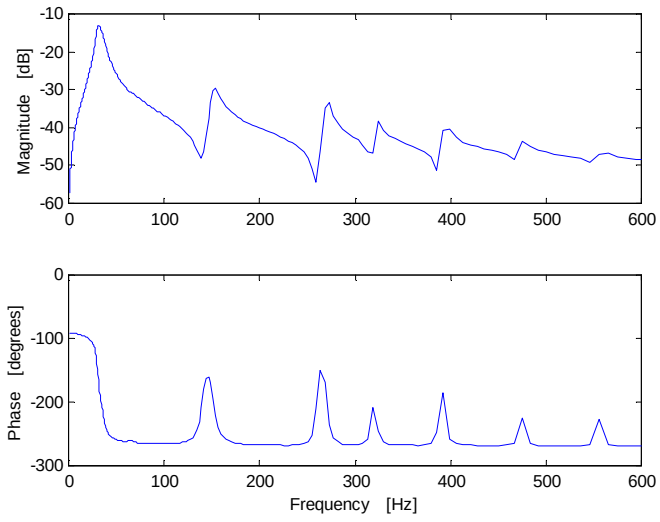

Figure 2.38: Simulated plant response for input on left mount of tile one with collocated error sensor

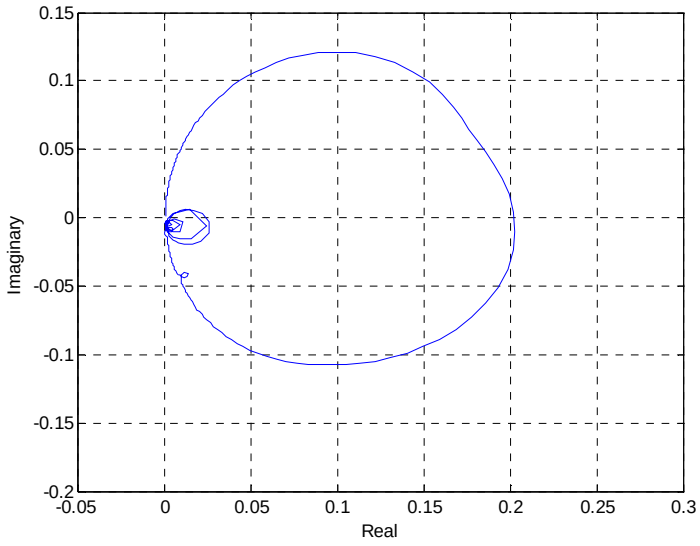

Figure 2.39: Simulated Nyquist plot for the one actuator plant response of the four tile-plate system

The transfer function between the output at the collocated and non-collocated sensors for an input at a single actuator is shown in Figure 2.40. Note the strong inter-tile coupling due to the presence of the air cavity. The inter-tile coupling is stronger around 30 Hz corresponding to a rocking mode of the tile and around 250 Hz corresponding to a piston type rigid body motion resonance of the tiles on the base plate. Strong coupling also occurs around 277 Hz corresponding to the natural frequency of the (3,1) vibration mode of the base plate.

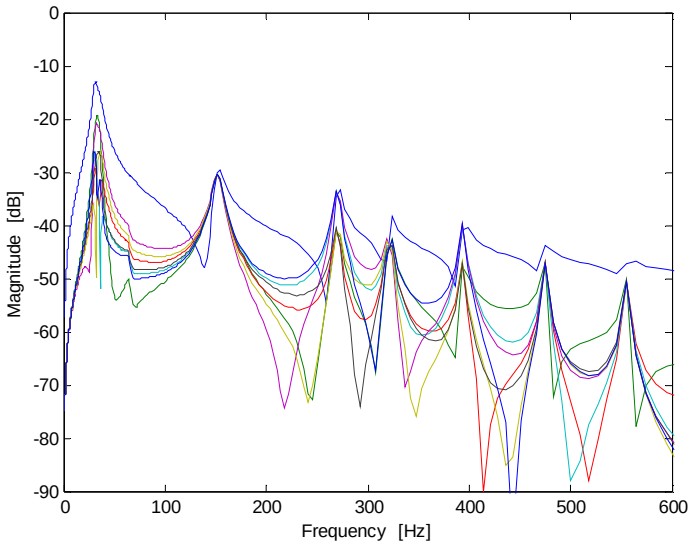

Figure 2.40: Collocated (thick blue trace) and non-collocated plant responses

The surface displacement of the tiles at the frequencies of 35 Hz, 151 Hz, 273 Hz and 400 Hz corresponding to peaks of the tile response curve shown in Figure 2.40 are shown in Figure 2.41 to Figure 2.44.

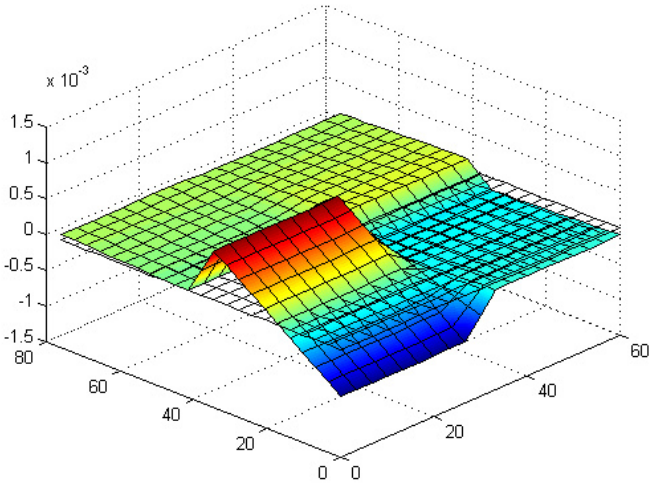

Figure 2.41: Displacement of the tiles at 35 Hz

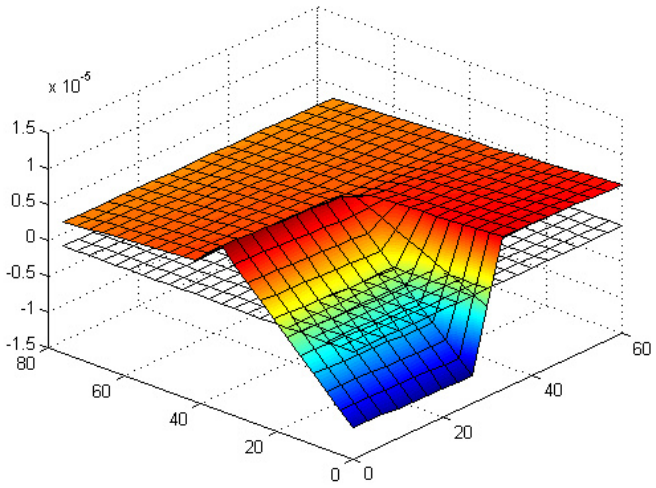

Figure 2.42: Displacement of the tiles at 151 Hz

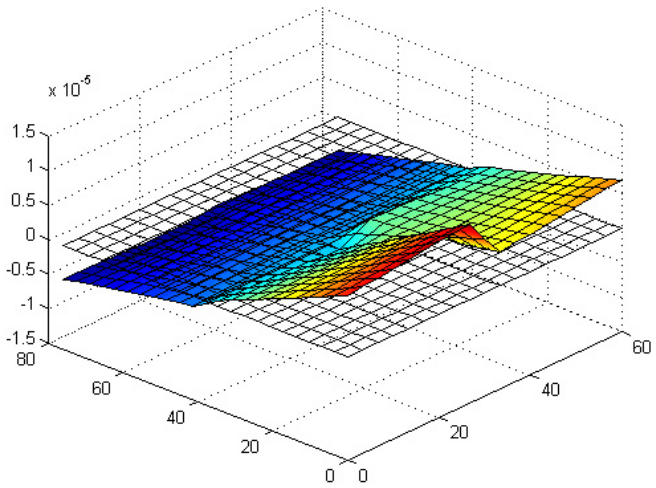

Figure 2.43: Displacement of the tiles at 273 Hz

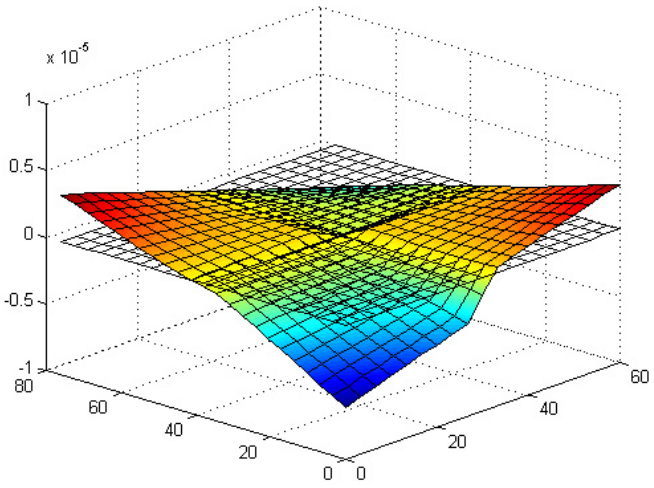

Figure 2.44: Displacement of the tiles at 400 Hz

For the case of structural borne transmission only (Figure 2.45), the mechanical coupling is only significant for the error sensors located on the same tile. The response at the error sensors located at the other tiles are about 40dB lower that the responses and have peaks at frequencies corresponding to the natural frequencies of the base plate, indicating that a small degree of coupling can occur by vibration transmission through the base plate.

The tile velocity in the passive and active cases for different feedback gains is shown in Figure 2.46. Good attenuation of the tile mass-spring resonance close to 250 Hz and also around 350 Hz.

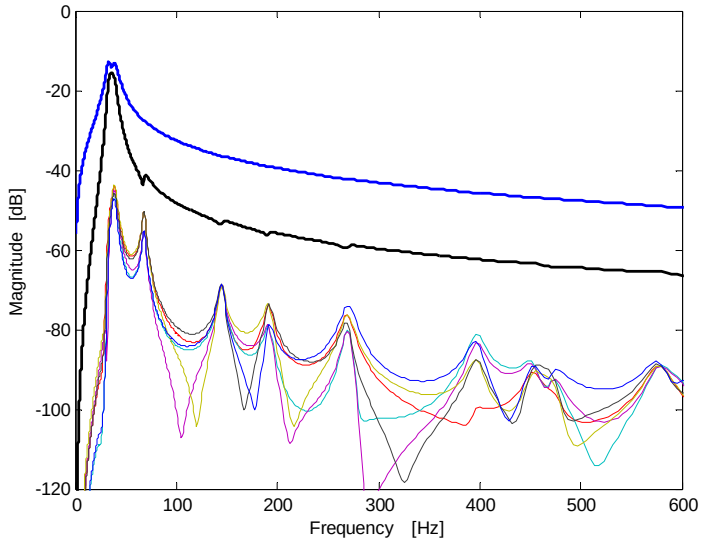

Figure 2.45: Collocated (thick blue trace) and non-collocated plant responses with structural borne path only

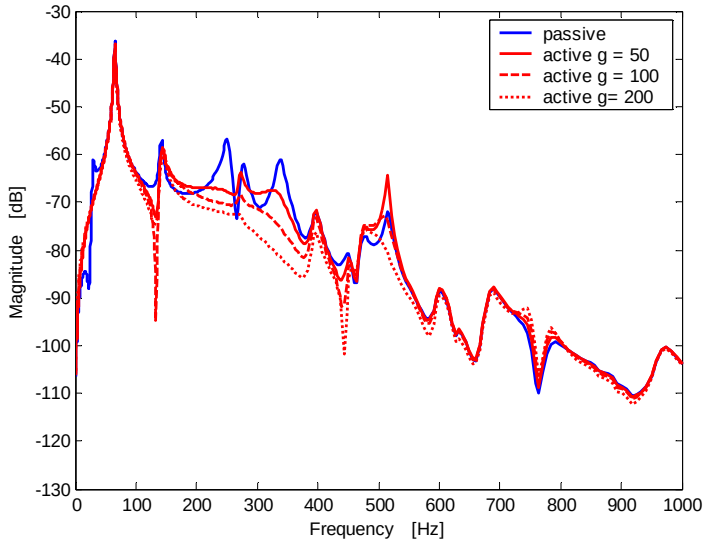

Figure 2.46: Magnitude of the tile velocity at the error sensor for the passive case (blue trace) and active case with different feedback gains (red traces)

The sound power radiated by the tile for the passive case and active case with different feedback gains is presented Figure 2.47. It worth noting the good correspondence between the attenuation of the tile velocity and the attenuation of the sound radiated. As discussed before, when the tile behaves as a flexible structure, reductions in the tile velocity at the error location do not necessarily correspond to attenuations of sound radiation.

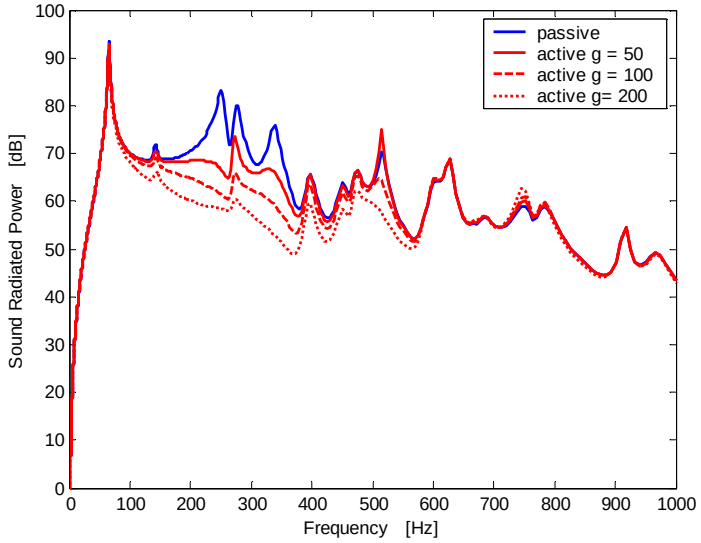

Figure 2.47: Sound power radiated by the tiles for the passive case (blue trace) and active case with different feedback gains (red traces)

2.5.5 Feedforward Control

Active attenuation results for velocity of the tile and sound radiated power using a feedforward control strategy applied to the multiple tile system are presented here. Two control strategies are investigated, as described earlier: 1) minimization of the normal velocity of the tile at the mount locations applying optimal control forces in parallel with the mounts; 2) minimization of the total sound power radiation of the tile applying optimal control forces in parallel with the mounts.

Figure 2.48 shows the velocity of one of the tile at one of the error sensors without

control and then the different control strategies are applied, namely, feedforward control of the tile velocity at the error sensor, feedback control and feedforward control with minimization of sound radiated power. Note once more that since harmonic feedforward control is considered, the minimization of the tile velocity at the mounts positions using harmonic feedforward control completely cancels the velocity of the tile at the error location.

The resulting sound radiated power for the various control strategies is shown in Figure 2.49. Using feedforward cancellation of the tile velocity good attenuation of sound power is observed up to around 650 Hz. It is also worth observing that through minimization of the sound radiated power, the bandwidth of effective control is extended to above 800 Hz. The application of feedback and feedforward control strategies demonstrates that the transmission loss of the partition using active tiles can be improved in the entire frequency range when compared to the transmission loss of the single base plate.

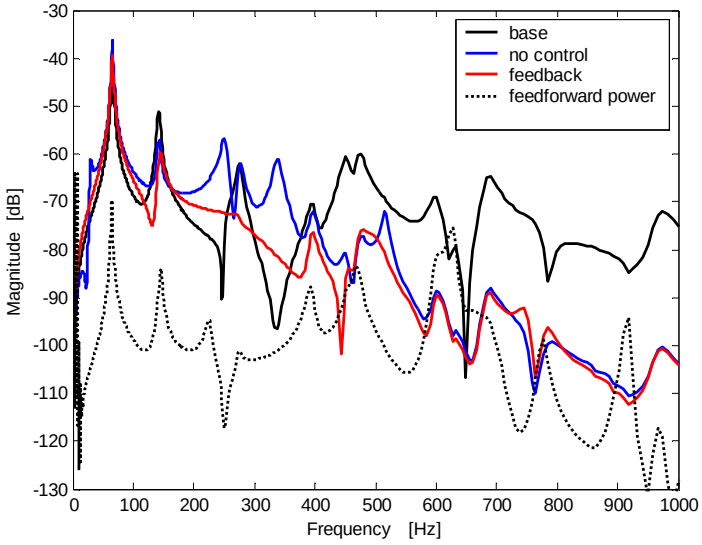

Figure 2.48: Tile at one of the mount positions. (a) black trace: base vibration (b) blue trace: tile vibration, control off (c) red trace: tile velocity with feedback control d) black dashed trace: feedforward control and minimization of the radiated acoustic power.

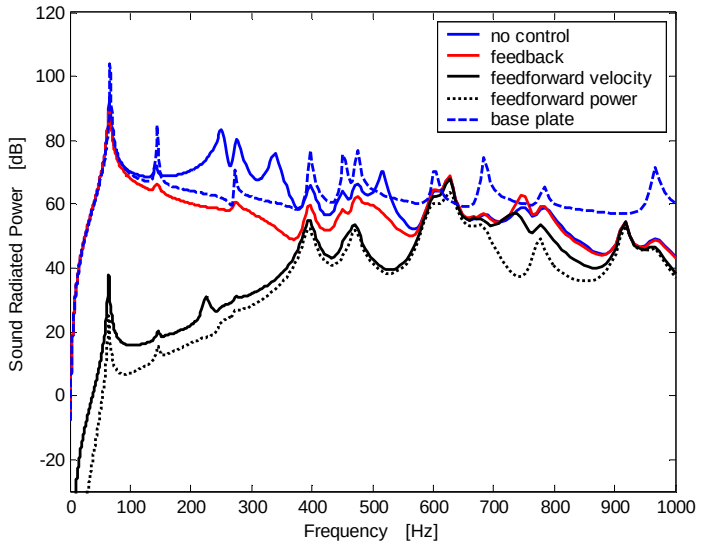

Figure 2.49: Total sound power radiated by a stiffer tile when the base plate is excited by an acoustic plane wave. (a) blue trace: sound radiated by tiles with control off (b) blue dashed trace: sound radiated by base plate only (c) red trace: tile radiation with velocity feedback control d) black dashed trace: feedforward control and minimization of the radiated acoustic power e) black trace: feedforward control and minimization of the tile velocity

2.6 Summary

This chapter investigated the sound transmission through double panel partitions consisting of a base plate and active tiles. Initially a double panel system was investigated assuming non-flexible panels. Using an impedance mobility approach allowed the model of the single active tile to be extended to include panel flexible behavior and the coupling of the tile to the base vibration through the air cavity that is created between the tile and the base structure. A fully coupled structural acoustic model was presented for a single flexible tile mounted through two mounts to a clamped plate that represents the base structure. The plate was modeled as excited by an acoustic plane wave and the total sound radiated power was computed. The active and passive performance of the tile in reducing the sound transmitted through the plate was then

simulated for the feedback and feedforward approaches introduced previously. It was shown that for the model simulated, most of the sound radiation from the tile is resultant from the acoustic coupling to the base vibration via the air cavity. In addition, the stiffness of the air cavity raises the tile mass-spring resonance and shifts the passive isolation to a higher frequency range. The simulations showed that effective control of the sound radiated power can be accomplished by controlling the tile velocity as long as the tile vibrates as a rigid piston or as long as the tile vibration mode are inefficient radiators. In addition it was shown that the bandwidth of control could be extended if sensors are used that estimate the tile radiated power, like for example distributed PVDF sensors. Finally, it was shown that increasing the tile stiffness is an effective way to extend the bandwidth of control even further.

The impedance mobility model was also applied to a four-tile system mounted on a simply supported plate. The model results showed that inter-tile coupling occur via the air cavity present between the tiles and the base plate. The application of feedback and feedforward control strategies demonstrated that the transmission loss of the partition using active tiles could be improved in the entire frequency range when compared to the transmission loss of the single base plate.

Chapter 3

3 Active-Passive Tile Approach Implementation

In a practical application of the active tile approach some assumptions of the analytical model formulated in Chapter 2 might not be true. For example, in practice the mounting system has internal dynamics that limit the performance of simple velocity feedback control schemes. In addition, there might be additional coupling not represented in the model and that can affect the control performance. These are some of the reasons that motivate the experimental investigation presented in this and the next Chapters.

In this chapter the practical feasibility of implementing the active tile approach is investigated. The main goal of this Chapter is to design and evaluate an active-passive tile prototype for controlling the low frequency sound transmission through a plate. In particular the following points are addressed: 1) selection of an adequate tile material that is light and stiff, 2) design of the active-passive mount including the selection of an actuator that has the necessary characteristics of being lightweight and with adequate force and displacement, 3) Test the performance of the active tile in controlling the sound radiation through a plate.

In the next sections the experimental implementation of the active tile is presented. Initially, the design of an active tile is discussed, including the selection of tile material and actuator. Subsequently, experimental tests are performed with prototype active tiles using two different setups. The first setup consists of a vibration isolation test, where a SDOF tile is mounted on top of a large shaker to directly measure its passive and active isolation performance. The second test consists of an acoustic transmission loss experiment using a single tile mounted on an aluminum panel than serves as base structure.

3.1 Prototype Design

The design of the active tile involves three main tasks: selection of the tile material, design of the passive/active mount, and design of the active controller. The first and second tasks are going to be considered in this section. The tile material has to be very lightweight and stiff, ideally with no flexible modes of vibration in the frequency range of interest.

The second important task is the design of the active-passive isolation mounts. In general, passive mounts have their performance limited by the contradicting requirements of having appropriated stiffness to provide static stability and being compliant so as to limit the vibration transmission caused by the dynamic excitation of the source [51]. The use of active mounts can overcome these limitations and allow higher performance. In this work, a THUNDER piezoelectric actuator is used in a novel way as passive-active mount. As is shown next, the chosen mount presents the required characteristics of being compact and lightweight, have good passive isolation characteristics and have adequate stroke, bandwidth, and control authority for the practical application of the active tile approach in noise control problems.

3.1.1 Tile Material

Any real tile exhibits flexible structural behavior above a certain frequency. The tile material properties, dimensions, and boundary conditions determine the frequency where the tile stops behaving like a rigid panel. For the active tile approach proposed, which uses a single error sensor to measure the tile velocity, the first flexible structural mode with high radiation efficiency frequency sets the upper frequency limit of control performance. This maximum frequency limit occurs because when the tile is flexible, the minimization of the tile velocity does not correspond to a reduction in the sound radiation. The mount vibration can be reduced at a single point while the rest of the tile surface continues to vibrate and radiate sound.

Given the requirements of lightweight and high stiffness, the selected tile material should maximize the ratio of flexural stiffness to mass. Considering that a rocket payload fairing is made of composite material that has typical surface density of 9.0 kg/m^2, in order to keep the added mass to around 10%, the panel materials should have a surface density of 0.9 kg/m^2.

A common approach to design a panel with high stiffness to mass ratio is to use a sandwich plate structure. In general, sandwich structures have two faces separated by a lightweight core. The faces usually have the same material and thickness and carry the primary in-plane and bending loads. The core of the sandwich panel can be of several types of materials, including honeycomb core, foam or solid core, and corrugated or truss core. The core resists the transverse shear loads and keeps the faces in place. The honeycomb core structure with hexagonally shaped cells has been used widely since World War II in commercial and military aircraft applications.

The advantage of using a sandwich structure can be seen by the following analysis. Consider a uniform plate of thickness h replaced by a sandwich plate of the same material. Assume also that the thickness of each plate of the sandwich structure is one half that of the uniform plate, that $t = h/2$, and that the thickness of the core is h_c. Because the density of the core of a typical sandwich panel structures is very low, the total weight of the sandwich structure can be assumed to be almost like that of the uniform plate. The bending stiffness of the uniform plate is give by:

$$D_{unif} = \frac{E_f (2t_f)^3}{12(1-\nu^2)} \tag{3.1}$$

where E_f is the modulus of elasticity of the panel material and ν is the Poisson's ratio. In the case of the sandwich plate the bending stiffness is given by:

$$D_{sand} = \frac{E_f t_f h_c^2}{2(1-\nu^2)} \tag{3.2}$$

The ratio of the bending stiffness of the sandwich plate to that of the uniform plate will be:

$$\frac{D_{sand}}{D_{unif}} = \frac{3}{4}\left(\frac{h_c}{t_f}\right)^2 \tag{3.3}$$

For example, if the ratio of the core thickness to the face plate thickness, $h_c/t_f = 20$, the bending stiffness of the sandwich plate will be 300 times that of the uniform plate, which is $D_{sand}/D_{unif} = 300$.

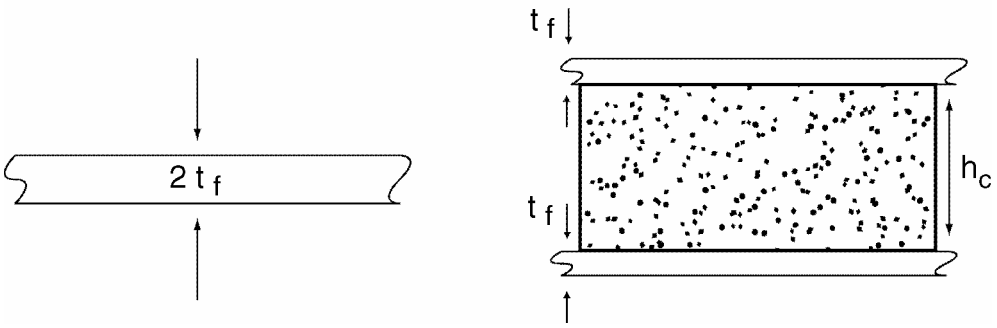

Figure 3.1: Cross section of uniform and sandwich construction

In this work, a sandwich panel structure with a honeycomb core is used for the construction of the active tiles. The honeycomb material is selected from datasheets of commercially available honeycomb panels and no attempt will be made to design or analyze in detail the sandwich panel structural response. It is outside the scope of this work to present a detailed treatment of the sandwich structure behavior. The reader can find such in depth analysis in for example reference [54]. Note also that it is possible to optimize the panel design for a given application. One can for example select the best face and core materials to minimize the total weight or minimize the absolute weight for a given geometry, material properties and mechanical loads [72].

3.1.2 Tile Sizing

The size of each tile is an important consideration for the successful implementation of the active tile approach. The decision of tile size is made taking into account the frequency bandwidth of control, the tile material properties and controller design approach.

For a given material, the tile size has to be selected so that the first flexible mode of vibration occurs above the control frequency bandwidth of interest. In addition, as shown by [48], the tile size will influence the radiation efficiency of the tile rocking modes. For a tile with a SISO controller capable of controlling the piston mode of vibration, the tile size should be selected so that the rocking modes contribution to the sound radiation becomes insignificant.

3.1.3 Active-Passive Mount

The design of the active mount is also of critical importance to the success of the active tile approach. The best actuator for a given application must be selected according to requirements such as, force, stroke, bandwidth and mass. An experimental investigation and discussion of different actuator technologies can be found in reference [55]. In addition, the stiffness of the mount influences its passive isolation characteristics.

In this work the active tile mount was implemented using a piezoelectric THUNDER actuator. This device is relatively light (around 20 grams) and has very good stroke and force characteristics. The *Thunder* actuator was mounted in such a fashion that it integrates the passive and active mounts. This actuator was be tested and the following measurements were performed:

- Free displacement
- Blocked force

- Open circuit dynamic stiffness

- Vibration isolation performance

Thunder is an acronym for Thin Layer Composite UNimorph Ferroelectric Driver and SEnsoR. This actuator is a composite of three thin layers that consists of a steel base layer, a piezoelectric patch and an aluminum top cover bonded together under pressure and high temperature with the LaRC SI polyimid adhesive. Applying a voltage across the PZT causes the actuator to bend and generate a force. During the manufacturing process a mechanical pre-stressing of the piezoceramic layer is accomplished and this is the key characteristic that gives *Thunder* devices their numerous inherent advantages as its very rugged and yet unusually flexible characteristics.

This device can be mounted and loaded in several different ways depending on the specific application, each of which result in slightly different force displacement characteristics. When mounting the device it is very important that at least one of the edges is allowed to move freely, so that the actuator is able to deform. The most common mounting configurations are the cantilevered and simple beam configurations. In this work a different mounting configuration is used that approximates simply supported boundary conditions. In this case the *Thunder* actuator is glued at its straight edges to very thin aluminum strips that have their top edge bonded to the steel skirt of the *Thunder* actuator and the bottom edge clamped to a stiff base, as illustrated in Figure 3.2. This mounting allows almost free horizontal displacement of the actuator edges while allowing force transmission to the attached structure, as the aluminum strips are very stiff in the vertical direction. An actual prototype of the tile is shown in Figure 3.3 where the topside of the *Thunder* is attached to a square sandwich honeycomb panel through a small balsa wood rectangular rod. The actuator used is TH 7-R whose specifications are shown in the Table 3.1.

Table 3.1 : Thunder actuator specifications

Characteristic	Thunder TH 7R
Weight	18.0 grams
Dimensions	96 x 71 x 0.56 mm
Ceramic Thickness	0.25
Arch Height	9.0 mm
Capacitance	166 nF
Maximum voltage	595 V_{pp}
Resonance Frequency	106 Hz (simply supported)
Typical Displacement	7.62 mm
Blocked Force	133 N

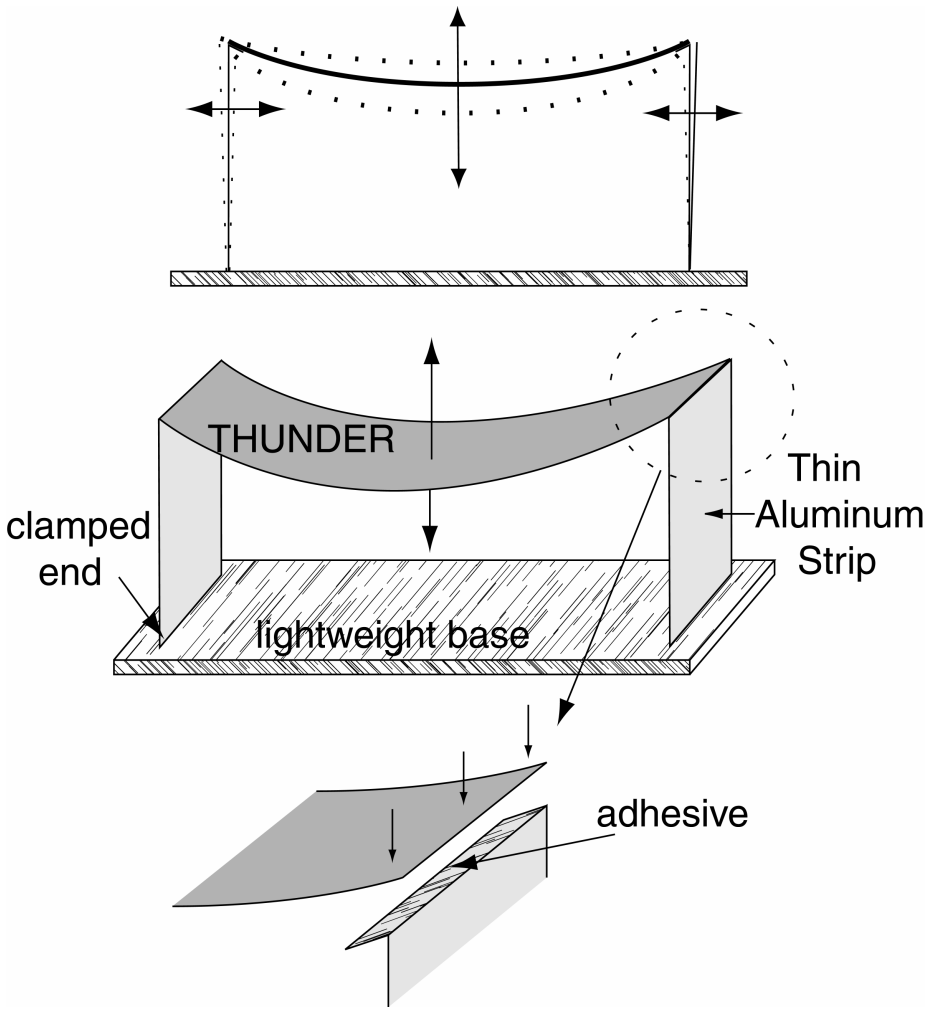

Figure 3.2: Active-passive isolation mount using a THUNDER element mounted in a simply supported fashion

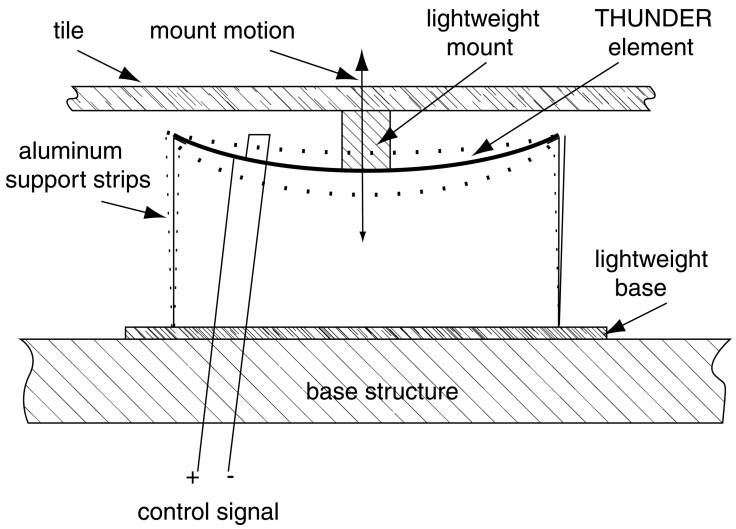

Figure 3.3 Schematic of the active-passive isolation mount installation

In the case of a vibration isolation problem, such as discussed in this dissertation, the actuator requirements for isolation of a receiving structure need to be defined, so that a proper actuator can be selected. A simple analysis can be performed using the system presented in Figure that shows an actuator placed between a source and receiver structures. The dynamic stiffness of the receiver, source and actuator are k_r, k_s and k_i and the actuator is capable of producing a force f_a. Note that the dynamic stiffness is defined, as the complex harmonic force required generating a unit harmonic displacement. The function of the actuator is obviously bringing the receiver to rest. The dynamic behavior of the system can be expressed in the frequency domain as:

$$f_r = k_r x_r$$

$$f_a - f_r = k_i (x_r - x_s)$$

Assuming that the receiver is brought to rest, then $x_r = 0$ and $f_r = 0$ and the force required by the actuator in this situation is given by:

$$f_a = -k_i x_s \tag{3.4}$$

In addition, note that when the receiver is kept at rest by the actuator, the source displacement is equal to its free displacement. This can be seen observing that at the junction between the actuator and the source, $f_a = -f_s$, which is the force applied by the actuator has the same magnitude and opposite direction to the force applied by the source to the internal dynamic stiffness of the actuator. Thus, there is no internal force between the source and the actuator and the source vibrates as if it was unconstrained. In view of this, one concludes that the actuator needs to be able to generate a displacement equal to the free displacement of the source [55]. This is a parameter that can be measured and that allows the selection of an actuator with adequate characteristics.

The actuator by itself can be characterized by two parameters, namely, its blocked force f_a and its free displacement x_f. The blocked force is the force that the actuator is able to generate when it is constrained not to move, while the free displacement is the displacement generated by an actuator when unconstrained to move [55]. These two parameters are related by the actuator internal dynamic stiffness, which is:

$$f_b = -k_i x_f \tag{3.5}$$

Under optimal control conditions the actuator has zero displacement at the receiver end and the free source displacement at the source end, while the force is zero at the source end and equals to f_a at the receiver end. Comparing equation 4 and 5 its possible to conclude that the actuator needs only to be able to overcome its internal dynamic stiffness and that the actuator will be able to isolate the receiver if its free displacement is larger than the free displacement of the source. Note that a stiffness element in parallel with the actuator will cause the effective internal dynamic stiffness of the actuator to be the sum of its internal dynamic stiffness and the parallel dynamic stiffness. This will cause the free displacement of the actuator to be reduced by $1+k_{parallel}/k_i$, while the blocked force remains the same.

The free displacement of the active-passive isolation mount using the *Thunder* actuator

was measured with the mount rigidly attached to a heavy base and electrically excited with a white noise signal. The acceleration at the top of the actuator was measured with a small accelerometer and a B&K frequency analyzer was used to compute the frequency response function of acceleration/input voltage. The obtained frequency response was then divided by $-\omega^2$ to get the free displacement. The free displacement per unit volt input measured for the *Thunder* actuator is shown in Figure 3.4

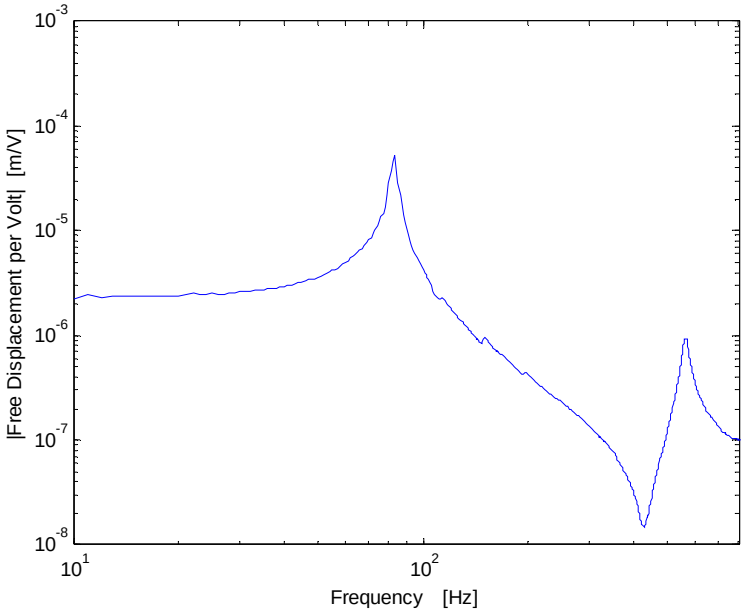

Figure 3.4: Free displacement per unit volt input for the *Thunder* actuator

In order to measure the blocked force, the active-passive isolation mount was attached to a fixture illustrated in Figure 3.5. The fixture consisted of two ¾ MDF wood panels connected to each other by 4 metal screws that had each end bolted to panel corners. The base of the mount was fixed to the base panel and the top of the actuator was attached via small screw to a force transducer. The topside of the force transducer was attached to a metal rod that had its other end fixed at the top panel. The blocked force generated for a white noise input was measured with frequency analyzer. Figure 3.6 shows the measured blocked force for unit electrical input for the Thunder actuator in a SDOF

active isolation mount configuration.

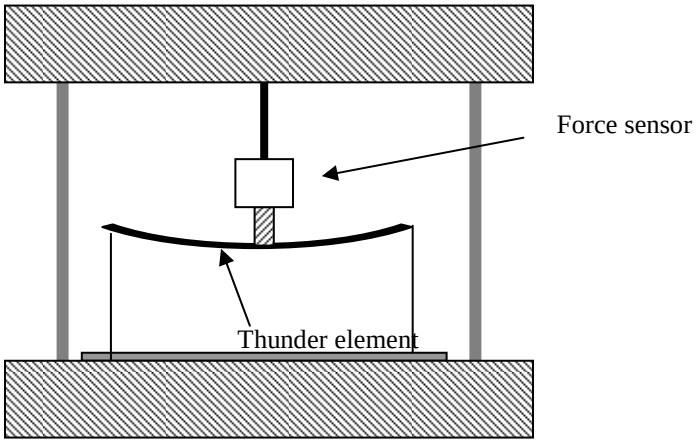

Figure 3.5: Fixture used to measure blocked force

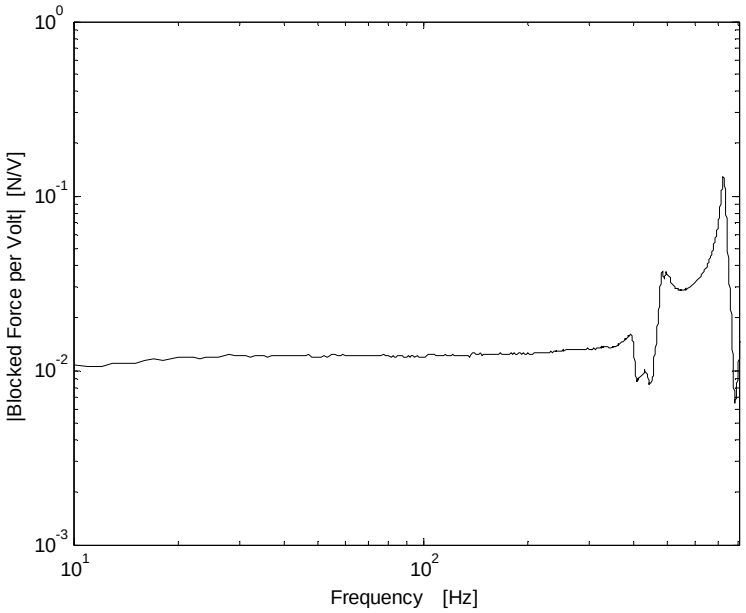

Figure 3.6: Blocked force per unit volt input for the *Thunder* actuator

The dynamic stiffness of the actuator was obtained by first measuring the force over acceleration transfer function, which was then multiplied by $-\omega^2$ to give the dynamic stiffness. The actuator base was fixed to the surface of heavy bench top, set in open circuit condition and mechanically excited with a shaker. The applied force was measured with a force gauge attached to the shaker. A small accelerometer was attached to the actuator in order to measure the resultant acceleration. The measured dynamic stiffness was then post-processed to remove the added mass of the measuring transducer by subtracting is dynamic stiffness. The dynamic stiffness obtained this way is shown in Figure 3.7 . It can be seen that the actuator behaves as a simple stiffness at low frequencies and at higher frequencies additional dynamics are present, related to actuator internal structural resonances.

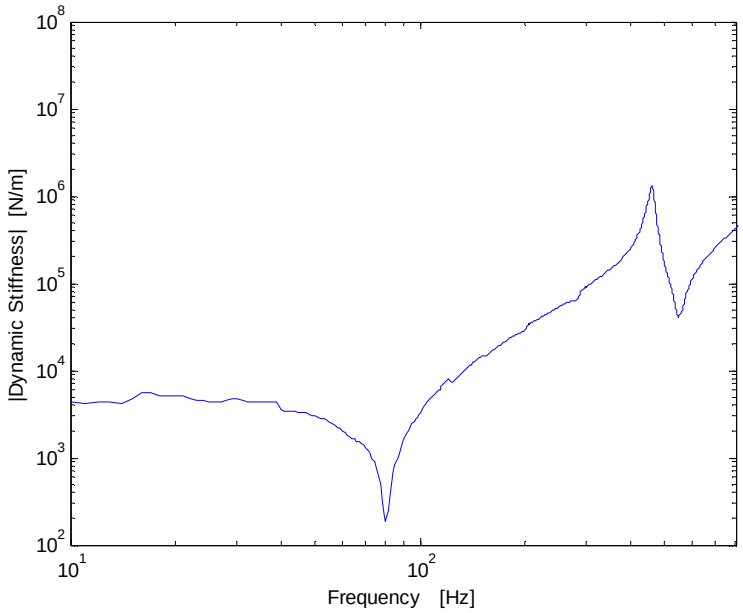

Figure 3.7: Dynamic stiffness of the *Thunder* actuator

These plots show that the Thunder actuator performs very well when compared to other actuator technologies for active vibration control as reported in [55]. The Thunder

actuator has dynamic stiffness and free displacement characteristics that are comparable to that of an electrodynamic tweeter. However, the blocked force is similar to other piezoelectric actuators such as a PZT tube or Rainbow actuator used in [55]. Another important advantage of the *Thunder* actuator is the low weight, approximately 20 grams for the version employed in this work. The mechanical characteristics of the *Thunder* actuator and the actuators studied in [55] in terms of the maximum electrical input and associated mechanical outputs computed from the product of the maximum input and the low frequency straight trace characteristics of Figure 3.4 and Figure 3.6 are presented in Table 3.2.

Table 3.2: Mechanical characteristics of *Thunder* and actuators tested in [55]

Actuator	Max Electrical Input (peak)	Max. Blocked Force (N)	Max. Free displacement (m)	Stiffness (N/m)	Loss factor (η)	Moving Mass (kg)
AVC	200 V	9.00	0.03×10^{-3}	5.77×10^{5}	0.074	2.6×10^{-2}
PZT tube	3180 V	47.5	0.032×10^{-3}	9.3×10^{5}	0.180	
Rainbow	200 V	3.0	0.03×10^{-3}	1.19×10^{5}	0.090	1.1×10^{-2}
Magnetostrictive	1 A	100	0.01×10^{-3}	1.5×10^{7}	0.050	
Tweeter	0.5 A	0.35	0.15×10^{-3}	3.92×10^{3}	0.100	4.8×10^{-3}
Thunder	300 V	3.6	0.75×10^{-3}	4.1×10^{3}	0.014	1.5×10^{-2}

3.2 Broadband Feedforward Control

In Chapter 2 the application of feedforward control to the active tile assumed, for the purposes of analysis and simulations, that the disturbance was deterministic, which is harmonic and that the control solution could be obtained frequency by frequency. In this section, an adaptive digital feedforward control system is introduced and used to investigate the performance of the active tile for random disturbances. Only a brief treatment of the broadband feedforward control is presented and a more complete discussion can be found in Chapter 2 of reference [62].

3.2.1 Single Channel Feedforward Control

The block diagram of a SISO filtered LMS-x feedforward controller is shown in Figure 3.8. The primary path P(z) represents the transfer function of the physical system from the reference input sensor signal x(n) to the error sensor signal e(n). W(z) is the adaptive filter, in this case a finite-impulse-response (FIR) filter with coefficients adapted by an LMS algorithm with the goal of minimizing the error signal e(n). S(z) is called the secondary path and represents the transfer function from the adaptive filter output to the error signal. The secondary path S'(z) represents the active-tile system including the D/A converter at the output of the adaptive filter, reconstruction filter, power amplifier, Thunder actuator, transfer function from Thunder actuator to error accelerometer, error accelerometer, preamplifier, antialiasing filter and D/A converter. S'(z) represents an estimated model of the secondary path S(z) and is used to filter the input signal x(n) to generated the filtered reference signal x'(x) used by the LMS algorithm. Assuming that the response of the reconstruction filter and the plant attenuates any frequency component produced by the D/A converter above the Nyquist frequency and that the anti-aliasing filter removes any component of the continuous disturbance above half the sampling rate, the discrete error is a good representation of the continuous time error signal.

The model of the secondary path S’(z) is obtained by an off-line modeling technique represented in Figure 3.9. A broadband white noise signal input to the actuator is used as the training signal in the system identification procedure, which adapts the coefficients of a FIR filter that models the secondary path. After the identification is completed the coefficients of the FIR filter that models the secondary path are set to fixed values.

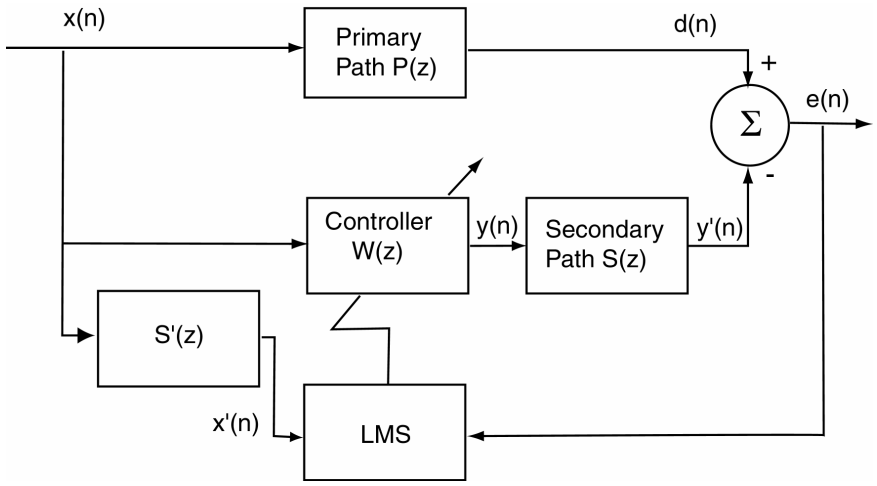

Figure 3.8 Block diagram of control system using filtered LMS-x feedforward algorithm

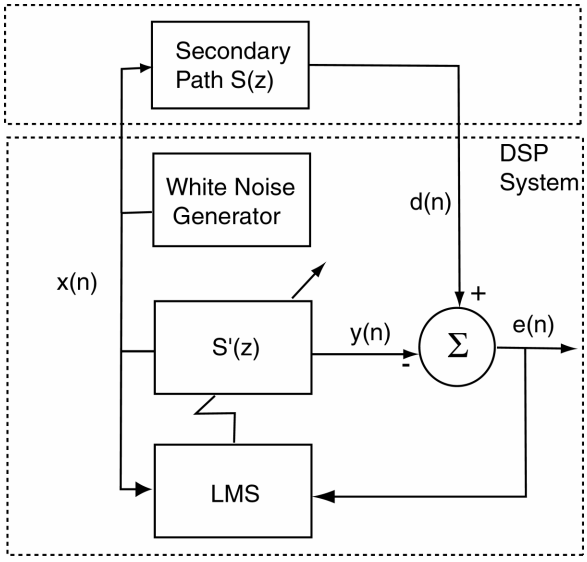

Figure 3.9: Schematic of experimental setup for off-line secondary path modeling

From this block diagram shown in Figure 3.8 the discrete time error signal can be written as the sum of the disturbance in the absence of control *d(n)* with the effect of the secondary control signal, *y'(n)* as:

$$e(n) = d(n) + y'(n) = d(n) - s(n) * y(n) \tag{3.6}$$

The output of the digital FIR filter *W(z)*, depicted in Figure 3.10 , is computed as:

$$y(n) = \sum_{l=0}^{L-1} w_l(n) x(n-l) \tag{3.7}$$

Defining the input vector at $\mathbf{x}(n)$ time *n* as:

$$\mathbf{x}(n) \equiv [x(n) \quad x(n-1) \quad \cdots \quad x(n-L+1)]^T \tag{3.8}$$

and defining the weight vector $\mathbf{w}(n)$ at time *n* as

$$\mathbf{w}(n) \equiv [w(n) \quad w(n-1) \quad \cdots \quad w(n-L+1)]^T \tag{3.9}$$

where the superscript *T* denotes the transpose of the vector and *L* is the order of the filter *W(z)*. Now, the output signal *y(n)* in equation (7) above can be written in vectorial form as:

$$y(n) = \mathbf{w}^T(n)\mathbf{x}(n) \tag{3.10}$$

Substituting (10) into (6) results in:

$$e(n) = d(n) - s(n) * [\mathbf{w}^T(n)\mathbf{x}(n)] \tag{3.11}$$

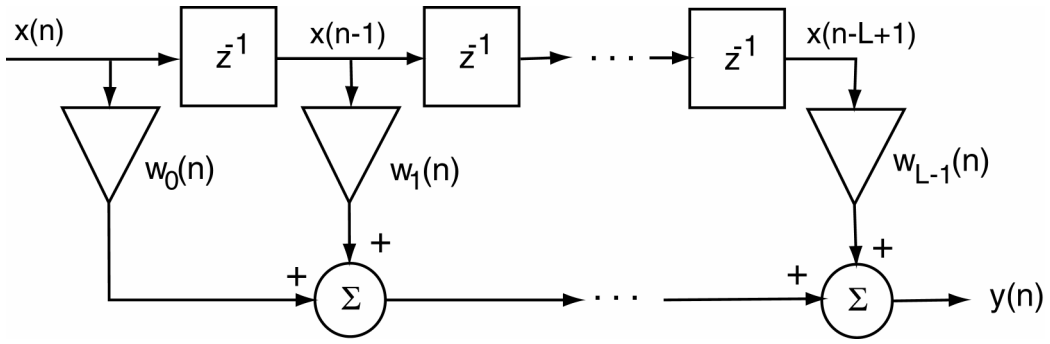

Figure 3.10: Block diagram of digital FIR filter

The *z*-transform of the error signal is:

$$E(z) = [P(z) - S(z)W(z)]X(z) \tag{3.12}$$

and for broadband disturbance signals $\mathbf{w}(n)$ must represent the impulse response of the transfer function:

$$W^o = \frac{P(z)}{S(z)} \tag{3.13}$$

This is the same as saying that the adaptive filter *W(z)* has to model the primary path P(z) and inversely model the secondary path *S(z)* and the FIR filter has to be of sufficiently high order. Note that it is impossible to compensate for the innate delay of the secondary path *S(z)* due to the antialiasing filters and wave propagation unless the primary path *P(z)* contains a delay of at least same length. In other words, this limitation is the causality constraint of broadband feedforward control systems [62].

The goal of the adaptive filter is the minimization of the instantaneous squared error $e^2(n)$. Although the filter coefficients can be calculated directly from the knowledge of the auto-correlation and cross-correlation properties of the disturbance and filtered

reference signals (Elliot,signal processing), in practice an adaptive algorithm is generally used. In this work an LMS-x approach is used to adapt the filter coefficients. For the filtered LMS-x algorithm the adaptive filter weights are adapted in real time as:

$$\mathbf{w}(n+1) = \mathbf{w}(n) + \mu \mathbf{x}'(n)e(n) \tag{3.14}$$

where $\mathbf{x}'(n)$ is the filtered reference signal obtained by filtering the excitation signal *x(n)* through the estimate of the secondary path and μ is the convergence coefficient. The algorithm is implemented in practice by filtering the reference signal *x(n)* by FIR filter estimate of the secondary plant. The output of the filter is then multiplied by the error signal *e(n)* and the convergence coefficient μ to compute the estimate of the change required for each filter weight.

The selection of the convergence coefficient μ controls the speed of the adaptation as well as the stability of the adaptive algorithm. A value μ of that is too small will result in slow adaptation and possibly interrupt the adaptation before optimum filter weights are achieved. A value of μ that is too large can cause the instability of the algorithm. In general, at the beginning of the adaptation a larger value of μ is used and once good convergence of the filter weights is obtained μ value is reduced to guarantee stability and steady state attenuation.

The selection of the sampling rate generally depends on a trade-off between performance and cost. While a faster sampling rate allows smaller delays in the system and better steady state performance for broadband disturbances it requires a faster and more costly processor. The increase in the computational cost comes because of the necessity of a larger number of coefficients to implement the FIR filter with certain impulse response duration. In addition, real time digital processing requires that the processing time required to complete the calculations involved in implementing the control filter has to be less than the sampling period. A sampling rate that is too fast results in a required filter length that is excessive to achieve a particular result. Long filters reduce system stability, increase computational overhear and memory requirements for the DSP. It is

generally accepted that the optimum sampling rate in active noise and vibration control systems is about 10 times the frequency of the noise or vibration to be controlled [64]. The control performance decreases as the sampling rate moves away from the optimal value.

3.2.2 Multi Channel Feedforward Control

The detailed analysis of a multi channel active noise control system is presented in Chapter 5 of reference [62]. Only a brief treatment is presented next. The block diagram in Figure 3.11 represents the reference/multiple output feedforward control system. There are *K* adaptive filters using a single reference *x(n)* and output signal vector **y***(n)*. The goal is to minimize the sum of the squares of the *M* error signals **e***(n)*. The matrix P represents M primary path transfer functions from x(n) to the error sensor output em(n). In addition, there are *K x M* secondary path estimates contained in the matrix *S'(z)*. The coefficients associated with all K adaptive filters are represented in Figure 3.11 by the vector **w***(n)*:

$$\mathbf{w}(n) \equiv [\mathbf{w}_1^T \quad \mathbf{w}_2^T \quad \cdots \quad \mathbf{w}_K^T]^T \tag{3.15}$$

where

$$\mathbf{w}_k(n) = [w_{k,0}^T \quad w_{k,1}^T \quad \cdots \quad w_{k,L-1}^T]^T, \qquad \text{k=1,2,….K} \tag{3.16}$$

are the coefficients of each of the *K* adaptive filters of length. The K canceling signals $y_k(n)$ generated by the control filters are represented as:

$$\mathbf{y}_k(n) \equiv [y_1 \quad y_2 \quad \cdots \quad y_k]^T \tag{3.17}$$

The *K* canceling signals $y_k(n)$ are generated by the control filters by filtering the reference signal *x(n)* by the corresponding adaptive FIR filter $\mathbf{w}_k(n)$:

$$y_k = \mathbf{w}_k^T \mathbf{x}(n) \qquad \text{k} = 1, 2, \ldots, \text{K} \tag{3.18}$$

where

$$\mathbf{x}_k(n) \equiv [x(n) \quad x(n-1) \quad \cdots \quad x(n-L+1)]^T \tag{3.19}$$

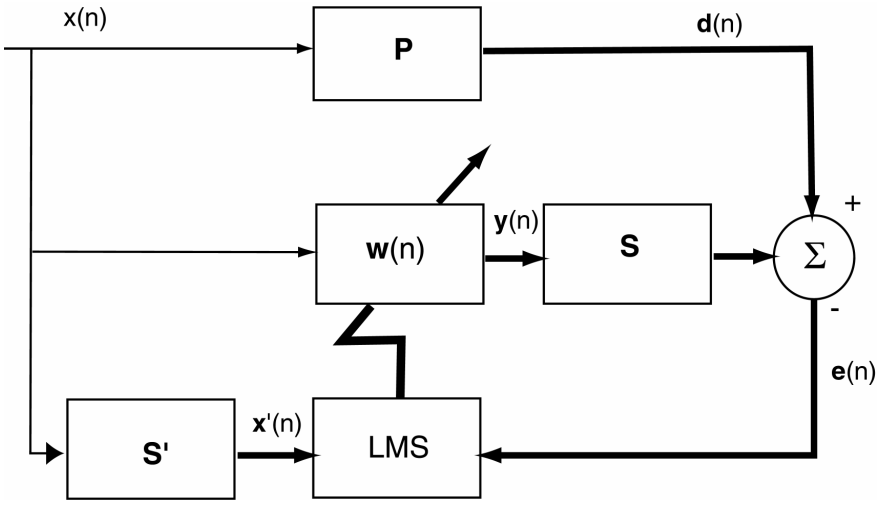

Figure 3.11: Block diagram of single-reference multiple output active noise control system using the filtered x-LMS algorithm

Combining equation (15), (17) and (18) it is possible to write:

$$y_k = \mathbf{X}^T(n)\,\mathbf{w}(n) \tag{3.20}$$

where $\mathbf{X}(n)$ is a *KL x K* block diagonal matrix defined as:

$$\mathbf{X}(n) = \begin{bmatrix} \mathbf{x}(n) & 0 & \cdots & 0 \\ 0 & \mathbf{x}(n) & 0 & \cdots \\ \vdots & 0 & \ddots & 0 \\ 0 & \cdots & 0 & \mathbf{x}(n) \end{bmatrix} \tag{3.21}$$

The error signal vector **e***(n)* measured by *M* error sensors is represented as:

$$\mathbf{e}(n) = \mathbf{d}(n) - \mathbf{y}'(n) \tag{3.22}$$

where $\mathbf{d}_k(n) \equiv [d_1(n) \quad d_2(n) \quad \cdots \quad d_m(n)]^T$ is the disturbance vector with $d_m(n)$ representing the disturbance at the *m*th error sensor, and $\mathbf{y}'_k(n) \equiv [y'_1 \quad y'_2 \quad \cdots \quad y'_m]^T$ is the control vector at the error sensors, where y'_m is the sum of the control signals from the *K* secondary sources to the *m*th error sensor. The vector $\mathbf{y}'_k(n)$ can be expressed as:

$$\mathbf{y}'_k(n) = \mathbf{S}(n) * \mathbf{y}(n) \tag{3.23}$$

where * stands for linear convolution and $\mathbf{S}(n)$ is a matrix that contains *M x K* impulse response functions:

$$\mathbf{S}(n) = \begin{bmatrix} s_{11}(n) & s_{12}(n) & \cdots & s_{1k}(n) \\ s_{21}(n) & s_{22}(n) & \cdots & s_{2k}(n) \\ \vdots & \vdots & \ddots & \vdots \\ s_{m1}(n) & s_{m2}(n) & \cdots & s_{mk}(n) \end{bmatrix} \tag{3.24}$$

where $s_{mk}(n)$ is the impulse response from the *k*th control actuator to the *m*th error sensor.

The error signal vector can be rewritten using the equations above as:

$$\mathbf{e}(n) = \mathbf{d}(n) - \mathbf{S}(n) * [\mathbf{X}^T(n)\mathbf{w}(n)] \tag{3.25}$$

As mentioned earlier the goal is to minimize the sum of the mean-square errors that can be expressed as:

$$\xi(n) = \sum_{m=1}^{M} E[e_m^2(n)] \tag{3.26}$$

The single reference/ multiple output FXLMS algorithm used to update the adaptive coefficient vector to minimize the cost function above is:

$$\mathbf{w}(n+1) = \mathbf{w}(n) + \mu \mathbf{X}'(n)\mathbf{e}(n) \tag{3.27}$$

where $\mathbf{X}'(n) = \mathbf{S}^T(n) \otimes x(n)$, and $\otimes$ denotes a Kornecker product convolution obtained by the convolution of each element of $\mathbf{S}^T(n)$ with **x***(n)*.

In the experimental tests for control of sound transmission the error signal is obtained from two accelerometers positioned on the tile surface at the locations where the mounts are attached. In this case, the *1 x 2 x 2* (single reference two-input two-output) feedforward controller is implemented in a C40 DSP board using the filtered-x LMS algorithm. Note that the use of a *1 x 2 x* 2 feedforward control system allows controlling the rocking mode of vibration of the tile. The block diagram of the two-input two-output feedforward controller is shown in Figure 3.12.

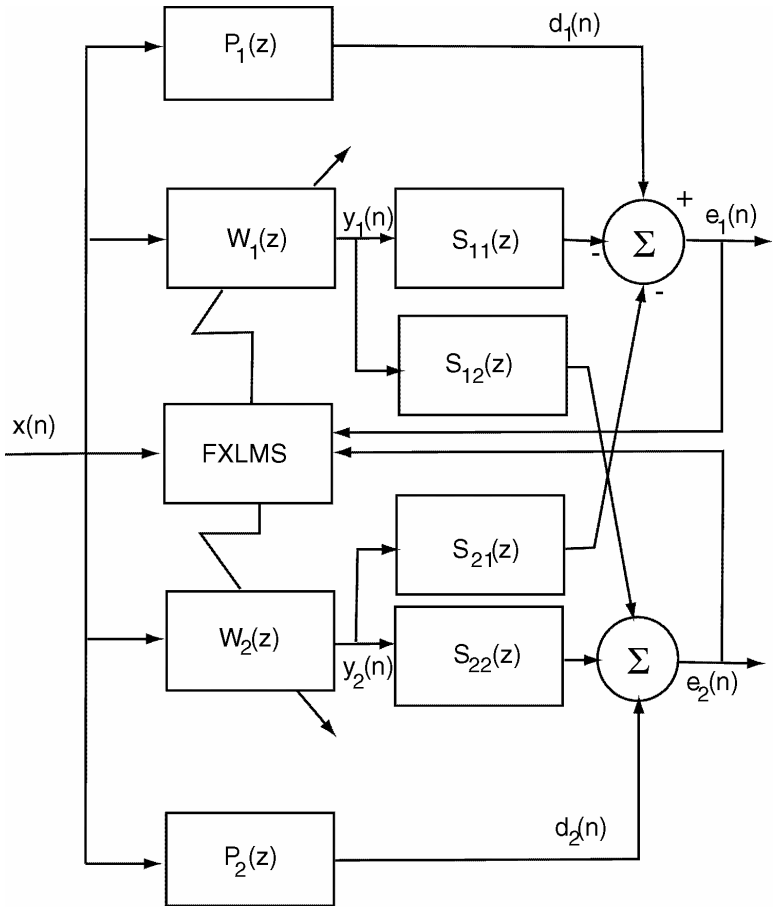

Figure 3.12: Block diagram of 1 x 2 x 2 multi channel active control system

In Figure 3.12, $e_1(n)$ and $e_2(n)$ are the error signals coming from accelerometers positioned on the surface of the tile at the location where the mounts are attached to the tile; $y_1(n)$ and $y_2(n)$ are the control signals generated by the adaptive filters $W_1(z)$ and $W_2(z)$ and sent to the *Thunder* elements; $P_1(z)$ and $P_2(z)$ are the primary path from the disturbance to the error sensors; $S_{11}(z)$ and $S_{21}(z)$ are the secondary paths consisting on the transfer functions between the control input $y_1(n)$ and the two error sensors; and $S_{12}(z)$ and $S_{22}(z)$ are the secondary paths consisting on the transfer functions between the control input $y_2(n)$ and the two error sensors. Thus, four *(2 x M)* FIR filters for modeling the secondary paths are needed for the *1 x 2 x 2* feedforward controller. In general, a *1 x M x N* system would require *M x N* FIR filters for the secondary path estimates and *M* FIR filters for the controllers. Note that in Figure 3.12 it is assumed that there is no

feedback between the control inputs to the reference sensor.

3.2.3 Decentralized Feedforward Control

In a multiple channel feedforward controller represented by the block diagram depicted in Figure 3.11 the inputs to the secondary sources are simultaneously adjusted to minimize the sum of the squared outputs from multiple error sensors. This type of controller can be called centralized or fully coupled feedforward control system. In contrast, a decentralized adaptive feedforward control system consists of a number of independently implemented adaptive controllers that drive subsets of the total number of secondary sources for minimizing the squared sum of a subset of error sensors. The extreme case of a decentralized controller is obtained when each secondary control source is adapted to minimize the output of a single error sensor.

A decentralized feedforward controller can be advantageous for large systems where a fully coupled controller would imply in great amount of wiring and great amount of processing power to implement. The block diagram of a single-reference, multi-channel decentralized feedforward controller is depicted in Figure 3.13.

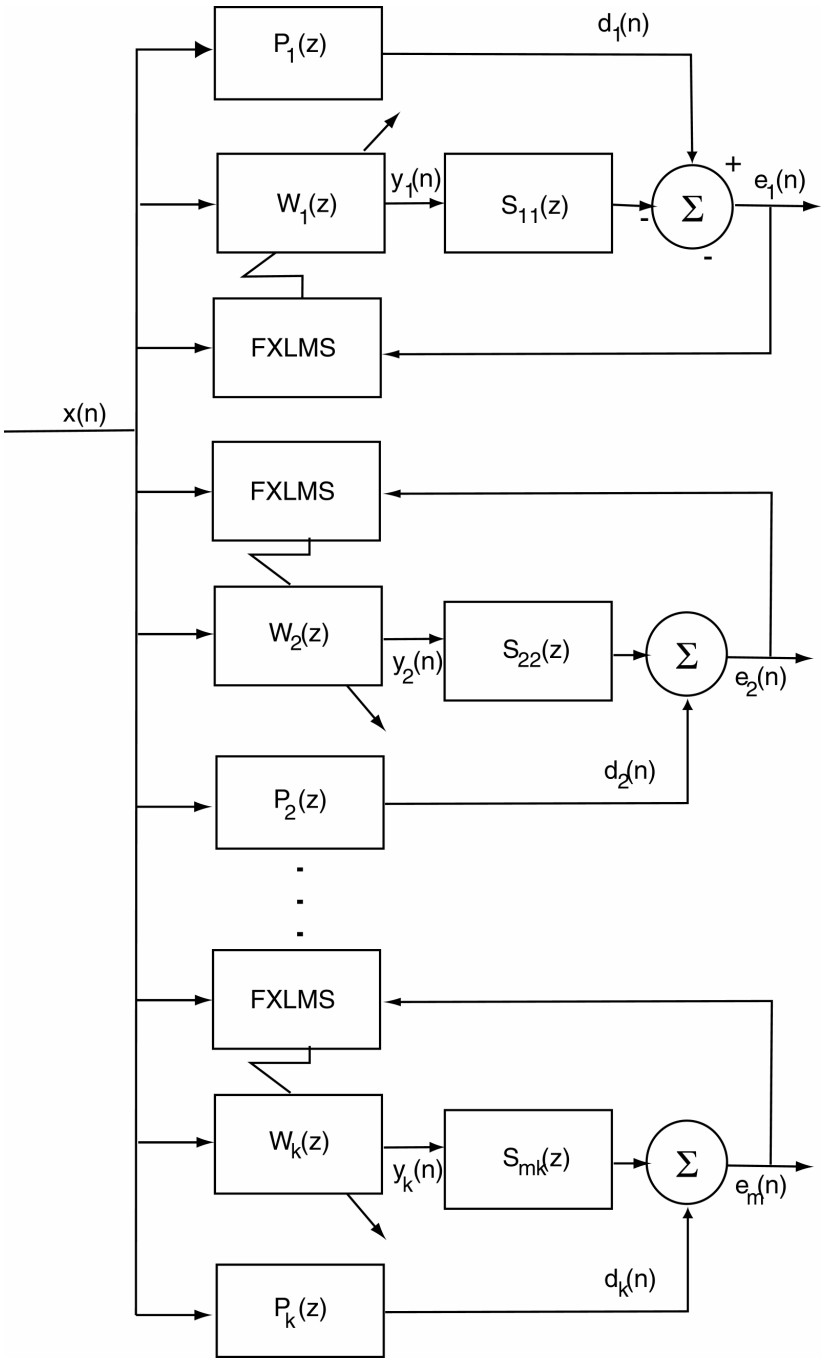

Figure 3.13: Block diagram representing a multi channel decentralized feedforward active control system

The signals coming from the M error sensors can be written as

$$\mathbf{e}(n) = \mathbf{d}(n) - \mathbf{S}_d(n) * y(n) \tag{3.28}$$

where * stands for linear convolution and $\mathbf{S}_d(n)$ is a diagonal matrix that contains *M x 1* impulse response functions:

$$\mathbf{S}_d(n) = \begin{bmatrix} s_{11}(n) & 0 & \cdots & 0 \\ 0 & s_{22}(n) & \cdots & 0 \\ \vdots & \vdots & \ddots & \vdots \\ 0 & 0 & \cdots & s_{mk}(n) \end{bmatrix} \tag{3.29}$$

where $s_{mk}(n)$ is the impulse response from the *k*th control actuator to the *m*th error sensor.

The single reference/ decentralized multiple output FXLMS algorithm used to update the adaptive coefficient vector to minimize the error is:

$$\mathbf{w}(n+1) = \mathbf{w}(n) + \mu \mathbf{X}_d'(n)\mathbf{e}(n) \tag{3.30}$$

where $\mathbf{X}_d'(n) = \mathbf{S}_d{}^T(n) \otimes x(n)$ is a diagonal matrix, and $\otimes$ denotes a Kronecker product convolution obtained by the convolution of each element of the diagonal matrix $\mathbf{S}_d{}^T(n)$ with **x***(n)*.

The stability conditions of decentralized feedforward controllers were investigated by Elliott and Boucher [69] for active noise control systems. It was shown that as long as the error sensors are closed to the secondary sources used to control them than the other secondary sources, the stability of the system is very robust to decentralization with similar steady-state performance. In addition, in order for (27) to converge, the real parts of all the eigenvalues of the matrix $S_d^H S$ must be positive. A simple method of establishing if a decentralized control system is guaranteed stable is to examine the relative magnitude of the elements of **S**. For a decoupled control system a sufficient

condition (but not necessary) for stability is given by:

$$|s_{ii}| \geq \sum_{\substack{j=1 \\ j \neq i}}^{M} |s_{ij}|, \qquad \text{for all } i \tag{3.31}$$

Which is equivalent to say that the matrix **S** is *diagonally dominant*.

3.3 Active Vibration Isolation

This section presents an experimental investigation of the vibration isolation characteristics of an active-tile. A tile prototype is constructed and tested for both passive and active vibration isolation. Active control of vibration isolation is implemented with both feedforward and feedback control.

3.3.1 Experimental Setup

A 25cm x 25cm tile made of composite sandwich material, with fiberglass faces and Nomex honeycomb core is used for the tests (see Figure 3.14). The active tile is mounted on the top of a 50 lbs-f electrodynamic shaker as shown in Figure 3.16. Band limited white noise from 0-250 Hz is used as input to the electrodynamic shaker and the normal acceleration of the base and of the tile are measured using small PCB accelerometers. These accelerations are used to compute the transmissibility of the tile-mount system. In the first test, the LMS-x feedforward algorithm implemented in real time in a PC-based system was used to minimize the signal coming from the accelerometer attached to the tile. The disturbance signal, delayed to the shaker by a few sample periods to ensure the system is causal, is used as the reference signal for the controller. The schematic of the experimental setup is shown in Figure 3.15.

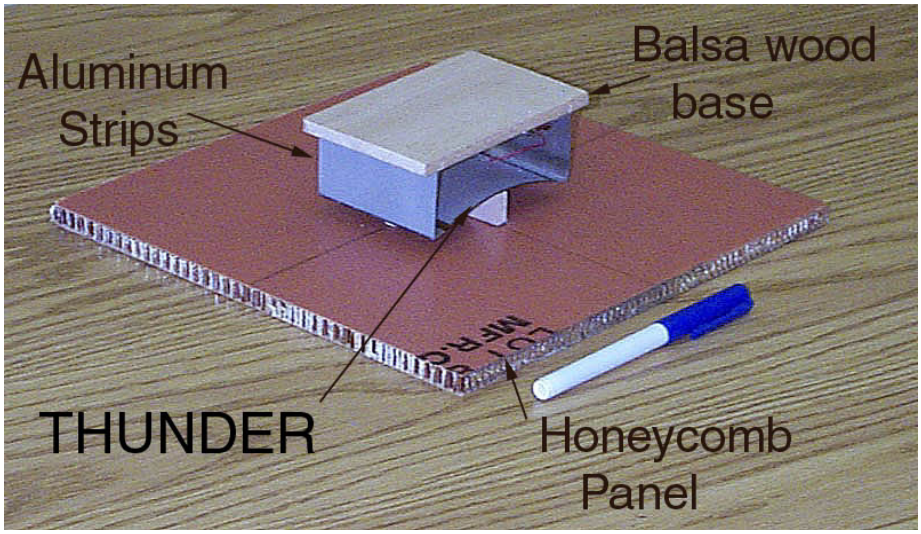

Figure 3.14 Tile prototype used for vibration isolation tests

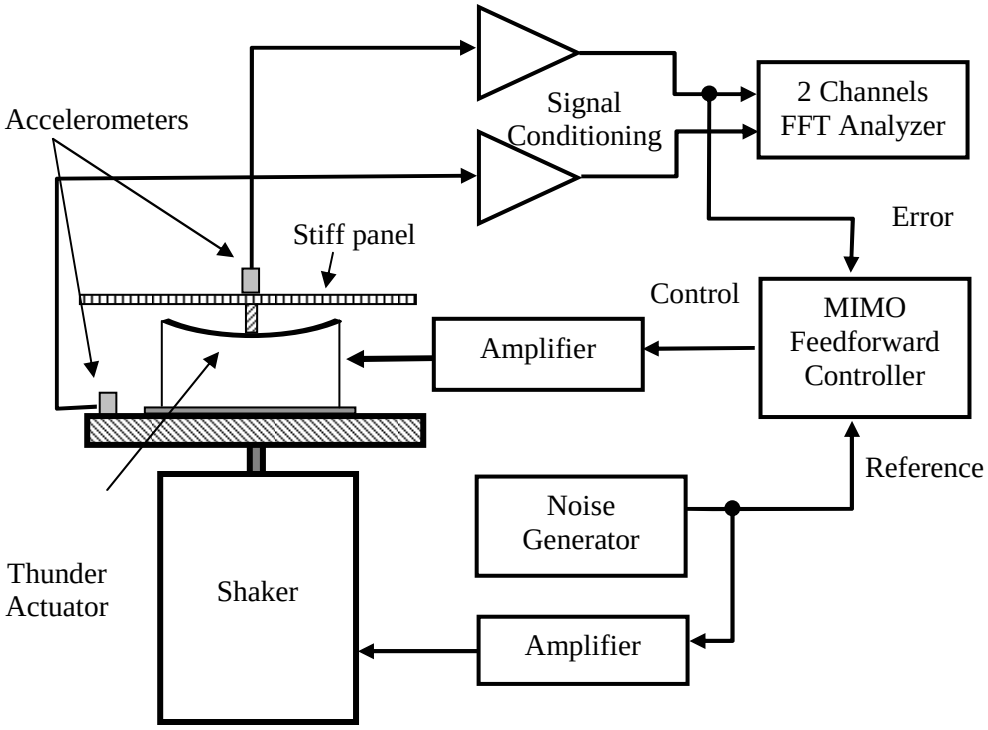

Figure 3.15 Schematic of instrumentation used for LMS-x feedforward control tests

The second test consisted in the implementation of a velocity feedback controller. The plant frequency response obtained by measuring of the tile acceleration divided by the input voltage is shown in Figure 3.18. Notice that the crossover frequency occurs at about 800 Hz and a feedback controller cannot be implemented without some form of plant compensation. In this simple experiment a fourth-order butterworth low-pass filter with cut-off frequency set at 400 Hz, was introduced in the feedback loop to attenuate the plant gain near the crossover frequency and avoid instability of the closed-loop caused by the high frequency dynamics of the actuator.

The negative velocity feedback controller was implemented by integrating the acceleration signal obtained from an accelerometer at the top of the tile. The resultant velocity signal is inverted and amplified for feedback into the actuator. The schematic of the experimental setup is presented in Figure 3.17.

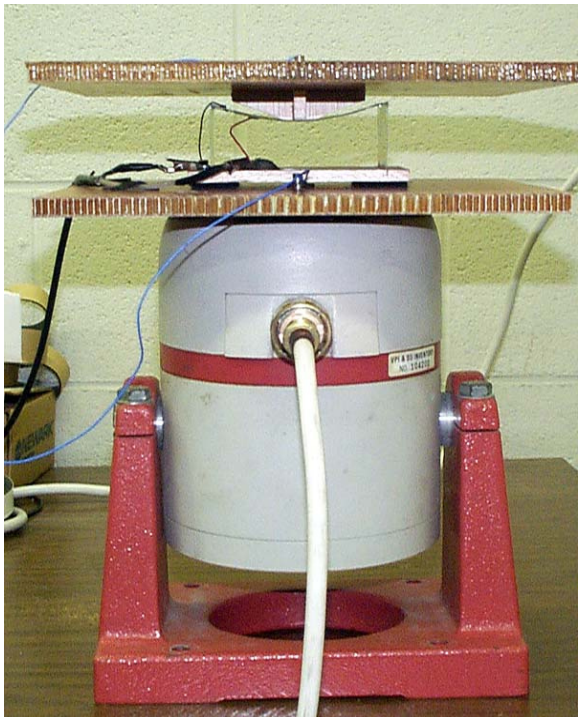

Figure 3.16: Experimental setup for the vibration isolation tests.

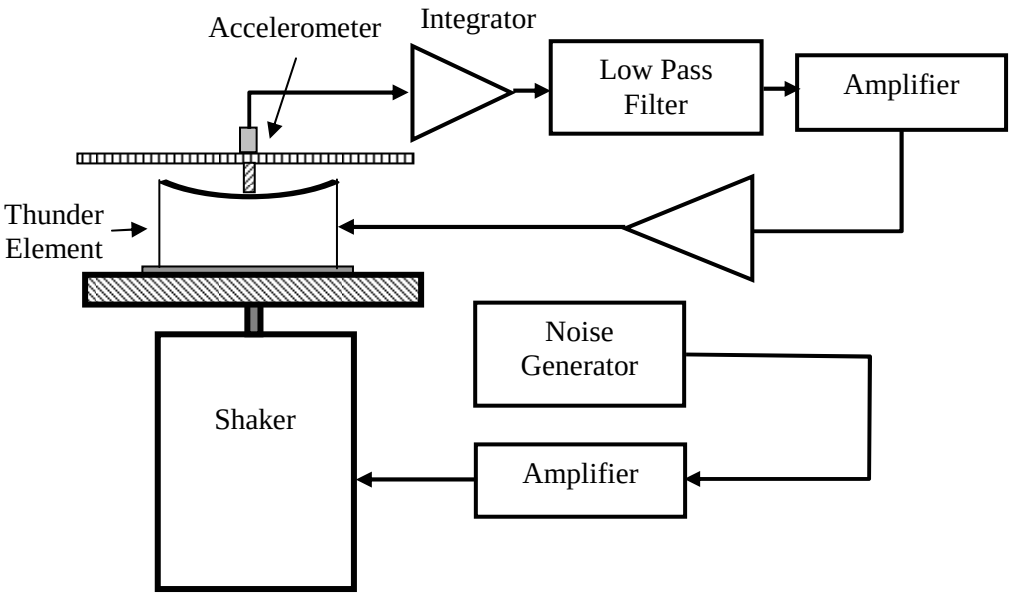

Figure 3.17 Schematic of instrumentation used for negative velocity feedback control tests

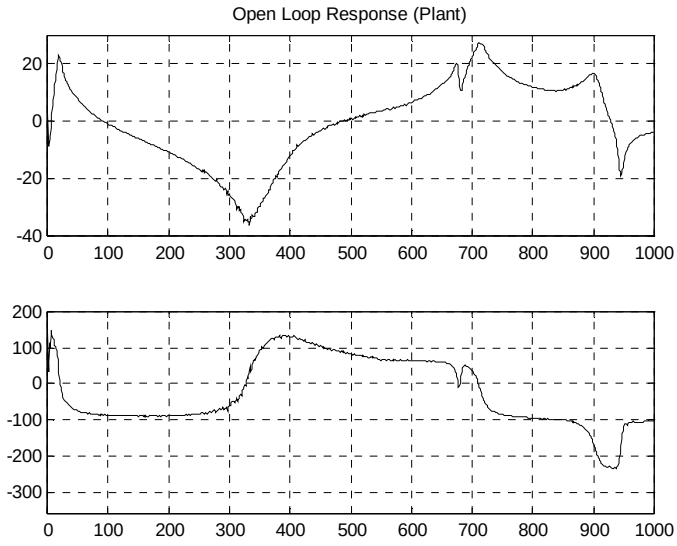

Figure 3.18 Open loop frequency response of the active tile prototype used for the vibration isolation tests

3.3.2 Vibration Isolation Results

The passive and active transmissibility of the system in for the feedforward and feedback control tests are shown in Figure 3.19 and Figure 3.20. The fundamental resonance of the tile-mount system is observed at 20 Hz. Above the resonance good passive vibration isolation was obtained.

In the feedforward control case, the amplification around the resonance frequency was eliminated and with the vibration of the tile reduced by about 15 dB in the entire frequency band.

The velocity feedback controller is very effective in minimizing the transmissibility at the fundamental tile-mount resonance. The performance of the feedback loop is peaks at the mass spring resonance of the tile and reduces at higher frequencies as the velocity decreases. The peak in transmissibility is reduced by about 16 dB with attenuation extending to about 100 Hz. It is also possible to observe some velocity amplification (spillover) at frequencies above 100 Hz. The amplification around 5 Hz is caused by the phase shift of the integrator circuit. The bandwidth of the controller could possibly be improved by the design of a more complex feedback controller.

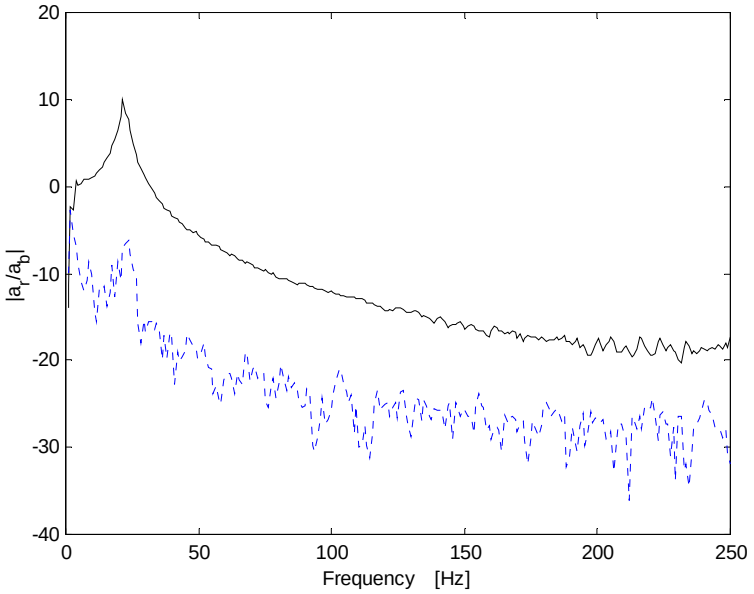

Figure 3.19: Experimental transmissibility results for the active-tile in the passive (solid trace) and active cases (dashed trace) using feedforward control.

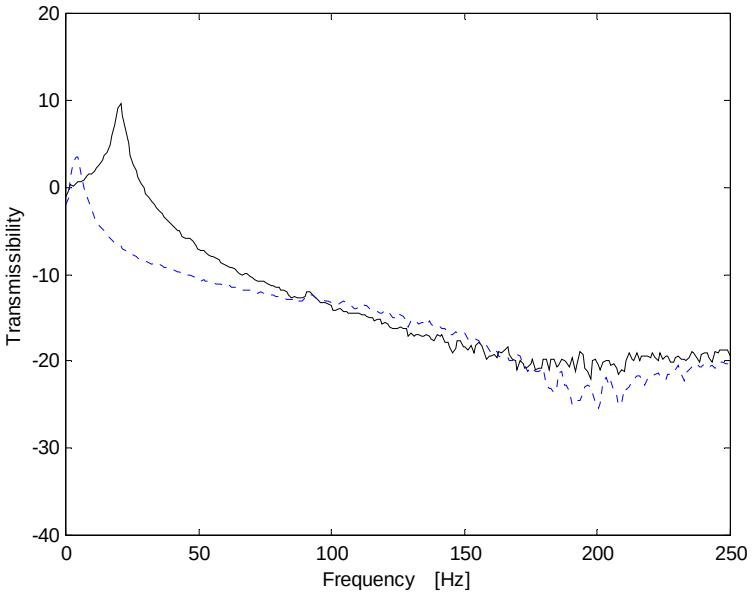

Figure 3.20: Experimental transmissibility results for the active-tile in the passive (solid

trace) and active cases (dashed trace) using velocity feedback control.

These results show the potential of the active-passive tile concept proposed in this work. In the next section the active tile concept is mounted on a flexible base and tested for its ability to reduce the sound transmission through the base plate. In this situation the tile vibration is coupled to the base structural vibration by the acoustic field between the tile and the base structure. The passive isolation of the tile now depends also of the stiffness of the air gap.

3.4 Active Control of Sound Transmission: Preliminary Experiments

This section presents the experimental setup, procedures and results of the testing of an active tile to control sound transmission through a rectangular plate. The controller used a filtered LMS-x feedforward algorithm implemented in a C40 DSP board. Results for tile acceleration and sound radiated power before and after control are presented. The feedforward controller is implemented using both an ideal reference case and realistic reference obtained from a microphone positioned close to the base plate. In addition, tests are performed for a single channel control, and two channels control in a coupled and decoupled controller. Finally, the tests are repeated for a stiffer active tile.

3.4.1 Experimental Setup

Figure 3.21 shows the actual active tile prototype used in the tests and a schematic of the experimental setup is depicted in Figure 3.22. In this setup a 1.6 mm thick aluminum plate is clamped in a 30 x 38 cm window between a reverberant and an anechoic room. The resonance frequencies of the clamped plate are given in Table 3.3.

A 29.5 x 37.5 cm honeycomb tile is mounted to the top of the clamped plate using 2 active-passive mounts as shown in Figure 3.22. The tile outer surface is flush with the

anechoic room wall surface leaving a 4.5 cm gap between the aluminum panel and tile internal surface. The gaps between the tile and the wall are sealed with compliant adhesive foam strips to avoid sound transmission via air leaks.

The tile consists of a composite sandwich plate, 6 mm thick, with carbon fiber faces and Nomex honeycomb sandwich core with surface density of 1 kg/m^2. The total weight of the tile and actuators is around 160 g. The first two flexible modes of the tile with free boundary conditions are experimentally identified to be 130 Hz and 337 Hz.

Table 3.3: Resonance Frequencies of Plate, Tile and Acoustic Cavity (in Hz)

Base plate	Tile	Cavity
113 (1,1)	40	0
198 (2,1)	130	452
258 (1,2)	337	556
334 (2,2)	417	725
336 (3,1)	518	913

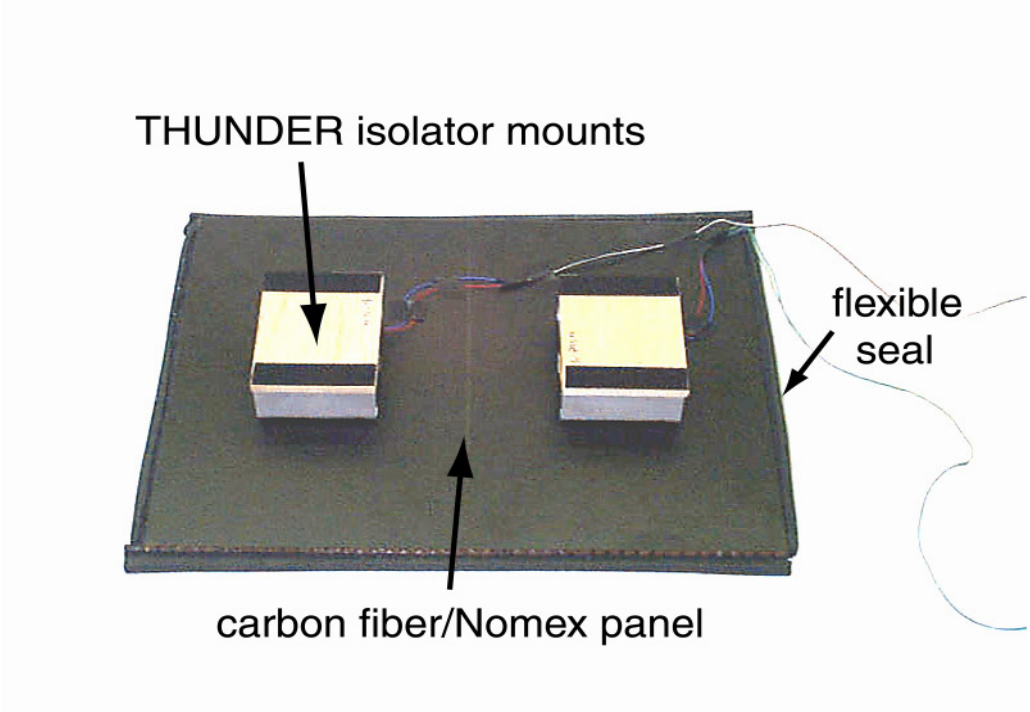

Figure 3.21: Active tile prototype for active sound transmission experiments.

A loudspeaker driven by an audio power amplifier fed with random noise signal limited from 20-400 Hz is positioned inside the reverberant room in front of the plate for generating the acoustic disturbance. A single microphone positioned in front of the loudspeaker is used to measure the incident sound power. This microphone can also serve as a reference signal for feedforward control tests. A foam barrier is placed around the disturbance speaker inside the reverberant room in order to attenuate the contributions of the reverberant environment on the disturbance and maximize the contribution of the incident plane wave.

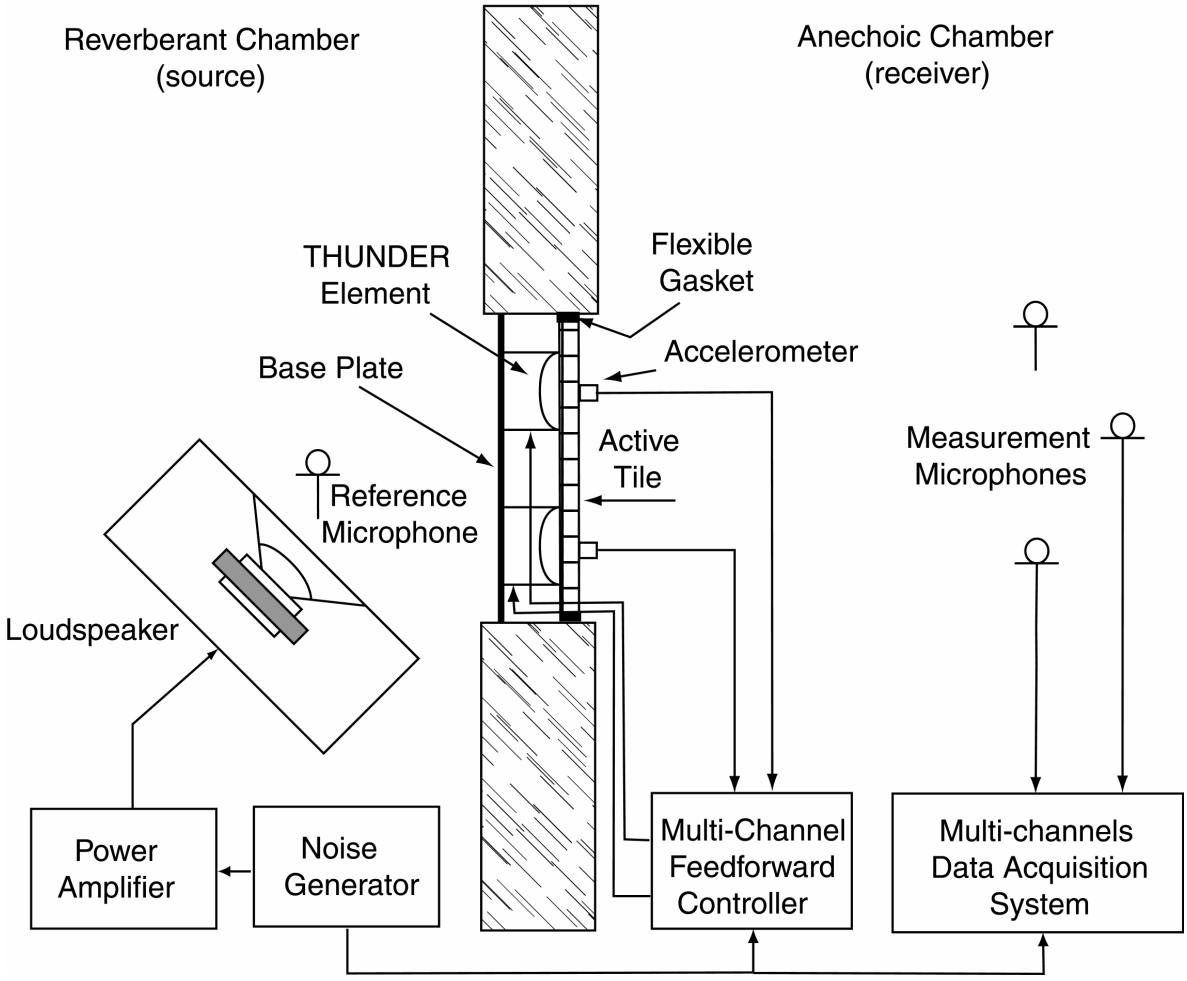

Figure 3.22: Schematic of experimental setup of transmission-loss test.

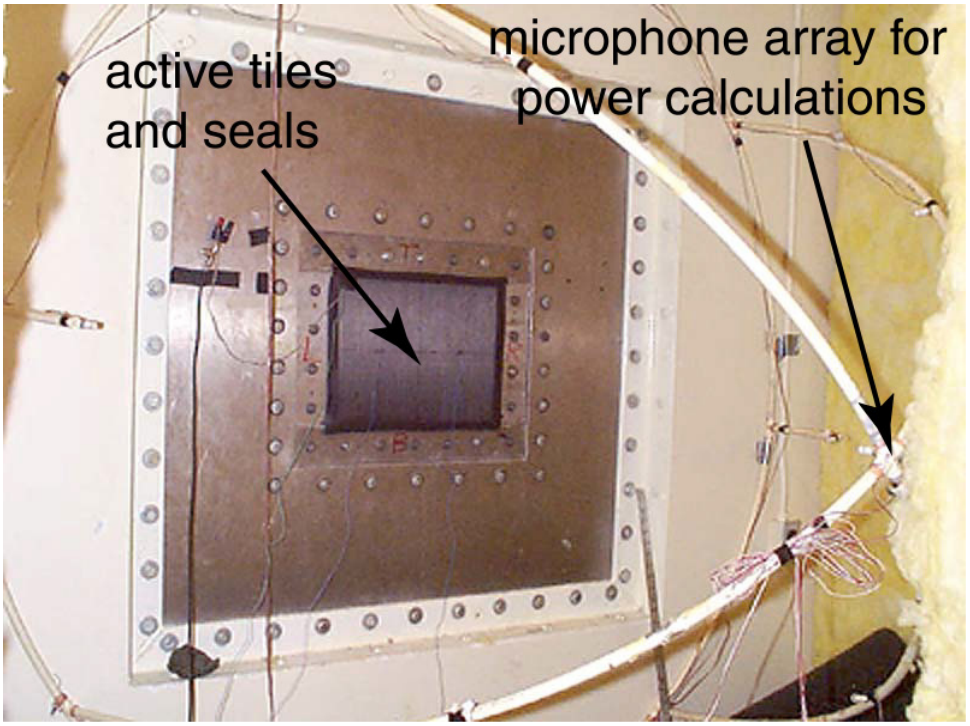

Figure 3.23: Active-tile mounted on clamped plate in wall of transmission loss test facility.

The transmitted sound is measured inside the anechoic room using an array of 9 microphones positioned in a hemispherical arrangement in the far-field of the plate radiation. The microphone signals are collected by a 16 channels DAQ system and referenced to the noise signal for computation of the radiated power. The details of the procedure for computing the total radiated sound power from the microphone pressure signals can be found in [61]. A picture of the experimental setup is shown in Figure 3.23.

3.4.2 Ideal Reference Feedforward Control Results

In this section, it is investigated the performance of the feedforward controller using an ideal reference. This means that the reference signal used for the feedforward controller was the obtained directly from the noise generator used to create the disturbance signal. The results of active attenuation obtained using an ideal reference, delayed by a few sample periods to ensure causality, are the best possible using a feedforward controller

and serve as benchmark for comparing to implementations using realistic reference signals.

Single Error Sensor Results

A SISO feedforward control system was implemented in a C40 DSP board. A single error accelerometer is attached at the center of the tile. The system was setup with a sampling rate of 3000 Hz. The FIR filter used to model the secondary path was set as 100 coefficients and the FIR control filters were set to 500 coefficients. The use of signal of a microphone placed between the disturbance speaker and the base plate as the reference signal will be shown later. The disturbance and reference signals were band limited to 20-400 Hz. In addition a 4th order low-pass filter with cut-off frequency of 1000 Hz was used before the actuator as a reconstruction filter.

After the secondary path, from the actuator to the error sensor, is identified the disturbance is turned on and the control filter adaptation starts. Initially a relatively larger convergence coefficient μ is used and after convergence of the filter coefficients is reached, the value of μ is reduced. The acceleration of the tile and the microphone array signals are then measured for control on and control off cases.

Figure 3.24 shows the active attenuation of the tile acceleration, which is the difference between the acceleration of the tile at the error accelerometer location with and without control. Note that the error sensor is attached to the center of the tile. An overall active attenuation of 12.5 dB is achieved. Good active reduction (about 10 x) of the tile velocity from 100 Hz to 300 Hz. No attenuation of the tile velocity is observed around 330 Hz probably due to vibration modes of the base plate at this frequency. Further attenuation of the tile velocity occurs above 340 Hz to about 500 Hz.

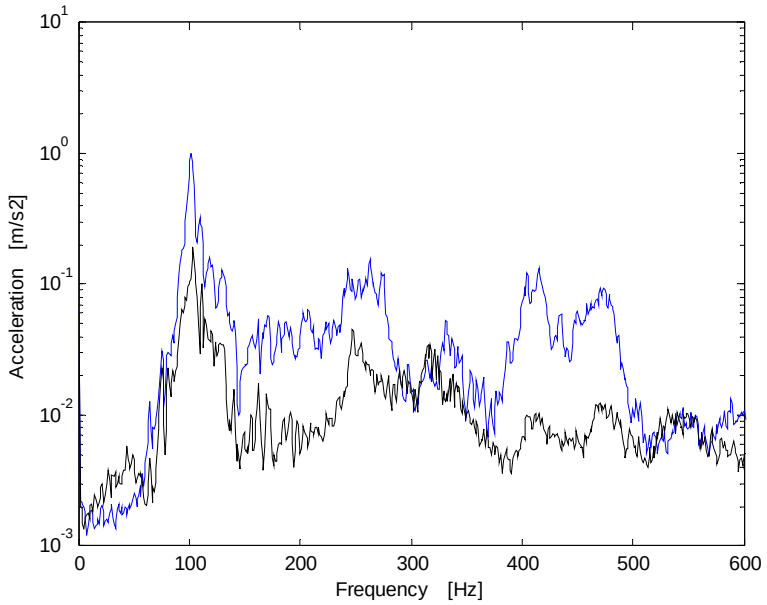

Figure 3.24: Experimentally measured acceleration for with single accelerometer at the center of the tile. (a) blue trace: tile without control and (b) black trace: tile with active control.

The sound power radiated by tile with control on and control off is shown in Figure 3.25 together with the plots of the sound power radiated by the base plate without the tile. A total attenuation of 15 dB was measured, with 7 dB of passive attenuation and 8 dB of active attenuation. Good broadband attenuation of the sound radiated power was obtained for the frequency band of 100-250 Hz and 350-400 Hz. Good correspondence between velocity amplitude and radiated sound power is observed to about 300 Hz, indicating that the tile behaves like a piston radiating in a baffle. Above 300 Hz the flexible modes of the tile imply that a reduction in the velocity of the tile does not correspond to a reduction in sound radiation.

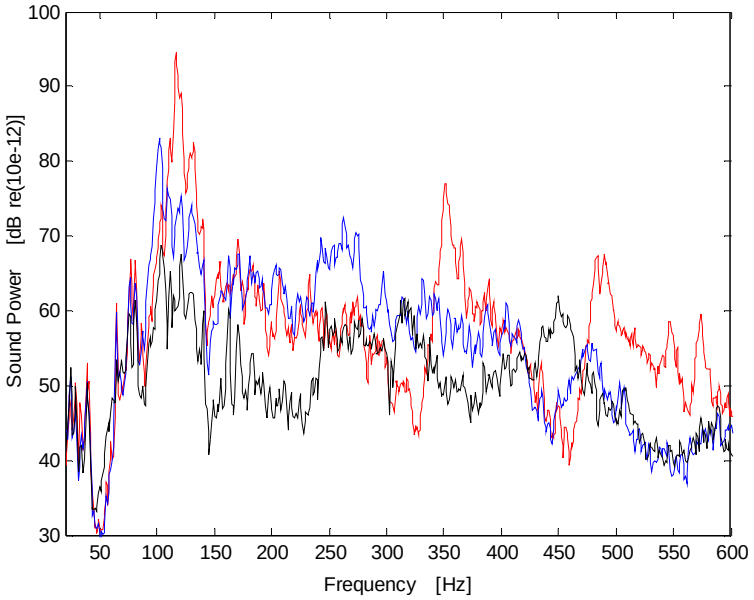

Figure 3.25: Experimentally measured total sound power radiated: single error sensor at the center of the plate. (a) red trace: base plate without tile. (b) blue trace: plate-tile without control and (c) black trace: plate-tile with active control.

Two-Channel Feedforward Controller

If a single error accelerometer located at the center of the tile is used, the control system does not attenuate any of the rocking modes of vibration of the tile, because of the nodal line of the modes passing through the center of the tile. The importance of controlling the rocking modes depend on the size of the panel and the frequency range of interest [47,48]. A rocking mode correspond to an acoustic dipole which starts radiating as efficiently as a piston mode for $ka \approx 1$, where k is the acoustic wavenumber and a is the largest dimension of the radiating tile. In this section, a single reference multi-output feedforward LMS-x controller is used to minimize the tile velocity, which allows controlling one of the rocking modes of vibration of the tile, along the line where the mounts are attached. For the tile in this experiment $ka=1$ at 144 Hz.

The system was set with a sampling frequency of 3000 Hz. 100 coefficients were used for the secondary path identification filters and 500 coefficients for each of the control

filters. Once again the disturbance signal is used as the reference. After the four secondary paths are identified, the disturbance is turned on and the control filter adaptation starts. Initially a relatively larger convergence coefficient μ is used and after convergence of the filter coefficients is reached, the value of μ is reduced. The acceleration of the tile (error signals) and the microphone array signals are then measured for control on and control off cases.

Figure 3.26 shows the acceleration of the baseline plate (without the tile on the top) and of the tile in the passive (without control) and active (with control) cases. For this case, 15.7 dB of overall active attenuation of the tile acceleration was obtained, compared to 12.5 for the single channel control case (see Figure 3.24). The plot shows that active control can effectively reduce the acceleration of the tile at the mount positions for frequencies up to 500 Hz, except around the resonance of the tile at about 330 Hz.

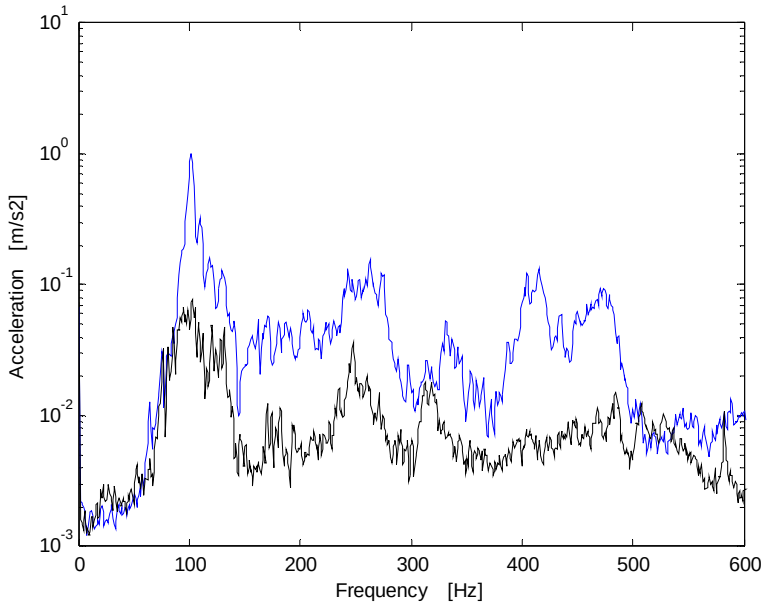

Figure 3.26: Experimentally measured tile acceleration: one sensor at each actuator position and coupled controller. (a) blue: control off and (b) black trace: control on

Figure 3.27 shows the transmitted sound powers for the baseline plate and for the plate-tile system in the passive and active cases. Good attenuations up to 20 dB for the

entire frequency band of interest (up to 400 Hz) were observed for the active case. An overall attenuation of 16 dB relative to the baseline plate was obtained, with 9 dB active attenuation and 7 dB of passive attenuation of the sound power transmitted through the plate. Note that the overall active attenuation results obtained for the 1 x 2 x 2 controller were about 1 dB better than the attenuation obtained for the 1 x 1 x 1 controller, with better performance particularly around 250-300 Hz. This seems to indicate that the rocking modes of vibration of the tile have contribution to the sound radiated by the tile in this frequency range.

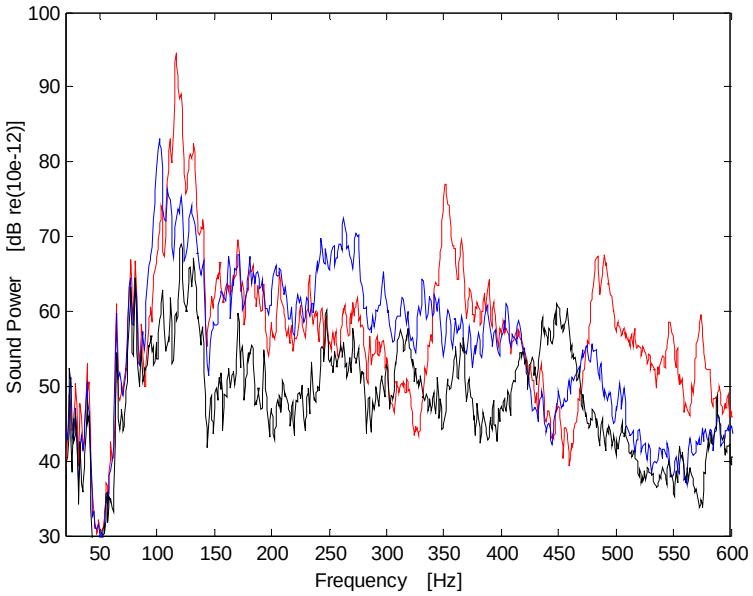

Figure 3.27: Experimentally measured total sound power radiated: one sensor at each actuator position. (a) red trace: base plate without tile. (b) blue trace: plate-tile, control off and (c) black trace: plate-tile, control on.

Figure 3.28 and Figure 3.29 show the performance of the tile with two error sensors for the case where the two the control channels are decoupled (decentralized control). This means that each actuator is controlled by an independent SISO controller that minimizes the error signal coming from the sensor collocated with the actuator. The decoupled multi channel controller is setup by setting the off-diagonal terms of the secondary paths

transfer function matrix equal to zero. This is performed during a step of the controller software setup. The results for the two channel decoupled controller show degradation in the performance of the system, suggesting that the tile active mounts are physically coupled. The acceleration of the tile at the error sensor position is actively attenuated by 5.6 dB while the total active attenuation of the sound power radiated by the tile is 3 dB.

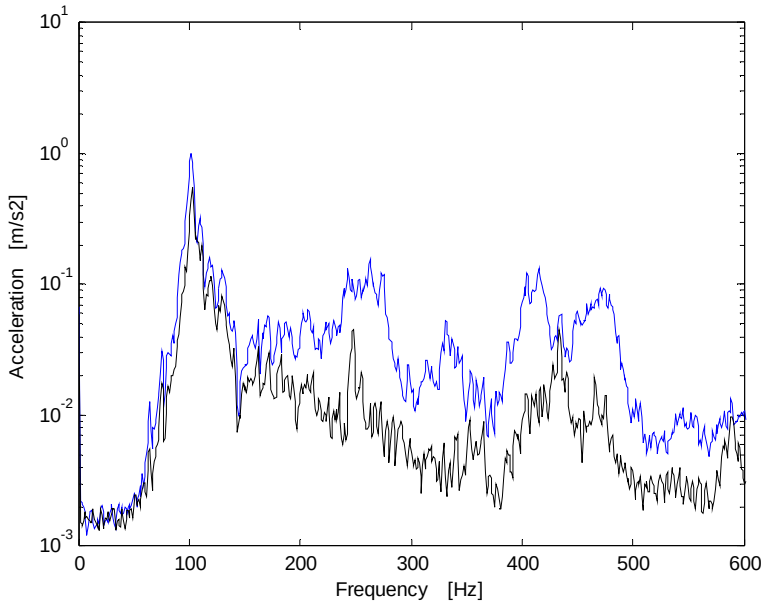

Figure 3.28: Experimentally measured tile acceleration, control with 2 decoupled control channels. (a) blue trace: control on and (b) black trace: control off (attenuation of 5.6 dB)

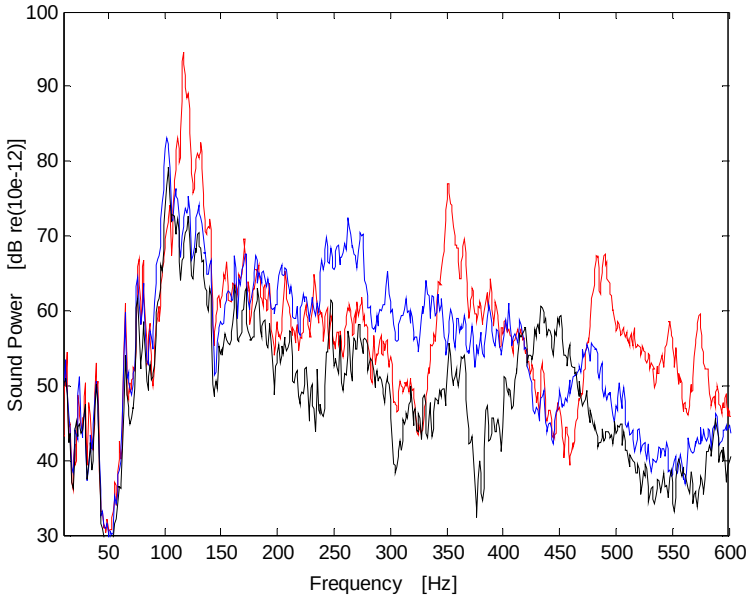

Figure 3.29: Experimentally measured total sound power radiated. 2 error sensors decoupled. (a) red trace: base plate without tile. (b) blue trace: plate-tile, control off and (c) black trace: plate-tile, control on.

3.4.3 Real Reference Feedforward Control Results

The previous section presented feedforward control results obtained using the disturbance signal as the reference signal for the feedforward controller. In practice, the implementation of a feedforward control system will require the reference signal to be obtained either from the vibration of the base structure or the external acoustic field.

The reference signal has influence on the control system performance [64]. First the delay for the disturbance signal to propagate from the reference sensor location to the controller location has to greater than the electronic delay through the control system, including the antialiasing filter, A/D interface, signal processing, D/A converter, reconstruction filter and delays associated with the sensor and actuators. In other words, the reference has give time advanced information about the disturbance. After the reference signal is picked up by the reference sensor, the control has a limited amount of

time to compute the control signal. If this electrical delay is longer than the propagation delay from the reference sensor to the actuator location, the system performance is substantially degraded. This is the condition of causality and needs to be fulfilled for realizable controllers.

Second, the following characteristics regarding the quality of the reference signal are important: coherence between reference and error signals; feedback from the control signal to the reference signal; and the spectral content of the reference signal. For a SISO system, the maximum possible fractional reduction in the power spectrum of the system error signal is given by:

$$\frac{S_{ee}(\omega)_{controlled}}{S_{ee}(\omega)_{uncontrolled}} = 1 - \gamma^2(\omega)$$

where $S_{ee}(\omega)_{controlled}$ and $S_{ee}(\omega)_{uncontrolled}$ are the power spectra of respectively the controlled and uncontrolled error signals and γ^2 is the coherence coefficient between the reference and the error signal. Note that $S_{ee}(\omega)_{uncontrolled} = S_{dd}(\omega)$, which is the power spectrum of the disturbance signal *d(n)*. For best attenuation, γ^2 has to be very close to unit for frequencies where there is disturbance energy. For example, a value of 0.90 is required for 10 dB of attenuation and a coherence of 0.99 is necessary for 20 dB of active noise attenuation.

For the experimental setup considered in this section a vibration reference signal obtained from the vibration of the base structure does not work because of the relative low mobility of the base plate. In this case there will be a feedback of the control signal back to the base plate vibration, which can lead to system instability [64].

A practical reference signal was obtained from a B&K microphone placed near the base plate structure, and in front of the loudspeaker that was generating the disturbance acoustic field. A large sheet of 3 inches thick acoustic foam was placed around the microphone in an attempt to minimize the influence of the reverberant sound field on the

microphone signal, which could degrade the coherence.

The acceleration of the tile before and after control is applied is presented in Figure 3.30 for the ideal reference and for the microphone signal as a reference. The results show an overall 5 dB of active attenuation for real reference case and 12 db for ideal reference. It is observed that although the control performance is less than that obtained with the ideal reference as expected because of the additional time delay and worse coherence between the error signal and the reference signal, it is still possible to obtain significant attenuation of the sound transmission with the active tile using a microphone near the base structure for providing a reference signal.

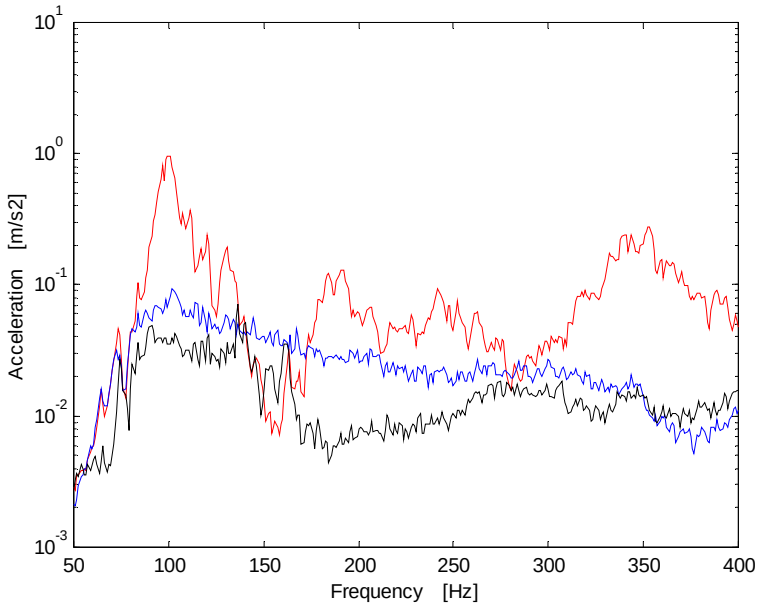

Figure 3.30: Experimentally measured tile acceleration using a microphone as the reference sensor: a) red trace: control off b) blue trace: control on and microphone reference c) black trace: control on and ideal reference

3.4.4 Effect of Increasing the Tile Stiffness

In this section results are presented for the active control of sound transmission through a plate using a stiffer tile. The experimental setup and procedure is the same employed in

the tests discussed in the previous section. The tile used in the experiments is the same carbon-fiber/Nomex sandwich tile but now with thickness of 1cm. The total weight of the tile increases from 115 grams of the 6mm thick tile to 160 grams. This increase in weight is solely due to an increase in the thickness of the Nomex core.

Figure 3.31 presents the acceleration of the tile in the passive case and for the active case when a **SISO feedforward controller** is employed and the error accelerometer is attached to the center of the tile, with 16.2 dB of active attenuation of the acceleration. Figure 3.32 shows the total sound power radiated by the baseline plate and by the tile in the passive and active cases and SISO control. A total of 17.4 dB of attenuation is obtained, 11.5 dB active. Comparing this result with the results shown in Figure 3.36 we observe that a SISO controller achieves similar performance levels to the levels of performance obtained with two SISO controllers. This indicates that the rocking mode of the tile does not have significant contribution to the total sound radiated power for this system configuration.

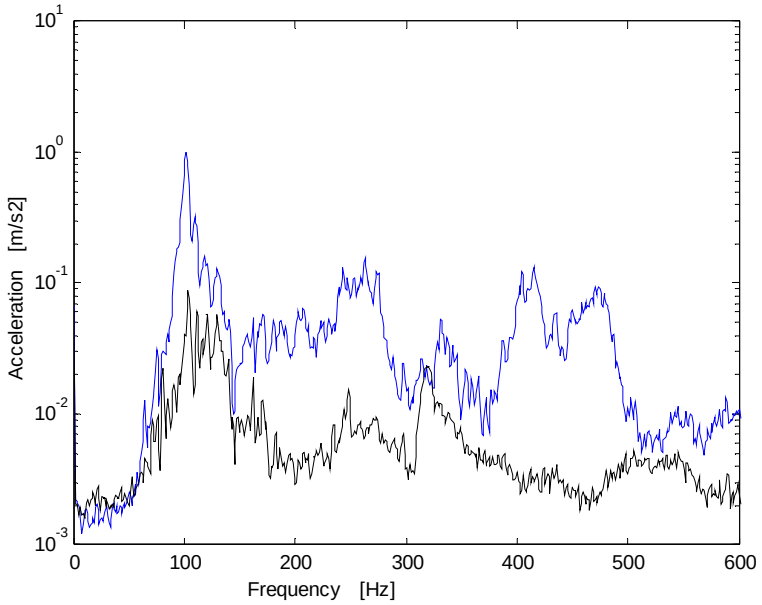

Figure 3.31: Measured tile acceleration for 10 mm thick tile, single channel control and error sensor tile center. (a) blue trace: control off and (b) black trace: control on

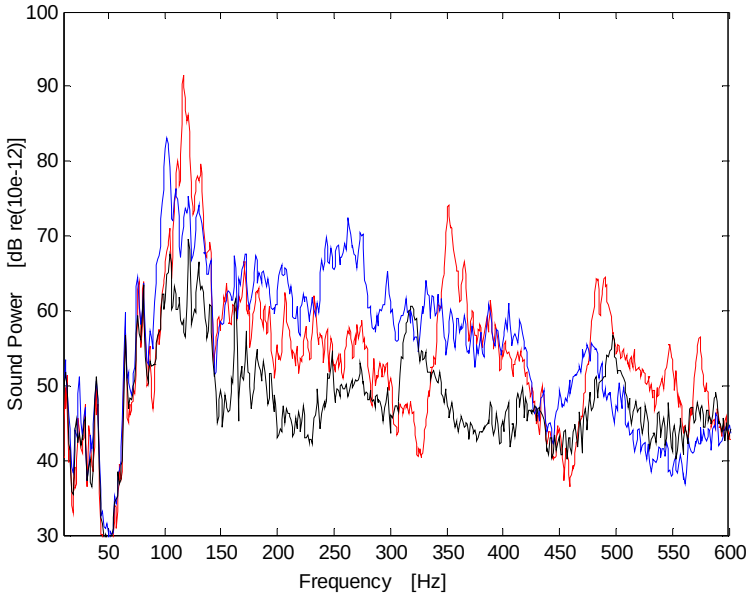

Figure 3.32: Experimentally measured total sound power radiated: single error sensor at the center of the plate. (a) red trace: base plate without tile. (b) blue trace: plate-tile, control off and (c) black trace: plate-tile, control on

Next, a **coupled two-channel controller** is used to minimize the acceleration signals obtained from two small accelerometers attached to the tile surface at the mounts locations. The controller was set with a 3000 Hz sampling rate and used 100 coefficients filters for the secondary paths and 500 coefficients for the optimal control filter. The acceleration signal obtained with the left accelerometer (the right accelerometer gives a similar result) before and after control is applied is shown in Figure 3.33. An overall acceleration attenuation of 17.2 dB is obtained throughout the frequency band of control. When this plot is compared with the plot shown in Figure 3.26 for the 6 mm thick tile, we observe that the use of a stiffer tile allows better minimization of the tile acceleration up to higher frequencies. The lower reduction of the peak acceleration can be attributed to the larger mass of the tile that would imply in the necessity of higher control authority by the actuators. Figure 3.34 shows the total sound power radiated by the baseline plate, and by the passive and active tile. A total attenuation of 18.7 dB is obtained, 12.8 dB of active and 5.9 dB of passive attenuation.

The use of a stiffer tile allows the control of sound transmission to be extended up to 500 Hz, in contrast to roughly 300 for the 6mm tile.

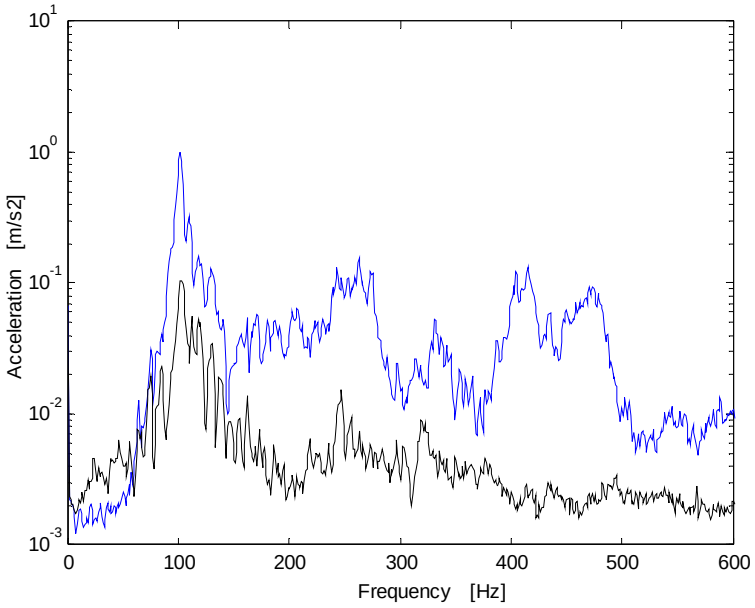

Figure 3.33: Experimentally measured tile acceleration for 10 mm thick tile using two-channel controller: (a) blue trace: control off and (b) black trace: control on.

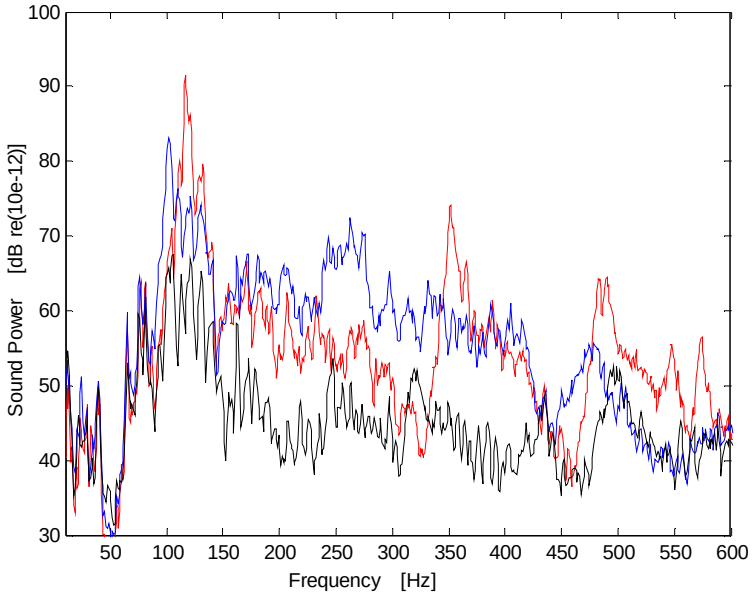

Figure 3.34: Experimentally measured total sound power radiated by tile: two channels controller. (a) red trace: base plate without tile. (b) blue trace: plate-tile control off and (c) black trace: plate-tile, control on.

Figure 3.35 shows the acceleration of the tile when a **two-channel decoupled controller** is employed. In this setup, each actuator control input is obtained using information coming only from the accelerometer collocated with the actuator. This setup is obtained by configuring the secondary path filter matrices in the controller software by nullifying the value of the off-diagonal terms. The plot shows that a decoupled controller can successfully reduce the acceleration of the tile from the low frequencies up to 300 Hz with 16.7 dB of overall reduction. This should be contrasted with the results obtained with the 6.0 mm tile that is shown in Figure 3.29 where the controller could not minimize the tile acceleration at frequencies around 100 Hz. The lack of control effectiveness in the case of the 6.0 mm tile is explained by the presence of a tile flexible mode around 100 Hz, that couples the control channels. In the case of the 10.0 mm thick tile, the first flexible mode occurs at 240 Hz, and the control channels are effective decoupled at lower frequencies.

Figure 3.36 shows the total sound power radiated by the baseline plate and by the tile in the passive and active cases. Good active reduction of the sound radiated power is obtained through the entire frequency range of control and the levels of reduction are similar to those obtained in the case of the coupled controller: 18.4 dB total, 12.5 dB active.

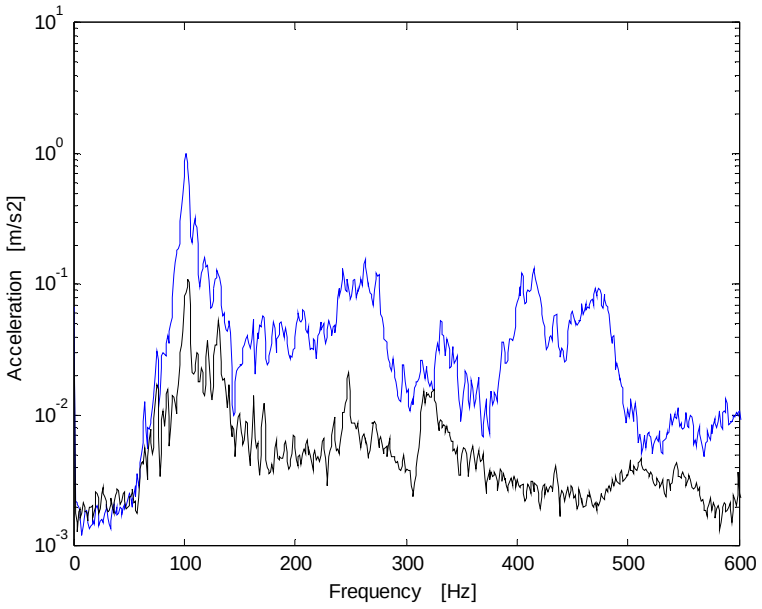

Figure 3.35: Experimentally measured tile acceleration for 10 mm thick tile using two channels decoupled control. (a) blue trace: control off and (b) black trace: control on

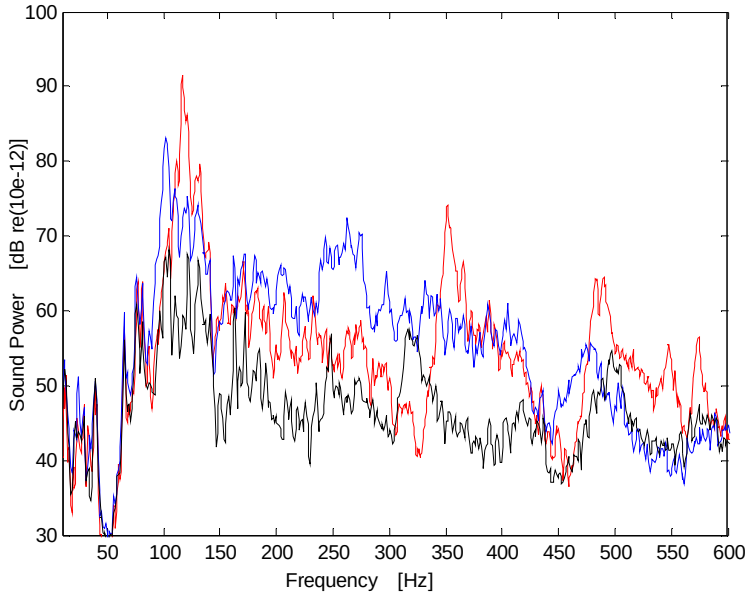

Figure 3.36: Experimentally measured total sound power radiated: two channels decoupled control. (a) red trace: base plate without tile. (b) blue trace: plate-tile, control off and (c) black trace: plate-tile, control on

3.4.5 Estimation of the Sound Radiated Power via Velocity Measurements

The normal velocity of the 10mm thick tile was measured with a laser vibrometer at 30 points distributed along the tile surface area. The measured velocity data was used to estimate the total sound power radiated by the tile with control on and control off, for the feedforward control with single error sensor and two error sensors cases. The active attenuation estimated from the velocity measurements was respectively 8.2 dB and 8.8 dB. The estimated active control performance using surface velocity measurements is about 2 dB smaller than the performance estimated based on sound radiated power measurements with the microphone array. This good agreement between the sound power estimated with velocity measurements and pressure measurements shows that the measurement of the surface velocity of the tile can provide a good prediction of the total sound radiated power with and without control. It also indicates that the sound radiated through the sealing gaskets that would not be taken into account in the velocity

measurements, is insignificant assuming that a good acoustic seal is achieved. The estimation of the sound radiated power based on surface velocity measurements was used in the experimental setup described in the next Chapters.

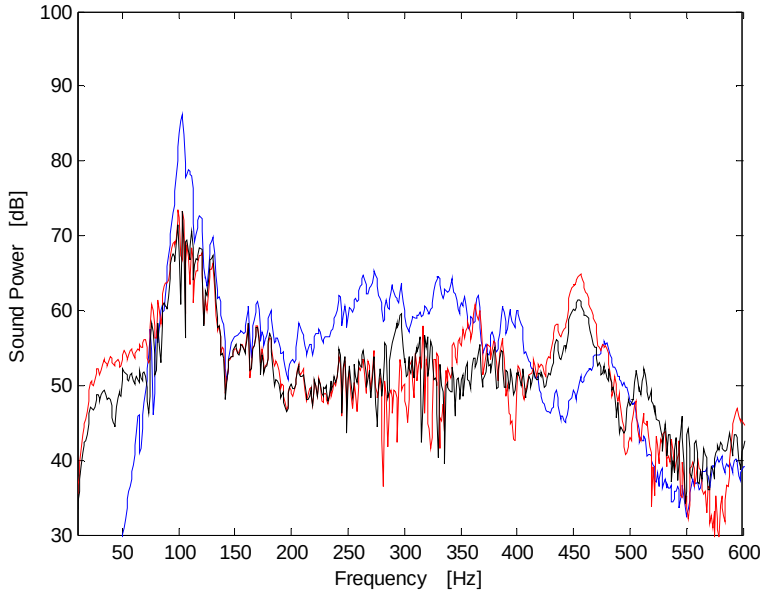

Figure 3.37 - Experimentally estimated total sound power radiated based on velocity measurements. (a) blue trace: tile with control off. (b) black trace: tile with control on and single sensor at the tile center and (c) red trace: tile with control on and 2 error sensors one at each actuator position

3.5 Summary

This chapter the experimental implementation of the active tile approach was carried out and active-passive tile prototypes were built. The tiles were made with lightweight stiff composite panels and the mounts were implemented with *Thunder* piezoelectric actuators. It was shown possible to take advantage of both the passive and active effects provided by the *Thunder* actuators, which have the additional characteristics of being compact, lightweight and have large stroke capabilities. A prototype tile with Thunder

mount was shown to have good passive vibration isolation characteristics. In addition both feedback and feedforward control were implemented and significant active vibration isolation performance was demonstrated.

The application of the active tile approach in controlling sound transmission was demonstrated for the case of a double-panel partition. A single active tile was designed and mounted over an aluminum plate clamped in window between two acoustic chambers. The sound power radiated by the baseline (bare) plate, for the passive tile and for the active tile cases was computed. In the case of the active tile, a feedforward control approach using a filtered x-LMS algorithm was employed. Both an ideal reference (disturbance generator signal) and a real reference signal (microphone on the disturbance sound field) were implemented with success. In addition, it was shown that increasing the stiffness of the honeycomb tile, by increasing its core thickness, could extend the bandwidth of effective control. Future work could include the minimization of the tile mass per unit area, which can be achieved by proper optimization of the core material density and thickness of the core and skin layers [72]. The active sound power radiation suppression results obtained in the transmission loss tests are summarized in Table 3.4.

Table 3.4: Active attenuation results for 6mm and 10mm thick tiles [dB]

	6mm tile		10mm tile	
	Velocity	Radiated Power Active/Total	Velocity	Radiated Power Active/Total
Single Channel	12.5	8 (15)	16.2	11.5 (17.4)
Two-channels coupled	15.7	9 (16)	17.2	12.8 (18.7)
Two-channels decoupled	5.6	3 (10)	16.7	12.5 (18.4)

Chapter 4

4 Active Control of Sound Transmission

The active tile approach is a potential solution for the control of sound transmission through large partitions when the use of an ASAC MIMO control system is impractical. In this Chapter a new experimental setup is used for investigating the use of active-passive tiles to control sound transmission. This second experimental setup is different from the experimental setup used in the last Chapter (section 3.4) in that it better approximates the dynamics of large, low mobility systems where the active tile approach might be used. A larger and heavier plate is used as the base structure and a larger acoustic cavity is created between the tile and the base structure approximating better the system dynamics of the target application. For this larger base structure with relatively low mobility it is expected that the lightweight active tiles do not modify the dynamic behavior of the structure. This low mobility base structure also allows the application of skyhook damping in a similar fashion to that used for active vibration isolation in base excited systems. In addition, a low mobility base structure allows that an accelerometer placed on the base structure be used as reference sensor in feedforward control systems since there is not a feedback path from the control forces to the reference signal.

The same experimental setup is used for a single active-passive tile, as presented in this Chapter and a multiple (four) active-passive tile system (see Chapter 5) allowing direct comparison of the performance of the systems and assessing the effects of inter-tile coupling dynamics on the system performance. This Chapter presents the results for the single tile system. Initially, a SISO feedback controller is designed and used to attenuate the tile velocity. Then a feedforward control system is implemented for the cases of an ideal and a real reference signal. Similar control systems with decentralized implementation are used in Chapter 5.

4.1 Experimental Setup

The experimental setup described in this section is illustrated in Figure 4.1. The base structure consists of an *80 cm x 60 cm x 0.635 cm* aluminum plate mounted in a metal frame in a simply supported configuration by bonding its edges to thin steel shims. The bottom end of the metal shim was fixed to a rigid metal frame as illustrated in Figure 4.2. The metal frame was bolted down to a large wood table (see Figure 4.2 and Figure 4.1). To check if the simply supported boundary conditions were achieved successfully, the resonance frequencies of the plate were measured with a modal hammer test and compared to analytical results obtaining good agreement as shown in Table 4.1. A *1.2 m x 1.6 m* wood baffle was placed surrounding the plate as shown in Figure 4.3 and another baffle with a rectangular window was positioned on top of the base panel creating a double wall type structure. The tiles are placed in the baffle window on top of the plate, as illustrated.

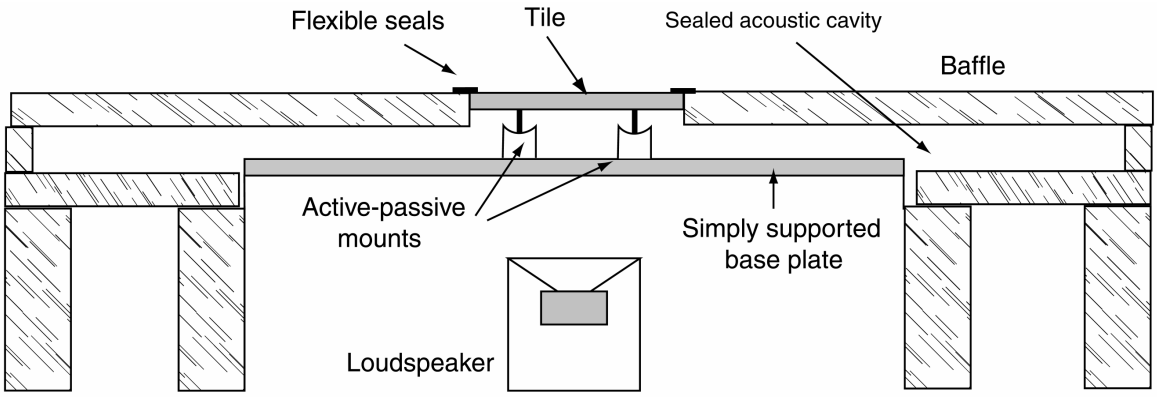

Figure 4.1: Cross section view of the experimental setup showing the simply supported base plate and double wall construction.

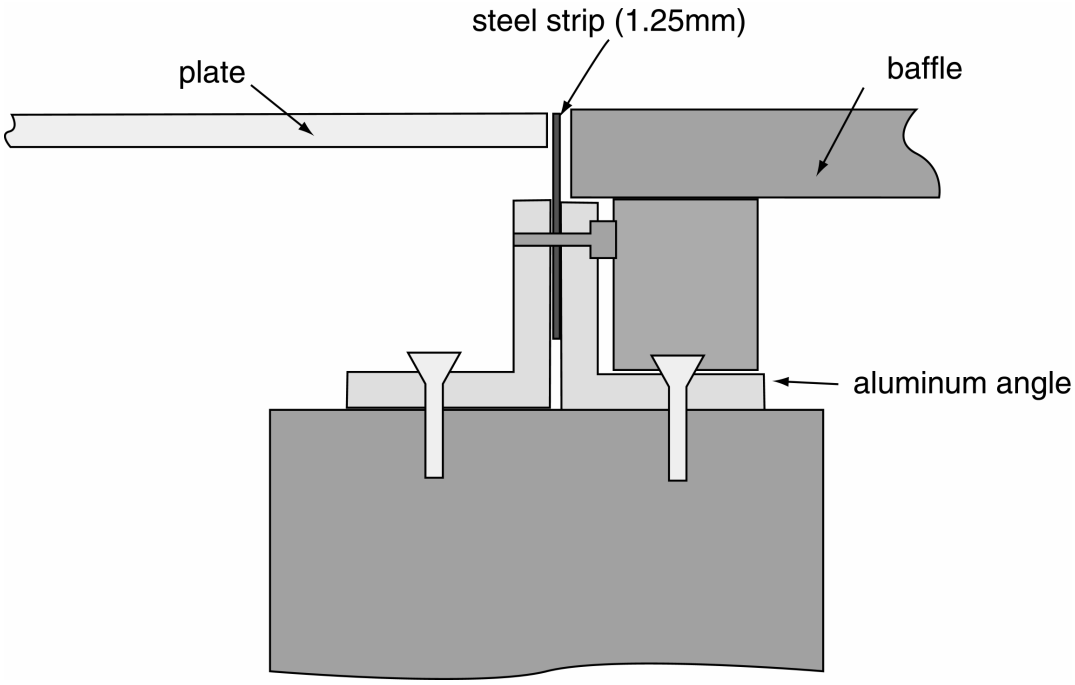

Figure 4.2: Detail of the test rig showing how the aluminum plate was mounted with its edges attached to steel strips to achieve simply supported boundary conditions.

Table 4.1: Resonance frequencies of the base panel

Analytical			Experimental		
m	n	f_r Hz	m	n	f_r Hz
1	1	66	1	1	68
2	1	144	2	1	149
1	2	190	1	2	210
2	2	272	2	2	315
3	1	267	3	1	272
3	2	396	3	2	343
1	3	397	1	3	392
4	1	452	4	1	424
2	3	576	2	3	590
4	2	602	4	2	621

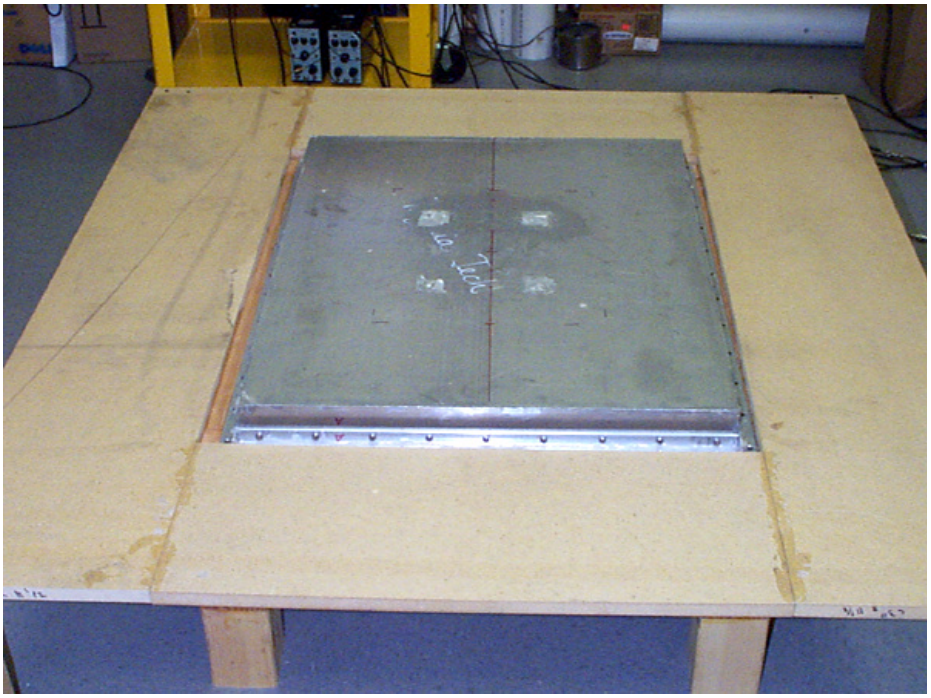

Figure 4.3: Simply supported aluminum frame used for the multi-tiles tests shown mounted on wood panel baffle

The tile used in the experiments consisted of a carbon-fiber/Nomex honeycomb sandwich panel with dimensions of *18cm x 15cm x 1.0cm*. The tile has 2 active-passive mounts attached as shown in Figure 4.4. Each tile actuator has a *2.5cm x 2.5cm* stiff pad on its base to reduce the contact area and was attached to the plate with high strength double-sided tape. After the tiles are attached to the base plate, the air gaps around the tiles were sealed with a self-adhesive strip of compliant rubber. The first vibration mode of the tile was measured to occur at 800 Hz and thus the tile can be considered to behave as a rigid panel up to this frequency.

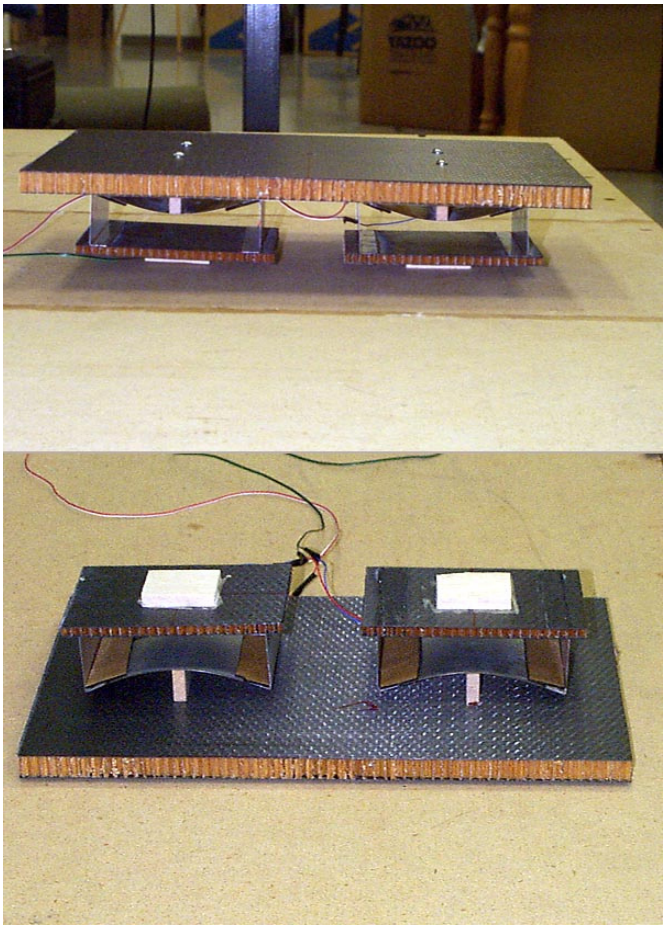

Figure 4.4: Honeycomb sandwich tile with two active mounts

The active tile prototype mounted on the base plate and surrounded by the MDF baffle is shown in Figure 4.5. The single error accelerometer is seen in the center of the tile. The photo also shows nine reflective strips attached to the tile and that are used for tile surface velocity measurements that were performed using a laser vibrometer.

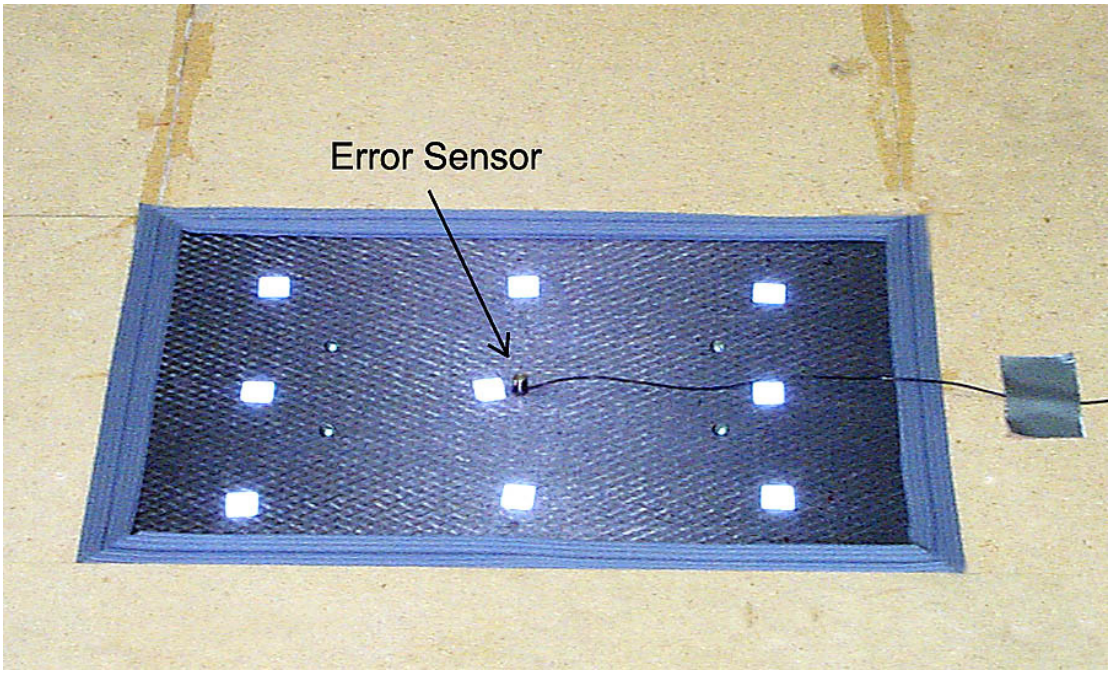

Figure 4.5: Single active tile prototype mounted in a baffle with error accelerometer located at the center of the tile

4.2 Feedback Control

As discussed earlier, the control objective of the active tile control approach is to reduce the normal velocity of the tile, which is the same as isolating the tile from the base structural vibration by applying active control signals to the active mounts. The low mobility of the simply-supported plate used as the base structure in this experimental setup, allows the implementation of skyhook damping control in a similar fashion to that used in active vibration isolation of base excited systems, where the actuator control forces reacting between the tile and base do not affect the response of the base.

It is well known that soft passive mounts provide good vibration isolation characteristics for frequencies above the resonance frequency created by the mass of system being isolated and the stiffness of the mount. Note that, in the case of a surface treatment using active tiles, the resonance frequency of the tile piston mode depends on the stiffness of

the air trapped in the gap between the base structure and the tiles. In addition, in order to obtain good high frequencies isolation, the damping of the mount should be small, which results in amplification of the vibration of the equipment at the resonance of the mass-spring system.

One method of improving the vibration isolation performance of the system around the resonance frequency, while keeping the good passive isolation performance at high frequencies, is to use the “skyhook damping” method, as discussed in Chapter 3. In this approach the feedback controller generates a control signal proportional to the velocity of the tile. Ideally, this force is applied between the system to be isolated and an inertial ground, which is then equivalent as having a passive damper element between the system and the ground (so the origin of the term “skyhook damping”). In this ideal configuration the feedback system is unconditionally stable for any feedback gain as shown by Elliott et al. [66].

In practice, there is no inertial ground, thus the actuator has to react against the base structure or against the inertia of its own mass. In the active tile proposed in this work, the actuator is reactive type and control force appears in parallel with the passive mount. In most practical cases, the base structure is flexible and the reactive force affects the base velocity, which affects the velocity of the system. Note that under the conditions of a rigid tile and a massless mount, the feedback control system can be shown to be unconditionally stable [66].

In the system being investigated in this work, neither the tile is rigid nor is the mount massless for the entire frequency range of interest. Thus, simple skyhook damping control using negative feedback will not be conditionally stable and in order to improve the stability characteristics of the system and the frequency bandwidth of control, a feedback compensator has to be designed.

Experiments were performed on an experimental setup consisting of a single tile mounted on the plate, as shown in Figure 4.5. This single tile system is useful for investigating the performance of the feedback control system without the effects of mechanical coupling to

the neighboring tiles. A frequency response design technique was employed to design a simple feedback controller that was implemented using analog electronics filters. The design procedure is detailed in the sections that follow.

4.2.1 Loop shaping approach

In this section the design of a feedback controller applied to the prototype active tile system is detailed. The controller design was based on classical control techniques and the frequency response analysis method [67]. This approach is effective for designing simple SISO systems that can be implemented using analog electronics.

The first step in the feedback controller design procedure is the experimental identification of the plant frequency response function (FRF), which is the transfer function of the path between the controller output (equal to the input voltage into the actuator) and the error sensor (acceleration of the tile measure at the accelerometer location). Then, the stability of the closed-loop system is investigated based on the open-loop frequency response by using the Nyquist stability criterion. Using the measured plant FRF, a suitable analog compensator can be design for the plant, so that closing the loop around the compensator results in suppression of the output signal, which in this case is the acceleration of the tile.

The equivalent block diagram shown in Figure 4.6 represents the feedback control system. In this diagram $G(\omega)$ represents the plant transfer function, $H(\omega)$ represents the controller transfer function (compensator), u is the controller output, e is the error signal and d is the primary disturbance. The goal of the feedback system is to minimize the error signal, in other words, provide disturbance rejection. The closed loop response for a stable system is given by:

$$\frac{E(\omega)}{D(\omega)} = \frac{1}{1+G(\omega)H(\omega)} \tag{4.1}$$

The goal is to design a compensator that modifies the response of the plant to maximize

the bandwidth and suppression of the closed loop system response. The compensator is generally designed by cascading basic compensator elements with know frequency response, such as integrators, lead-lag networks and complex poles/zeros. The procedure employed to select the compensator response is based on trial and error. First, a mathematical model of the control system is obtained and then parameters of the compensator are interactively adjusted. At each adjustment of the controller parameters the performance and stability specifications are checked until a satisfactory closed loop response and associated stability margins is obtained.

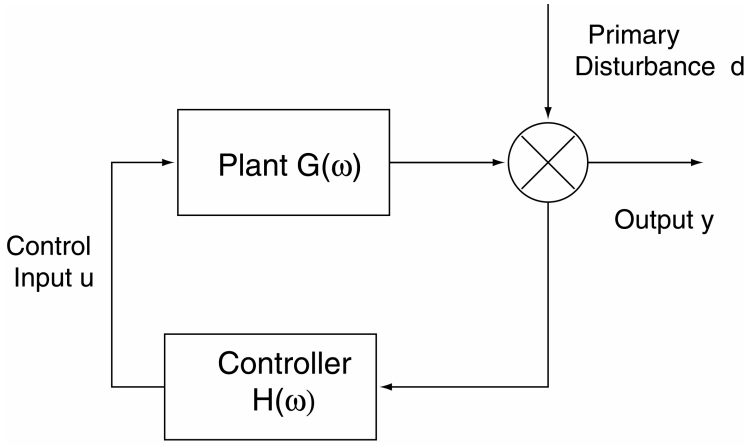

Figure 4.6: Equivalent block diagram of the feedback control system

The mathematical model of the plant was obtained using *MATLAB*, by performing a curve fit of the experimentally obtained frequency response of the plant. This curve fitting routine allowed to obtain the plant model in terms of the coefficients of the numerator and denominator of the plant transfer functions or alternatively by its zeros, poles and gain. The transfer function model of the plant can then be cascaded with models of the compensator and the resulting open loop and closed loop responses can be computed. After a satisfactory performance was achieved, the compensator response was implemented using analog electric circuits and experimental tests were performed to verify the closed loop response of the system.

4.2.2 Active Tile Design Considerations

One of the challenges involved in designing a feedback controller for the tile system comes from the fact that the *Thunder* actuator combined with the tile has several high-frequency lightly damped structural resonances (see Figure 4.7). Attempts were made to improve the plant dynamics for the control design.

Figure 4.7 shows the response of the Thunder active mount shown in Figure 4.4. It's observed that the actuator has several lightly damped resonances above the fundamental mass-spring resonance, caused by the actuator structural resonances. One way to improve the system response is to add damping to these resonances so that the gain stability margin can be increased, resulting in increased control bandwidth.

Additional damping was added to the system by attaching strips of damping material to the Thunder actuator. After several trials, best results were obtained by attaching 2.0 cm wide strips of damping material to the edges of the actuator (see Figure 4.4), being possible to attenuate the resonance peaks up to 15dB. The active mount acceleration frequency response before and after the addition of the damping is plotted together in Figure 4.7.

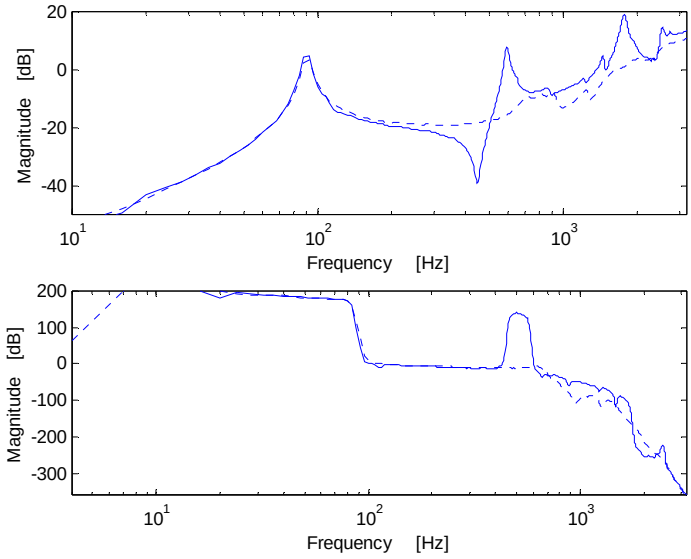

Figure 4.7: Thunder element mount acceleration response before (solid trace) and after (dashed trace) the installation of damping material.

In order to achieve good plant response characteristics for the controller design, attention was given to the way the mounts were attached to the tile. In the initial experiments a single mount was attached to the center of the tile. A mount attached to the center of the tile excited the first structural mode of the tile, around 800 Hz, decreasing the gain stability margin of the system. A better configuration was obtained by using two mounts per tile. The frequency response of the plant with a single and with two mounts is shown Figure 4.8 where it is observed the lower magnitude of the two tile system response around 800 Hz. The two mounts configuration also provided additional mechanical stability to the tile and increased control authority.

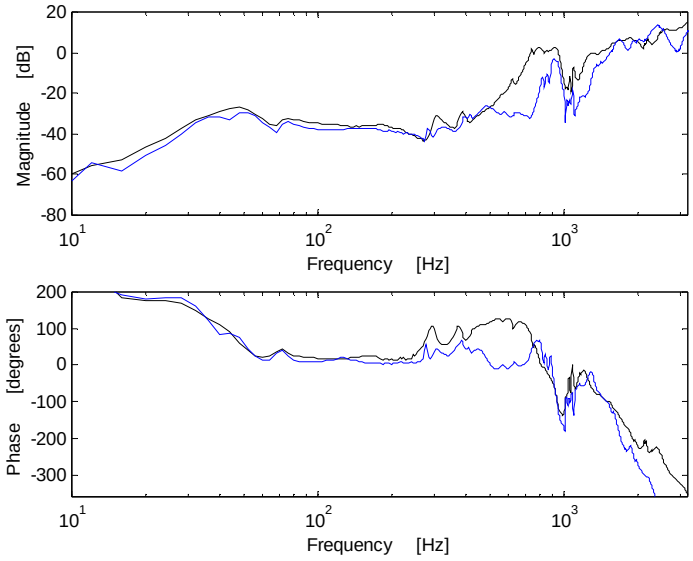

Figure 4.8: Tile acceleration response for a tile with a single mount (black trace) and two mounts (blue trace)

4.2.3 Controller Design

The frequency response of the active tile plant used in the control design is shown in Figure 4.9. In this plot it is observed that the phase response of the system crosses 180 degrees around 800 Hz. Thus, in order to have a stable loop, it is necessary that the open loop magnitude response is less than unity at this frequency.

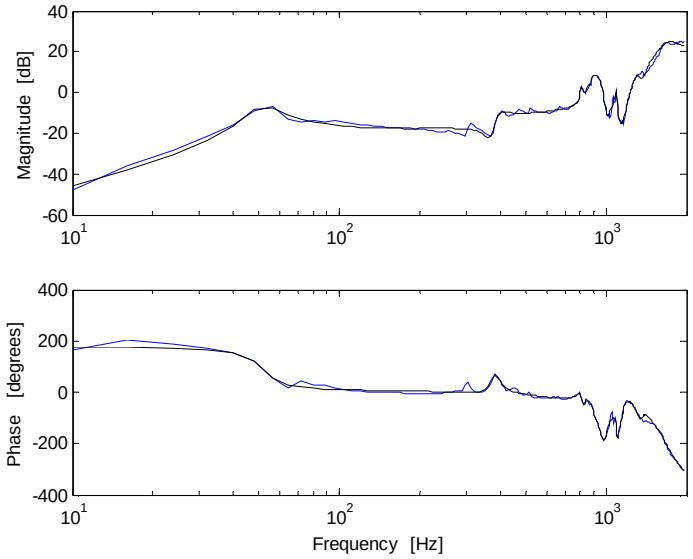

Figure 4.9: Plant frequency response data (black trace) and curve fit (blue trace)

The frequency response of the feedback compensator is shown in Figure 4.10. This compensator is the combination of an integrator, a lag network and a 2nd order low pass filter (pair of complex poles). The transfer function of the compensator is given by the following rational function:

$$H(s) = \frac{10^6(s+1258)}{s(s+104)(s^2+6143s+10^6)} \tag{4.2}$$

This feedback compensator was implemented with analog circuits using analog filter synthesis techniques as described in [68]. The details of the synthesis procedure and the circuit implementation are presented in Appendix B.

Figure 4.11 shows the open loop response of the original plant and of the plant combiner with the compensator. Note that the bandwidth of the system extends to about 160 Hz and the phase and gain margins are respectively 30 degrees and 6dB. Another way to

visualize the open loop response is by plotting the logarithmic Nyquist plot, shown in Figure 4.12.

The system closed loop magnitude response that represents the attenuation provided by the feedback control is shown in Figure 4.13. The frequency bandwidth where active attenuation is achieved is approximately 160 Hz with an attenuation of about 25 dB at around 50 Hz. Note that there is some response amplification (control spillover) above 160 Hz and that reaches about 10 dB at 250 Hz.

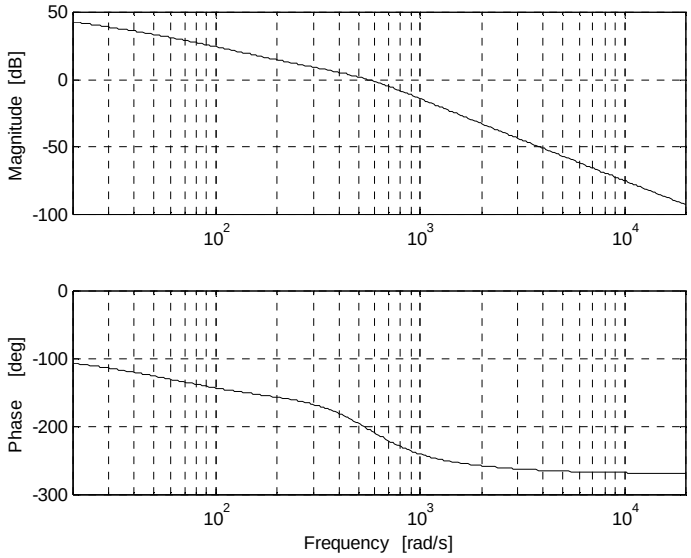

Figure 4.10: Feedback controller frequency response

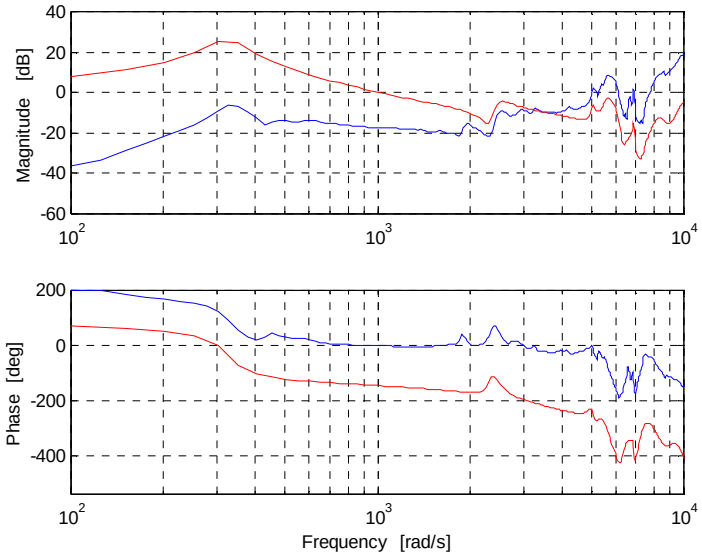

Figure 4.11: Open loop frequency response of the original (blue trace) and compensated (red trace) plant

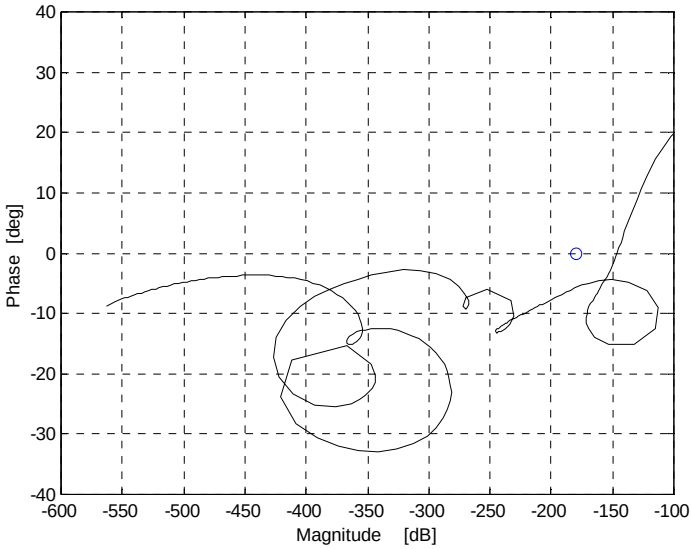

Figure 4.12: Open loop frequency response of the compensated system in the Nyquist plane

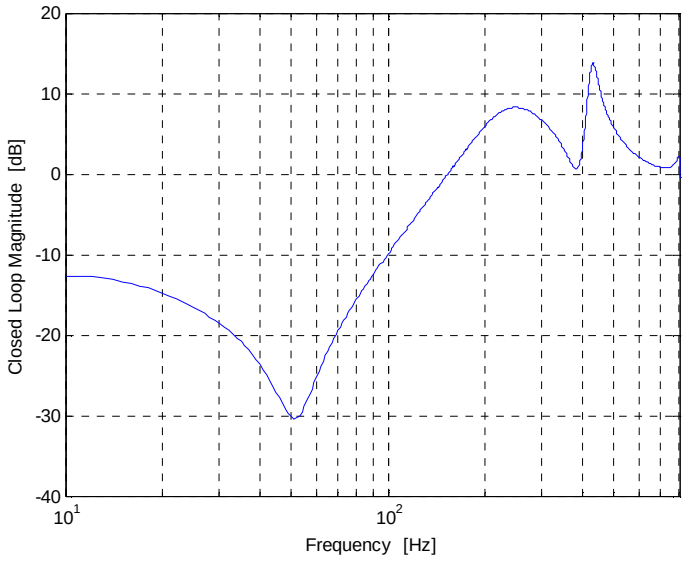

Figure 4.13: Predicted closed loop frequency response of the feedback control system

4.2.4 Experimental Results

This section presents the experimental results of tile acceleration and sound radiated power of the tile obtained using the feedback controller discussed above.

Experimental Setup

The error sensor used for the feedback control system was a small *2.0* grams accelerometer attached with bee wax to the center of the tile. The acceleration signal was sent to an accelerometer power supply with built-in integrator circuit and the resultant output velocity signal was the input of the feedback compensator circuit. The output of the compensator was then connected to an adjustable gain amplifier suitable for driving piezoelectric capacitive loads. The gain of the amplifier was set to 40 times and a single amplifier was used to drive both active mounts electrically connected in parallel. The combined capacitive load of both mounts was measured to be *320 nF*, within the operation range of the amplifier as stated in the amplifier operation manual. A schematic of the instrumentation interconnection used for the tests is shown in Figure 4.14.

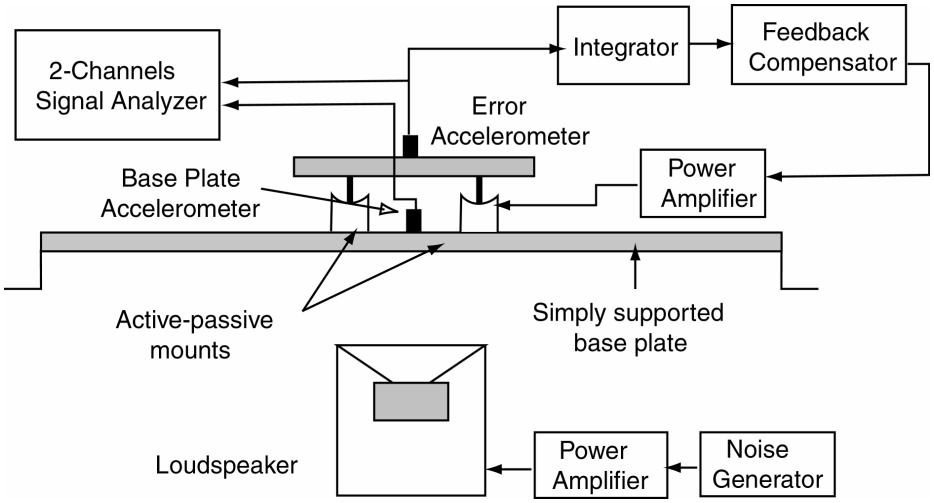

Figure 4.14: Schematic of the experimental setup used for the SISO feedback control tests

An audio power amplifier with white noise input was used to drive a 10 in. loudspeaker that acted as an acoustic disturbance source for exciting the base aluminum plate. In addition, a small *2.0* grams PCB accelerometer was attached to the base plate in order to measure its acceleration. The measurement of the both the tile and base plate accelerations using a two-channels FFT analyzer allows computing of the transmissibility characteristics of the active tile.

Experimental Results

Figure 4.15 shows the velocity of the center of tile measured with the accelerometer, for an acoustical excitation of the base plate, before and after control. An attenuation of about 15 dB is obtained at the base first structural resonance at around 60 Hz with an overall active attenuation of 8 dB. It's also observed that the control bandwidth extends to about 200 Hz and that slight spillover of about 5-10 dB occurs above this frequency. The corresponding experimental closed loop attenuation of the SISO feedback control system is shown in Figure 4.16.

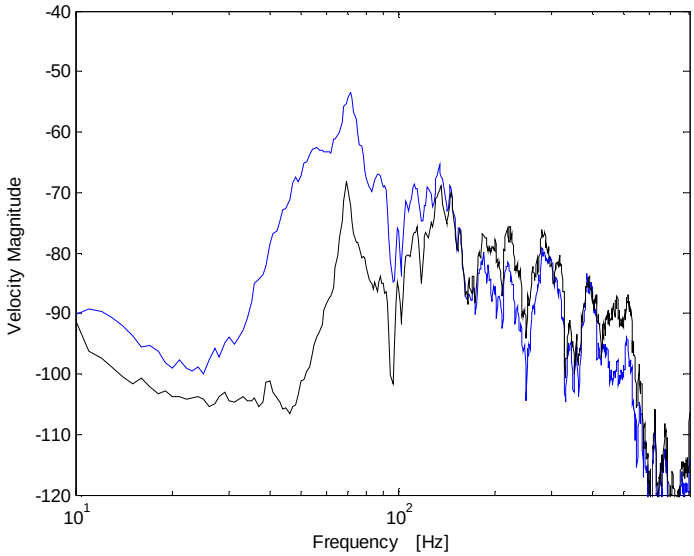

Figure 4.15: Velocity measured at the center of the tile before control (blue trace) and with control (black trace)

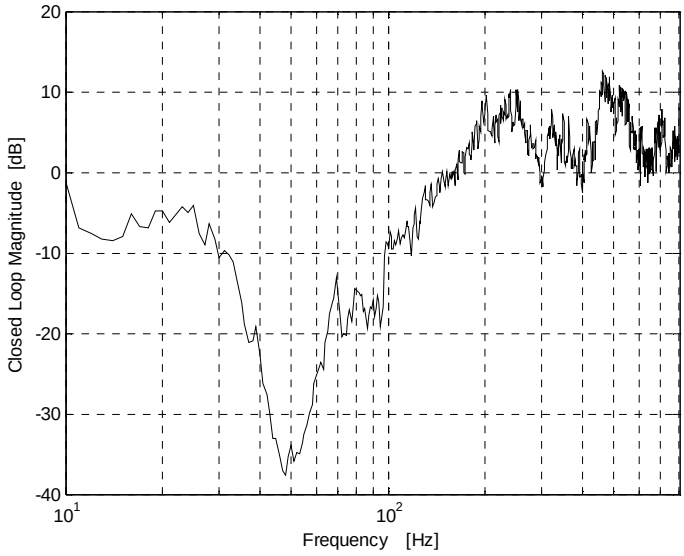

Figure 4.16: Experimentally measured closed loop response of the SISO feedback control

Sound Radiated Power

If the tile vibrates as a rigid piston, the sound radiated power is directly proportional to its normal surface velocity. Thus attenuation in the velocity of the tile should correspond to an attenuation of the acoustic radiated power and the control of sound radiation can then be achieved with a single sensor on the center of the tile. In order to verify this, the sound power radiated by the tile was computed based on tile surface velocity measurements at 9 points using a laser vibrometer (see Figure 4.5). The resulting sound radiated power was computed using equation (2-63) using different numbers of velocity measurements. The total sound radiated power obtained with control off for 1, 3 and 9 points velocity measurements is plotted in Figure 4.17 where it is observed that the same result is obtained for all cases, indicating that a single point velocity measurement can be used to estimate the sound radiated power with control off. The same procedure, but now for the case with control on, is shown in Figure 4.18. Again, good agreement is obtained for all cases, except for around 90 Hz, where there is a discrepancy between the single point velocity measurement estimation versus the multiple point measurement curves. This can probably be attributed to the existence of a tile rocking mode at this frequency. The tile vibrating in its rocking mode is a poor sound radiator (low radiation efficiency) and its contribution to the sound radiation only becomes apparent with control on, when the radiation of the piston mode is greatly attenuated. Thus, it is possible to estimate the sound radiated power for the cases of control off and control on, by measuring the tile velocity at three locations, in this case, points 4, 5 and 6 of Figure 4.5.

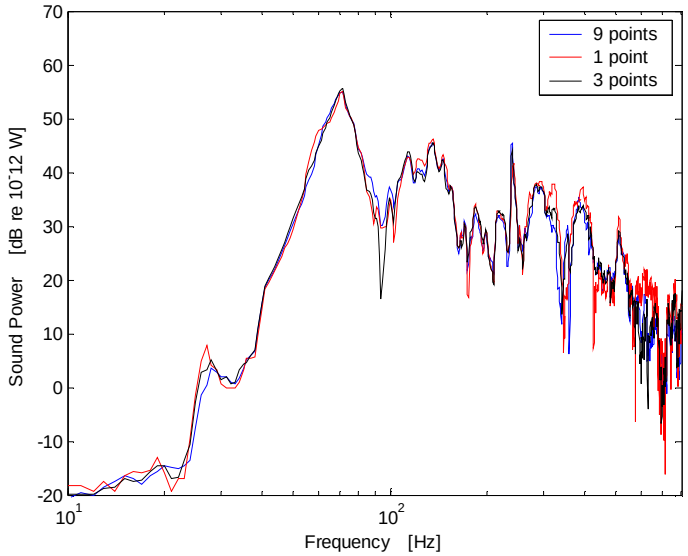

Figure 4.17: Tile total acoustic radiated power with control off, computed using different number of surface velocity measurements locations.

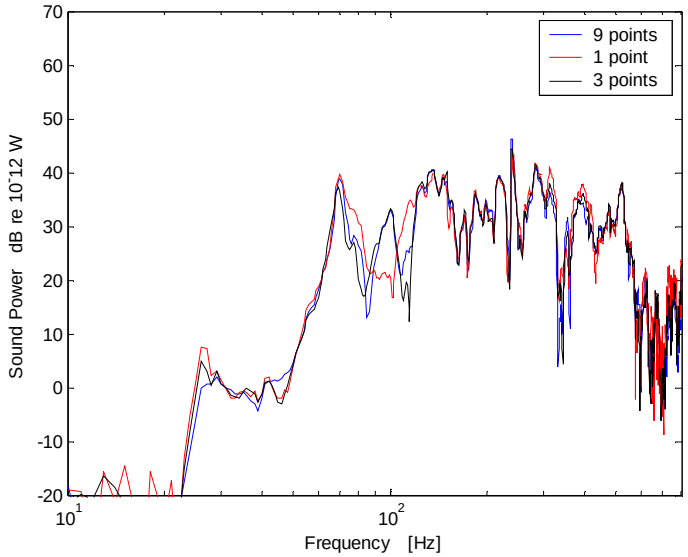

Figure 4.18: Total acoustic radiated power of the tile with control on, computed using different number of surface velocity measurements locations.

The total sound radiated sound power estimated using the velocity measurements, before and after feedback control is applied is shown in Figure 4.19 below. A total overall active attenuation of 5.5 dB was obtained.

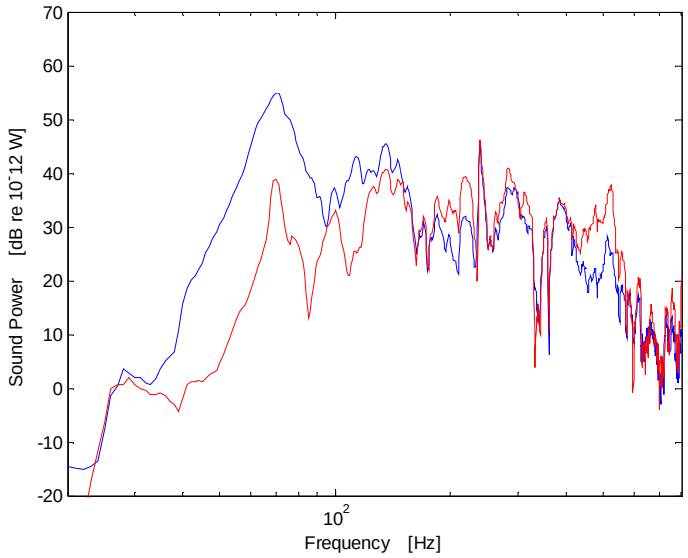

Figure 4.19: Estimated sound radiated power before (blue trace) and after (red trace) feedback control.

4.2.5 Optimal Feedback Control

Although optimal feedback control is not investigated in detail in this work or neither implemented experimentally, it is interesting to simulate the performance of the active tile when optimal control design techniques are employed. The design of the LQG controller is performed in MATLAB. Note that the resulting controller is usually high order and has to be implemented digitally, usually with an IIR filter. The magnitude of the closed loop results are shown in Figure 4.20 where it is observed that the bandwidth of control can be extended to about 230 Hz with 20 dB of peak active attenuation from 40-120 Hz.

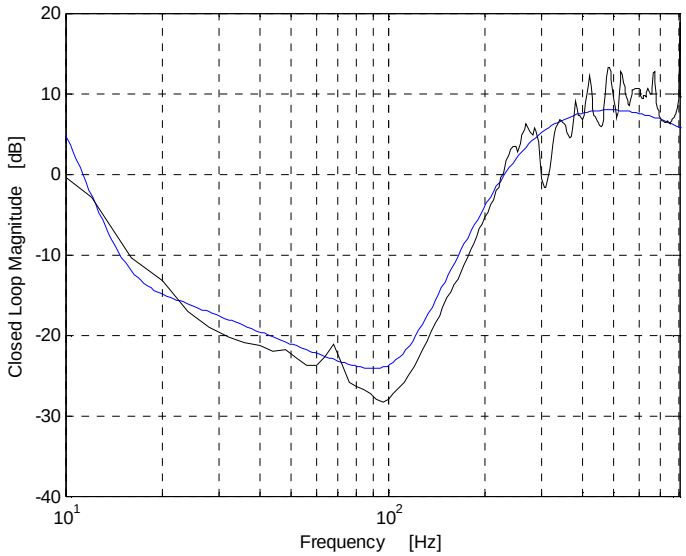

Figure 4.20: Closed loop magnitude of the single tile system for a feedback control system designed with LQG approach.

4.3 Feedforward Control

The single tile mounted in baffled shown in Figure 4.5 was used for the feedforward control tests presented in this section. The error signal was the acceleration signal from a small B&K accelerometer attached to the center of the tile and with output connected to a B&K power supply was used as the error signal. The output of the controller was connected to a PCB piezoelectric amplifier used to drive the active mounts. A 10 inches woofer mounted in a sealed box and electrically driven with band-limited white noise via an audio power amplifier was used as a disturbance source. The schematic of the experimental setup is shown in Figure 4.21.

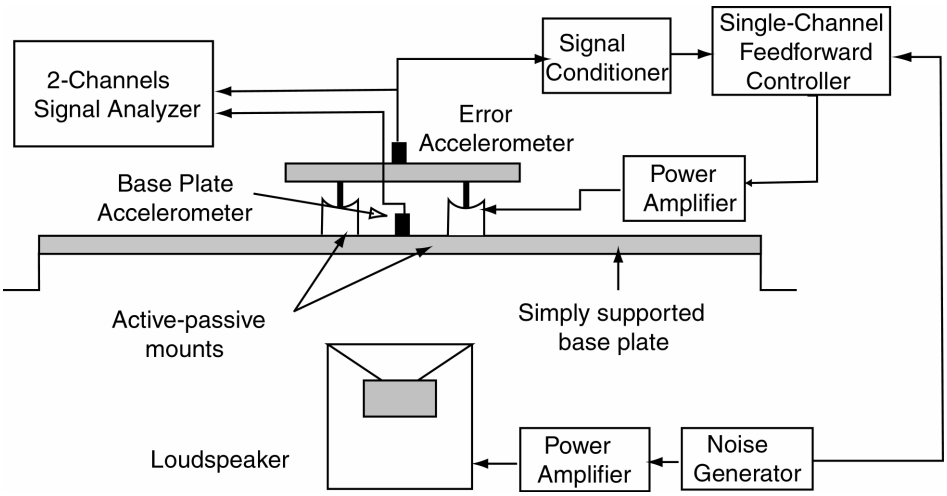

Figure 4.21: Schematic of the experimental setup used for the SISO feedforward control tests

A feedforward filtered-x LMS algorithm was implemented in a controller board based on Texas C-30 DSP, running on a PC system and operated via a LabView interface. The procedure for setting up the controller consists in first defining the sampling frequency of the controller and the number of coefficients used for the plant identification filter and for the control filter. Initially, an offline secondary path modeling procedure is executed. The active mounts are driven with a white noise signal generated by the control board and the resulting acceleration response is measured. A LMS algorithm is used to adapt the coefficients of an FIR filter that models the secondary path (see Figure 3.9). After the plant is identified the control algorithm is started. The convergence coefficient μ is adjusted to ensure the proper convergence of the control filter. Initially a larger value of μ is used until the filter coefficients converge. Then the value of μ is decreased for steady state stability. The quadratic sum of the error signal is used to check the convergence of the control filter. In addition, the input and output signal levels have to be scaled to make best use of the dynamic range of the A/D and D/A stages of the control board. The proper input and output signal levels were monitored on an oscilloscope.

Both an ideal reference and a real reference signals were used for the feedforward control tests. The ideal reference was obtained by feeding into the controller the white noise

disturbance. For the case of a real reference, another B&K accelerometer was attached to the base structure under the active tile, to provide the reference signal.

After several interactions, best performance was obtained with the controller adjusted to run at 3000 Hz. The FIR filter used in the secondary path identification used 128 coefficients and 300 coefficients were used for the control filter. The control results are presented next for the ideal and real reference cases.

4.3.1 Ideal Reference Signal Results

The feedforward control ideal reference signal was obtained by feeding into the controller, the generator white noise disturbance signal delayed to made causal. Figure 4.22 shows the acceleration of the base structure (aluminum simply supported plate) measured by an accelerometer located under the tile, the acceleration of the tile without control and the acceleration of the active tile with feedforward control. A total active attenuation of 20 dB was obtained, with 14.2 dB of active attenuation and 5.8 dB of passive attenuation. Comparing the acceleration of the base and the acceleration of the passive tile, good passive vibration isolation performance for frequencies above 100 Hz can be observed. Relatively low passive isolation occurs at the first base structural resonance frequency due to the proximity to the tile mass-spring fundamental resonance. Note that good active control performance is obtained (10-20 dB of active attenuation) for the entire frequency band of control from 40-500 Hz.

The total sound power radiated by tile with and without control was computed based on measurements of the tile velocity at 3 points along its width. The results are presented in Figure 4.23 and show 14.7 dB of overall active attenuation of the sound radiated power. In order to check that the acceleration of the tile at the error sensor location can give good estimates of the sound radiated power, sound radiated power was estimated from velocities measured at 1, 3 and 9 points on the tile. The results obtained were very similar, with 1dB overall difference between the measurements with 1 and 9 points.

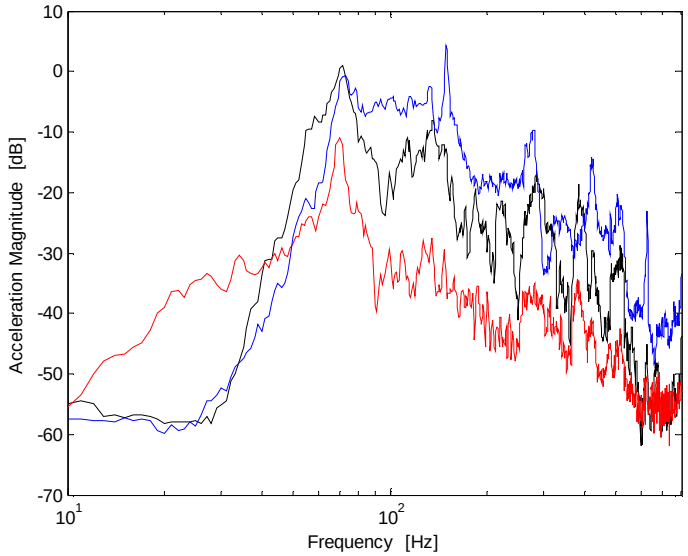

Figure 4.22: Experimental results for feedforward control with an ideal reference. Acceleration response of base plate (blue trace), tile without control (black trace), tile with active control (red trace).

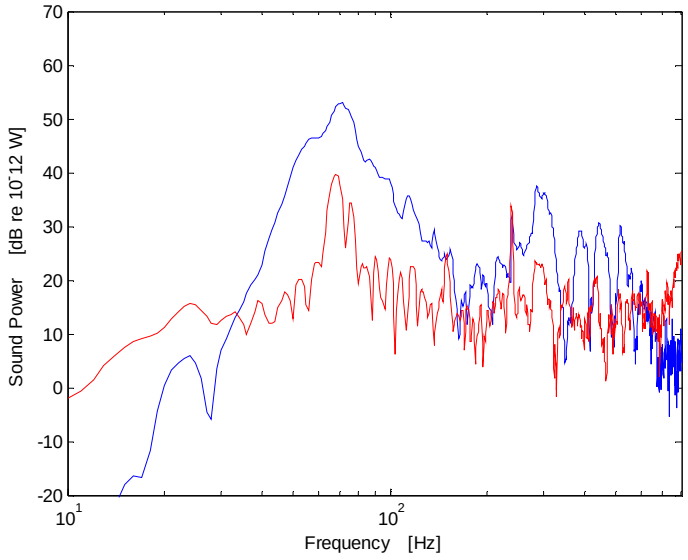

Figure 4.23: Single tile sound power results for feedforward control with an ideal reference: tile without control (blue trace), tile with active control (red trace)

4.3.2 Real Reference Signal Results

A more realistic reference signal that can be implemented in a practical application of the active tile system was obtained by using the acceleration signal measured at the simply supported aluminum plate at a position near the tile mounts. Figure 4.24 shows the measured acceleration of the base structure, the acceleration of the tile without control (passive) and the acceleration of the active tile with feedforward control. For the active control case it is observed good attenuation (10-20 dB) of the tile acceleration for the frequency band of 40-400 Hz with more than 20 dB of attenuation at 85 Hz, the first resonance frequency of the base structure. A total attenuation of 20.5 dB over the measured frequency range was obtained, with 14.7 dB of active attenuation and 5.8 dB of passive attenuation. The total sound power radiated by tile with and without control was computed by measuring the tile velocity at 3 points along its width. The results are presented in Figure 4.25 with 10.7 dB of active attenuation of the sound power radiated by the tile was obtained.

The good active control results obtained indicate that the acceleration of the base plate provides a good reference signal. Given its relatively high input mobility the base plate vibration was not affected by the control force generated by the active mounts. In other words there is no feedback path from the control signal back to the reference signal.

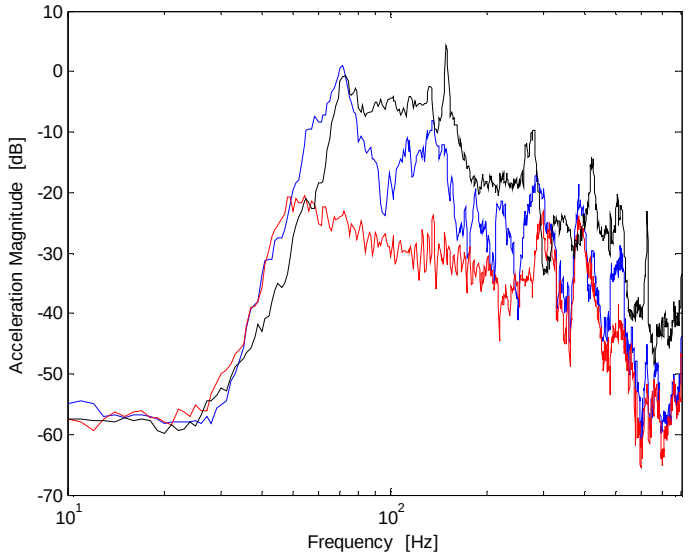

Figure 4.24: Experimental results for feedforward control with a realistic reference signal. Acceleration response of base plate (blue trace), tile without control (black trace), tile with active control (red trace).

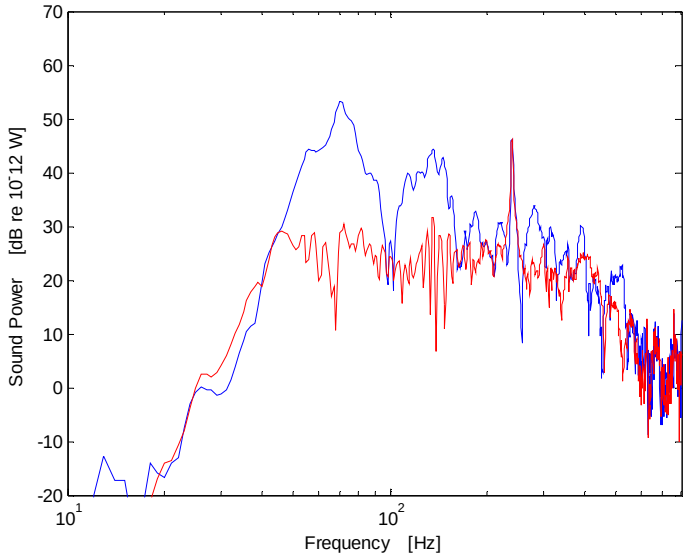

Figure 4.25: Single tile sound power results for feedforward control with an ideal reference: base plate (blue trace), tile control off (black trace), tile control on (red trace).

4.4 Summary

In this Chapter the performance of a single active tile system is investigated. The results shown demonstrate the successful application of both feedback and feedforward SISO system for controlling sound radiation.

A large aluminum simply supported plate was used as a low mobility base structure. The tile is mounted in a baffle that covers the base plate and is attached to the plate via two active-passive mounts (*Thunder* actuators). The base plate was acoustically excited and the resulting tile velocity was measured for the passive condition and when active control was applied to the active tile to reduce its normal velocity. Both SISO feedback and feedforward control systems were investigated.

A single accelerometer located at the center of the tile was used as the error sensor for single-input single-output (SISO) control. The use of a SISO control system implies that the rocking mode of vibration of the tile cannot be controlled. Thus, the tile has to be small enough so that the rocking mode of vibration does not contribute significantly to the sound radiated power in the frequency range of interest. The first flexible mode of vibration of the tile occurs at 800 Hz and the tile can be considered rigid in the control band of interest. This also implies that the sound radiated by the tile, except by the contribution of rocking modes of vibration, can be well estimated from measurement of the tile velocity at a single location.

A velocity feedback control system was designed and implemented with analog electronic circuits. Analog circuits were used because of the desire to keep the control system implementation as simple and low cost as possible, due to the large number of active tiles that have be used for a large structure. The SISO velocity feedback controller was designed in the frequency domain-using loop shaping techniques. The designed compensator response was then implemented with analog electronic circuit and tested for controlling the normal velocity of the tile. Good active control was obtained around the mass-spring resonance of the tile and up to 150 Hz with an overall active attenuation of 5-

6 dB. The frequency bandwidth where control was successfully achieved was limited by the lightly damped high frequency dynamics of the tile-mount system. The frequency bandwidth of feedback control was maximized by attaching damping to the *Thunder* element and attenuating the high frequency dynamics of the mount. Finally, it was shown that designing the controller using optimal design techniques could extend the frequency bandwidth of control. However, the resulting controller is in general of high-order and requires a digital filter implementation.

A single channel feedforward controller based on the filtered x-LMS algorithm was investigated for the cases of an ideal reference and a real reference signals. The practical reference signal was obtained from an acceleration measurement of the base plate vibration. It was shown possible to use of the acceleration of the base plate as a reference signal thanks to the lack of a feedback path from the control signal to the reference signal, given the high input mobility of the base plate. The use of the feedforward controller with ideal reference achieved active attenuation of the tile velocity up to 600 Hz and about 15 dB overall attenuation of the sound radiated power. The control system using the acceleration of the base plate as reference signal achieved control up to 500 Hz and about 10dB overall attenuation of the sound radiated power.

Chapter 5

5 Control of Sound Transmission with Multiple Active-Passive Tiles

In the previous chapter, the control of sound transmission through a plate using the active-passive tile approach was investigated experimentally for a single tile system. Although the results obtained clearly demonstrated the potential of the proposed active tile approach to control sound transmission at low frequencies, a single tile system ignores the physical coupling between neighboring tiles, as shown in the multi-tile analytical simulations. This has important implications regarding the use of multiple independent control loops (decentralized control), either feedforward or feedback. This Chapter presents experimental results obtained for an experimental setup using four active tiles and that allows investigating the inter-tile coupling effects on the control performance. After the description of the experimental setup, results obtained using a decentralized analog feedback control scheme applied to the multiple tile system is detailed. Finally, experimental tests and results are presented for the active control of multiple tiles using a decentralized feedforward control system.

5.1 Feedback Control

This section presents the experimental results obtained by applying independent SISO feedback controllers to each of the four tiles for controlling the tile normal velocity signal measured by an accelerometer at the center of each tile. The description of the experimental setup is presented first, followed by the controller design and experimental results including the feedback attenuation of tile velocity and estimated sound radiated power.

5.1.1 Decentralized Feedback Control

The block diagram representing a decentralized feedback control system is presented in Figure 5.1. The *m x m* square plant *G(s)* with elements g_{ij} is to be controlled using a diagonal controller:

$$H(s) = diag\{h_i(s)\} = \begin{bmatrix} h_1(s) & 0 & 0 & 0 \\ 0 & h_2(s) & \cdots & 0 \\ \vdots & \vdots & \ddots & \vdots \\ 0 & 0 & \cdots & h_m(s) \end{bmatrix} \tag{5.1}$$

The optimal solution to the decentralized feedback control problem is mathematically complex because the optimal control solution is obtained solving an infinite dimensional optimization problem and maybe non-unique [70,71]. General guidelines for the design of decentralized feedback control systems are given in [70].

The matrix of diagonal elements of *G(s)* can be written as:

$$\tilde{G}(s) = diag\{g_{ii}(s)\} = \begin{bmatrix} g_{11}(s) & 0 & 0 & 0 \\ 0 & g_{22}(s) & \cdots & 0 \\ \vdots & \vdots & \ddots & \vdots \\ 0 & 0 & \cdots & g_{mm}(s) \end{bmatrix} \tag{5.2}$$

where g_{ii} are the diagonal elements of *G*. Now, the feedback control loop transfer function for the loop *i* is denoted as $L_i=g_{ii}k_i$ which is the *i*th diagonal element of the matrix $\tilde{G}(s)H$.

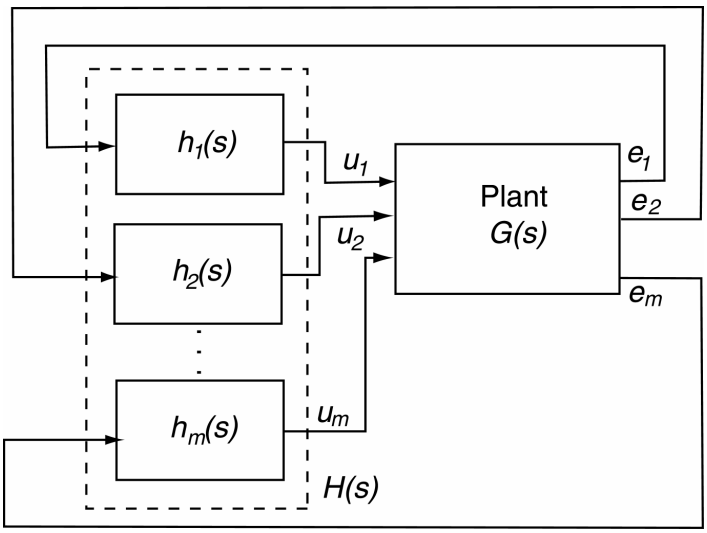

Figure 5.1: Block diagram of decentralized diagonal control of a *m x m* plant

When applying a decentralized feedback controller to a system is important to choose the best error sensor-actuator pairs, in order to minimize the influence of coupling between control loops in the control system performance. The decentralized control system will work well if *G(s)* is close to diagonal, in which case the plant can be considered as a set of independent sub-plants and the individual controllers can be designed independently. If the off-diagonal elements of *G(s)* are large, the performance of the decentralized control system will decrease because of the effect of interactions between the control loops.

The magnitudes of the off-diagonal elements of G relative to its diagonal elements are called *interactions* and are given by the matrix:

$$E \equiv (G - \tilde{G})\tilde{G}^{-1} \tag{5.3}$$

The closed loop transfer function from the disturbance to the error signal is called the sensitivity function and gives a measure of the disturbance attenuation provided by the feedback control system.

The sensitivity function is defined as:

$$S = (I - GH)^{-1} \tag{5.4}$$

For a decentralized feedback control system the sensitivity function can be factorized as:

$$S = \tilde{S}(I - E\tilde{T})^{-1} \tag{5.5}$$

where $\tilde{S}$ and $\tilde{T}$ contain respectively the sensitivity and the complementary sensitivity for the individual control loops *i.*

$$\tilde{S} \equiv (I - \tilde{G}H)^{-1} = diag\{\frac{1}{1 + g_{ii}k_i}\} \tag{5.6}$$

and

$$\tilde{T} = I - \tilde{S} \tag{5.7}$$

The degree of influence of the off-diagonal elements of G for decentralized control is given by the relative gain array (RGA) defined in the equation below [70]:

$$\mathrm{RGA}(G) = \Lambda(G) = G \times (G^{-1})^T \tag{5.8}$$

where $\times$ denotes element by element multiplication.

The preferred pairing between inputs and outputs for avoiding instabilities in the crossover frequency region should result in a RGA matrix close to identity. In other words, for stability of a decentralized feedback control system the input-output pairings should results in a RGA $\Lambda(G(j\omega)) \approx I$ at frequencies around the crossover frequency.

The RGA can also be used to measure diagonal dominance by the RGA-number defined as:

$$\text{RGA} - \text{number} = \left\| \Lambda(G) - I \right\|_{sum} \tag{5.9}$$

For decentralized control it is preferred to have pairings for which the RGA-number at crossover frequencies is close to 0.

5.1.2 Experimental Setup

The experimental setup studied in this chapter is similar to the one used in the single tile experiments of Chapter four, but now four tiles are used as depicted in Figure 5.2. The multiple tile system investigated in this work employs four *18 x 15 cm* tiles placed in a baffle and with the edges sealed by a flexible rubber strip as shown in Figure 5.2. Each tile is mounted to the base plate via two active-passive mounts implemented with *Thunder* actuators electrically connected in parallel. Figure 5.2 also shows a single small accelerometer placed at the center of each tile, which is used as error sensor. Each accelerometer is connected to a power supply with built-in integrator, so that velocity can be directly measured. A schematic of the experimental interconnections is presented in Figure 5.3.

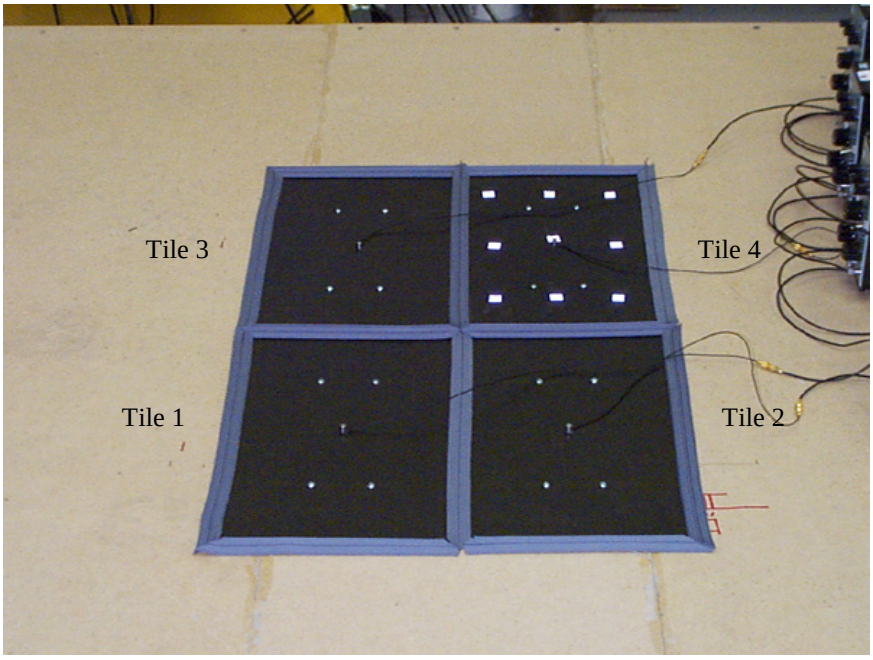

Figure 5.2: Photo shows the multiple tile setup system with 4 tiles mounted in a baffle and with the gaps sealed with strips of flexible rubber. The accelerometers (error sensors) are positioned at the center of each tile

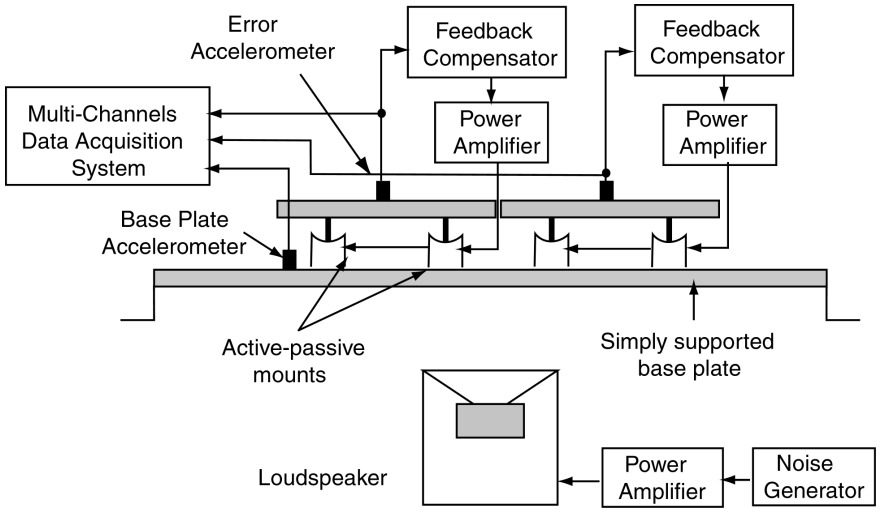

Figure 5.3: Experimental setup used for the multiple independent SISO feedback control

The velocity output of each power supply was used as input each of the SISO feedback compensator circuits. The outputs of each of the feedback compensator channels were run through an adjustable gain amplifier used to drive the pair of active mounts of each tile electrically connected in parallel.

5.1.3 SISO Feedback Controller Design

The controller design approach was performed in the frequency domain, using loop-shaping techniques, as already detailed in Chapter 4. For an ideal system with no inter-tile coupling, each tile would have the exact same dynamic response (same plant) and the same feedback controller used for each tile would result in the same closed loop performance. In practice, differences in the actuator characteristics and tile construction cause each plant to be slightly different. In addition, inter-tile coupling can degrade the performance of the decentralized feedback control system. Thus, if a single feedback controller is to be used for every tile, it has to be robust to variations in the plant responses. It is not the purpose of this work to study in detail robust control design. The same feedback controller is applied for all the plants by adjusting the applied control gain in order to leave suitable stability margins to accommodate the variations between the plants responses.

Figure 5.4 presents the four measured magnitude and phase responses for each active tile, plotted together. Each tile of the multiple tile system utilized the same controller configuration used on the previous tests. Four identical independent feedback compensators were built using analog electronic circuits.

The transfer function of the plant g_{ii} for each loop i is the ratio of the output of the sensor i to an input to the actuator i. The transfer function g_{ij} from the ith actuator to the jth sensor ($i \neq j$) is called the coupling transfer function. If these coupling transfer functions are zero, then the system is just a set of individual single loop systems.

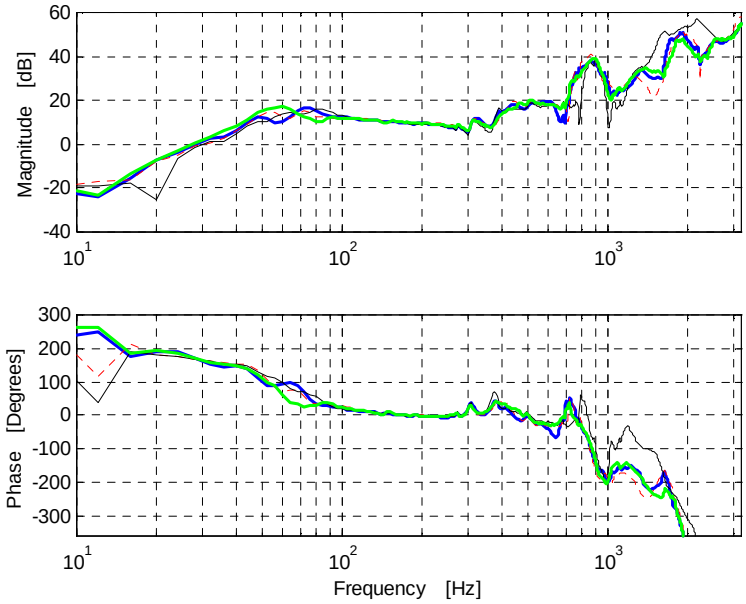

Figure 5.4: Frequency response of the four active tiles shown in Figure 4.1

In order to assess the degree of the mechanical coupling between the tiles the 16 plants transfer functions from each sensor to all actuators were measured. Initially the transfer functions were measured without the sealing gaskets around the tiles leaving a 3-4mm gap between the tiles. A single tile was excited at each time, and all the four accelerometers signals were measured simultaneously. The transfer functions consisting of the tile acceleration over input voltage into each tile, obtained for tile number 2 (see Figure 5.2) are shown in Figure 5.5. The same transfer function for the tile number 2 when the tiles are mechanically connected to each other via the sealing gaskets is shown in Figure 5.6. Note that the coupling transfer functions have large magnitude around the mass-spring resonance frequency of the tiles, 40 Hz for the case with no sealing gasket and 50 Hz with gasket. The magnitude is also large around 800 Hz, which correspond to the first flexible mode of the tile. Although the magnitude of the coupling transfer functions increases when the gaskets are used, relatively large coupling occurs even without gaskets indicating that coupling occurs via the base structure and air cavity.

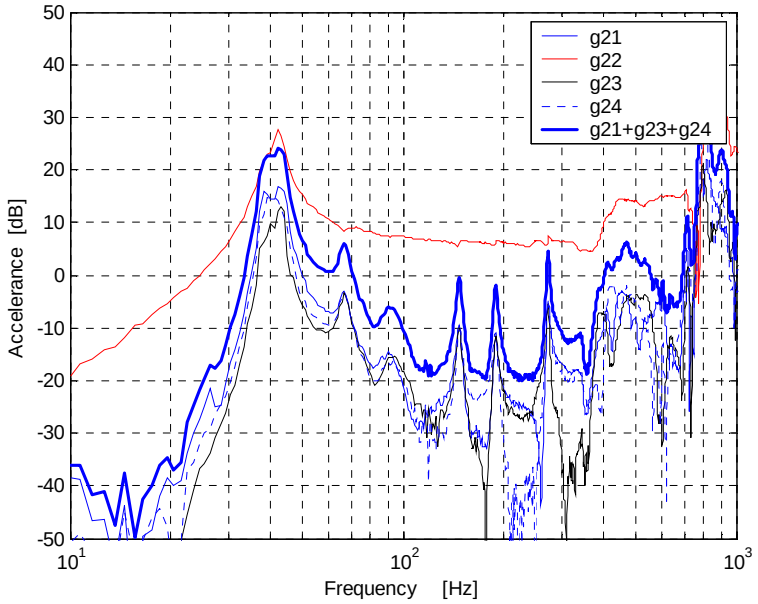

Figure 5.5: Output of tile 2 for inputs on all tiles. Tiles without sealing gaskets.

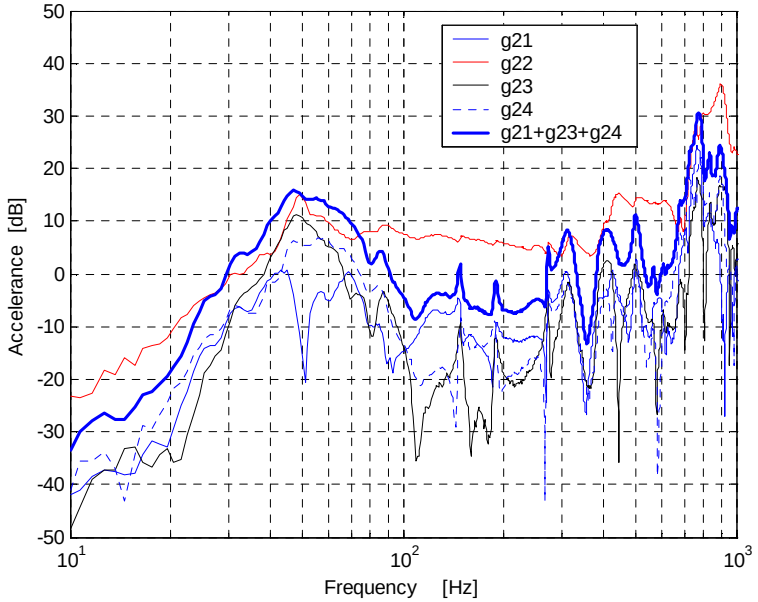

Figure 5.6: Output of tile 2 for inputs on all tiles. Tiles with sealing gaskets.

The RGA-number defined in equation (5-9) is computed using the 16 measured plant transfer functions for the tiles with and without gaskets and plotted in Figure 5.7. Note that an RGA-number close to 0 means that the matrix is diagonally dominant and the RGA is closer to identity, which is preferable for decentralized control. It is possible to observe that the use of the sealing gaskets increases the inter-tile coupling and RGA-number values. Larger values of the RGA-number occur around 50 Hz and 80 Hz corresponding to resonance frequencies of the tile-mount system and first mode of vibration of the base plate. RGA-number values are also large between 700-800 Hz, which could be caused by the first flexible mode of vibration of the tiles.

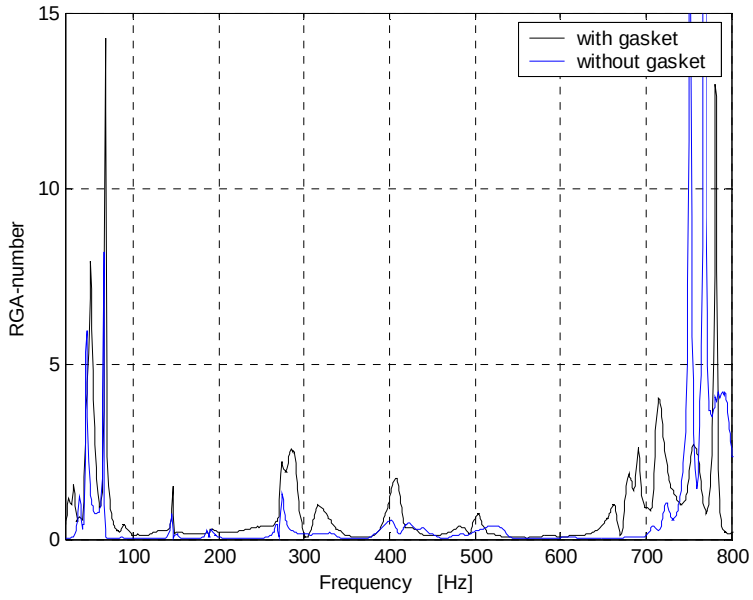

Figure 5.7: RGA-number for multiple tile plant, with and without gaskets

For SISO systems, evaluating $|S(j\omega)|$ as a function of frequency gives a measure of the effectiveness of the closed loop feedback control performance. For MIMO systems this result can be generalized considering the ratio $\|e(\omega)\|_2 / \|d(\omega)\|_2$, where *e* is the vector of errors, *d* is the vector of disturbance and $\| \, . \, \|_2$ is the vector 2 norm. The ratio above depends on the direction of *d* and is bounded by the maximum and minimum singular values of *S* as

detailed in reference [70]:

$$\sigma_{\min} \leq \frac{\|e(\omega)\|_2}{\|d(\omega)\|_2} \leq \sigma_{\max} \tag{5.10}$$

The singular values of the sensitivity matrix of the individual control loops (equation (6)) $\tilde{\mathbf{S}}$ are plotted in Figure 5.8 and the singular values of the sensitivity matrix **S** for the full system (equation (5)) is presented in Figure 5.9. Comparing Figure 5.8 and Figure 5.9 it is observed that the estimated performance of the decentralized control system degrades due to interaction effects of the off-diagonal elements of the plant matrix *G(s)*. The stability of the MIMO control system can be assessed observing the magnitude level of the spillover, which is the high-frequency amplification. In Figure 5.9 the spillover amplitude of the high frequency peaks around 400 Hz reach 20 dB indicating possible system instability. The singular values of the sensitivity matrix of for the full system (equation (5)) are presented in Figure 5.10 when the gain of the control loops is reduced by a factor of 3 for increased stability margins. The thick line represents the average performance assuming all disturbances have the same direction.

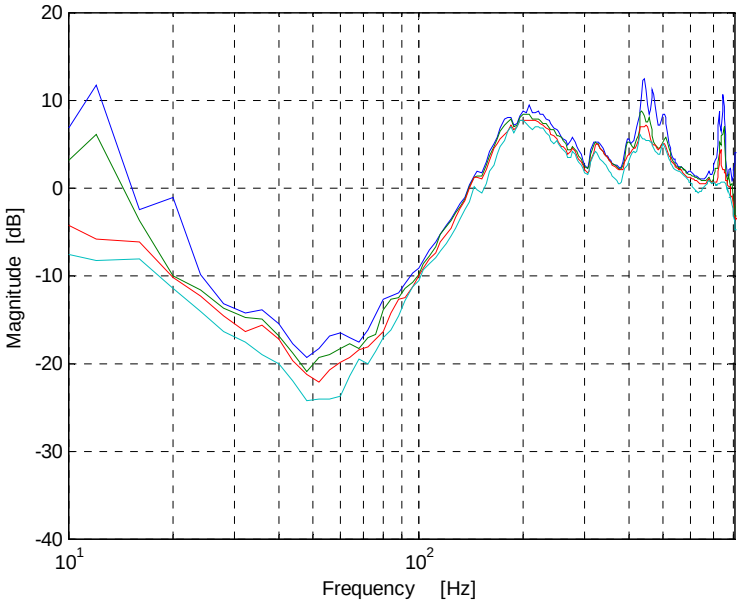

Figure 5.8: Singular values of sensitivity matrix $\tilde{\mathbf{S}}$

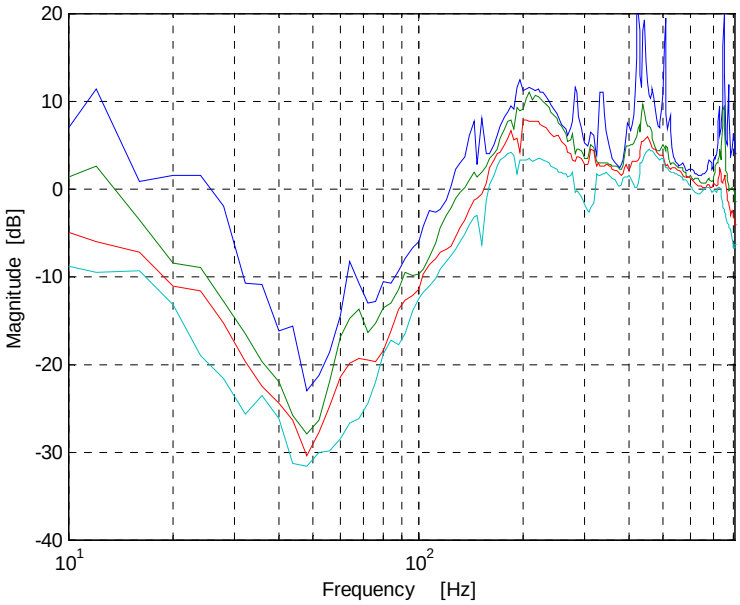

Figure 5.9: Singular values of sensitivity matrix **S**

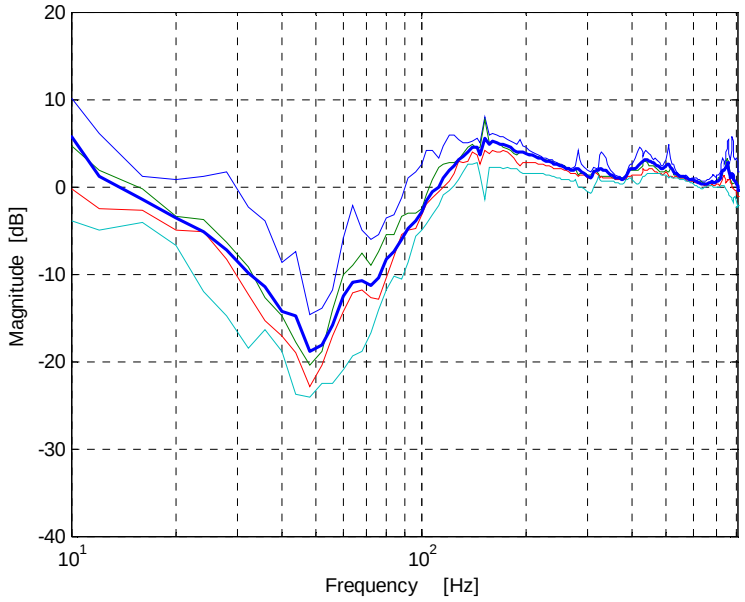

Figure 5.10: Singular values of sensitivity matrix **S** with reduced loop gain

5.1.4 Experimental Results

This section presents the experimental results obtained by applying decentralized feedback control to the four-tile setup shown in Figure 5.2. The velocity of the base plate under the tile and the velocity of the tile # 2 are presented in Figure 5.11 where it is observed significant passive vibration isolation for frequencies above 120 Hz. The measured velocity of each tile with control off and with control on are shown in Figure 5.12 to Figure 5.15. The same SISO feedback compensator was applied to each tile. The gain of each control loop was adjusted by iteration with the goal of maximization of the control performance while avoiding instabilities. The control bandwidth extended to about 130 Hz for all tiles and the overall active attenuations obtained for tiles one to four are respectively 3.6 dB, 2.0 dB, 7.4 dB, 6.9 dB. The closed loop active attenuations measured for the four tiles obtained with the decentralized feedback controller are presented in Figure 5.16. The thick line represents the average performance which has good agreement with the predicted performance shown in Figure 5.10.

The feedback control performance obtained for each of the four tiles of the multiple tiles system is clearly lower than the performance achieved for the single tile case investigated in Chapter 4. The reduced performance can be explained by the coupling between the tiles that limited the amount of gain that could be applied the to the feedback loop before instability occurs (about half the gain applied to the single tile case).

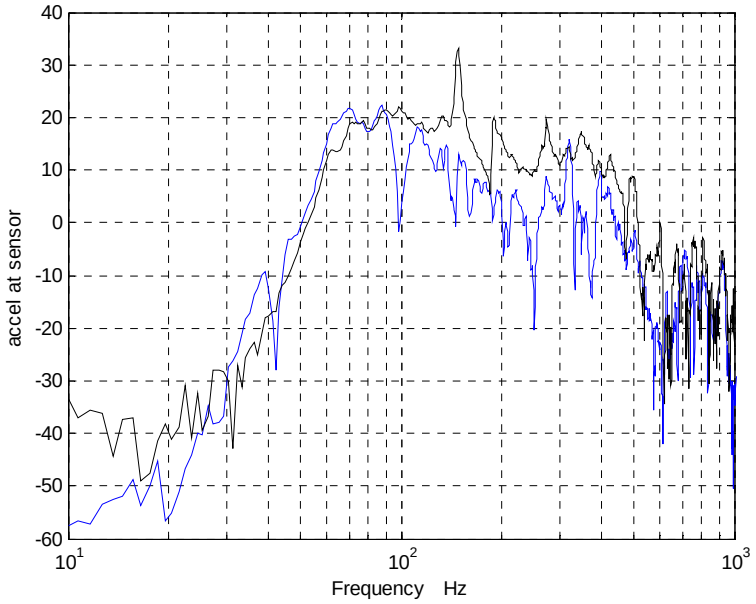

Figure 5.11: Measured acceleration of base plate (black trace) and tile (blue trace)

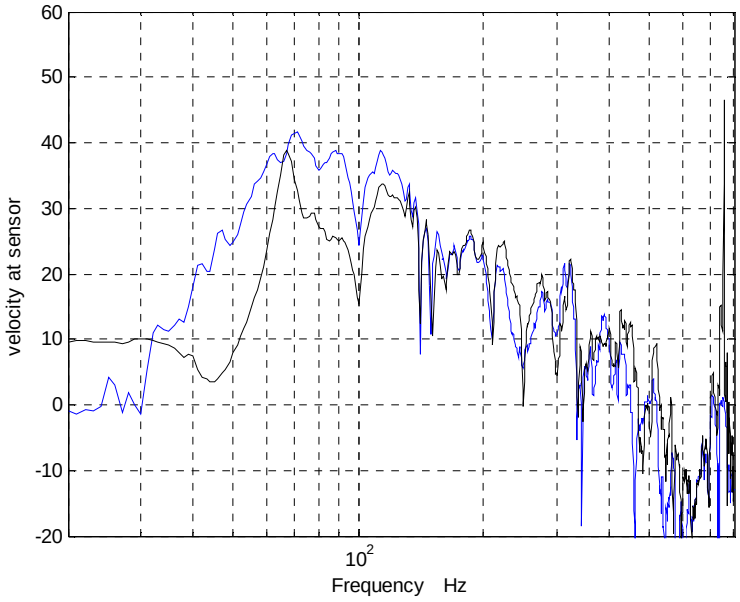

Figure 5.12: Velocity signal of tile # 1 control off (blue trace) and control on (black trace)

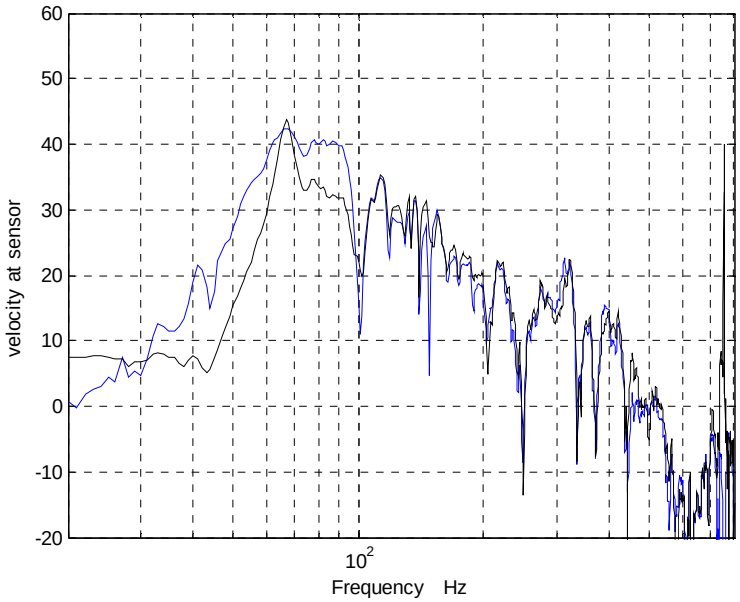

Figure 5.13: Velocity signal of tile # 2 control off (blue trace) and control on (black trace).

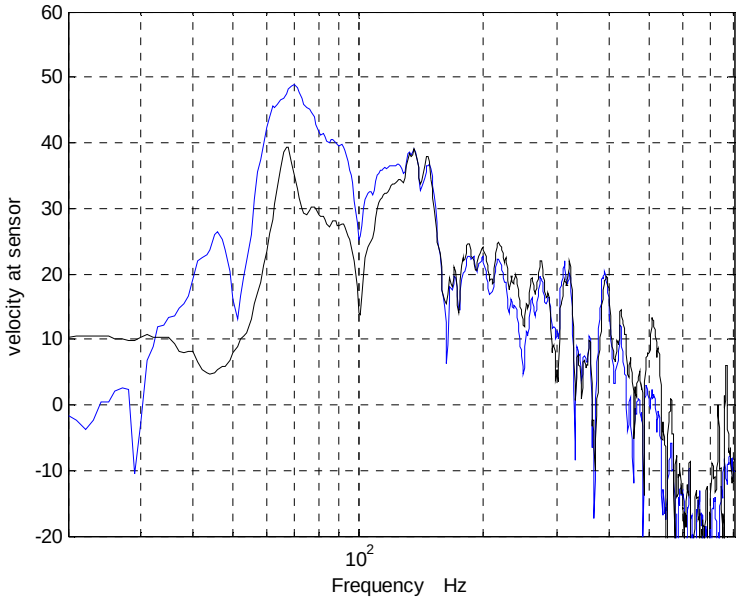

Figure 5.14: Velocity signal of tile # 3 control off (blue trace) and control on (black trace).

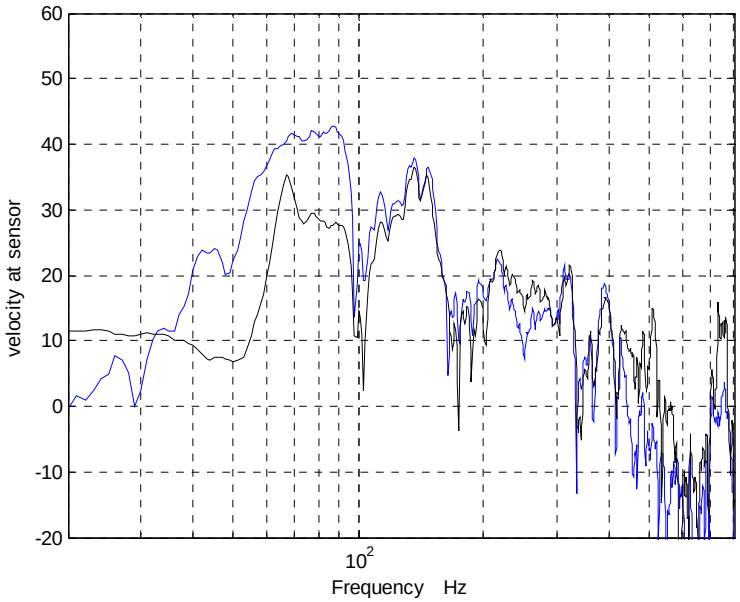

Figure 5.15: Velocity signal of tile # 4 control off (blue trace) and control on (black trace)

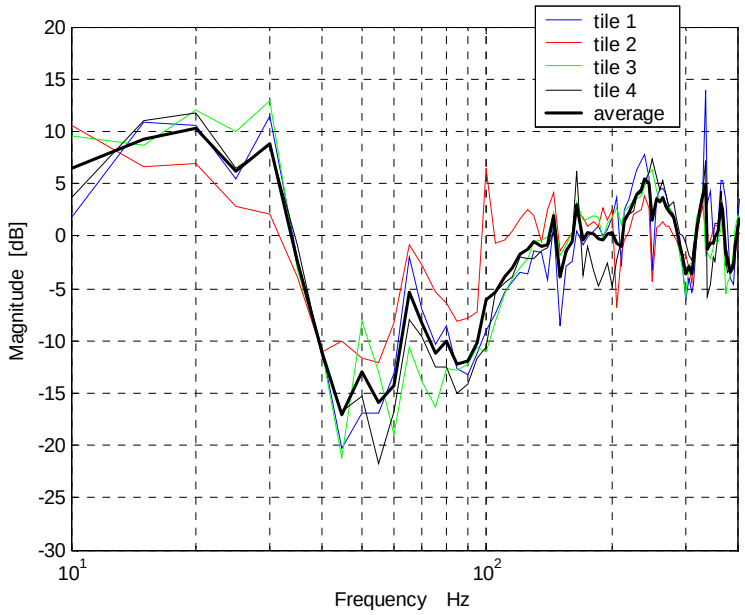

Figure 5.16: Active attenuation for the four tiles using a decentralized feedback controller

In order to estimate the total sound radiated power from the tiles before and after feedback control is applied, the velocity of each tile was measured using a laser vibrometer at 3 points along the width of each tile. The measured velocities were used to compute the total acoustic radiated power of the tiles in the passive and active cases. This assumes that there is no sound radiated by acoustic leaks on the sealing gaskets around the tiles or any other flanking path. The sound radiated through the sealing was verified to be insignificant based on a comparison of the sound radiated by the tile estimated using surface velocity measurements and a far-field microphone array as discussed in Section 3.4.5. The sound power radiated by the base plate without the tiles is also estimated from velocity measurements. Comparing the sound radiated by the plate to the sound radiated by the tiles, the total passive attenuation provided by the tiles in the passive case (with control off) is about 16 dB. Applying feedback control provides an additional 4.2 dB of attenuation of the sound radiated power.

Next section presents experimental results obtained applying feedforward control to the multiple tile system.

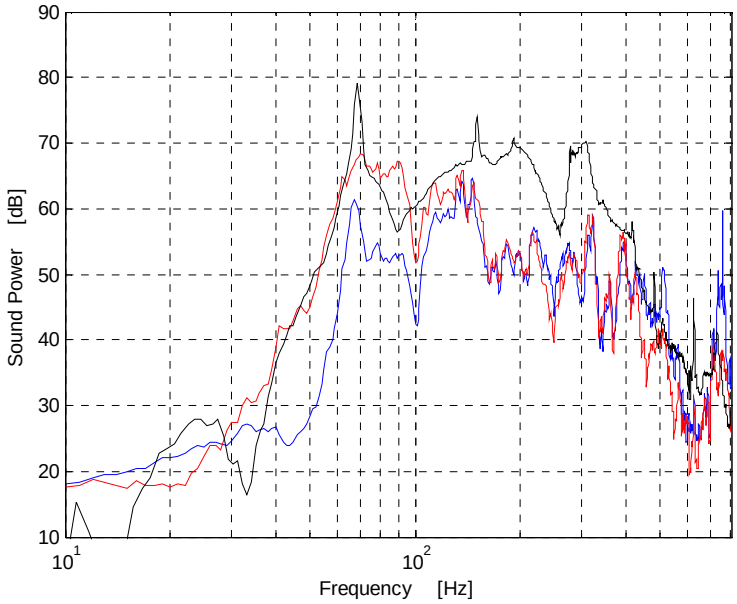

Figure 5.17: Estimated sound radiated power of the base structure without the tile treatment (black trace), the radiated power of the tiles with control off (red trace) and the radiated power of tiles with control on (blue line).

5.2 Decentralized Feedforward Control

Last section investigated the use of multiple independent SISO feedback controllers (decentralized feedback control) to control the tile normal velocity in a multiple tile application. Feedback control has the advantage of not requiring a reference signal and thus can be applied to problems when no information of the disturbance can be obtained in advance. However, the performance of the feedback control system was largely limited by the tile-mount high frequency dynamics, control plant phase lag (delay in the feedback loop) and the inter-tile coupling.

Chapter 4 presented active control results of a single tile system applying feedforward control. A single accelerometer placed on the base structure was used as a reference sensor, with good control results being obtained. In this section the use of feedforward control is

investigated for a four tiles system. Both an ideal reference and real references were used in the tests and both coupled and uncoupled feedforward controllers are tested. The experimental setup and results were presented next.

5.2.1 Experimental Setup

The multiple-tile setup studied in this section consisted of the four-tile system described in the feedback control section and shown in Figure 5.2. Four B&K accelerometers were attached to the center of each tile and used as error signals. Four additional PCB miniature accelerometers were attached to the base plate for monitoring the base structural vibration and also served as reference signals. The outputs of the controller were connected to PCB piezoelectric amplifiers used to drive the *Thunder* active mounts. Band limited white noise from 50-500 Hz was input to a loudspeaker via an audio power amplifier for generating the acoustic disturbance to the base plate.

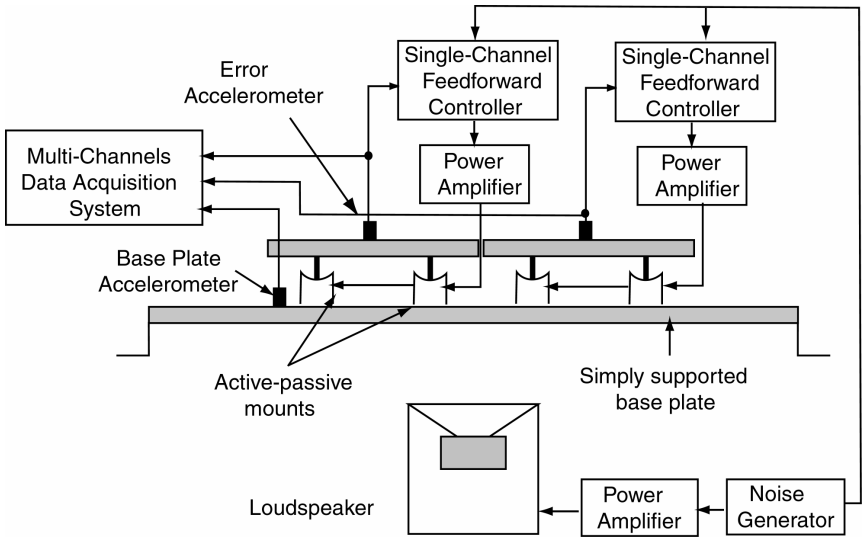

Figure 5.18: Experimental setup used for the multiple independent SISO feedforward control of multiple tiles with ideal reference

A feedforward filtered x-LMS algorithm was implemented in a controller board based on Texas C-40 DSP and running on a PC system operated via a LabView interface. The same

procedure described for the single tile system was used to setup the controller. The system identification of the secondary path models were done by successively driving with white noise each tile active mount and measuring the correspondent accelerometer response signal.

As mentioned above, both an ideal reference and a real reference signals were used for the multiple tile feedforward control tests. The ideal reference was obtained directly from the noise generator signal that served as disturbance to the system. Several PCB miniature accelerometers attached to the base plate were used to generate reference signals in a scheme that could be used in a practical application of an active tile system.

Initially, prior to running the feedforward control tests the configuration of the multiple channel system has to be defined. This involves defining the coupling of the control system channels, which defines if each control filter will control a single or a combination of the error signals. In addition, for the case of multiple reference signals is it necessary to define if each control filter will use a single or a combination of reference signals.

5.2.2 Active Control Results Using an Ideal Reference Signal

The initial active control tests of the multiple tile system using feedforward control used a delayed ideal reference obtained from the disturbance generator signal. Best control performance was obtained by setting the controller sampling rate at 2000 Hz. The secondary path FIR filter used 256 coefficients and 512 coefficients were used for the control filter.

Decentralized Feedforward Control

As discussed in Chapter 3, a decentralized feedforward controller can be advantageous for large systems where a fully coupled controller would imply in great amount of wiring and great amount of processing power to implement. Figure 5.19 shows plots of the acceleration of the base structure under the tile, the acceleration of the passive tile and the acceleration of the active tile with feedforward control for one of the tiles (tile 3). Only the results of a single tile are presented, since the performances of the other tiles are very similar. Good active reduction of the tile vibration is obtained throughout the frequency band of 40-600 Hz

with a total overall active attenuation of 13 dB. In addition, the tile acceleration has an overall passive reduction of 10 dB with relation to the base plate acceleration.

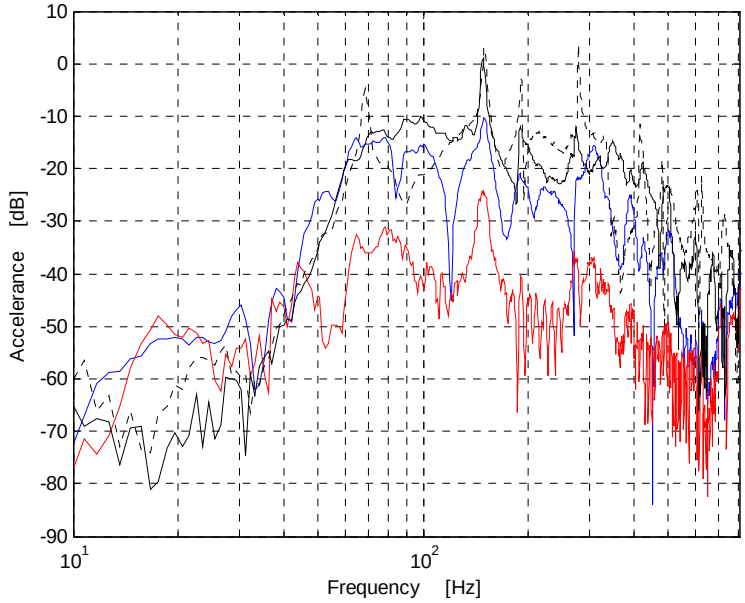

Figure 5.19: Acceleration results for a tile (tile 3) using feedforward control with an ideal reference. Shown are the acceleration response of base plate (black line), acceleration of the tile with control off (blue line) and acceleration of the tile with control on (red line). The acceleration of the base plate before the tiles were installed is also shown (dashed black line).

The total sound power radiated by the four tiles with and without active control was estimated based on measurements of the velocity of each tile at 3 points along its width using a laser vibrometer. The estimated total sound radiated power results are presented in Figure 5.20 for the base plate without tiles, for the tiles with control off and for the tiles with control on. The sound radiated power of the base plate was estimated from measurements of the plate acceleration at 12 points before the tiles were installed. The estimated sound radiated power was attenuated by 21.8 dB, with a passive attenuation of 9 dB and an overall active attenuation of 12.8 dB.

The complete set of the tile surface velocities measurements results is included in Appendix C. Included in the Appendix C is also the sound power estimated using 3 velocity

measurement points along the length of each tile and a single point at the center of each tile. The results show no significant difference, indicating that a single point measurement at the center of the tile is sufficient to estimate the sound radiated by the tile.

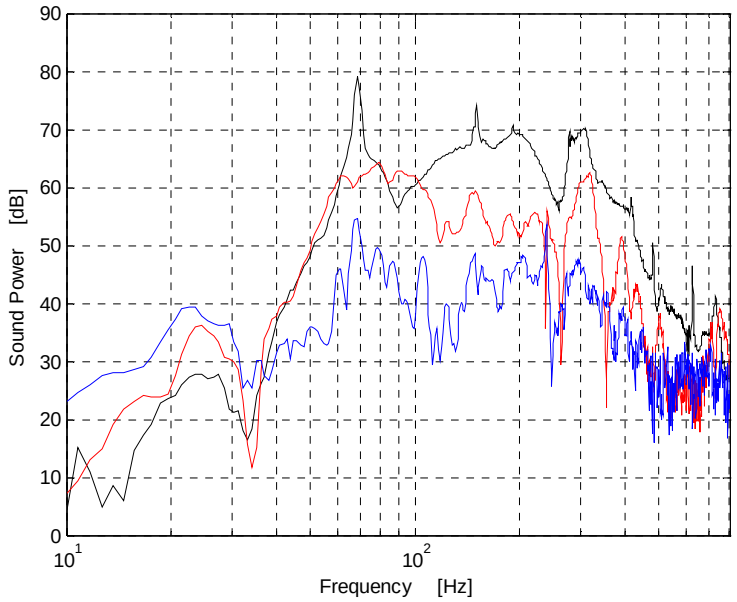

Figure 5.20: Total sound radiated power for 4 tiles. Radiated power of uncovered base plate (black line), radiated power of tiles without control (dashed line) and radiated power of tiles with feedforward control and ideal reference (blue line).

Fully Coupled MIMO Feedforward Controller

The results presented above were obtained in a decentralized controller configuration, where each adaptive filter is updated to control the signal of a single error sensor. However, as discussed earlier, the tiles are mechanically coupled to each other through the base structure, through the acoustic cavity between the base structure and the tiles and through the sealing gaskets. A centralized multiple channel feedforward controller can be setup so that the coupling between the tiles is taken into account so that all the output control signals are used to minimize the sum of the squared error signals. The system setup is done during the secondary paths identification step, by driving a tile with white noise and measuring the

resulting acceleration of all the tiles of the system. This procedure results in 16 secondary paths filters and 16 control filters, which increases significantly the computational burden of the controller system.

Figure 5.21 presents the tile acceleration results measured for one of the tiles with control off and control on, in a coupled (MIMO) and decoupled controller (SISOs) configurations. It is observed that using a centralized MIMO controller allows only slightly better performance than the multiple SISO controllers in the low frequency range below 50 Hz. The overall attenuation of MIMO controller is similar to the four SISO controllers indicating that decentralized feedforward controller can successfully be applied to multiple tiles system without significant performance loss.

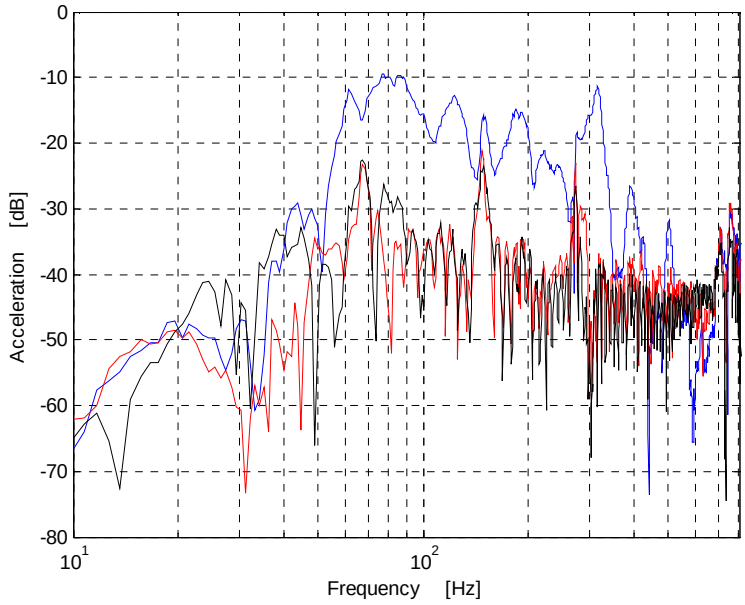

Figure 5.21: Acceleration of tile number 2. Control off (blue line), four SISO feedforward controllers (black line), MIMO feedforward controller (red line)

5.2.3 Control Results Using Base Acceleration Reference Signals

This section presents experimental results of the active control of the multiple tile system shown in Figure 5.2 using feedforward control with acceleration measurements of the base

structure as the reference signals.

It is well known that in order to obtain good control performance with a feedforward controller, the reference signal has to be well correlated to the disturbance [62,63,64]. When using a reference signal obtained from acceleration measurements of the base plate vibration, it is important that the accelerometer locations are chosen such as to avoid nodal lines of the vibration modes of the base plate. Initial active control tests were performed using a single accelerometer attached near the center of the base plate used as a reference signal. Figure 5.22 shows the acceleration of the base structure under the tile, the acceleration of the passive tile and the acceleration of the active tile for this case.

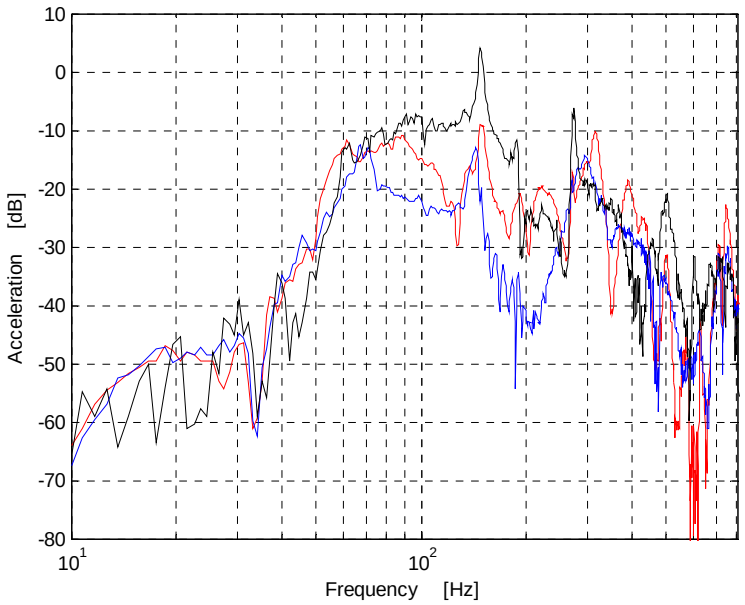

Figure 5.22: Acceleration of the tile for feedforward control using single error sensor at the center of the base plate as the reference signal. Black trace is the acceleration of the base plate, the red trace is the acceleration of the tile with control off and the blue trace is the acceleration of the tile with control on.

An overall active attenuation of 3.9 dB was obtained. Note the low control performance at the peaks around 150 Hz and 300 Hz that correspond respectively to the (2,1) and (2,2) vibration modes of the base plate. Note also that an accelerometer placed at the center of the

base plate will be located at the nodal lines of these modes. In addition, low control performance was obtained at the fundamental frequency of the base plate. A possible reason for this low control performance is that the mechanical input impedance of the base plate is small at its resonance and thus, the control forces applied by the active mounts affect the vibration of the base plate and feedback onto the reference signal.

As mentioned earlier, the performance of a feedforward control system depends on the coherence between the error and reference signals. Figure 5.23 shows the coherence between the one of the error signals and the reference signal, measured for the cases of an ideal reference and for the acceleration reference. Note the low coherence values at the frequencies corresponding to the resonances of the base plate and in particular at around 100 Hz, that corresponds to the base plate first resonance frequency.

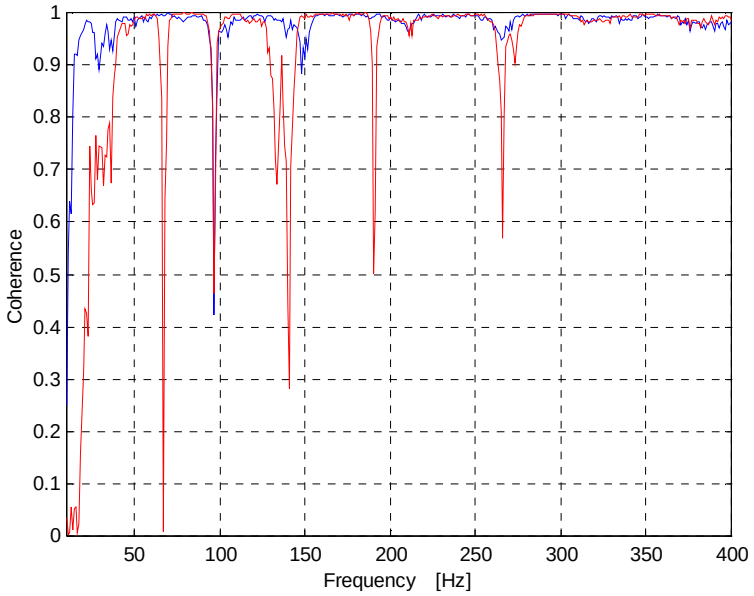

Figure 5.23: Coherence between the error signal and the reference signal. Blue trace is for the ideal reference and the red trace is for the base plate acceleration as a reference.

Further feedforward control tests were performed using four reference signals obtained from base plate acceleration measurements at locations near the tile mounts. Each reference signal is used only for the corresponding tile, thus implementing four independent SISO systems.

Figure 5.24 shows the corresponding acceleration of the base structure under the tile, the acceleration of the passive tile and the acceleration of one of the active tile. In this case, an overall active attenuation of 4.8 dB was obtained.

Additional tests were performed using two reference signals obtained from two acceleration measurements, under one tile and at the center of the plate. Figure 5.25 shows the acceleration of the base structure under the tile, the acceleration of the passive tile and the acceleration of the active tile for this case. For this choice of reference signal an overall active attenuation of 8.3 dB was obtained. The combination of the two acceleration measurements allows detecting all the base plate vibration modes and good performance is obtained throughout the entire frequency band (60-400 Hz).

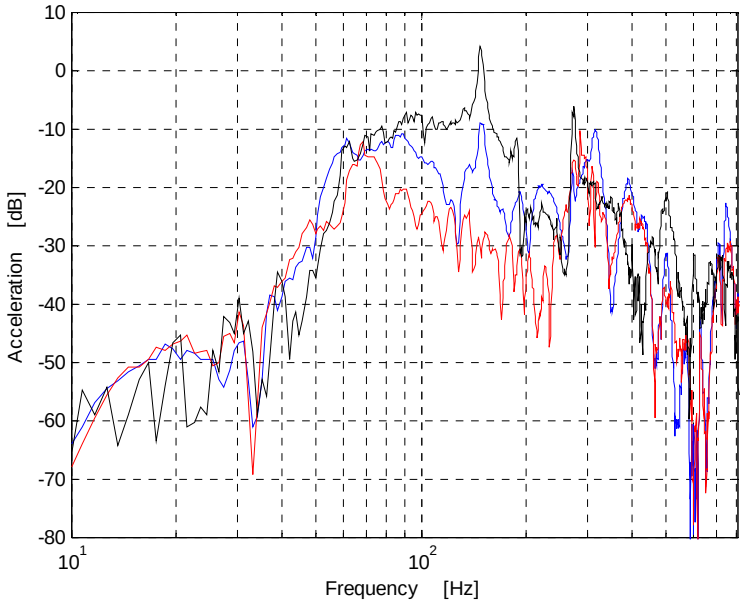

Figure 5.24: Feedforward control results using 4 decoupled reference sensors near the mount of each tile as reference signals. Black trace is the acceleration of the base plate, the blue trace is the acceleration of the tile with control off and the red trace is the acceleration of the tile with control on.

The total sound power radiated by the four tiles with and without control was estimated by measuring the surface velocity of each tile at 3 points along its width using a laser

vibrometer. The sound radiated power results for the base plate before installing the tiles, for the tiles with control off and for the tiles with control on and four independent reference signals are presented in Figure 5.26. Observe the relatively poor control performance around 300 Hz, since the reference signal setup used for this test did not measure the (3,1) mode of the base plate, that is an efficient sound radiator. An overall active performance of 7.2 dB was obtained.

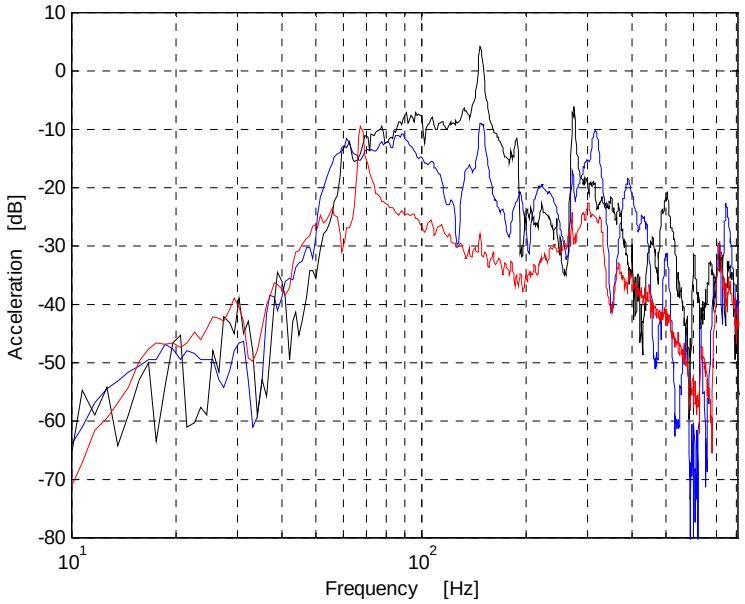

Figure 5.25: Feedforward control results for 2 references, one at the center of the plate and one near the mount of one the tiles. Black trace is the acceleration of the base plate, the blue trace is the acceleration of the tile with control off and the red trace is the acceleration of the tile with control on.

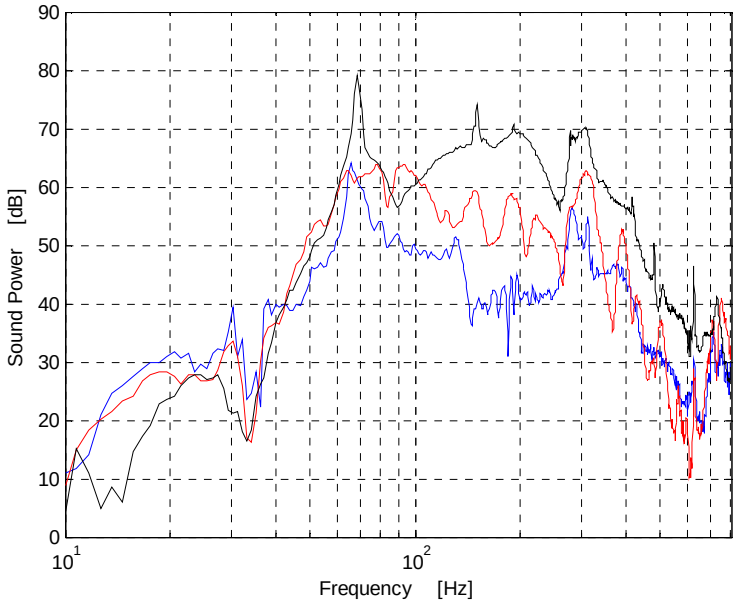

Figure 5.26: Sound radiated power for 4 tiles computed from velocity measurements at 3 points on each tile. Base plate without tiles (black trace), tiles with control off (red trace) and tiles with control on and 4 uncoupled reference sensors (blue trace).

5.2.4 Intensity Measurements

Last section the sound power radiated by the tiles was obtained from velocity measurements of the tile surface that should give an accurate estimate of the sound power as long as there are no leaks through the tile gaskets or other flanking paths. In order to have an acoustic measurement of the sound radiated power outside an anechoic chamber, intensity measurements were performed.

The measurement procedure employed is detailed in the ISO 9614-2, “Determination of sound power levels of noise sources using sound intensity - Part 2: measurement by scanning”. In this procedure the probe is used to scan the measurement surface during the date acquisition to obtain a space averaged value of the intensity. A box shaped measurement surface enclosing the source should be initially defined. The scan should follow equally spaced parallel lines along each measurement surface with the probe normal

to the measurement surface and turning at each edge. The scanning speed should be between 0.1m/s and 0.5 m/s and the duration of the scan over an area segment should be no less than 20 seconds. In addition, the recommended distance to the source is between 10cm to 30cm.

The sound radiated power obtained following the procedure described above is plotted in the Figure 5.27 below for the passive case and for active case using feedforward control with an ideal reference. An overall attenuation of 8.5 dB was measured. This is lower than the attenuation predicted with tile velocity measurement of 13 dB. This difference can probably be attributed to the presence of acoustic leaks or sound radiation by the sealing gaskets in the velocity measurement procedure, and sound radiation from the adjacent MDF board baffle in the intensity measurement procedure.

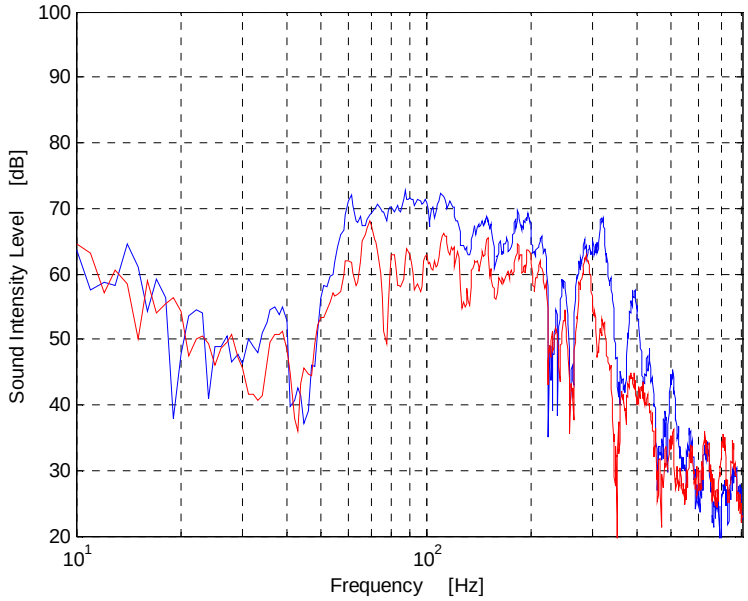

Figure 5.27: Sound radiated power for 4 tiles computed from measured intensity. Blue trace is for control off and red trace is for feedforward control on with ideal reference.

5.3 Multiple Tile Performance Prediction

From the point of view of system design it would be desirable that the performance of the

multiple tile system could be predicted based on the performance of a single tile. The use of an analytical approach to model a multiple tile system is complicated due to the large system of equations that needs to be solved. In addition it is very challenging to realistically model the inter-tile coupling mechanisms, which affect the performance of the multi-tile system.

An alternative approach is to estimate the performance of a multi-tile system based on the measured experimental performance of a single tile. This approach can only give approximate results because the performance of a single tile is larger than the performance of a multiple tile system due to the inter-tile coupling that will affect to some degree the performance of the multi-tile system. In addition it considers that each tile has the same vibration response or in other words, the base plate excites each tile in the same way. If the coupling between the tiles is small, the performance of the multi-tile system should approach that of the single tile. Next, we will investigate this approach.

First, the performance of a four tiles system was estimated based on the performance of a single tile for a feedforward controller using an ideal reference. The sound radiated power for the single tile case with control off and control on was shown in Figure 3.50. The active control performance for this case was 14.5 dB. The performance of the multiple-tile system will be estimated using the velocities measured at 9 points on the surface of the single tile and assuming that the four tiles vibrate with the same displacements. The total sound radiated power predicted in this manner is shown in Figure 5.28. Note that the overall sound power levels are 12 dB higher than for the single tile, as is expected since the sound power should increase 6 dB for each doubling in the area. The estimated multiple tile results in an active performance of 15.3 dB, which is 2.5 dB higher than the actual active performance of 12.8 dB measured for the four tile system and shown in Figure 5.20.

The same approach is repeated now for the case of feedforward control and reference signals derived from base acceleration measurements. The performance of the single tile system is shown in Figure 3.51 and an active performance of 10.8 dB was obtained.

The total sound radiated power for the four tiles system estimated from the single tile result with and without control is shown in Figure 5.29 and an active performance of 11 dB is

obtained. This estimation is 3.5 dB higher than the best-measured performance of the multi-tile system of 8.5 dB for a 2 references system, which is shown in Figure 5.30.

The results discussed above shows that the multiple tile system performance predicted based on the response of a single tile overestimates the performance of the real four tile system by about 2-4 dB. The lower performance of the real system can be attributed to coupling between the tiles and feedback from the control forces to the reference signal. Thus, the performance of a multiple tile system can be reasonably predicted from the performance of a single tile system as long as the quality of reference signal is similar for both the single and multi-tile systems and that inter-tile coupling is small.

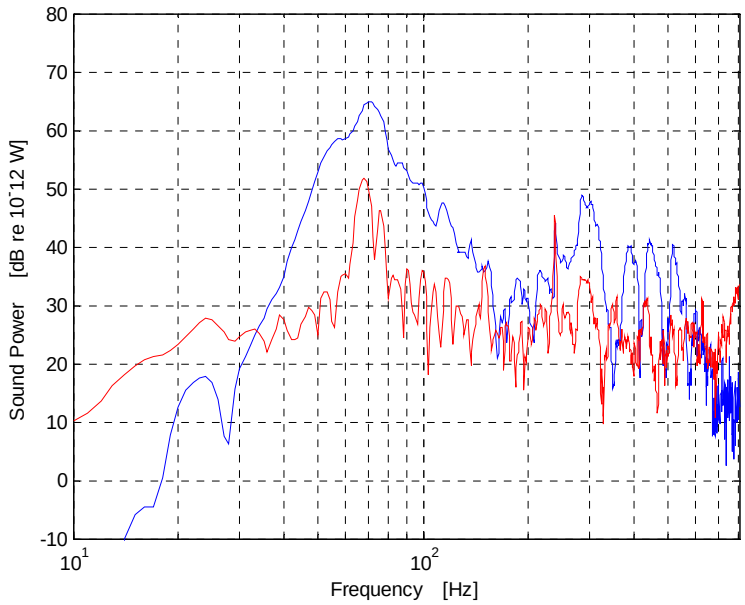

Figure 5.28: Sound radiated power prediction for 4 tiles base on velocity measurements at 9 points on a single tile system. Tiles with control off (red trace) and tiles with control on (blue trace), ideal reference case.

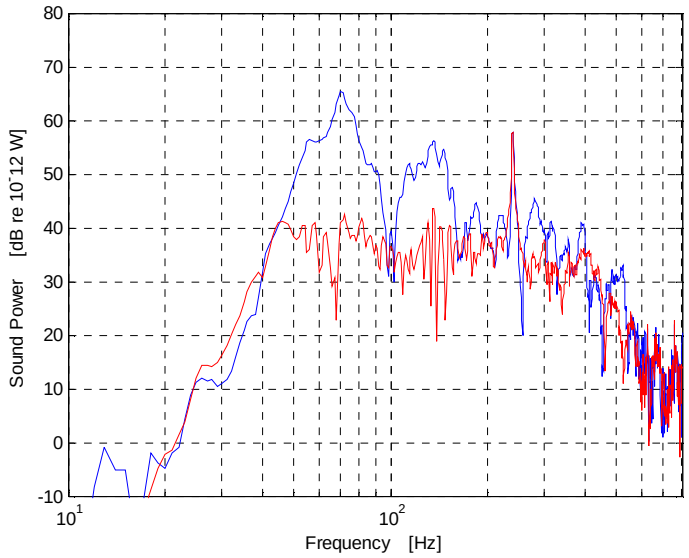

Figure 5.29: Sound radiated power estimated for 4 tiles computed based on velocity measurements at 9 points on a single tile system. Tiles with control off (blue trace) and tiles with control on (red trace)

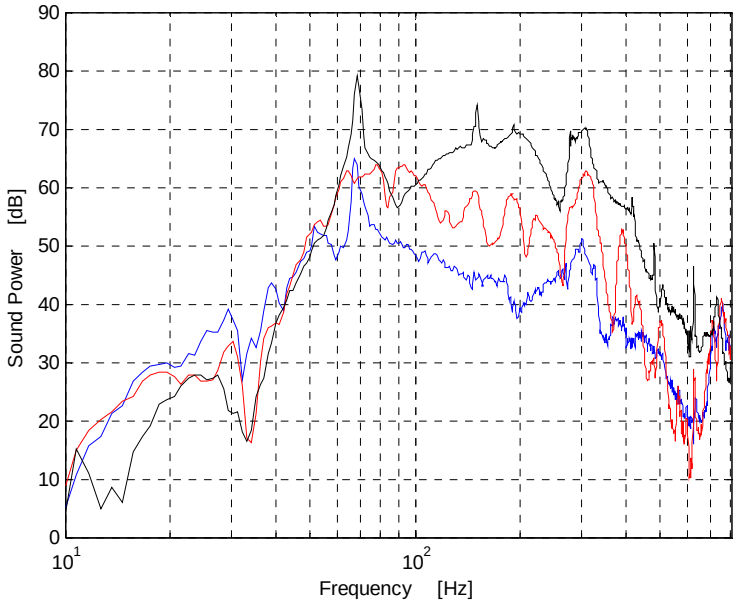

Figure 5.30: Sound radiated power for 4 tiles computed from velocity measurements at 3 points on each tile. Base plate without tiles (black trace), tiles with control off (red trace)

and tiles with control on (blue trace), 2 acceleration reference signals.

5.4 Summary

In this Chapter the active performance of a multiple-tile system with four tiles for controlling sound radiation was experimentally investigated and both feedback and feedforward control schemes were applied. The decentralized feedback control tests used the same SISO analog feedback controller designed for the single tile system studied in Chapter 3 for each of the four tiles. The experimental results showed that the performance of the feedback control system suffered when compared to the single tile performance because of the inter-tile coupling. The inter-tile coupling was predicted using the analytical model and occurs through the base plate, air gap and the sealing gaskets interconnecting the tiles. In the experimental setup the inter-tile coupling results in a reduction in the feedback gains that can be applied before instability occurs. Nevertheless an overall active reduction in the sound power of about 4.5 dB in the bandwidth up to 130 Hz was demonstrated for the multi-tile system with independent feedback control loops.

The multiple tile system was also tested with a decentralized feedforward control approach. Both an ideal reference and a more practical reference signal using base acceleration measurements were tested. The active performance of the multiple tile system with an ideal reference was measured as 12.8 dB with bandwidth up to 400 Hz, which is about 2 dB lower than the performance of the single tile system.

The feedforward control approach was also tested using accelerations measurements on the base plate as reference signals. The measured performance is about 2 dB lower than the results obtained for the single tile system. The results suggest that performance of the multiple tile system is reduced by the presence of a certain degree of feedback from the control forces to the reference signal, which did not happen in the single tile case. This occurs due to the low input mobility of the base structure at its resonance. In addition it was observed that is it important to select carefully the number and location of the acceleration

measurements on the base plate in order to achieve best performance.

The sound radiated power for the case of active control on and off was measured using intensity measurements. Up to this point the sound radiated power results presented were based on velocity measurements and would be accurate assuming that there are no acoustic leaks. The results showed an attenuation of 8.5 dB, about 4.5 dB lower than the performance predicted based on the velocity measurements. However, the intensity measurements were made difficult by the low levels of sound pressure being radiated by the plate and also by the radiation of the adjacent wooden baffle and cannot be considered totally accurate.

Finally, the Chapter ends with a brief investigation of the prediction of the four-tile system performance based on velocity measurements performed on a single tile system. The results showed that the predictions overestimate the performance of the multi-tile system in about 2-4 dB, which can be attributed to the lower performance of the controller in the multi-tile system because of effects as coupling between the tiles and feedback from control to the reference signal.

The results presented in this Chapter clearly demonstrate the potential of the active tile approach in a multiple tile system. The coupling between the tiles was shown to be less of a problem in the feedforward control system case, which can be implemented in practical applications using acceleration measurements on the base structure as reference signals.

Chapter 6

6 Conclusions and Future Work

This work demonstrated analytically and experimentally the control of low frequency sound transmission through plates using a novel active-passive sound transmission control approach. The approach consists of using arrays of lightweight stiff panels (or tiles) attached to a radiating surface through active-passive mounts. The tile array is designed to cover the entire (or most of the) target structure surface. At low frequencies, the sound radiated by the tiles is mostly due to the tile piston mode of vibration (or volume velocity mode) and is proportional to its normal velocity. Thus, reductions in the total sound radiated power can be achieved by reducing the vibration levels of the tiles. This is performed by using independent single-channel controllers on each tile to generate control signals that are applied to the active mounts to reduce the normal velocity of the tile.

The active tile approach can be applied to numerous applications of active sound transmission control that require lightweight partitions with high transmission loss over a broad frequency range and simple control strategies. Note that one of the main motivations for using the active-passive tile approach is when the source levels and structural vibrations are very large, as for example in the rocket payload fairing application. Thus, mechanical actuators attached directly to the shroud will have to be large and exert enough control force. The use of active-passive tiles enables passive isolation to reduce the levels and then active inputs to act on the tiles, thus requiring much smaller and lighter actuators, as for example piezoelectric actuators as used in this work. The main goal of the present work was to investigate the sound transmission control characteristics of the proposed active-passive tile arrangement and approach.

The investigation was divided into a companion analytical and an experimental effort.

The motivation for the analytical component of the work was to determine the potential sound transmission control performance of the system. A coupled structural-acoustic model of the system was formulated based on an impedance-mobility matrix approach. The formulation was applied to model double-panel systems consisting of a rectangular base plate connected to a single or multiple tiles through active-passive isolators and an acoustic cavity. Initially, a single tile system was investigated that consisted of a single tile connected via two active mounts to a plate with clamped boundary conditions. The analytical model was validated by comparing analytical and experimental results for the control plant frequency responses and sound radiated power results. Simulations results showed significant passive attenuation of the sound transmission in the frequency range above the mass-air-mass resonance frequency of the system. Sound transmission was shown to be mostly due to the air-borne path that strongly couples the vibration of the tiles to the base structure vibration. Increased passive attenuation was demonstrated for an increase in the volume of the air gap formed between the tiles and the base structure. For the active control case, good attenuation of the sound radiated power was obtained and the frequency bandwidth of control extended up to the resonance frequency of the second flexible vibration mode of the tile (saddle type flexible mode). Further improvements of control bandwidth were shown possible if stiffer tiles were used or if an error sensor that directly measured sound radiated power was used. Then, the impedance-mobility model was extended to model a system with four tiles connected to a simply supported plate. The analytical model of the control plant showed the existence of inter-tile coupling mainly through the acoustic cavity. Despite the inter-tile coupling, good active attenuation was obtained with both feedback control and feedforward control approaches. Simulations of the plant response indicated that the system should be unconditionally stable for velocity feedback control in the case where the mounts have no internal dynamics.

The experimental part of the work was performed to evaluate the practical application of the active tiles approach in controlling sound transmitted through plates. Active tile prototypes were designed using lightweight composite panels and Thunder piezoelectric elements as integrated passive-active mounts. Two main experimental setups were used

for the investigations. The first experimental setup studied was a double panel partition consisting of a single tile mounted on a plate clamped in a window between acoustic chambers. This setup was used for preliminary investigations and for assessing the potential performance of a single tile system. It also allowed for direct measurements of the sound radiated power by the partition with an array of microphones and comparison to the sound radiated power estimated from velocity measurements on the tile surface. Optimal feedforward control algorithm implemented on a DSP-based system was used to reduce the velocity of the tile measured by accelerometers placed on the tile surface at the mount attachment locations. Both an ideal reference sensor obtained from the primary disturbance generator and a realistic reference, obtained by using a microphone close to the base plate (source side), were used. Significant reduction in the sound power radiated by the tiles was measured using an array of microphones and good correspondence was observed between attenuation of sound radiated power and attenuation of the tile velocity. In addition, an extension in the control bandwidth was demonstrated possible with the use of a stiffer tile, with little increased weight penalties.

The second experimental setup investigated approximated better the dynamics of large, low mobility systems where the active tile approach might be used. A larger and heavier plate was used as the base structure and a larger acoustic cavity was created between the tile and the base structure approximating better the system dynamics of the target application. This low mobility base structure allowed the application of skyhook damping in a similar fashion to that used for active vibration isolation in base excited systems. In addition, a low mobility base structure allowed that an accelerometer placed on the base structure to be used as reference sensor in feedforward control systems, since there is not a feedback path from the control forces to the reference signal. The same base structure was used for a single active-passive tile, as presented in this Chapter and a multiple (four) active-passive tile system (see Chapter 5) allowing direct comparison of the performance of the systems and assessing the effects of inter-tile coupling dynamics on the system performance. The attenuation of sound radiation by the active tiles was estimated based on measurements of the tile surface velocity obtained using a laser vibrometer. Both feedback and feedforward decentralized control schemes were demonstrated despite the

existence of the inter-tile coupling.

The main contributions and findings of this work are summarized as follows:

1) A lightweight and compact active-passive tile system with fully decentralized control and that can be applied for the control of sound transmission through large and low mobility structures was analyzed, designed and tested. Decentralized active vibration control of the tiles using SISO controllers with collocated force actuators and velocity sensors were demonstrated able to globally reduce the sound radiated power in the low frequency range before the flexible behavior of the tile is significant.

2) Novel active-passive tile prototypes were implemented and tested: tiles made of composite honeycomb material and active-passive mounts implemented with Thunder actuators resulted in a system that is lightweight, has good control authority and good passive vibration isolation characteristics. Because of its particular fabrication process, it was possible to use the Thunder actuator as an integrated passive-active isolation mount, where the passive vibration isolation capabilities comes from the flexibility provided by the curved steel plate to which the piezoelectric element is attached. By properly mounting the actuator it was possible to create a normal active force between the base and tiles while providing good passive isolation effect at high frequencies.

3) A coupled structural-acoustic model was developed for a single and a multiple tile systems and used to investigate sound transmission in the passive and active cases, with feedback and feedforward control approaches. Using the model it was shown that the frequency bandwidth of the system control performance was limited by flexible behavior of the tiles. In addition, for the multiple tile system it was possible to predict the inter-tile coupling through the air cavity.

4) A multiple tile system was used to investigate experimentally the feasibility of decentralized control implementation and expansion of the tile approach over larger areas (i.e. many tiles). Fully decentralized control systems were designed and implemented for both feedback and feedforward control approaches. Good performance was demonstrated

for a decentralized feedforward control system using measurements of the vibration of the base plate as reference signals. The performance of the feedback control system in the multiple tiles setup was lower than in the single tile setup because of inter-tile coupling effects.

Based on the results obtained in this work the proposed tile approach has good potential for application in practical control of launch vehicle payload noise and other applications. However, additional work needs to be performed before the tile approach can be implemented in a large scale realistic application. Future is necessary in hardware development including optimized tiles and actuators, low-power consumption controllers and lightweight power supply systems. In addition, additional work needs to be performed to improve the performance of the decentralized feedback control system that would reduce the complexity of the control hardware. Recommendations for future work are presented below.

Future Work

Some suggestions of future work are as follows:

- Optimization of the tile design using composite materials to achieve optimal flexural stiffness to mass ratios;
- Optimize the actuator design to achieve desired passive vibration isolation characteristics, high authority and insignificant internal dynamics to extend bandwidth of feedback control;
- Investigate the use of shaped distributed sensors that estimate sound radiation modes to extended bandwidth of control;
- Investigate analytically and experimentally the control of sound transmission into an enclosure;
- Investigate the use of a hybrid feedback-feedforward controller;

- Optimize the distribution of vibration reference sensors on the base structure for best feedforward control performance;
- Integrate the active tile design to conventional passive liners;
- Investigate tile seal and edge effects;
- Investigate the effect of base structure curvature on the system performance;
- Investigate required size of tile relative to the structural wavenumber spectrum of the base vibration.
- Develop low cost controller hardware and power supply systems.

References

[1] Fahy, F., and Walker, J., Fundamentals of Noise and Vibration, (London: E \& FN Spon, 1998).

[2] Timmins, A., and Heuser, R., "A Study of First-Day Malfunctions," NASA TN D-6474}, 1971.

[3] The Boeing Company, "Delta II Payload Planners Guide," 2000.

[4] Bradford, L., and Manning, J. E., "Attenuation of the Cassini Spacecraft Acoustic Environment," Sound and Vibration 30-37, October, 1996.

[5] Nelson, P.A., and Elliott, S. J., Active Control of Sound, (San Diego:Academic Press Inc., 1995).

[6] Fuller, C.R., et al., Active Control of Vibration, (San Diego: Academic Press Inc., 1996).

[7] Deffayet, C., and Nelson, P. A., "Active Control of Low-Frequency Harmonic Sound Radiated by a Finite Panel," J. Acoust. Soc. Am., 84 (6), 2192-2199, 1988.

[8] Pan, J., et al, "Active Control of Far-Field Sound Radiated by a Rectangular Panel: a General Analysis," J. Acoustical Soc. Am. 91 (4), pt.1, 2056-2066, 1992.

[9] Snyder, S. D., and Hansen, C. H., "The Design of Systems to Control Actively Periodic Sound Transmission into Enclosed Spaces, Part I: Analytical Models," J. of Sound and Vibration, 170 (4), 433-449, 1994.

[10] Snyder, S. D., and Hansen, C. H., "The Design of Systems to Control Actively Periodic Sound Transmission into Enclosed Spaces, Part II: Mechanisms and Trends," {J. of Sound and Vibration, 170 (4), 451-472, 1994.

[11] Fahy, F., Sound and Structural Vibration, (London: Academic Press, 1985).

[12] Kim, S-M and Brennan, M. J., "Active Control of Harmonic Sound Transmission into an Enclosure Using Both Structure and Acoustic Actuators," J. Acoust. Soc. Am., 107 (5), pt. 1, 2523-2534, 2000.

[13] Pan, J. and Hansen, C. H., "Active Control of Noise Transmission Through a Panel into a Cavity: I. Analytical Study," J. Acoustical Soc. Am, 87 (5), 2098-2108, 1990.

[14] Niezrecki, Christopher, Structural & Internal Acoustic Response of Cylinders with Applications to Rocket Payload Fairings, PhD Thesis, Mechanical Eng. Dept,

Virginia Tech, 1999.

[15] Griffin, S. F., et al., “Power Consumption for Active Acoustic Control of Launch Vehicle Payload Fairings,” Adaptive Structures and Material Systems ASME Conference, AD-vol 60, 85-93, 2000.

[16] Griffin, S., Hansen, C. and Cazzolato, B., “Feedback Control of Structurally Radiated Sound into Enclosed Spaces Using Structural Sensing,” J. Acoust. Soc. America, 106 (5), 2621-2628, 1999.

[17] Van den Dool, T., et al., “Broadband MIMO ANC in an Ariane Fairing Model,” Proceedings of the Active 97, Budapest, Hungary, 861-872, 1997.

[18] Denoyer, K. K., et al., “Hybrid Structural/Acoustic Control of a Sub-Scale Payload Fairing,” SPIE Conference on Smart Structures and Integrated Systems, SPIE vol. 3329, 237-243, 1998.

[19] Fuller, C.R., et al., “Active control of Sound Radiation from a Vibrating Rectangular Panel by Sound Sources and Vibrational Inputs: an Experimental Comparison,” J. of Sound and Vibration, 145, 195-215, 1991.

[20] Dimitriadis, E. K., and Fuller, C. R., “Active Control of Sound Transmission Through Elastic Plates Using Piezoelectric Actuators,” AIAA Journal, 29 (11), 1771-1777, 1991.

[21] Wang, B-T., Fuller, C. R. and Dimitriadis, E. K., “Active Control of Sound Transmission Through Rectangular Plates Using Multiple Piezoelectric or Point Force Actuators,” J. Acoustical Soc. Am. 90 (5), 2820-2830, 1991.

[22] Thomas, D. R., et al., “An Analytical Investigation of the Active Control of the Transmission of Sound Through Plates,” J. of Sound and Vibration, 181 (3), 515-539, 1995.

[23] Beranek, L. L. and Work, G. A., “Sound transmission through multiple structures containing flexible blankets”, J. of the Acoustical Society of America, 21, 419-428, 1949.

[24] Carneal, J. P., and Fuller, C.R., “Active Structural Acoustic Control of Noise Transmission Through Double Panel Systems,” AIAA Journal, 33 (4), 618-623, 1995.

[25] Sas, P., Bao, C., Augusztinovicz, F. and Desmet, W., “Active Control of Sound Transmission Through a Double Panel Partition,” J. of Sound and Vibration, 180 (4), 609-625, 1995.

[26] Pan, X., Sutton, T. J. and Elliott, S. J., “Active Control of Sound Transmission Through a Double-Leaf Partition by Volume Velocity Cancellation,” J. Acoustical

Soc. Am.104 (5), 2828-2835, 1998.

[27] Gardonio, P. and Elliott, S. J., “Active Control of Structure-Borne and Airborne Sound Transmission Through Double Panel,” Journal of Aircraft, 36 (6), 1023-1032, 1999.

[28] Pan, J.and Hansen, C. H., “Active Control of Noise Transmission Through a Panel into a Cavity: II. Experimental Study,” J. Acoustical Soc. Am, 90 (3), 1488-1492, 1991.

[29] Pan, J.and Hansen, C. H., “Active Control of Noise Transmission Through a Panel into a Cavity: III. Effect of the Actuator Location,” J. Acoustical Soc. Am, 90 (3), 1493-1501, 1991.

[30] Cazzolato, B.S. and Hansen, C. H.,”Active Control of Sound Transmission Using Structural Error Sensing,” J. Acoust. Soc. Am., 104 (5), 2878-2889, 1998.

[31] Leo, D. J. and Anderson, E. H., “Vibroacoustic Modeling of a Launch Vehicle Payload Fairing for Active Acoustic Control”, AIAA paper 98-2086, 3212-3222, 1998.

[32] Glaese, R. M. and Anderson, E. H., “Active Structural-Acoustic Control for Composite Payload Fairings, ” Proceedings of the SPIE vol 3668, 450-461, 1999.

[33] Johnson, M. E. and Elliott, S. J., “Active Control of Sound Radiation Using Volume Velocity Cancellation,” Journal of the Acoustical Society of America, 98, 2174-2186, 1995.

[34] Griffin, S., Lane, S. A., Hansen, C. and Cazzolato, B., “Active Structural-Acoustic Control of a Rocket Fairing Using Proof-Mass Actuator,” Journal of Spacecraft and Rockets, 38 (2), 219-225,2001.

[35] Lane, S. A., Kemp, J. D., Griffin, S. and Clark, R., “Active Acoustic Control of a Rocket Fairing Using Spatially Weighted Transducer Arrays,” Journal of Spacecraft and Rockets, 38 (1), 112-119.

[36] Osman, H., Johnson, M., Fuller, C. R. and Marcotte, P., “Interior Noise Reduction of Composite Cylinders Using Distributed Vibration Absorbers,” AIAA paper 2001-2230, 2001.

[37] Johnson, M., Fuller, C. R. and Marcotte, P., “Optimization of Distributed Vibration Absorbers for Sound Transmission into a Composite Cylinder,” AIAA paper 2001-2232, 2001.

[38] Guigou, C., and Fuller, C. R., “Adaptive Feedforward and Feedback Methods for Active/Passive Sound Radiation Control Using Smart Foam,” J. Acoust. Soc. Am.,

104 (1), 226-231, 1998.

[39] Guigou, C., and Fuller, C. R., “Control of Aircraft Interior Broadband Noise with Foam-PVDF Smart Skin,” J. of Sound and Vibration, 220 (3), 541-557, 1999.

[40] Johnson, B. D., and Fuller, C. R., “Broadband Control of Plate Radiation Using a Piezoelectric Double-Amplifier Active Skin and Structural Acoustic Sensing,” J. Acoust. Soc. Am, 107 (2), 876-884, 2000.

[41] Leishman, T. W., and Tichi, J., “A Fundamental Investigation of the Active Control of Sound Transmission Through Segmented Partition Elements,” Proceedings of the Noise-Con 97, 137-148, 1997.

[42] Hirsch, S. M. and Sun, J. Q., “An Analytical Study of Interior Noise Control Using Segmented Panels", J. of Sound and Vibration, 231(4), pp. 1007-1021, 2000.

[43] Hirsch, S. M. et al, “Experimental Study of Smart Segmented Trim Panels for Aircraft Interior Noise Control”, J. of Sound and Vibration, 231(4), pp. 1023-1037, 2000.

[44] Ross, B. W. and Burdisso, R. A., “Low Frequency Passive Noise Control of a Piston Structure with a Weak Radiating Cell,” J. Acoust. Soc. Am., 106 (1), 226-232, 1999.

[45] Elliott, S. J. and Johnson, M.E., “Radiation Modes and the Active Control of Sound Power,” J. Acoust. Soc. Am, 94 (4), 2194-2204, 1993.

[46] Thomas, D. R., et al., “An Experimental Investigation into the Active Control of Sound Transmission Through Stiff Light Composite Panels,” Noise Control Engineering Journal, 41 (1), 273-279, 1993.

[47] Sharp, S. J., et al., “Transmission Loss Characteristics of an Active Trim Panel,” Proceedings of the Noise-Con 97, 149-160, 1997.

[48] Johnson, M. E., Elliott, S. J., “Active Control of Sound Radiation from Vibrating Surfaces Using Arrays of Discrete Actuators,” J. of Sound and Vibration, 207 (5), pp. 743-759, 1997.

[49] Thomas, D. R., and Nelson, P. A., “Experiments on the Active Control of Broadband Sound Radiation from a Lightweight Partition,” J. of Sound and Vibration, 202 (3), pp. 438-445, 1997.

[50] Dowell, E. H., et al., “Acoustoelasticity: General Theory, Acoustic Natural Modes and Forced Response to Sinusoidal Excitation, Including Comparisons with Experiment,” J. of Sound and Vibration, 52 (4), 519-542, 1977

[51] Gardonio, P., Elliott, S. J. and Pinnington, R. J., “Active Isolation of Structural

Vibration on a Multiple-Degree-of-Freedom System, Part I: The Dynamics of the System," J. of Sound and Vibration, 207 (1), 61-93, 1997

[52] Gardonio, P., Elliott, S. J. and Pinnington, R. J., "Active Isolation of Structural Vibration on a Multiple-Degree-of-Freedom System, Part II: Effectiveness of Active Control Strategies," J. of Sound and Vibration, 207 (1), 95-121, 1997

[53] Kinsler, L. E., Frey, A. R., Coppens, A. B. and Sanders, J. V., Fundamentals of Acoustics, (New York, John Wiley \& Sons, 3rd Ed., 1982).

[54] Vinson, J. R., The Behavior of Sandwich Structures of Isotropic and Composite Materials, (Lancaster, PA, USA : Technomic Publishing Company, Inc., 1999).

[55] Brennan, M. J., Garcia-Bonito, J., Elliott, S. J., David, A., and Pinnington, R. J., "Experimental Investigation of Different Actuator Technologies for Active Vibration Control," Smart Materials and Structures, 8, 145-153, 1999

[56] Chen, W-K, Active Network Analysis, New York, 1989

[57] Ewins, D. J, Modal Testing: Theory, Practice and Applications, 2001

[58] ANSYS Inc, Instruction Manual, 1999.

[59] Inman, D. J., Engineering Vibration, 2nd ed., Prentice Hall Inc, New Jersey, 2001.

[60] Esteve, S. J. And Johnson, M. E, "Reduction of Sound Transmission into Circular Cylindrical Shells Using Distributed Vibration Absorbers and Helmoltz Resonators," J. of the Acoustical Society of America, 112(6), 2840-2848, 2002

[61] Bies, D.A and Hansen, C. H., Engineering Noise Control, 2nd Edition, E&FN Spon, New York,1999.

[62] Kuo, S.M and Morgan, D. R., "Active Noise Control Systems: Algorithms and DSP Implementations," John Wiley & Sons, Inc., New York, 1996.

[63] Elliott, S., Signal Processing for Active Control, Academic Press, London, 2001.

[64] Hansen, C. H., Understanding Active Noise Cancellation, Spon Press, London 2001.

[65] Waser, P. M. and Crocker, M. J., "Introduction to the Two-Microphone Cross-Spectral Method of Determining Sound Intensity," Noise Control Engineering Journal, 22(3), 76-85, 1984.

[66] Elliott, S. J., Serrand, M and Gardonio, P., "Feedback Stability Limits for Active Isolation Systems with Reactive and Inertial Actuators," Journal of Vibration and Acoustics, 123, 250-261, 2001

[67] Franklin, G. F., Powell, J. D. and Emami-Naeini, A., Feedback Control of Dynamic

Systems, 4th Edition, Prentice Hall, 2002.

[68] Natarajan, S., "Theory and Design of Linear Active Networks," MacMillan Publishing Company, New York, 1987.

[69] Elliott, S. J. and Boucher, C. C., "Interaction Between Multiple Feedforward Active Control Systems," IEEE Transactions on Speech and Audio Processing, 2(4), 521-530, 1994

[70] Skogestad, S. and Postlethwaite, I., Multivariable Feedback Control – Analysis and Design, John Wiley & Sons, New York, 1996.

[71] Sourias, D.D. and Manousiouthakis, V., "Best Achievable Decentralized Performance," IEEE Transactions on Automatic Control, 40 (11), 1858-1871, 1995.

[72] Wennhage, P., "Weight Minimization of Sandwich Panels with Acoustic and Mechanical Constraints," Journal of Sandwich Structures and Materials, 3, 22-49, 2001.

[73] Elliott, S. J., "Distributed Control of Sound and Vibration," Proceedings of the Active 04, pp 1-25, Williamsburg, VA.

[74] X. Huang, S. J. Elliott and M. J. Brennan, "Active Isolation of a Flexible Structure from Base Vibration," Journal of Sound and Vibration, 263, 357-376, 2003.

[75] Kim, S-M, Elliott, S. J. and Brennan, M. J., "Decentralized Control for Multichannel Active Vibration Isolation," IEEE Transactions on Control and Systems Technology, 9(1), 93-100, 2001.

[76] Serrand, M and Elliott, S. J., "Multichannel Feedback Control for the Isolation of Base-excited Vibration," Journal of Sound and Vibration, 234(4), 681-704, 2000.

Appendix A- Intensity Measurements

An alternative method to determine the sound radiated by a structure is to measure the sound intensity over a surface enclosing the structure. Sound intensity can be defined as the measure of the rate of flow of sound energy per unity area oriented normal to a wave front [1]. It can be shown to equal the product of sound pressure and particle velocity, hence being a vector quantity.

The use of sound intensity measurement instead of sound pressure is useful to determine the sound power of individual sources in the presence of other sources. In addition it is very useful to measure the sound insulation of partition without the necessity of special acoustic chambers [65].

The experimental determination of sound intensity requires the measurement of signals proportional to the instantaneous sound pressure and associated instantaneous particle velocity vector. In general, sound intensity measurements are performed using a so-called intensity probe that consists of a pair of phase matched pressure microphones separated a distance d from each other by a solid spacer. This device allows one to measure one component of the intensity vector at a time, in general the component normal to the surface of interest.

For $kd^2 << 1$, where k is the acoustic wavelength, the pressure at the midpoint between the microphones can be obtained from the average of the two pressure signals. In addition, the difference between the two microphone signals gives an approximation of the component of the pressure gradient along the trace connecting the two microphones. Observing that the pressure gradient is proportional to the particle acceleration, a signal proportional to the axial component of the particle velocity can be obtained by a temporal integration of the pressure difference signal.

As shown in [65] the sound intensity can be readily determined by the following

expression:

$$I = \frac{\mathrm{Im}\{G_{12}(\omega)\}}{\omega \rho d}$$

Where $G_{12}(\omega)$ is the cross spectrum of the two microphone signals and ρ is the air density.

When performing sound intensity measurement it's important to keep in mind the limitations of the two microphones measurement technique. One of the important limitations happens because of the approximation of the gradient of the pressure by a finite difference approximation. For a certain microphone distance d the approximation will be better for wavelengths much larger than d that is $\lambda >> d$.

On the other hand, for $\lambda >> d$ the actual physical phase difference between the microphone pressure signals becomes smalls and very well phase matched are required to avoid measurement errors. Due to these limitations, difference microphone distances d is employed for measurements in different frequency ranges.

Additional errors will occur if the intensity changes between the two microphones as in the case of high order sources and by interference of the intensity probe in the sound field. A good discussion of the errors and limitations of the two microphones measurement technique is presented in [65].

The actual sound power P can be determined from the intensity measurements by integrating the normal component of the intensity I_n over the measurement area S enclosing the source:

$$P = \int_S I_n dA$$

In practice the integral is in general replaced by a summation, corresponding to a discrete

point sampling of the intensity field over a number of elementary areas dividing the surface:

$$W = \sum_{k=1}^{K} I_{nk} \Delta A_i$$

The error involved in this sampling will be function of the spatial variation of the normal intensity component over the measurement surface, that is function of several factors such as the source directivity, the choose sampling surface and the proximity of other sources. An alternative method is to scan the measurement surface during the date acquisition to obtain a space averaged value of the intensity. This method will be present in the next Chapter.

A B&K intensity probe with 1/2 in microphones separated 50mm from each other, was used to measure the intensity field in 72 points over a box type surface over the tile. Each measurement position was averaged for 10 seconds. The detailed recommended measurement procedure for determining the sound power of sources using discrete point intensity measurements can be found in the ISO 9614-1 standard.

The total sound power of the 6mm tile in the passive and active cases found via the intensity measurements is shown in Figure A-1.

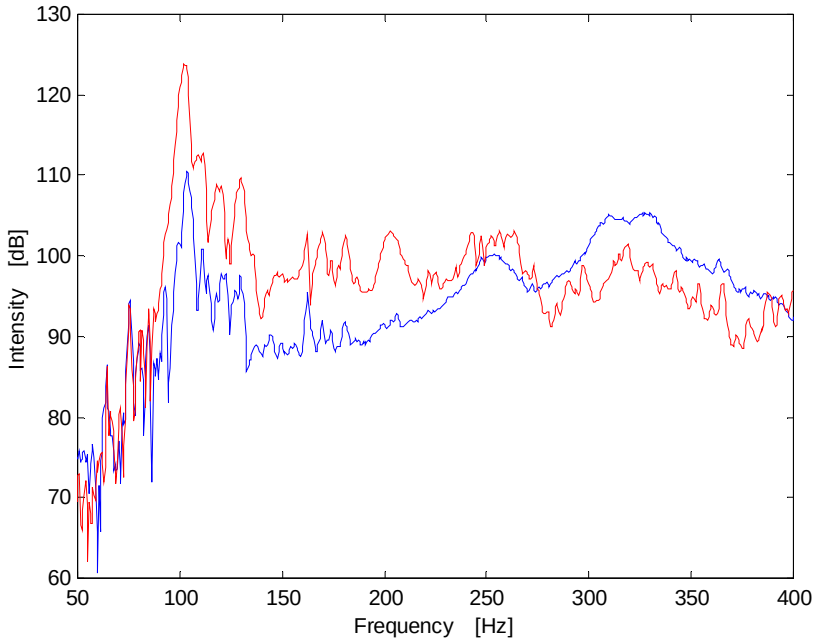

Figure A-1 Experimentally measured total sound power radiated using intensity measurements (a) red trace: without active control. (b) blue trace: with active control

Appendix B - Implementation of Analog Feedback Controller

Figure B- 2 shows the implementation of an inverting lag compensator using a single operational amplifier. The frequencies of the real zero ω_z and real pole ω_p and the gain k can be obtained using the following expressions:

$$\omega_z = \frac{1}{R_3 C}$$

$$\omega_p = \frac{1}{(R_2 + R_3)C}$$

$$k = \frac{R_2 R_3}{R_1 (R_2 + R_3)}$$

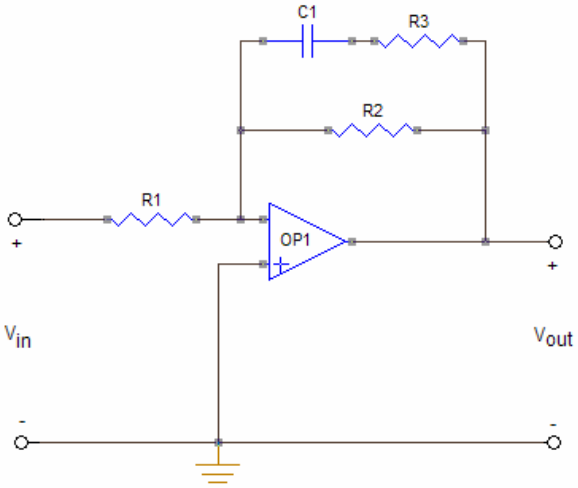

Figure B-1: Implementation of an inverting “lag” compensator

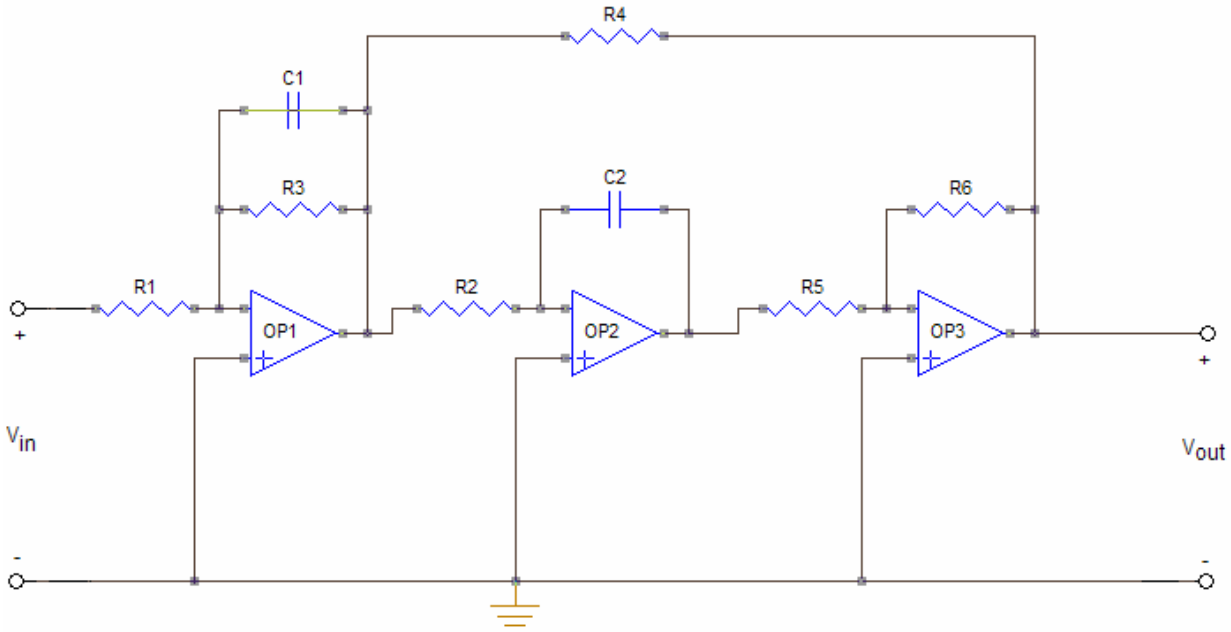

Figure B-2: Tow-Thomas biquad circuit

Figure B-3 shows the implementation of the Tow-Thomas biquad circuit. This circuit allows the implementation of both band-pass and low-pass filter functions given by second order functions of the form:

$$T(s) = \frac{V_{out}}{V_{in}} = \frac{kP(s)}{s^2 + (\omega_p / Q_p)s + \omega_p^2}$$

Where ω_p and Q_p describe the poles of the transfer function and k is the gain constant. Q_p is also known as the quality factor and it can be represented as Q = 1/(2ζ) where ζ is the damping factor. In addition, for the case of a low-pass filter we have $P(s) = \omega_p^2$.

Note that it is possible to implement second order transfer functions using different analog circuits. One advantage of the Tow-Thomas circuit when compared to other

biquad implementations is that it allows ω_p and Q_p to be controlled independently. In addition, Q_p and k can be controlled using individual resistors.

In the circuit of Figure B-3 V_{out}/V_{in} implements a low-pass type filter (complex pole pair) with transfer function given by:

$$\frac{V_{out}}{V_{in}} = \frac{1/(R_1 R_2 C_1 C_2)}{s^2 + s/(R_3 C_1) + 1/(R_2 R_4 C_1 C_2)}$$

Choosing $R_2 = R_4 = R$ and $C_1 = C_2 = C$ results in a simple design procedure for the filter.The design equations are as follows:

$$R = \frac{1}{\omega_p C}$$
$$R_3 = Q_p R$$
$$R_1 = \frac{R}{k}$$

Appendix C – Laser Velocity Measurements

The plots presented in this Appendix present the velocity measurements performed with a laser vibrometer at 9 points on the tile surface area, as shown in Figure 4.5, for velocity feedback control with a single error sensor at the tile center. The point velocity measurements were used to estimate the sound power radiated by the tile with control off and control on.

Single tile – Velocity Feedback Results

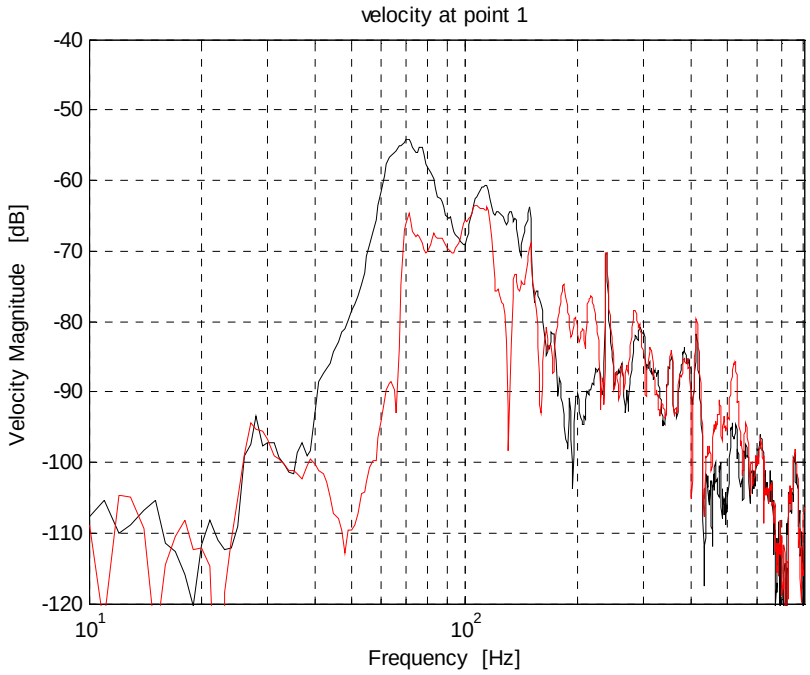

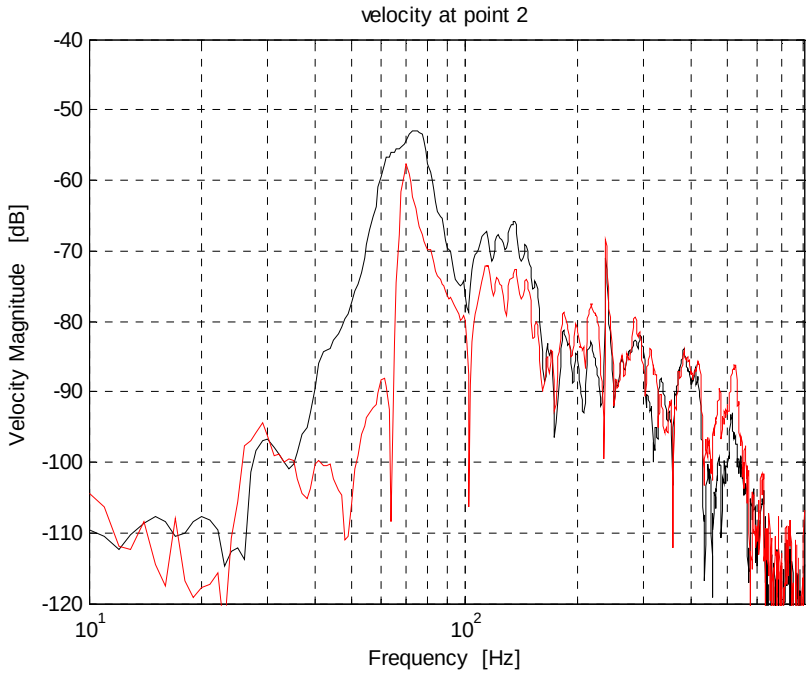
velocity at point 2
-40
-50
-60
-70
-80
-90
-100
-110
-120
Velocity Magnitude [dB]
10^1
10^2
Frequency [Hz]

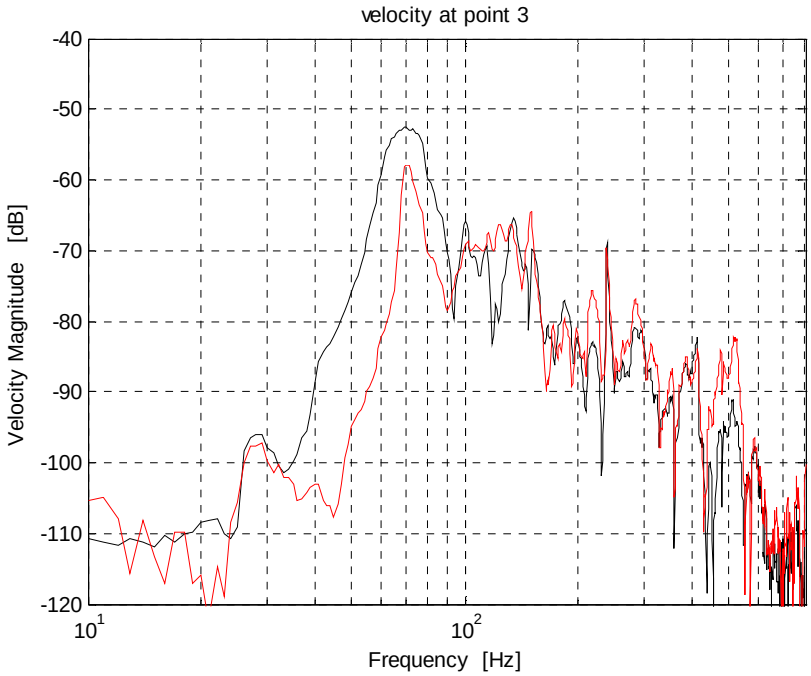
velocity at point 3
-40
-50
-60
-70
-80
-90
-100
-110
-120
Velocity Magnitude [dB]
10^1
10^2
Frequency [Hz]

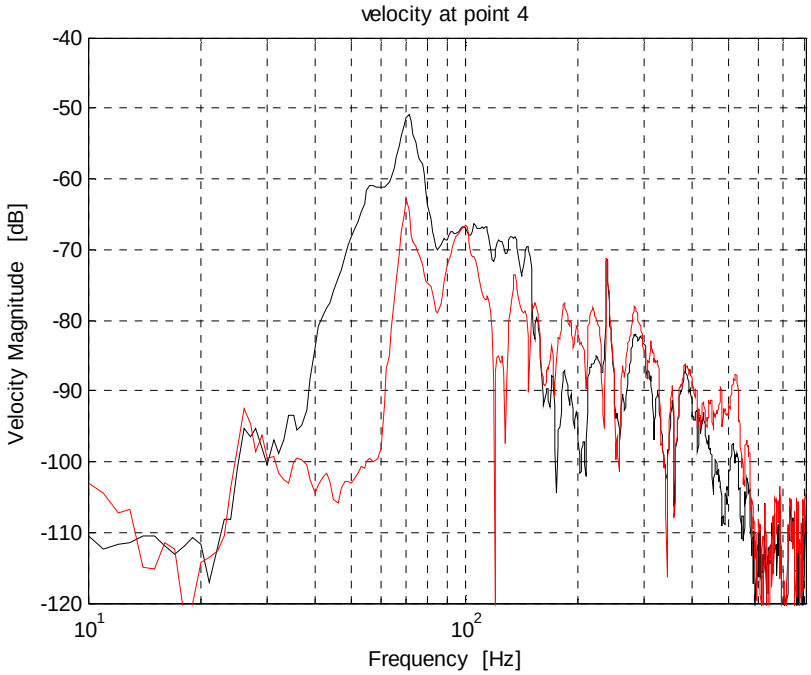
velocity at point 4
-40
-50
-60
-70
-80
-90
-100
-110
-120
Velocity Magnitude [dB]
10^1
10^2
Frequency [Hz]

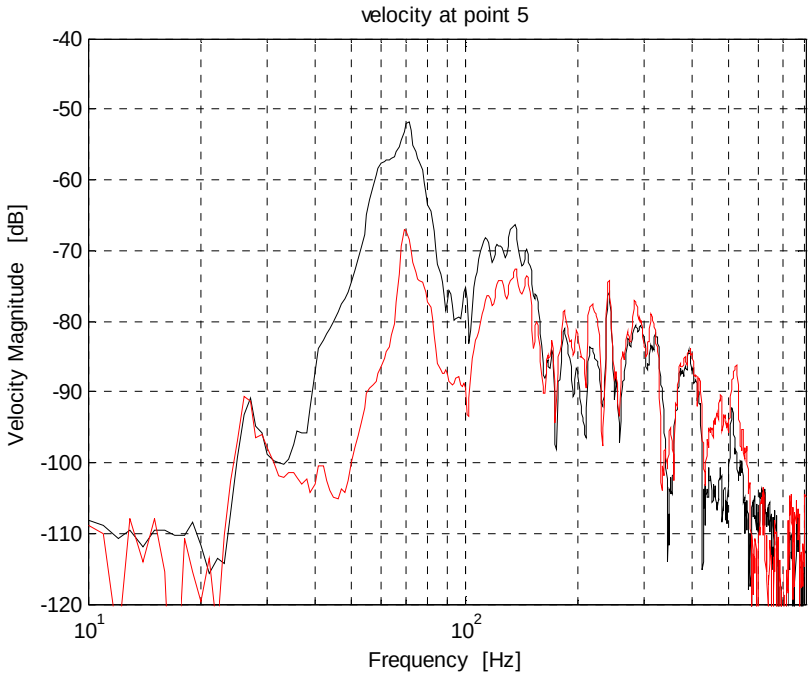
velocity at point 5
-40
-50
-60
-70
-80
-90
-100
-110
-120
Velocity Magnitude [dB]
10^1
10^2
Frequency [Hz]

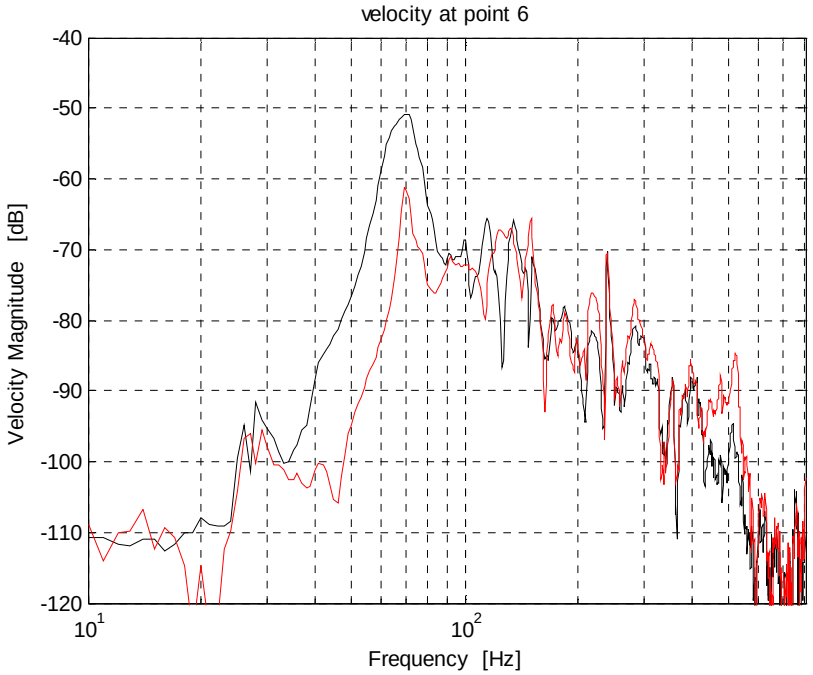
velocity at point 6
-40
-50
-60
-70
-80
-90
-100
-110
-120
Velocity Magnitude [dB]
10^1
10^2
Frequency [Hz]

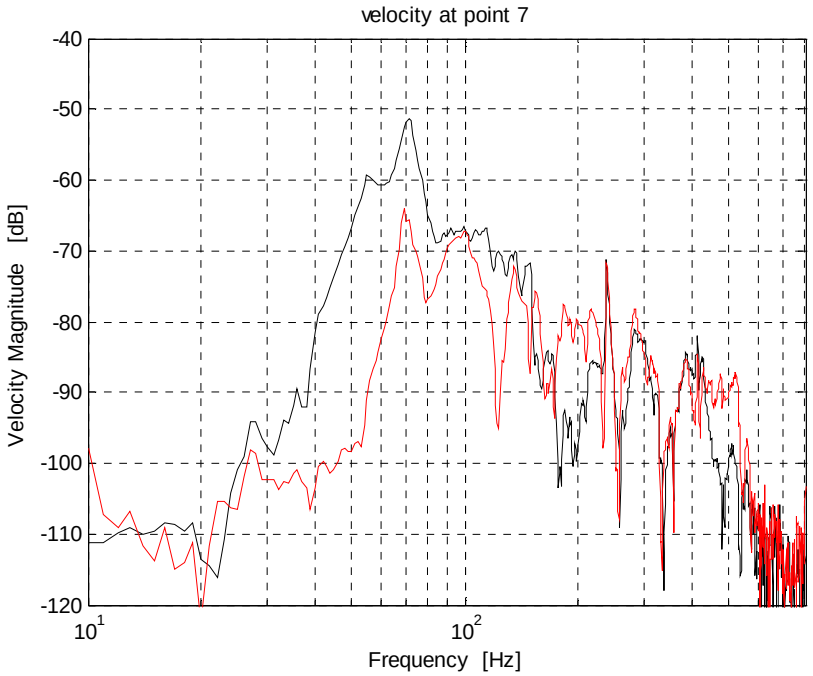
velocity at point 7
-40
-50
-60
-70
-80
-90
-100
-110
-120
Velocity Magnitude [dB]
10^1
10^2
Frequency [Hz]

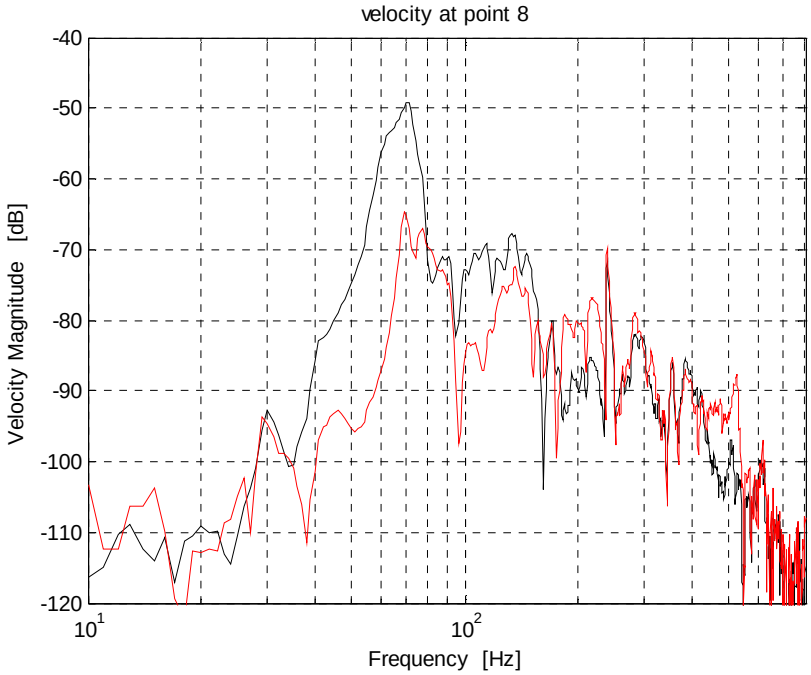
velocity at point 8
-40
-50
-60
-70
-80
-90
-100
-110
-120
Velocity Magnitude [dB]
10^1
10^2
Frequency [Hz]

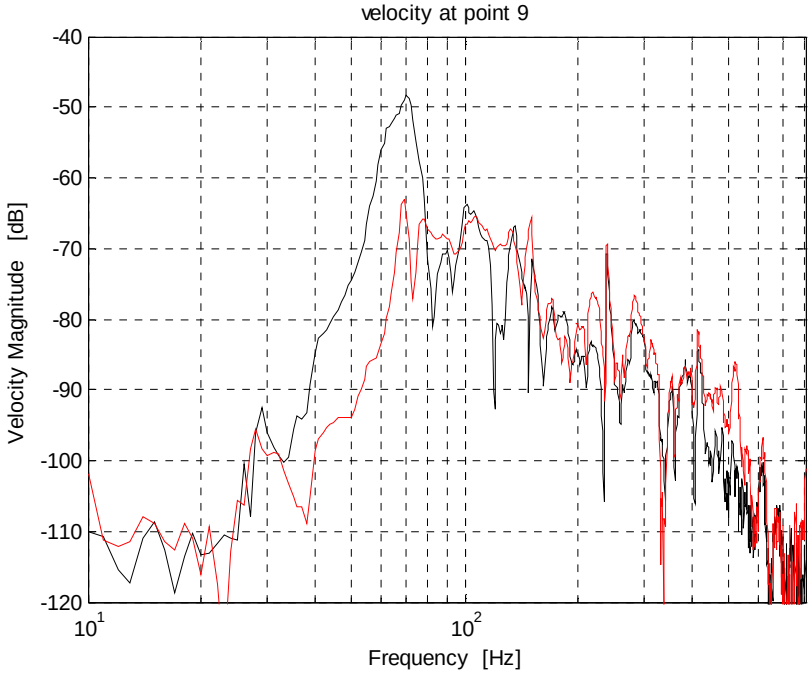
velocity at point 9
-40
-50
-60
-70
-80
-90
-100
-110
-120
Velocity Magnitude [dB]
10^1
10^2
Frequency [Hz]

Multiple Tile System Results

Velocity measurements performed with a laser vibrometer at 3 points on the each tile surface area for the four-tile system studied in Chapter 5, see Figure 5.2, for velocity decentralized feedforward control (ideal reference case) with a single error sensor at the tile center. The point velocity measurements were used to estimate the sound power radiated by the tile with control off and control on.

Velocity measurement at 3 points along the width of each tile.

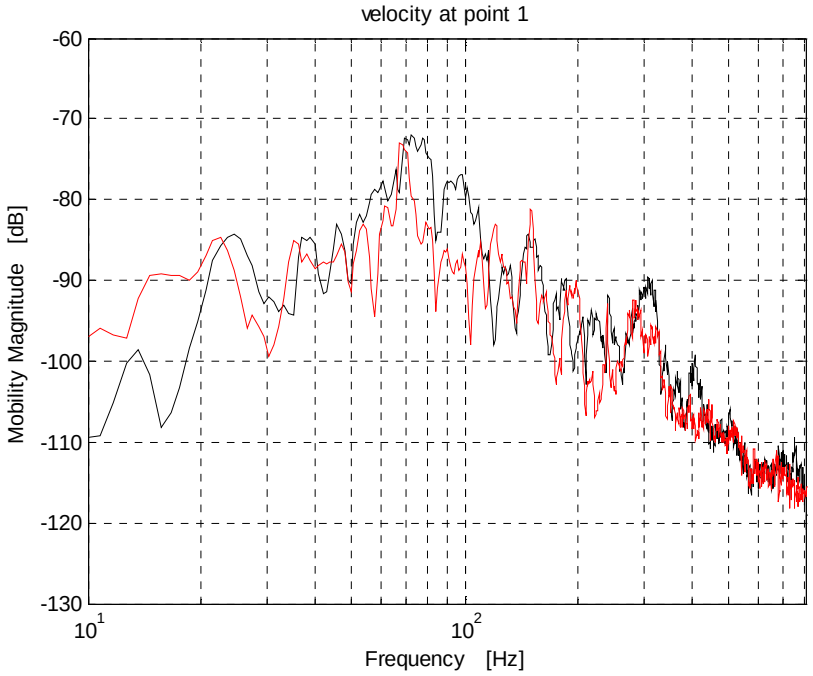

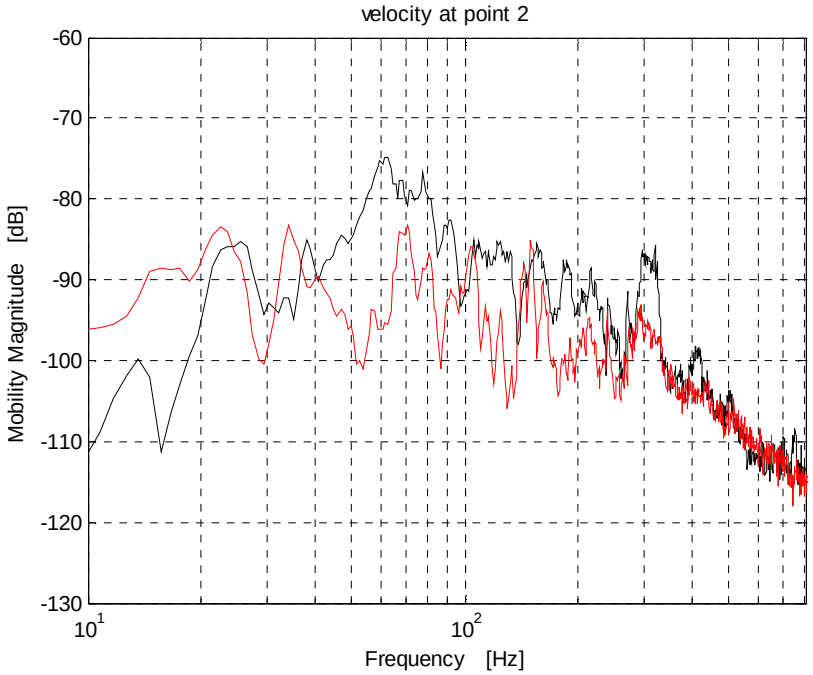
velocity at point 2
-60
-70
-80
-90
-100
-110
-120
-130
Mobility Magnitude [dB]
10^1
10^2
Frequency [Hz]

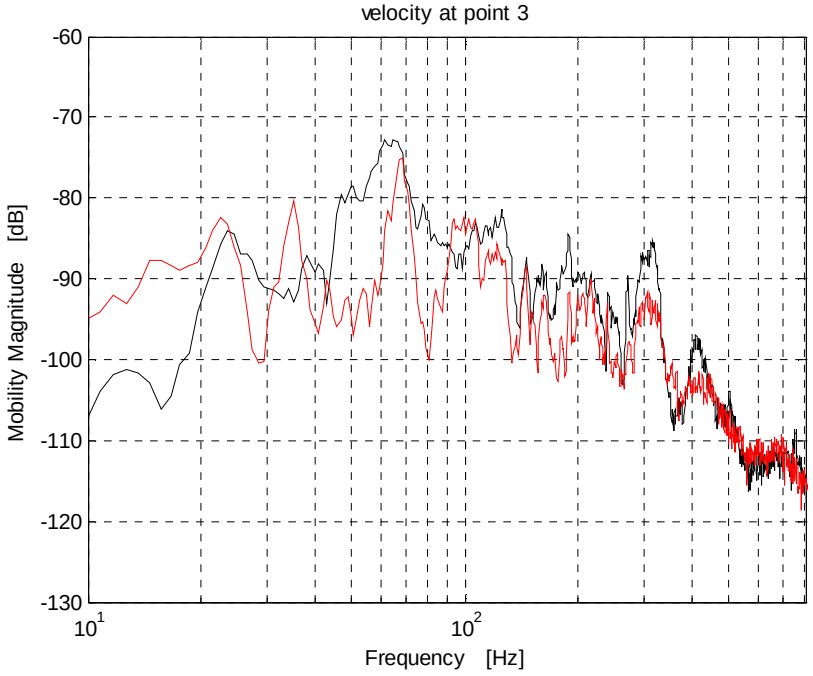
velocity at point 3
-60
-70
-80
-90
-100
-110
-120
-130
Mobility Magnitude [dB]
10^1
10^2
Frequency [Hz]

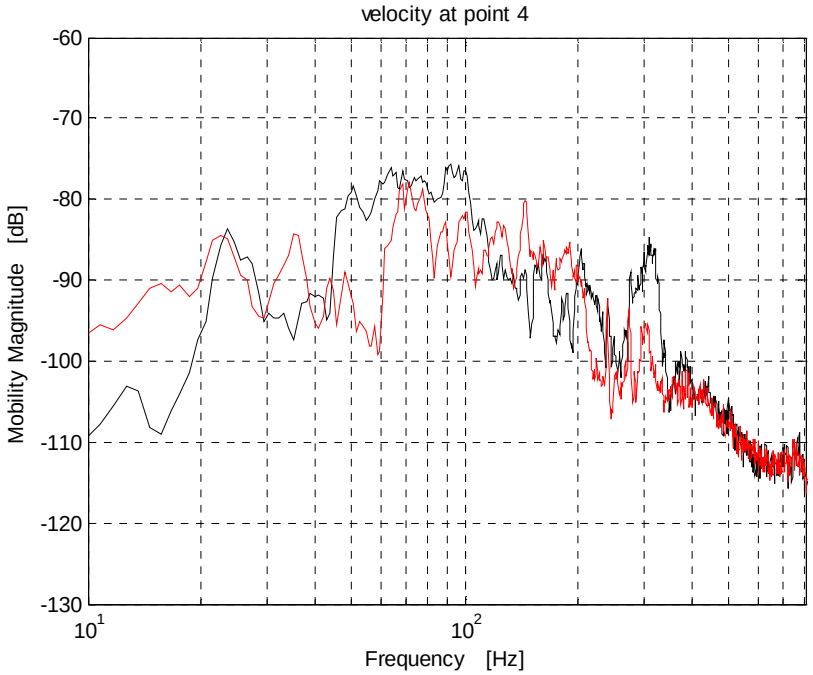
velocity at point 4
-60
-70
-80
-90
-100
-110
-120
-130
Mobility Magnitude [dB]
10^1
10^2
Frequency [Hz]

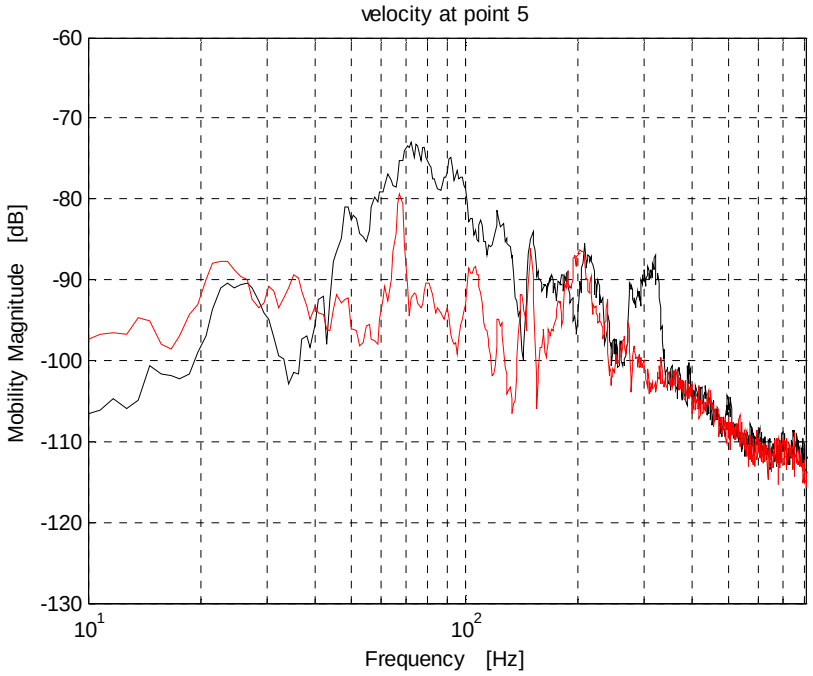
velocity at point 5
-60
-70
-80
-90
-100
-110
-120
-130
Mobility Magnitude [dB]
10^1
10^2
Frequency [Hz]

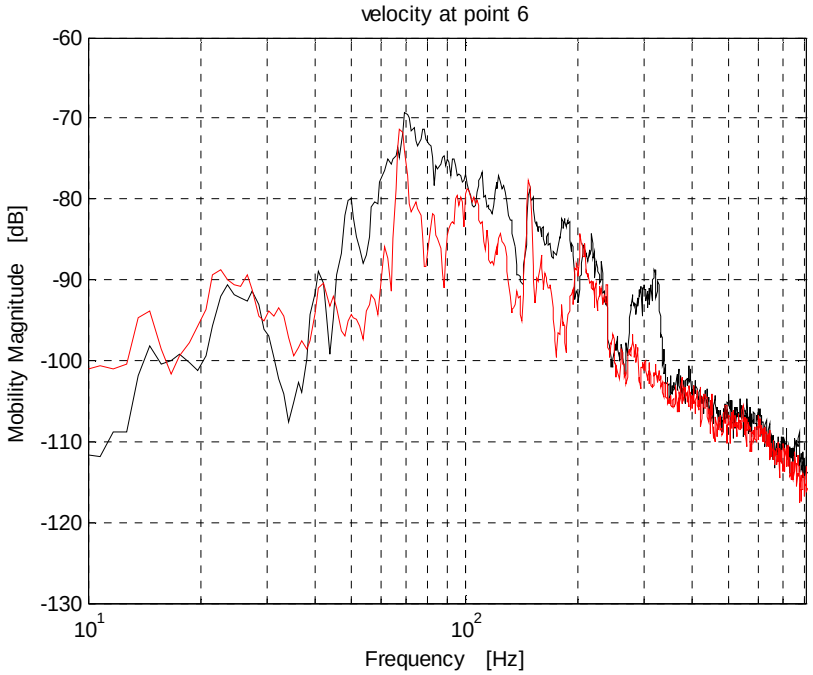
velocity at point 6
-60
-70
-80
-90
-100
-110
-120
-130
Mobility Magnitude [dB]
10^1
10^2
Frequency [Hz]

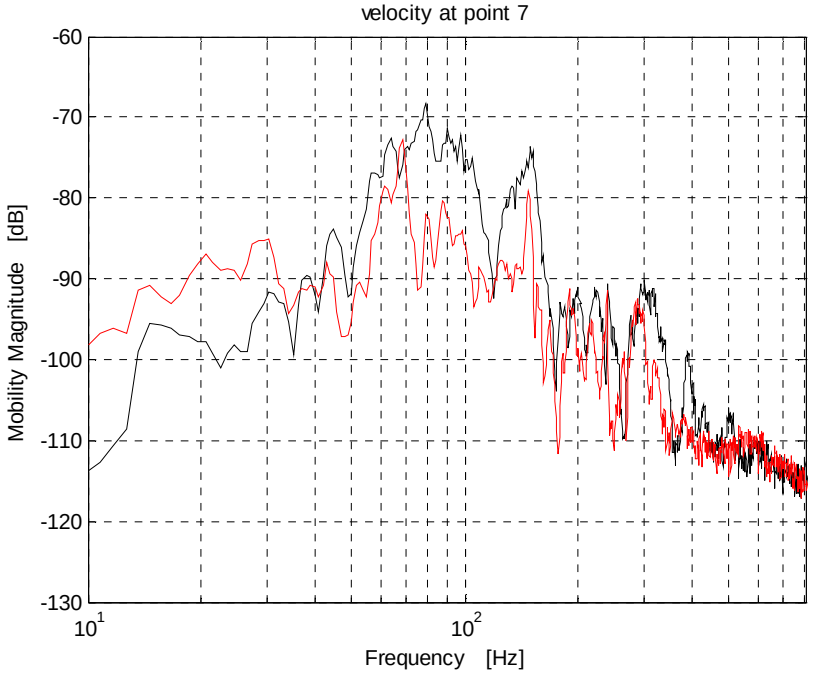
velocity at point 7
-60
-70
-80
-90
-100
-110
-120
-130
Mobility Magnitude [dB]
10^1
10^2
Frequency [Hz]

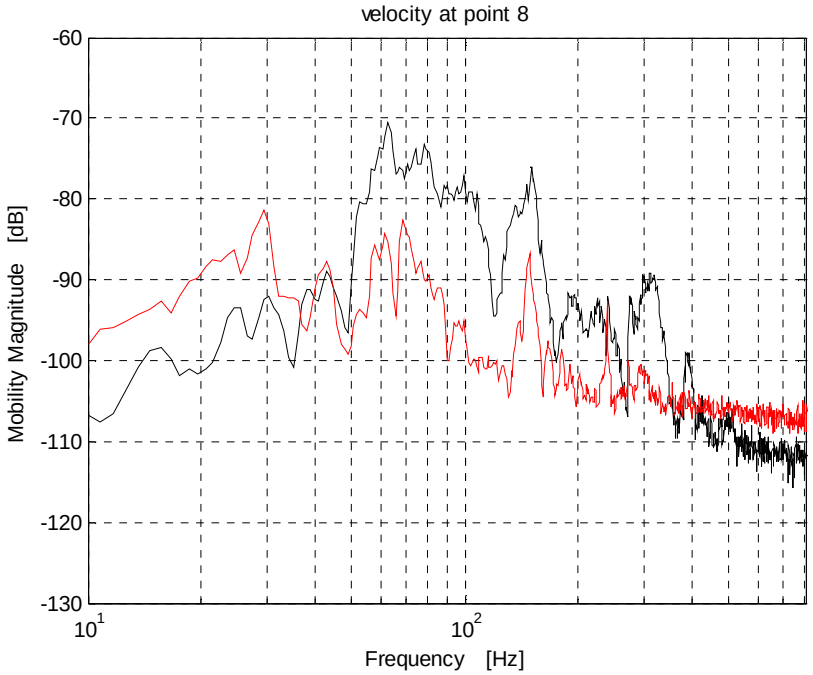
velocity at point 8
-60
-70
-80
-90
-100
-110
-120
-130
Mobility Magnitude [dB]
10^1
10^2
Frequency [Hz]

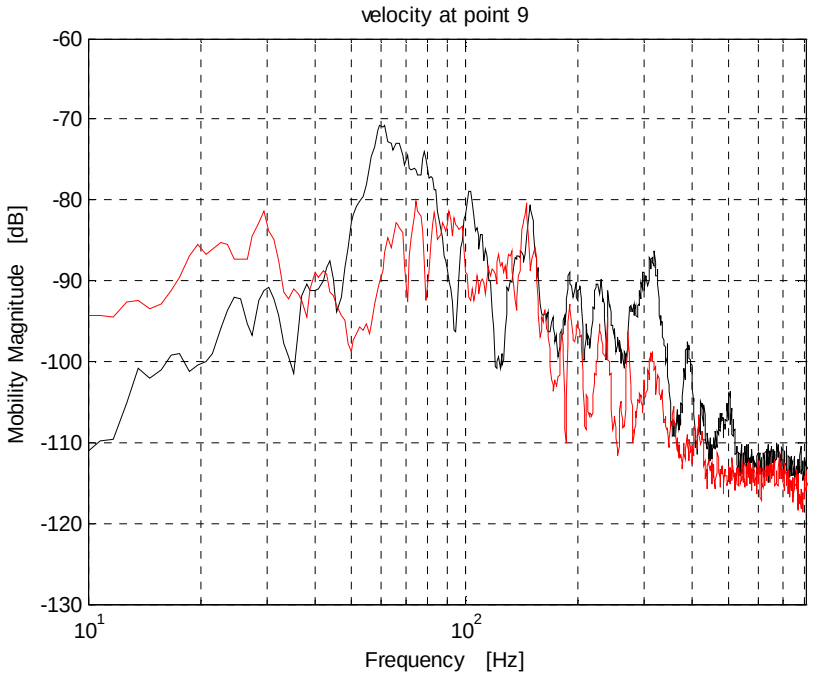
velocity at point 9
-60
-70
-80
-90
-100
-110
-120
-130
Mobility Magnitude [dB]
10^1
10^2
Frequency [Hz]

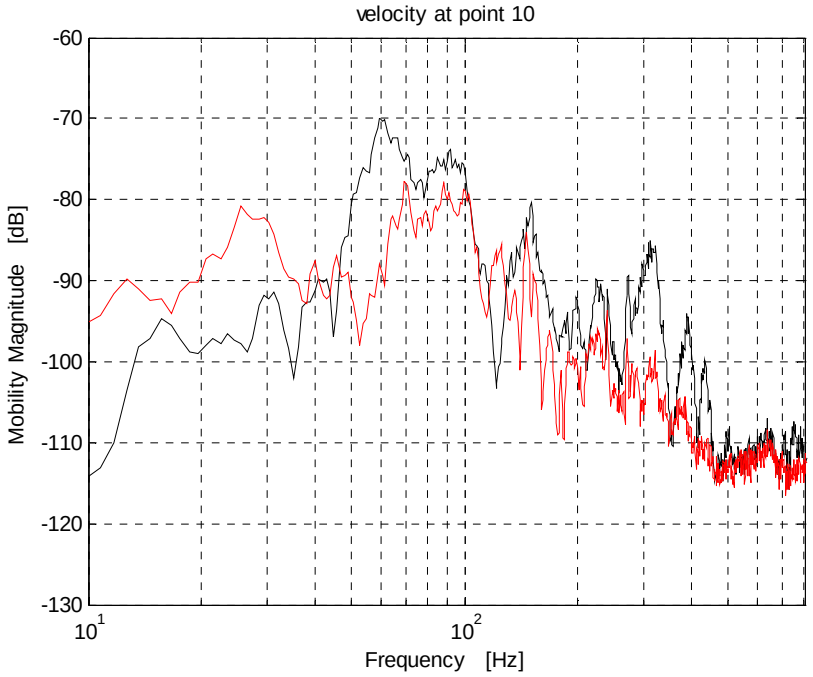
velocity at point 10
-60
-70
-80
-90
-100
-110
-120
-130
Mobility Magnitude [dB]
10^1
10^2
Frequency [Hz]

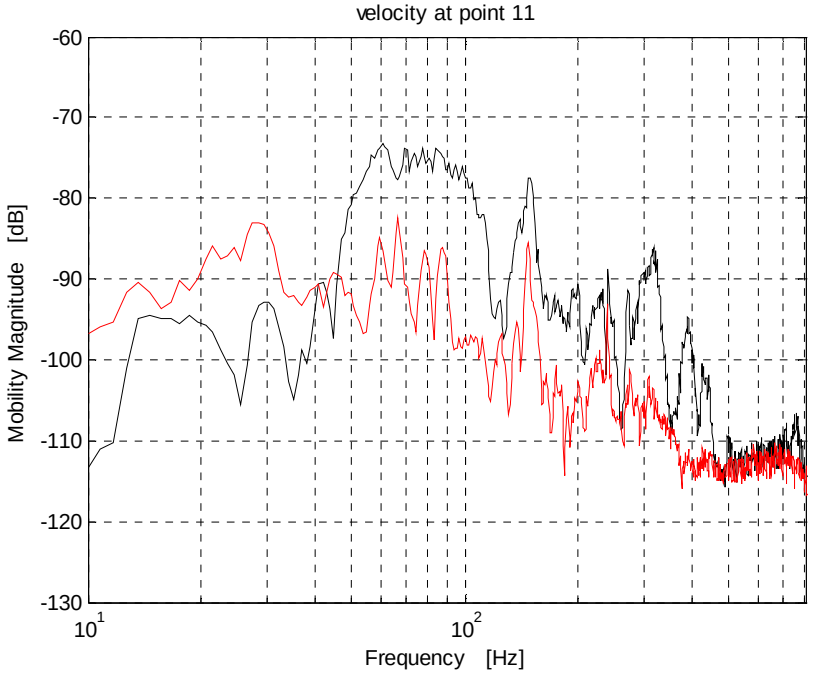
velocity at point 11
-60
-70
-80
-90
-100
-110
-120
-130
Mobility Magnitude [dB]
10^1
10^2
Frequency [Hz]

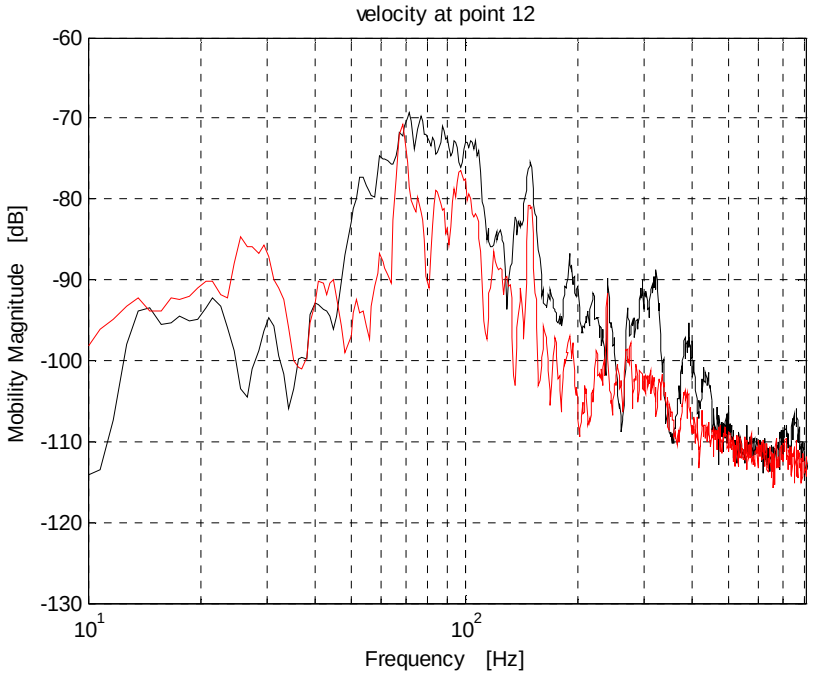
velocity at point 12
-60
-70
-80
-90
-100
-110
-120
-130
Mobility Magnitude [dB]
10^1
10^2
Frequency [Hz]

Sound power radiated by four-tiles estimated with 3 points (red trace) and 1 point (blue trace) at each tile.

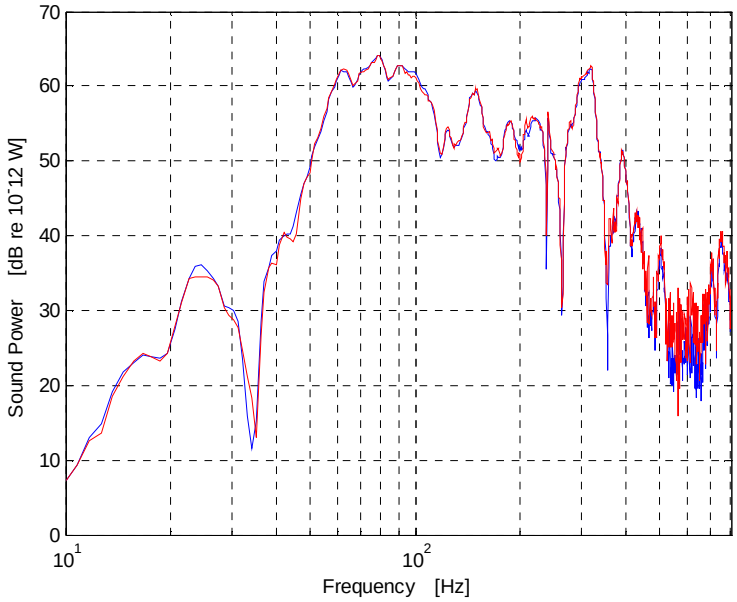

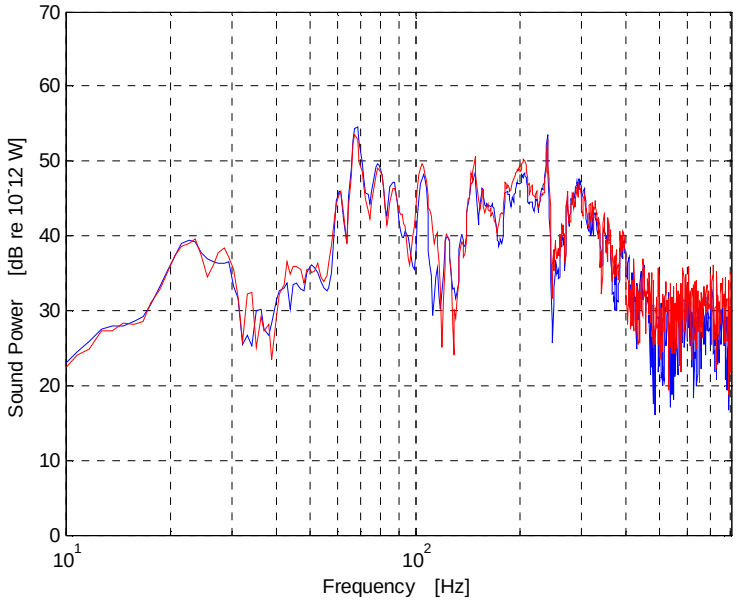

Appendix D - Modal Coupling Theory

In this section modal coupling theory is used for the modeling of the coupled structural-acoustic system shown in Figure 2.17. The detailed derivation of the coupled equations of motion of the system obtained using modal coupling theory can be found in [50].

In the model presented in this section, the vibration of the plate and the tile are coupled by the spring-damper mounts and by the dynamics of the air confined in the gap between the plate and the tile. The clamped plate and tile are assumed not to be influenced by the external acoustic radiated field. In addition, the tile is assumed to be in an infinite baffle and radiating into open-space. Furthermore, in the model presented, we assume the tile edges to be acoustically sealed.

The derivation of the response of the coupled system due to an arbitrary external excitation is presented next. The procedure involved in developing the model consists in expanding the pressure field of the internal cavity between the panels in terms of the rigid-walled cavity modes and writing the result in the form of a set of linear ordinary differential equations for each acoustic mode. In the same way the equations of motion of the plates are expanded using the in-vacuum structural modes. Next, the complete coupled structural-acoustic equations of motion of the double panel system are derived. Finally, the mechanical coupling of the tile to the base structure via the mounts is included. The model assumes that the mounts are simple spring-damper systems. The sound power radiated is estimated assuming that the radiating panel is in an infinite baffle and that there are no flanking paths.

Acoustic field problem

The set of ordinary differential equations for the acoustic modes of a system with arbitrary wall excitation is derived using the Green's theorem and the result applies to an arbitrarily shaped cavity.

Assume a structure defined by the surface S enclosing a fluid with volume V .The structure surface S_f is assumed flexible and is described by the normal displacement w, while the remainder of the structure surface S_r is assumed rigid. It is desired to predict the sound field due to the motion of the flexible wall.

If the fluid inside the cavity is assumed to be at rest before the motion of the wall (no internal acoustic sources), the perturbation pressure satisfies the following homogeneous wave equation and boundary conditions:

$$\nabla^2 p - \frac{1}{c^2}\frac{\partial^2 p}{\partial t^2} = 0 \qquad \text{D-1}$$

$$\begin{aligned} \frac{\partial p}{\partial n} &= -\rho \frac{\partial^2 w}{\partial t^2} \quad \text{on } S_f \\ \frac{\partial p}{\partial n} &= 0 \quad \text{on } S_r \end{aligned} \qquad \text{D-2}$$

where ρ and c are, respectively, the fluid density and acoustic velocity, and w is the normal displacement of the rigid wall.

The wave equation D for the case of a cavity with rigid walls has solutions given by normal modes Ψ_n that satisfy:

$$\frac{\partial \Psi_n}{\partial n} = 0 \text{ on } S = S_f + S_r \qquad \text{D-3}$$

and the orthogonality conditions:

$$\int_V \Psi_n \Psi_m dV = \Lambda_n \delta_{nm}$$
$$\int_V \Psi_n \nabla^2 \Psi_m dV = -k_n^2 \Lambda_n \delta_{nm} \qquad \text{D-4}$$

Where $k_n = -\omega_n/c$ and ω_n is the nth acoustic natural frequency. Using D-4 above we derive the following property:

$$\nabla^2 \Psi_n = -k_n^2 \Psi_n \qquad \text{D-5}$$

Now, using Green's second identity:

$$\int_V \{u\nabla^2 v - v\nabla^2 u\} dV = \int_S \{u \frac{\partial v}{\partial n} - v \frac{\partial u}{\partial n}\} dS \qquad \text{D-6}$$

where u and v are continuous scalar functions with continuous first and second partial derivatives, the wave equation D-1 can be transformed into a set of ordinary differential equations as:

$$\int_V \{p\nabla^2 \Psi_n - \Psi_n \nabla^2 p\} dV = \int_S \{p \frac{\partial \Psi_n}{\partial n} - \Psi_n \frac{\partial p}{\partial n}\} dS \qquad \text{D-7}$$

Using D-1, D-5 and boundary conditions given by D-2 and D-3, the integral equation above can be rewritten as:

$$\frac{1}{\rho c^2} \int_V \{\Psi_n \frac{\partial^2 p}{\partial t^2} dV + \frac{\omega_n^2}{\rho c^2} \int_V p \Psi_n dV = -\int_S \Psi_n \frac{\partial^2 \omega}{\partial t^2} dS \qquad \text{D-8}$$

Defining:

$$P_n \equiv \frac{1}{\rho c^2}\int_V \Psi_n p dV \qquad \text{D-9}$$

$$W_n \equiv \int_S \Psi_n \omega dS \qquad \text{D-10}$$

allows D-8 to be rewritten as an ordinary differential equation of the form:

$$\ddot{P}_n + \omega_n^2 P_n = -\ddot{W}_n \qquad \text{D-11}$$

where a dot (.) denotes differentiation with respect to time and P_n are coefficients of the mode expansion for the pressure:

$$p = \rho c^2 \sum_n (\frac{P_n}{\Lambda_n})\Psi_n \qquad \text{D-12}$$

Structural Model

Consider an isotropic plate radiating into an air cavity. Its equation of motion can be written as:

$$D\nabla^4 w + m\frac{\partial^2 w}{\partial t^2} = f_e - p \qquad \text{D-13}$$

where D is the bending stiffness, m is the mass per unit area, f_e is a external force and p is the pressure loading due to the air in the cavity.

Assume that the solution to the above equation can be obtained by expanding the displacement in terms of the in vacuum structural modes:

$$w = \sum_{m=1}^{M} q_m \Phi_m \qquad \text{D-14}$$

where q_m are the modal amplitudes and Φ_m are the in vacuum structural modes.

The modes Φ_m satisfy the following orthogonality conditions:

$$\begin{aligned} \int_S \Phi_m m \Phi_m &= M_n \delta_{mn} \\ \int_S \Phi_m D \nabla^4 \Phi_m &= M_n \omega_n^2 \delta_{mn} \end{aligned} \qquad \text{D-15}$$

Substituting D-12 into D-13, pre-multiplying by Φ_m, integrating over the domain of the structure and making use of the orthogonality conditions gives:

$$M_m (\ddot{q}_m + \omega_m^2 q_m) = F_e - \int_S p \Phi_m dS \qquad \text{D-16}$$

where F_e is the external modal force given by:

$$F_e = \int_S f_e \Phi_m dS \qquad \text{D-17}$$

Structural-Acoustic Coupling

The solution of the coupled structural acoustic system can be obtained by solving D-11 and D-16 together. First we need to rewrite D-10 in terms of the structural modal coefficients. Substituting expression D-14 into D-10, we get:

$$W_n = \sum_{n=1}^{N} C_{nm} q_m \qquad \text{D-18}$$

where $C_{nm\,i}$ is the modal coupling coefficient given by:

$$C_{nm} = \int_{S_f} \Psi_n \Phi_m dS \qquad \text{D-19}$$

Now D-11 can be rewritten as:

$$\ddot{P}_n + \omega_n^2 P_n = -\sum_{n=1}^{N} C_{nm} \ddot{q}_m \qquad \text{D-20}$$

In a similar way the pressure loading term in D-16 can be rewritten in terms of the pressure modal coefficients P_n. Using D-12 and D-19, D-16 can be rewritten as:

$$M_m (\ddot{q}_m + \omega_m^2 q_m) = F_e - \rho c^2 \sum_n \frac{P_n}{\Lambda_n} C_{nm} \qquad \text{D-21}$$

Equations D-20 and D-21 are coupled structural acoustic ordinary differential equations.

Additional insight into the nature of the structural acoustic coupling interaction can be obtained by using the acoustic velocity potential instead of the acoustic pressure. These are related by Bernoulli's equation:

$$p = -\rho\dot{\varphi} \tag{D-22}$$

Expanding φ in terms of the modes:

$$\varphi = \sum_{n=1}^{N} a_n \Psi_n \tag{D-23}$$

and using D-12, D-22 and D-23 it is possible to solve for a_n as:

$$\dot{a}_n = -c^2 \frac{P_n}{\Lambda_n} \tag{D-24}$$

Substituting this last expression into D-20 and D-21 we obtain:

$$\Lambda_n (\ddot{a}_n + \omega_n^2 a_n) = -c^2 \sum_{m=1}^{M} C_{nm} \dot{q}_m \tag{D-25}$$

and

$$M_m (\ddot{q}_m + \omega_m^2 q_m) = F_e - \rho \sum_n \dot{a}_n C_{nm} \tag{D-26}$$

The last two equations can be written in matrix form as:

$$\begin{bmatrix} \omega_{a1}^2-\omega^2 & 0 & 0 & \frac{i\omega\rho C_{11}}{M_{a1}} & \cdots & \frac{i\omega\rho C_{1m}}{M_{am}} \\ 0 & \ddots & 0 & \vdots & \ddots & \vdots \\ 0 & 0 & \omega_{a1}^2-\omega^2 & \frac{i\omega\rho C_{n1}}{M_{a1}} & \cdots & \frac{i\omega\rho C_{nm}}{M_{am}} \\ \frac{i\omega\rho C_{11}}{M_{s1}} & \cdots & \frac{i\omega\rho C_{n1}}{M_{s1}} & \omega_{s1}^2-\omega^2 & 0 & 0 \\ \vdots & \ddots & \vdots & 0 & \ddots & 0 \\ \frac{i\omega\rho C_{1n}}{M_{s1}} & \cdots & \frac{i\omega\rho C_{nm}}{M_{sm}} & 0 & 0 & \omega_{sm}^2-\omega^2 \end{bmatrix} \begin{bmatrix} a_1 \\ \vdots \\ a_n \\ q_1 \\ \vdots \\ q_m \end{bmatrix} = \begin{bmatrix} Q_1 \\ \vdots \\ Q_n \\ F_1 \\ \vdots \\ F_m \end{bmatrix} \quad \text{D-27}$$

or:

$$\begin{bmatrix} \boldsymbol{W_a} & \boldsymbol{Z_a} \\ \boldsymbol{Z_s} & \boldsymbol{W_s} \end{bmatrix} \begin{bmatrix} \boldsymbol{a_n} \\ \boldsymbol{q_m} \end{bmatrix} = \begin{bmatrix} \boldsymbol{Q_n} \\ \boldsymbol{F_m} \end{bmatrix} \quad \text{D-28}$$

Where:

$$\boldsymbol{W_a} = \begin{bmatrix} \omega_{a1}^2-\omega^2 & 0 & 0 \\ 0 & \ddots & 0 \\ 0 & 0 & \omega_{an}^2-\omega^2 \end{bmatrix} \quad \text{D-29}$$

$$\boldsymbol{W_p} = \begin{bmatrix} \omega_{s1}^2-\omega^2 & 0 & 0 \\ 0 & \ddots & 0 \\ 0 & 0 & \omega_{sn}^2-\omega^2 \end{bmatrix} \quad \text{D-30}$$

$$\boldsymbol{Z_a} = \begin{bmatrix} \frac{i\omega\rho C_{11}}{M_{a1}} & \cdots & \frac{i\omega\rho C_{1m}}{M_{am}} \\ \vdots & \ddots & \vdots \\ \frac{i\omega\rho C_{1n}}{M_{a1}} & \cdots & \frac{i\omega\rho C_{nm}}{M_{am}} \end{bmatrix} \quad \text{D-31}$$

$$\boldsymbol{Z}_s = \begin{bmatrix} \frac{i\omega\rho C_{11}}{M_{s1}} & \cdots & \frac{i\omega\rho C_{1m}}{M_{sm}} \\ \vdots & \ddots & \vdots \\ \frac{i\omega\rho C_{1n}}{M_{s1}} & \cdots & \frac{i\omega\rho C_{nm}}{M_{sm}} \end{bmatrix} \qquad \text{D-32}$$

Double Panel System

The analytical model of the complete double panel system can be obtained by a straightforward extension of the theory presented above by adding an additional equation to describe the behavior of the second plate.

The equations describing the behavior of the coupled structural acoustic system in matrix form are:

$$\begin{bmatrix} \boldsymbol{W}_a & \boldsymbol{Z}_{a1} & -\boldsymbol{Z}_{a2} \\ \boldsymbol{Z}_{p1} & \boldsymbol{W}_{s1} & \boldsymbol{0} \\ -\boldsymbol{Z}_{p2} & \boldsymbol{0} & \boldsymbol{W}_{s2} \end{bmatrix} \begin{bmatrix} \boldsymbol{a}_n \\ \boldsymbol{q}_{1m} \\ \boldsymbol{q}_{2m} \end{bmatrix} = \begin{bmatrix} \boldsymbol{Q} \\ \boldsymbol{F}_1 \\ \boldsymbol{F}_2 \end{bmatrix} \qquad \text{D-33}$$

Observe that as the cavity now couples with both plates, coupling terms appear in the acoustic equation.

The new terms in this matrix, $\boldsymbol{Z}_{a2}$, $\boldsymbol{Z}_{p2}$ and $\boldsymbol{W}_{s2}$ can be computed in a similar fashion as the terms for the single plate system.

Double Panels Connected by Isolators

In this section the equations of motion of a double-panel system connected by isolators are derived. The isolators are modeled simply as point spring-dampers connecting both plates.

The equations of motion of the incident (subscript 1) and radiating (subscript 2) plates connected by a set of spring-dampers can be written as:

$$D_1\nabla^4 w_1 + m_1\frac{\partial^2 w_1}{\partial t^2} = c(\frac{\partial w_1}{\partial t} - \frac{\partial w_2}{\partial t})\sum_{j=1}^{J}\sum_{i=1}^{I}\delta(x-x_j)\delta(y-y_i) + k(w_1 - w_2)\sum_{j=1}^{J}\sum_{i=1}^{I}\delta(x-x_j)\delta(y-y_i) = f_e - p(x,y,0) \quad \text{D-34}$$

$$D_2\nabla^4 w_2 + m_2\frac{\partial^2 w_2}{\partial t^2} = c(\frac{\partial w_2}{\partial t} - \frac{\partial w_1}{\partial t})\sum_{j=1}^{J}\sum_{i=1}^{I}\delta(x-x_j)\delta(y-y_i) + k(w_2 - w_1)\sum_{j=1}^{J}\sum_{i=1}^{I}\delta(x-x_j)\delta(y-y_i) = p(x,y,Lz) \quad \text{D-35}$$

Assuming that both plates have the same mode shapes and expressing the plate displacement as a modal expansion it can be substituted back into the equations above, making use of the orthogonality conditions and Dirac delta sifting property to get:

$$M_{1mp}(\omega^2 - \omega_{1m}^2)q_{1m} + i\omega c(q_{1m} - q_{2m})\sum_{j=1}^{J}\sum_{i=1}^{I}\sum_{m=1}^{M}\sum_{n=1}^{N}\Phi_m(x_j,y_i)\Phi_n(x_j,y_i) + k(q_{1m} - q_{2m})\sum_{j=1}^{J}\sum_{i=1}^{I}\sum_{m=1}^{M}\sum_{n=1}^{N}\Phi_m(x_j,y_i)\Phi_n(x_j,y_i) = F_e - P(x,y,0) \quad \text{D-36}$$

$$M_{2mp}(\omega^2 - \omega_{2m}^2)q_{2m} + i\omega c(q_{2m} - q_{1m})\sum_{j=1}^{J}\sum_{i=1}^{I}\sum_{m=1}^{M}\sum_{n=1}^{N}\Phi_m(x_j,y_i)\Phi_n(x_j,y_i) + k(q_{2m} - q_{1m})\sum_{j=1}^{J}\sum_{i=1}^{I}\sum_{m=1}^{M}\sum_{n=1}^{N}\Phi_m(x_j,y_i)\Phi_n(x_j,y_i) = P(x,y,L_z) \quad \text{D-37}$$

where

$$F_e = \int_S \Phi_n f_e dS \quad \text{D-38}$$

$$P = -\rho \sum_{n=1}^{N} \dot{a}_n C_{nm}(x, y, z) \qquad \text{D-39}$$

It is evident that the springs have coupled the structural modal equations. The equations above can be rewritten as:

$$\begin{aligned} &M_{1mp}[\omega^2 + (i\omega c + k) X_{nm}(x_j, y_i) - \omega_{1m}^2] q_{1m} \\ &-[(i\omega c + k) X_{nm}(x_j, y_i)] q_{2m} = F_e - P(x, y, 0) \end{aligned} \qquad \text{D-40}$$

$$\begin{aligned} &M_{2mp}[\omega^2 + (i\omega c + k) X_{nm}(x_j, y_i) - \omega_{2m}^2] q_{2m} \\ &-[(i\omega c + k) X_{nm}(x_j, y_i)] q_{1m} = P(x, y, L_z) \end{aligned} \qquad \text{D-41}$$

where

$$X_{nm} = \sum_{j=1}^{J} \sum_{i=1}^{I} \sum_{m=1}^{M} \sum_{n=1}^{N} \Phi_m(x_j, y_i) \Phi_n(x_j, y_i) \qquad \text{D-42}$$

Equations D-40 and D-41 together with the acoustic equation of motion can be written in matrix form as:

$$\begin{bmatrix} \boldsymbol{W_a} & \boldsymbol{Z_{a1}} & -\boldsymbol{Z_{a2}} \\ \boldsymbol{Z_{p1}} & \boldsymbol{W_{s1}} + X_{nm} & -\boldsymbol{X_{nm}} \\ -\boldsymbol{Z_{p2}} & -\boldsymbol{X_{nm}} & \boldsymbol{W_{s2}} + X_{nm} \end{bmatrix} \begin{bmatrix} \boldsymbol{a_n} \\ \boldsymbol{q_{1m}} \\ \boldsymbol{q_{2m}} \end{bmatrix} = \begin{bmatrix} \boldsymbol{Q} \\ \boldsymbol{F_1} \\ \boldsymbol{F_2} \end{bmatrix} \qquad \text{D-43}$$

The modal amplitude vector can be obtained by:

$$\begin{bmatrix} a_n \\ q_{1m} \\ q_{2m} \end{bmatrix} = \begin{bmatrix} W_a & Z_{a1} & -Z_{a2} \\ Z_{p1} & W_{s1} + X_{nm} & -X_{nm} \\ -Z_{p2} & -X_{nm} & W_{s2} + X_{nm} \end{bmatrix}^{-1} \begin{bmatrix} Q \\ F_1 \\ F_2 \end{bmatrix} \qquad \text{D-44}$$

Comparison to Impedance Mobility Model

The model based on Modal Coupling Theory was applied to a double plate system with two 30cm x 38cm aluminum plates, 1.5mm thick and spaced by 5cm. The base plate was excited by a point force applied and the resulting velocity of the radiating plate was computed. The same system was modeled using the Impedance-mobility matrix approach. The velocity results at two points on the radiating plate are shown in the next figures showing good agreement between the two model approaches.

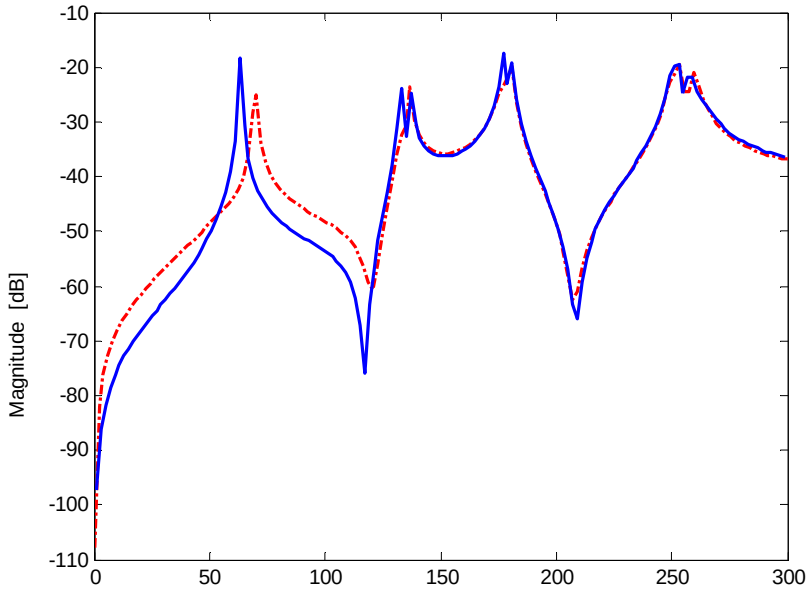

Figure D-1: Comparison of velocity results obtained with the Modal Coupling and Impedance-Mobility models

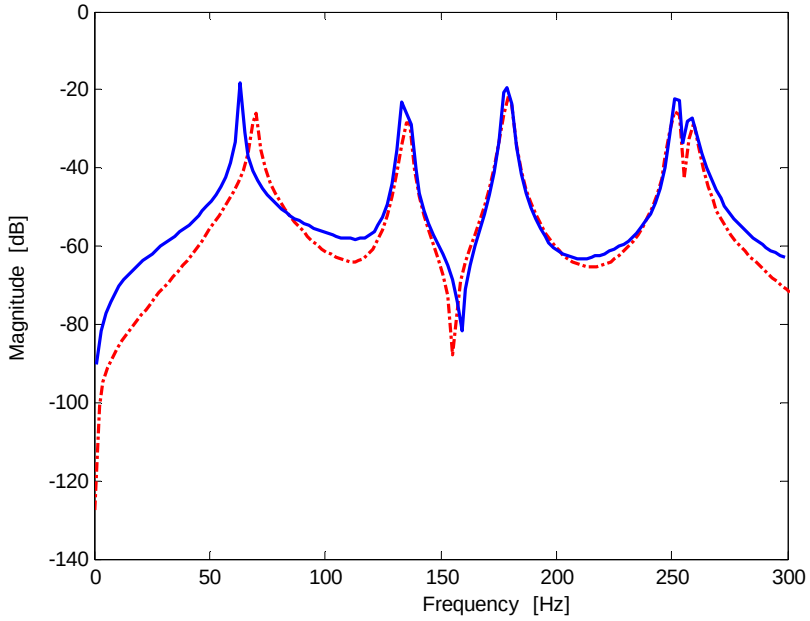

Figure D-2: Comparison of velocity results obtained with the Modal Coupling and Impedance-Mobility models